Prediction of Structural Health of Pavement Preservation Treated Pavements Using Neural Networks

by

Md Towhid Ur Rahman

A dissertation submitted to the Graduate Faculty of
Auburn University
in partial fulfillment of the
requirements for the Degree of
Doctor of Philosophy

Auburn, Alabama
August 5, 2023

Keywords: pavement, preservation, structural condition benchmarking, falling weight deflectometer, neural network

Approved by

Adriana Vargas-Nordcbeck, Chair, Associate Research Professor, NCAT
Benjamin Bowers, Assistant Professor, Dept. of Civil and Environmental Engineering
Carolina Rodezno, Associate Research Professor, NCAT
Fabricio Leiva-Villacorta, Assistant Professor, Clemson University

ABSTRACT

Structural testing of pavements is required to ensure their strength, durability, and longer service life. Destructive testing methods are less costly but more time-consuming and pose a safety risk for road users and crew members. On the other hand, nondestructive testing is faster and less intrusive, but the initial cost is very high for procuring and purchasing equipment. In network-level management, testing every road segment within a network is not feasible when the testing process is time-consuming and resource-demanding. Therefore, a tool or methodology to predict the structural condition of the pavements from the visible surface distresses is much needed. The present study used a neural network-based model for this purpose. Also, the existing benchmarking for the structural condition index was not found sensitive enough to capture the changes in structural condition due to the application of pavement preservation treatments. Therefore, a modified benchmarking was proposed in this study. Finally, a decision tree was developed for application in a Pavement Management System (PMS) that incorporates the structural health condition of the pavement while assigning a particular maintenance or rehabilitation activity that can directly benefit the agency providing recommended rehabilitation activities based on the overall pavement health.

ACKNOWLEDGEMENT

In this journey toward a Doctor of Philosophy degree, I acknowledge the support and contribution that my Professor and Committee Chair, Adriana Vargas, Ph.D., for her continuous support and guidelines. Special thanks to Dr. Carolina Rodezno, Dr. Benjamin Bowers and Dr. Fabricio Leiva for agreeing to serve on my Doctoral Committee. I also thank my Colleagues, Friends, Classmates and Project Sponsors who helped me every day to make my journey to success.

I would dedicate this Dissertation to my parents Mahbubur Rahman and Mahmuda Rahman- without whom I would not be here at this point in my career. I would also thank my Lovely Wife, Maliha Yel Mahi, who has supported my journey to this destiny. Finally, all praise to the Almighty for favoring me through this journey.

TABLE OF CONTENTS

LIST OF TABLES

LIST OF FIGURES

1 INTRODUCTION

1.1 Background

A Pavement Management System (PMS) is a pre-defined, well-structured, dynamic and evolving procedure to collect, analyze, maintain, and report pavement data which aids in finding optimum and economic pavement maintenance and rehabilitation strategies over a given period. The PMS does not provide a decision or planning but helps the managers make informed, educated, and unbiased decisions for improving pavement assets. Three major dimensions of PMS are data collection, modeling and analysis, and data management. Using all these data and analysis results, an agency can accomplish the following tasks: identification of data needs, short and long-term planning, treatment selection, and performance modeling (*1–8*). The success of a PMS largely depends upon the accuracy and variety of performance data to analyze and model to identify the most effective and economic solutions for the pavement network.

Over recent years many state and local agencies have effectively incorporated pavement preservation activities in PMS planning. Pavement preservation is defined as a series of activities performed to keep the pavement surface in a good state of repair. The pavement preservation activities can repair some minor or moderate distresses by sealing minor cracks, removing surface irregularities, and reducing rutting. Pavement preservation treatments are not intended to repair or restore the pavement's structural condition. The main purpose of these low-cost activities is to delay the need for major surface rehabilitation by applying them once or several times on the pavement surface before any major rehabilitation is warranted.

Treatments such as crack seal, chip seal, micro surfacing, cape seal and thin non-structural overlays seal up the open cracks and stop the surface run-off from penetrating into the pavement

surface. In addition, moisture damage and loss of elasticity due to ultraviolet rays in the wearing course are the two major damage types that can be corrected by applying preservation treatments, thus slowing the deterioration rate (*9, 10*).

Although pavement preservation treatments do not add structural capacity, selecting and treating structurally sound candidates can also extend the structural life of the pavement. Therefore, the structural benefit must also be incorporated into the PMS to optimize maintenance and rehabilitation planning for the network. Therefore, a study incorporating accurate, repeatable structural health condition parameters into the PMS decision tree while considering the benefits of pavement preservation treatments for network-level management is much needed.

Structural testing of the pavement layers is important in measuring the structural health of the pavement. There are two methods of structural testing (i) destructive testing (core extraction and trenches) and (ii) nondestructive testing (deflection testing, seismic pavement analyzer, dynamic cone penetrometer, ground penetrating radar, nuclear and non-nuclear density gauge). Destructive testing is expensive, time-consuming, and poses a safety risk to both the user and the agency, making it impractical for network-level project management. Falling Weight Deflectometers (FWDs) have been widely used for nondestructive structural testing of pavements over the past decades. They are accurate, but the cost of purchase and maintenance is high for agencies as lane miles of roads under maintenance ownership are increasing annually. In addition, some degree of destructive testing may be required to analyze results. On the other hand, functional pavement condition data such as surface distress and ride quality are easier and faster to obtain at the network-level and can indicate structural health.

As discussed, FWD testing is a much more reliable but expensive option to evaluate the structural condition of the pavement; an inexpensive but less-intrusive repeatable methodology of nondestructive testing. A few of the many significant efforts were to model the structural condition based on the surface condition, climate and traffic conditions, asphalt mix properties, base layer properties, subgrade properties etc. Based on available mathematical knowledge, regression modeling of heterogeneous structures like pavements is challenging as all the components may not exhibit a positive correlation with the predicted variable. However, with the advancement of computational ability, some model behavior variances can be explained using Neural Network (NN) modeling. In addition, some long-standing structural performance modeling issues have been successfully performed using neural networks on project-level pavement analysis.

The computational abilities of modern computers have enabled professionals to decipher complex phenomena using very basic but powerful techniques inspired by nature. The history of the mechanical brain started from the imagination of smart minds such as Homer, Blaise Pascal, Mark Twain, Jules Verne, Isaac Asimov, and L. Frank Baum. Artificial Intelligence (AI) was conceived in 1944 by Herb Simon, explaining the potential use of artificial computer brains in information processing, symbol manipulation, and psychological problems (*11*). NN adopts the way the human brain works toward problem-solving and pattern recognition. Each brain cell is connected to the next cells through axons, and information from one cell is transmitted to the next cell so that on each transmission of data, the brain can learn the pattern and channel the information in the right direction to categorize objects or learning patterns. In machine learning, the connections between each neuron are called nodes, and the nodes are arranged in a sequence of layers. An increased number of layers provides increased learning accuracy but reduced learning speed, so using an NN is a balanced tradeoff between learning speed and accuracy.

Many pavement research facilities have been studying pavement dynamics based on the collected data from the live traffic application to pavements. Collected pavement condition data from the live traffic application sites allow better relevance and validate the assumptions. Among several pavement research facilities in the United States, the National Center for Asphalt Technology (NCAT) at Auburn University was established in 1986 in collaboration with National Asphalt Pavement Association (NAPA), laying the foundation to provide innovative, relevant, and implementable research. One of the many significant and long-term experiments, the Pavement Preservation Group (PG) study has been conducted for over a decade to study the life-extending benefits of pavement preservation treatments. The expert panels for the experimental design, construction supervision, and data collection phase have employed the best knowledge to ensure that the collected data over 10 years are the most accurate and reliable. As a part of the experimental design, test locations were chosen in Alabama and Minnesota to capture the benefits of the preservation treatments under different traffic and climate conditions.

The researchers at NCAT identified several short-coming in the present methodologies: no prediction model that predicts the structural health of pavement that accounts for the application of the pavement preservation treatments, the existing Federal Highway Administration (FHWA) benchmarking of the structural health index is not sensitive to the small changes in structural health triggered by some minor improvement in the surface condition and finally, no existing PMS model to incorporate the pavement structural health alongside the functional condition of the pavement to assign right rehabilitation activity.

In summary, based on the discussion of the background, the need for a methodology to evaluate the structural condition of the pavement preservation treated HMA pavements and

incorporation of the structural health to the PMS decision tree is identified to achieve an inclusive and diverse pavement management plan for transportation agencies.

1.2 Objective

The main objectives of this study are to:

- Develop a Neural Network Model to predict the structural condition of the pavement based on the functional condition and incorporate the effect of pavement preservation treatments.
- Modify the existing FHWA deflection basin benchmarking system to identify initial structural distresses when those can be corrected with the application of light rehabilitation activities.
- Formulate a framework to incorporate the structural condition of the pavement into a Pavement Management System (PMS) decision tree based on the functional condition only.

The study's secondary objective is to validate the length of service life of pavement preservation treatments under different weather and traffic conditions.

1.3 Scope of Work

To accomplish the objectives mentioned above, data from the Pavement Preservation Group (PG) Study were used in this research. The PG Study was initiated in 2012 to determine the life-extending benefits of various pavement preservation treatments. The experimental design includes test locations in open roadways subjected to different climates and traffic conditions. Full-scale test sections were constructed on Lee County Road 159 in Auburn, AL, Highway US 280 in Opelika, AL, County State Aid Highway (CSAH) 8, and Highway US 169 near Pease, MN.

Pavement performance data over an analysis period of 10 years was employed to train a Neural Network Model to predict the FWD deflection basin parameters Base Damage Index (BDI) and Base Curvature Index (BCI), which represent the structural condition of the base and subgrade layers, respectively. In addition, functional condition parameters cracking, IRI, rutting, pre-application cracking, pre-application IRI, pre-application rutting, surface, and air temperature at the day of testing, 7-day average precipitation before the testing date was the input predictor parameters to develop two separate models to predict BDI and BCI. The MATLAB® 2021(b) Neural Network Tool was employed to train and measure the model performance. The training data was supplemented with the climatic data from the National Oceanic and Atmospheric Administration (NOAA).

1.4 Organization of the Dissertation

The dissertation consists of an elaborate and extensive literature review of past and recent studies on the application of neural networks in pavement engineering and pavement management systems in Chapter 2. Chapter 3 consists of a review of the testing methodology and test site information. The application of a neural network model to predict the deflection basin parameter (DBPs) from the functional condition data and model performance is discussed in Chapter 4. Chapter 5 presents a modified benchmarking for the DBPs to capture the structural benefits of pavement preservation treatments. Chapter 6 presents the proposed framework for integrating the structural condition of the pavement into the PMS decision tree. Finally, Chapter 7 discusses the findings from the dissertation, the limitations of the present study and recommendations for future research.

2 LITERATURE REVIEW

The present chapter discusses an extensive review of the present state of the practice for PMS, and the identification of needs, followed by an in-depth review of nondestructive pavement testing. Next, previous development and application of the neural network modeling methodology in pavement performance were reviewed so that the task of developing a model, significant input variables, and reduced bias with increased accuracy are investigated. Finally, the recent practices of pavement management and the incorporation of neural networks in PMS are also discussed.

2.1 Pavement Management Current State of Practice

In this section, needs and deficiencies in the existing PMS practices identified and acknowledged by the stakeholders were reviewed. In addition, the recent implementation of performance modeling for the pavement condition index to identify pavement needs was also reviewed.

2.1.1 Identification of Gaps in the Current Practice by FHWA in PMS Roadmap

FHWA, in the Pavement Preservation Research Roadmap (*5*), discussed various aspects of the PMS based on different studies conducted in the following areas of PMS, majorly six umbrella topics:

- Asset Management, Pavement Management, and Pavement Preservation
- Treatment Design
- Materials
- Treatment Application
- Performance

- Benefits

Based on the umbrella topics, the FHWA surveyed the asset stakeholders to identify the prioritization of the research topics. Figure 2-1 shows the stakeholders' response regarding the topic's priority to research need statement (RNS) and the budget allocation. It is clear from the responses that the six umbrella topics roughly received equal traction from the stakeholders.

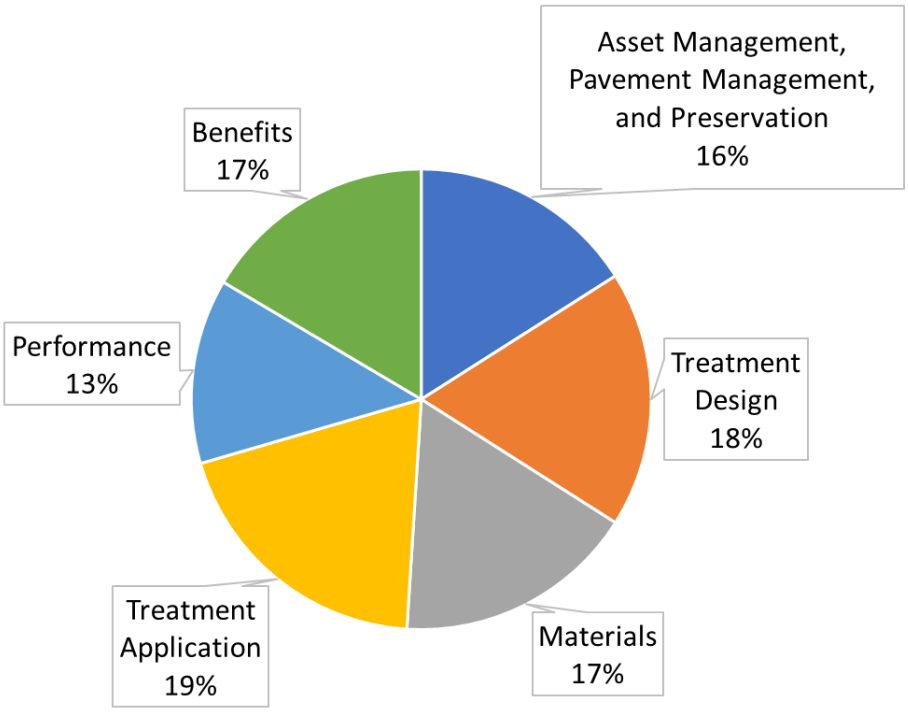

Figure 2-1 Stakeholder response for the priority of the umbrella topics by FHWA (Zimmerman et al., 2022)

Zimmerman et al. (*4*), in the 2022 Publication Titled "Pavement Management Roadmap," indicated some key areas to identify the gaps to achieve successful pavement condition goals by the stakeholders, summarized in Table 2-1.

Table 2-1 Overview of Gaps Identified by Agency Stakeholders (Zimmerman et al., 2022)

THEME 1: PAVEMENT MANAGEMENT DATA	Topic Area 1-1: Data
	Topic Area 1-2: Data Quality
THEME 2: PAVEMENT MANAGEMENT ANALYSIS TOOLS AND OTHER APPLICATIONS	Topic Area 2-1: Modeling
	Topic Area 2-2: Support for TPM and Transportation Asset Management (TAM)
	Topic Area 2-3: Project Selection
	Topic Area 2-4: Other Applications for Pavement Management Data and Analysis
THEME 3: WORKFORCE AND ORGANIZATIONAL ISSUES	Topic Area 3-1: People
	Topic Area 3-2: Pavement Management Funding Risks
	Topic Area 3-3: Integration into Existing Systems and Processes
	Topic Area 3-4: Data and Technology
	Topic Area 3-5: Communication and Outreach
THEME 4: TECHNOLOGICAL ADVANCEMENTS – NEW TOOLS, METHODOLOGIES	Topic Area 4-1: Advancements in Automated Pavement Data Collection Technologies
	Topic Area 4-2: Technologies to Assess Pavement Subsurface Characteristics and Structural Properties
	Topic Area 4-3: Emerging Data Collection Technologies and Methodologies for Assessing Pavement Distresses and Other Surface Characteristics
	Topic Area 4-4: Improving Pavement Management Data and Analysis Tools
	Topic Area 4-5: Next-Generation Performance Measures

In this dissertation, Topic Areas 2-3 and 4-2, shown in Table 2-1, are directly addressed to implement a more robust PMS tool to achieve longer pavement life by incorporating the pavement structural condition assessment in the decision tree for project selection and rehabilitation assignment.

2.1.2 Recent Advances in Performance Modeling in PMS

There have been several studies aimed at incorporating structural conditions in pavement management systems. Katicha et al. (*12*) developed a pavement structural deterioration model indicating the need to incorporate structural performance into PMS decisions to avoid less-than-optimal decisions. The model developed in the study combined the model critical condition index (CCI) and observed CCI to explain variability. The authors recommended that a negative binomial model better represents the data trends for CCI in Virginia Department of Transportation (VDOT) pavements. The deterioration index (DI) is calculated based on the CCI, which is $DI = 100 - CCI$. The modified strucutral index (MSI) developed by Bryce et al. (*13*), the Deteriroartion Index (DI) and pavement age (T) were used to fit the model for the DI_{model} and CCI_{model} as shown in Equation 2-1 and Equation 2-2.

$$DI_{\text{model}} = e^{\left(\beta_0+\beta_1\frac{1}{MSI^4}+\beta_2\ln(T)+\beta_3 T\right)} = T^{\beta_2}e^{\left(\beta_0+\beta_1\frac{1}{MSL^4}+\beta_3 T\right)} \quad \text{Equation 2-1}$$

$$CCI_{\text{model}} = 100 - DI_{\text{model}} = 100 - e^{\left(\beta_0+\beta_1\frac{1}{MSI^T}+\beta_2\ln(T)+\beta_3 T\right)} = 100 - T^{\beta_2}e^{\left(\beta_0+\beta_1\frac{1}{MST^T}+\beta_3 T\right)} \quad \text{Equation 2-2}$$

Based on the model, the agency developed different CCI deterioration curves for different MSI values, and the study concluded that incorporating structural condition models in the PMS decisions could improve the prediction by up to 21.6% more accurately.

Haider et al. (*14*) investigated the service life extension (SLE) of different pavement preservation treatments considering the pre-existing condition of the pavement. Long-Term Pavement Performance Specific Pavement Study -3 (LTPP SPS-3) data was utilized to perform the investigation. SLE can be explained as the extension of service life between treated and untreated sections. The measurement of SLE is based on the functional (cracking, IRI and rutting) and structural condition of the pavement. The study showed that the SLE of different treatments depends not solely on the treatment type but also on the type of distress dominant on the existing pavement, climatic region, traffic parameters, etc. Table 2-2 indicates the ranking of influence over different distresses for treatments based on the SLE. The study concluded that the surrounding environment largely impacts the choice of the right treatment type, pre-treatment distresses, and weather conditions of the road surface being treated. The study determined that thin overlay, slurry seal, and crack seal treatments had a statistically significant effect on the SLE with $p - value \leq 0.05$. The treatments were. As the table indicates, no treatment statistically significant on the SLE has a rutting reverting capability. Therefore, that treatment group has been identified as "N/A".

Table 2-2 Relative Ranking of Site Factors Affecting Treatment SLE (Haider et al., 2015)

Site factor	Flexible Pavement surface conditions							
	FC	LC	TC	IRI	Rutting	Bleeding	Raveling	Friction
Statistically significant treatments	Thin Overlay and Slurry Seal	Thin Overlay, Slurry Seal, Crack Seal, Chip Seal	Slurry Seal	Thin overlay	N/A	Thin Overlay	Thin Overlay and Slurry Seal	Slurry Seal and Chip Seal
Treatment Type	-	5	2	-	-	-	2	-
Pre-ext. cond,	5	2	-	-	-	3	-	-
Pre-ext. SN	-	-	-	-	-	-	3	-
Pre-ext. LTE	-	-	-	-	-	-	-	-
Pre-treatment d_0	3	-	4	4	2	4	-	-
Pavement thickness	2	3	-	-	3	-	-	-
AADT	4	4	-	2	-	-	-	2
ESALs	-	-	-	-	-	-	-	-
Age	-	-	-	3	-	2	-	-
Precipitation	-	-	3	5	-	-	5	3
Freezing index	-	-	-	6	-	-	4	-

Relative Ranking (1 = Most Influence; 6 = Least Influence)
FC = Fatigue Cracking, LC = Longitudinal Cracking, TC= Transverse Cracking, IRI – International Roughness Index, SN = Structural Number, LTE= Load Transfer Efficiency, d_0= Mean Center Deflection measurement from FWD

2.2 Falling Weight Deflectometer for Nondestructive Testing of Pavement Structure

Nondestructive testing is often performed with the falling weight deflectometer (FWD) to evaluate the structural condition of the pavement. However, this common practice still faces several limitations for network-level pavement management, which are discussed later in this section. Therefore, this current section discusses the evaluation of the pavement's structural health based on deflection testing and measurement of the structural condition index.

2.2.1 Evaluation of Structural Pavement Condition

Deflection-based pavement structural testing has evolved over the years to establish a standard method to perform nondestructive structural testing (NDT) of the pavement structure. The equipment has transitioned from the Benkelman Beam, Dynaflect, and Road Rater devices, to the modern impulse loading mechanism, the falling weight deflectometer (FWD). The FWD is now one of the major pieces of equipment for the structural testing of pavement for most agencies and research facilities worldwide. In addition, heavy weight deflectometer (HWD), FastFWD, and traffic speed deflectometer (TSD) have been employed for the structural testing of airport runways and pavement surfaces with higher capability and faster testing speed. However, FWD is the equipment that has exhibited the most correlation with the structural health of the pavement layers in most studies available based on years of user-end research experience. Though FWD devices are deployed for project-level analysis, many Departments of Transportation have incorporated FWD testing in network-level maintenance. Some known benefits of NDT over destructive testing are a more rapid testing duration, easier operation, lower operating cost, reduced workforce, less intrusive procedure, and an increased number of test points (*15*).

FWD deflections are commonly used for calculating layer moduli of different pavement layers for mechanistic empirical design procedures. The measured deflection, load magnitude, layer thicknesses, and temperature at the testing time are the mandatory inputs for the backcalculation of layer elastic moduli for AC pavements. In addition, the use of FWD devices is equally influential for the load transfer efficiency (LTE) for PCC pavements which is one of several important indicators of the overall performance of the PCC pavement. Figure 2-2 shows the schematic of the FWD testing method for structural testing of pavements.

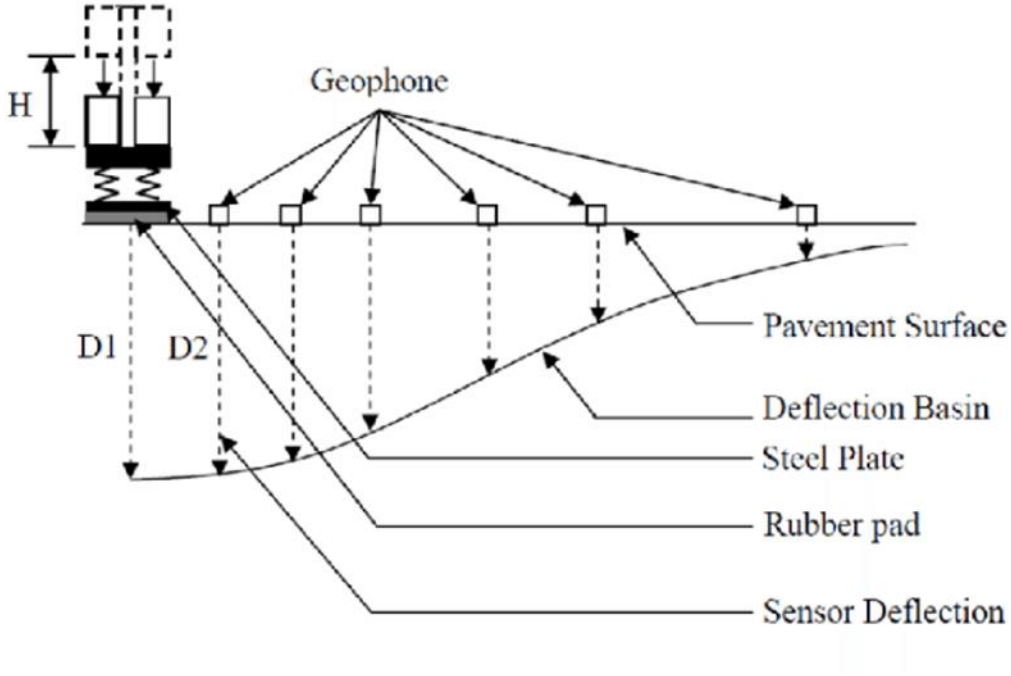

Figure 2-2 Schematic of FWD testing using impulse loading mechanism (Kavussi et al. 2017)

First, the drop location is selected where there is no discontinuation of the surface layer, such as cracking in the AC layer or slab joint in PCC pavements. The spacing between each consecutive drop location differs from network-level and project-level data collections, which are

designed based on the accuracy required for the project. Once the location is selected, the load plate is placed on the pavement where no dust or debris can cause seating errors in the data. The application of seating load is important for structural testing, as without a sitting load, the load plate cannot transfer the whole load magnitude to the pavement layers. Also, the magnitude of the seating load is equally important, as asphalt concrete is a visco-elastic material; the deflection or strain applied to the pavement surface does not dissipate immediately. Finally, the initial seating load or maximum applied load is selected based on the pavement layer conditions such as layer thicknesses, pavement age, preservation treatments, pavement use, type of roadway classification, etc.

ASTM D 4694 and ASTM D4695 (*16*, *17*) are the standards for the deflection testing procedure followed during the FWD testing in the present study. The basic testing procedure measures the surface deflection around the drop location at a known distance. To measure the deflections around the load plate, 9 geophones are located at 0, 8, 12, 18, 24, 36, 48, 60, and 72-in. spacing from the center of the load plate to measure the deflections. The geophones can measure up to ±0.01 mil accuracy where the minimum resolution for deflection measurement is ±0.04 mils.

Some of the pioneering work in 1992 laid the foundation of the present pavement mechanics and nondestructive testing of pavement materials by investigating using an FWD in pavement backcalculated layer moduli when sufficient structural geometry information is available (*18–22*). One of the challenges in network-level management is the availability of good quality and reliable thickness information.

2.2.2 Deflection Basin Parameters (DBPs)

Deflection basin parameters (DBPs) can predict the structural health of different pavement layers without using layer thickness information. Different studies have shown a positive correlation between DBPs and some structural health condition parameters, such as AC tensile strength, base layer moduli, subgrade modulus of resilience, and effective structural number (*23–28*).

Among several deflection basin parameters, the Base Damage Index (BDI), Base Curvature Index (BCI), and Area Under Pavement Profile (AUPP) have been found to correlate to many of the structural condition indicators, such as layer moduli, remaining service life, effective structural number of pavement, stress-strain condition etc. (*15*, *29*). Based on the literature, it was found that BDI estimates the base layer's structural health, and the BCI estimates the structural condition of the subgrade layer. Area under pavement profile (AUPP) is the area under the deflection curve when the FWD load is applied. BDI and BCI are measured in mils, which is $1/1000^{th}$ of an inch, and AUPP is unitless as this is the proportion of two deflections. The summary of the parameters is shown in Table 2-3. Understanding the need for pavement structural condition evaluation based on the FWD testing, FHWA recommended a set of benchmarking values for the BDI and BCI. The index represents the pavement's structural health; a higher value represents deteriorating structural health. The measured deflection at any location highly depends on the load magnitude and surface temperature at the testing time. Therefore, it is required to perform load normalization (9,000 lbs is standard) and temperature correction (68ºF) on the measured deflections.

Table 2-3 Common Deflection Basin Parameters

Parameter	Equation	Layer of significance
Base Damage Index (BDI), mils	$BDI = d_{12} - d_{24}$	Base layer
Base Curvature Index (BCI), mils	$BCI = d_{24} - d_{36}$	Subgrade
Area Under Pavement Profile (AUPP)	$AUPP = \frac{(5d_0 + 2d_{12} + 2d_{24} + d_{36})}{d_0}$	Surface layer

Note: $d_0, d_{12}, d_{24}, d_{36}$ are the deflections measured at 0",12",24",36" offset from the center of the load plate for standard 9-kips equivalent impulse loading at 68°F

2.3 Neural Network (NN) Basics and Development

Pavements are composite layered structures where each layer is significantly different from the point of material strength, stiffness, resistance to deformation, temperature susceptibility, time dependency and many other materials properties. The pavement structure is exposed to open weather and subjected to the abrasive behavior of tires and natural forces. This is why the response of the same pavement structure can vary in different climates and traffic conditions. Performance prediction using conventional methodologies doesn't help achieve the desired accuracy compared to field performance. When many variables are included as contributing factors, machine learning algorithms were found useful in cases of medical science and business model applications. Thus, several attempts have been made in previous studies by pavement engineers to predict the elastic modulus of different pavement layers, cracking performance, stress-strain behavior, roughness prediction, and other functional condition parameters.

Neural network (NN) is the machine-based replication of the mechanism the human brain follows to solve complicated mathematical or logic-based problems. The human brain contains billions of complex structured cells containing dendrons and axons where a synapse connects two neurons. In the same fashion, the NN mechanism also adopts the idea of the human neurons computing the desired output by optimizing the weight of a neuron in the neural network. This is called a "network" because there are several layers of input, intermediate, and output nodes similar to synapses inside the human brain but called "perceptron" in NN methodology. The human brain is more powerful than the artificial brain when there is a problem related to guessing, pattern recognition, or restoration of images where the computing processors are much faster than a human brain to perform computational analysis. Hubel and Wiesel laid the foundation of the artificial neural network in the Journal of Physiology, published in 1959. The idea of visual pattern recognition is based on the organization of the cat's visual cortex. They discovered from the study that the cat's brain activates a specific set of neurons to recognize a specific type of light and angle the cats were exposed (*30*).

Later studies asserted the idea of activating the different areas of brain cells in response to a specific problem statement, i.e., computation, pattern recognition, prediction and forecasting, etc. The idea steered the concept of assigning different network architectures for NN for different problem-solving purposes. The building block for NN is a set of nodes for the input layer and an output layer, combined as perceptrons. Based on the complication of the network, the neural network can be basically of two types: single-layer and multilayer neural networks. In a single-layer neural network, a set of inputs are channeled to the output by engaging a generalized variation of a linear function. For a multilayer neural network, the neural network is arranged in layers. A

group of hidden layers separates the input and outputs. The layer-like architecture and the input and output node(s) are combined and addressed as a feed-forward neural network.

In recent years, convolutional neural networks (CNN) have gained much popularity for their capabilities in deep learning problems. CNNs adopt a shared-weight architecture of the convolution kernels, which slides along the input features. Due to its architecture, this CNN is also named space invariant artificial neural networks (SIANN) (*31*). However, CNN is commonly used for visual imagery-related problems, not discussed in the present study. Therefore, the discussion of the NN is limited to multilayer perceptron feedforward and backpropagation training.

2.3.1 Network Architecture

Samarasinghe (*32*) and Aggarwal (*33*) discussed the basic architecture and capabilities of the artificial neural network. The idea of neural networks, a branch of machine learning, was inspired by the architecture of the human brain. The brain can receive a different form of data, perform a conversion to prepare the data to be processed (interpolation or extrapolation), recognize patterns, understand concepts, and make predictions even from noisy inputs. The biological neurons have three significant features: (i) dendrons (receive and transmit signals), (ii) cell body (processes data), and (iii) an axon (transmits the processed signal to the next neuron).

2.3.2 Activation Function and Loss Function

The primary use of the activation function is to provide nonlinearity to the inputs and prepare the model to capture complex attributes of the input dataset. The choice of the appropriate activation function is critical for multilayer perceptron (MLP) network design and also to consider the prediction of binary class labels. Different types of nonlinear activation functions are sign,

sigmoid or hyperbolic tangent functions. The mechanism within an activation function can be explained with the following terms: pre-activation and post-activation value. The computed value before applying the activation function on a node is called the pre-activation value, and the value achieved after the application of activation functions is called the post-activation function. The impact of the differences will be explained in detail during the discussion on backpropagation (*33*).

The choice of the loss function is important to measure the model's accuracy to quantify how much the model values deviate from the training or input values. However, a few important issues to consider while choosing the loss function in a neural network are the nature of output nodes, activation function, and the type of model being learned (regression fitting classification learning or image recognition etc.) (*32*, *33*).

2.3.3 Choice of Hidden Layer, Nodes per Hidden Layer, and Nodes in the Output Layer

Based on the literature, Zhang et al. (*34*) recommended that the number of hidden layers be more than or equal to two for a better prediction model, especially in time series predictions. If the number of input variables is i,the probable number of nodes within a hidden layer can be $\frac{i}{2}, 2i \; or \; 2i + 1$. The number of nodes in the output layer is solely dependent on the problem statement and research objective (*34*). Figure 2-3 shows a generic NN Feed Forward (4-8-4-1) network architecture for regression.

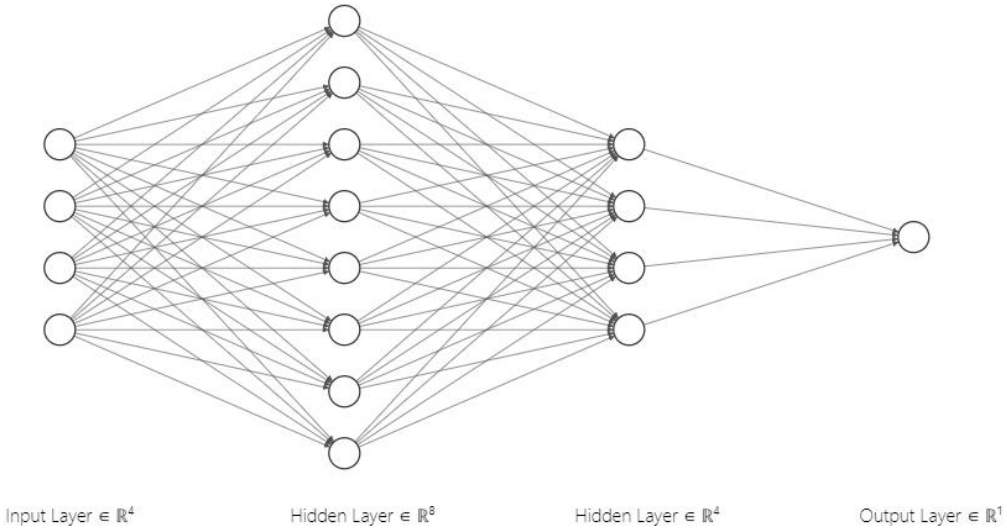

Figure 2-3: General architecture of an NN feed forward model

2.3.4 The Perceptron

The building block for neural network architecture is the perceptron which is like the brain cells, as in one dendron and one axon. Considering a computational architecture training of the form $(\overline{X}, y)$, where $\overline{X}$ is the input layer with d number of features available, such that $\overline{X} = [x_1, \dots, x_d]$, and y is the output variable as $y \in N$. During the training process, a random subset of y is fed into the module as training data which also can be identified as "observed value". A set of weights controls the output values between the input and output layers while changing values during training iterations. For d number of features, the weight be $\overline{W} = [w_1, \dots, w_d]$ to an output node. No calculation is performed on the input layer, and the calculations start from the weights and then bias (if any). The linear function for a perceptron without bias is shown in Equation 2-3.

$$\overline{W}.\overline{X} = \sum_{i=1}^{d} w_i.x_i \qquad \text{Equation 2-3}$$

For any binary classification problem solving where $y \in \{-1, +1\}$, the $sign$ function is useful for predicting the output values. Therefore, the predicted response of the model for $\hat{y}$ is shown in Equation 2-4. The sign functions are useful for the prediction of binary classification models. The equation provides both "value" and "class" solutions for the input variables.

$$\hat{y} = \text{sign}\{\overline{W} \cdot \bar{X}\} = \text{sign}\left\{\sum_{j=1}^{d} w_j x_j\right\} \qquad \text{Equation 2-4}$$

Another important feature of NN analysis is a discussion of the "bias". For example, in many problem statements, the mean of the outputs must not be 0. In that case, the bias is imposed on the model to shift the mean of the outputs. This is uncommon for classification problems but can be very common and useful for regression, prediction, and pattern recognition neural networks. The bias is incorporated into the NN architecture via $bias\ neuron$ to the output layer. The way bias works in a NN is shown in Equation 2-5.

$$\hat{y} = \text{sign}\{\overline{W} \cdot \bar{X} + b\} = \text{sign}\left\{\sum_{j=1}^{d} w_j x_j + b\right\} \qquad \text{Equation 2-5}$$

Further optimization for the equations is performed to improve the NN tool, but Equation 2-3 to Equation 2-5 is the skeleton of a basic NN network. In the next step of the analysis, further calculations are performed to achieve the accuracy and repeatability of the working model.

2.3.5 Loss Function

In the model development phase, the primary goal is to minimize the error of the prediction model. The error is expressed as $E = y_{pred} - y_{observed}$. In the early era of NN development, the correctness of the model was a controlled, heuristically motivated approach. This type of objective

minimization function is also known as the "loss function", L . A generalized loss function with a feature-label pair containing dataset $\mathcal{D}$ is shown in Equation 2-6.

$$\text{Minimize}_{\bar{W}} \; L = \sum_{(\bar{X},y)\in\mathcal{D}} (y - \hat{y})^2 = \sum_{(\bar{X},y)\in\mathcal{D}} (y - \text{sign}\,\{\bar{W} \cdot \bar{X}\})^2 \qquad \text{Equation 2-6}$$

The loss function is generally like least-square regression and a basic feature in modern NN tools. This tool aims to identify the model with the least errors and penalize for the higher degree of errors during model training. However, another challenge remains with the loss function based on the least-square form, and as the sign function is not differentiable, the loss function takes a jump on several parts, which is why a smooth approximation is required for the gradient descent. The objective function for gradient descent is shown in Equation 2-7.

$$\nabla L_{\text{smooth}} = \sum_{(\bar{X},y)\in\mathcal{D}} (y - \hat{y})\bar{X} \qquad \text{Equation 2-7}$$

It is to be noted that not all cases during the NN training exhibit a stair-case-like gradient, but in general, smoothing out this gradient is called the "perceptron criterion".

2.3.6 Backpropagation Training

Backpropagation is an application of dynamic programming consisting of forward and backward phases. The inputs are passed through the training in a cascade of computations based on the initial weights in the forward phase. After completing computations, the final outputs are compared with the inputs to estimate the errors. In the case of a single-layer feedforward network, the training is straightforward, while in the case of MLP, the process is complex as the accumulated error is the function of weights assigned in the previous layers. One of the methods of tracking the error is the derivative of the loss function with respect to the outputs. The error value is then passed

back to the layers according to the weights previously applied in the first iteration. In the backward phase, the weights are adjusted using the chain rule of the gradient of the loss function. In a real-world problem, the iteration for weight adjustment reaches up to a thousand epochs through training data (*33*).

2.3.7 Training Epochs and Training Rate

During the training of the NN, a set of small batches of data is passed through the model to train, calculate errors, and adjust the weights and bias to reduce the error indicated by reaching the convergence. One complete cycle of data feeding forward, calculating errors, and adjusting the weights and bias to reduce the error is called an "epoch". The parameter that controls how fast an epoch should complete is the "learning rate". A fast learning rate can take any number of epochs with less accuracy, but slow learning can cause longer training time with the risk of overfitting. The weight vector $\overline{W}$ can be expressed as a function of errors and training rate, as shown in Equation 2-8 and Equation 2-9.

$$E(\overline{X}) = y - \hat{y} \qquad \text{Equation 2-8}$$

$$\bar{W} \Leftarrow \bar{W} + \alpha(y - \hat{y})\bar{X} \qquad \text{Equation 2-9}$$

A balance between the training rate and the number of epochs is the key to achieving an accurate model and the least training time. However, this depends on the type of data being used to train the model, the quality of the training data and the level of accuracy expected by the user (*33*).

2.3.8 Risk of Overfitting

NN is a powerful tool for learning patterns and predicting values, but there is a high probability of overfitting the data. Increasing the number of training increases the generalization capacity; simultaneously, the increase in complexity increases the chance of overfitting. Also, big training data with a simpler model with a few variables would not capture the complexities within the dataset. There should be a balance between bias and variance with the practice of training the model. Aggarwal (*33*) recommends a good rule of thumb to avoid overfitting issues: the number of training data points should be 2 to 3 times larger than the number of parameters included in the study. The author also recommends applying proper care when adopting the NN model on an instance of much available training data to avoid overfitting during training.

2.3.9 Limitations and Cautions for Neural Network Training

One major limitation of neural network training is the computational ability of the equipment. Higher graphics processing capability is required to converge the complex and large training data. Levenberg-Marquardt training for small and medium-sized networks is recommended for quick convergence. If there is access to supercomputers or higher GPU, the "trainscg" or "trainnrp" activation functions can be used for the training.

Also, the error surface for a non-linear network is more complicated than the linear network, which can be identified with the local minima along the gradient. Local minima are the point where the value is the lowest within a neighborhood of numbers or distribution. Therefore, there remains a higher probability that the network solution can be trapped inside the local minima. Therefore, several iterations must be performed to avoid missing the network solution within the local minima.

Finally, too few neurons can lead to underfitting, or too many neurons might cause overfitting of the network. Unfortunately, there is no rule of thumb on how to assign the right number of neurons, but it is recommended to run several iterations to change the network architecture and check with the testing dataset RMSE if they are still the lowest or consistent along the iterations.

2.4 Implementation of Neural Network Modeling in Pavement Engineering

The success of a pavement management system largely depends on (i) the proper identification of the present condition of the pavement, (ii) the proper assignment of life of the maintenance and rehabilitation (M&R) activities, and (iii) the assignment of the right type of M&R to maximize the service life of the pavement. This literature review discusses the three major areas of the pavement management system from the neural network perspective and how improvements can be made to the PMS by incorporating the neural network methodology.

Banan and Hjelmstad (*35*) adopted a monte carlo hierarchical adaptive random partitioning (MC-HARP) process, replicating the idea of a neural network. First, the authors predicted the pavement's present serviceability index (PSI) from the thicknesses of AC, base, subgrade, axle load, and log of the equivalent single axle load (ESALs). Then, they followed the training and validation dataset at 48% and 52% split of the main database from the AASHO Road Test. Finally, they recommended that the MC-HAPR (a replicate of a neural network) can provide better results than the AASHTO Road test equations.

One of the recent works published by Kumar et al. (*36*) compared neural network architectures and training mechanisms for predicting the pavement condition index (PCI). Three major training algorithms that can be adopted for pavement engineering machine learning

problems are Levenberg–Marquardt (LM), bayesian regularization (BR), and scaled conjugate gradient (SCG). The best training method was selected based on the mean squared error (MSE) of the testing data. It was reported that the LM model showed better prediction performance than the rest. LM algorithms showed 89% prediction accuracy, whereas BR and SCG showed 76% and 58%, respectively.

Yang et al. (*37*) experimented with the Florida Department of Transportation (FDOT) pavement condition data to predict PCR from FDOT's Cracking Index, Rutting Index and Roughness Index. For their study, the NN architecture adopted was MLP with 11 input neurons, 11~22 hidden layers, and one output neuron for flexible pavements. To compare the performance of the NN model, the authors also performed three autoregressive (AR) prediction models. Overall, results indicated that NN worked better for prediction than AR models. Also, the finding was that the prediction is more accurate for asphalt pavements. Figure 2-4 shows the goodness-of-fit for different modeling tools and pavement types. It was observed that the NN model for the flexible pavement yielded the best prediction for the training data.

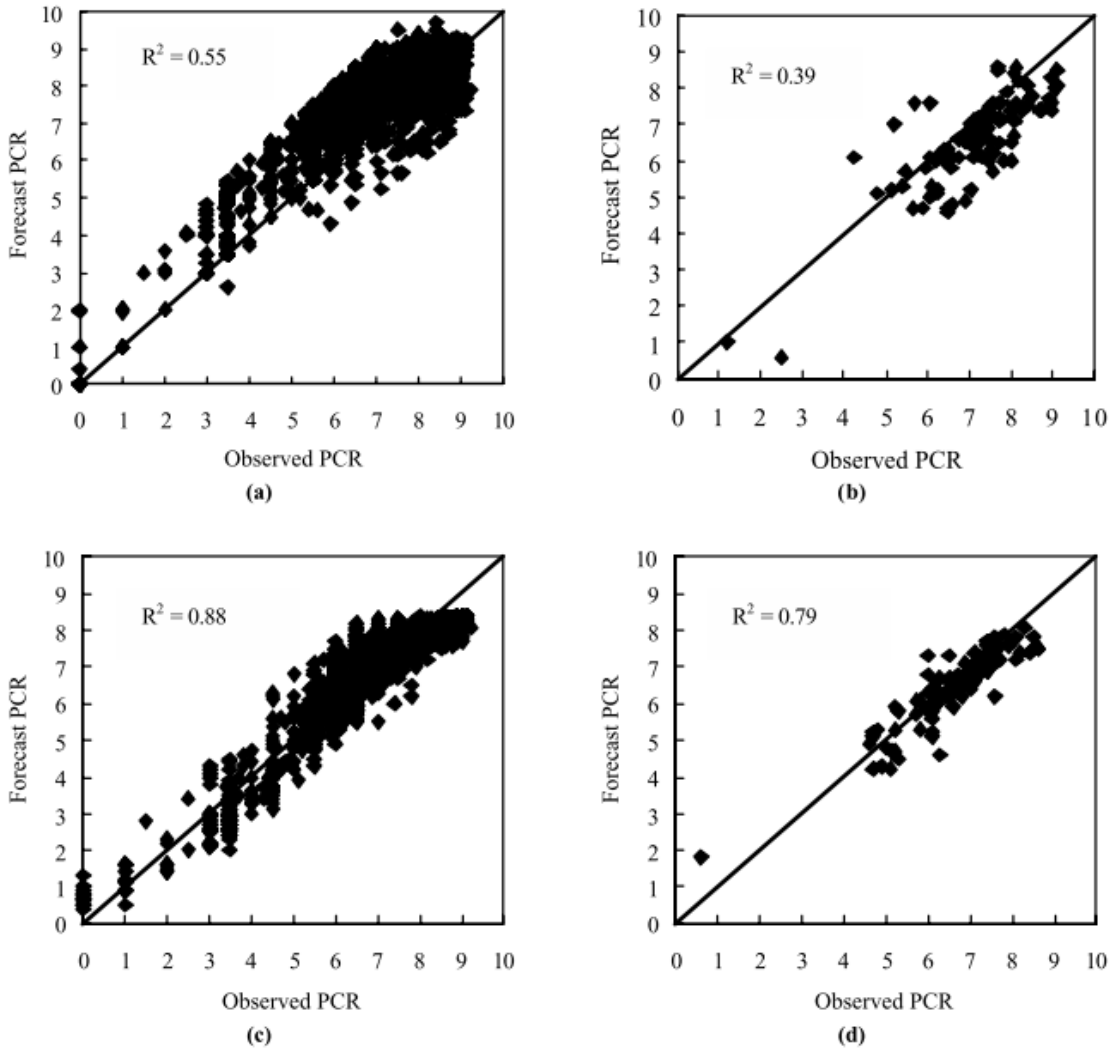

Figure 2-4 Goodness-of-fit: (a) AR model, flexible pavements; (b) AR model, rigid pavements; (c) NN model, flexible pavements; (d) NN model, rigid pavements. (Yang et al., 2003)

Terzi (*38*) measured the PSI of the pavement using data mining methodology. One of the major concerns mentioned in the study was which feature in the dataset had the greatest impact on the resultant PSI. Therefore, Terzi recommended a regression tree developed based on the data mining findings to model the PSI. Machine learning data mining and knowledge discovery and data mining (KDD) are the same methodologies that can be used interchangeably. Regression tree

(RT) splits the training data into heterogeneous sets generated by the binary splitting rule. This can be compared to small packets of neural network training to achieve the final model by adjusting weights in small increments. Overall, this data mining methodology yielded a better fit for the panel rating with an $R^2 = 0.89$.

Domitrović et al. (*39*) adopted the global performance index (GPI) to represent pavement conditions. GPI is a function of the transformed variables from IRI, rutting, mean profile depth (MPD), crack rating (CR), and surface defects (SD), which makes it equivalent to the conventional PCI or PSR. The training dataset comprises all ranges for the input variables from "very good" to "very poor". During the training process, the weightage of different input variables was collected. Also, during the training process, the proposed maintenance strategy was fed into the database to train the model to predict any need for a maintenance strategy. Based on the observation from

Table 2-4, this can be commented that rutting has the strongest influence on the GPI, and roughness (IRI) has the strongest influence on the maintenance strategy.

Table 2-4 NN Assigned Weight for Global Performance Index and Maintenance Strategy (Domitrović et al., 2018)

Adopted weights	Technical Parameter				
	IRI	Rut depth	Texture depth	Cracks	Patches
GPI	0.19	0.29	0.12	0.18	0.2
MS	0.35	0.2	0.09	0.18	0.15

Tabatabaee et al. (*40*) adopted the two-stage support vector classifier (SVC) and recurrent neural network (RNN) predictor for pavement performance prediction. This state-of-the-art tool uses the predicted information to refine the model and predict more accurately; as such, it gets

better at predicting unforeseen data. The process flow of the SVC-RNN model is shown in Figure 2-5.

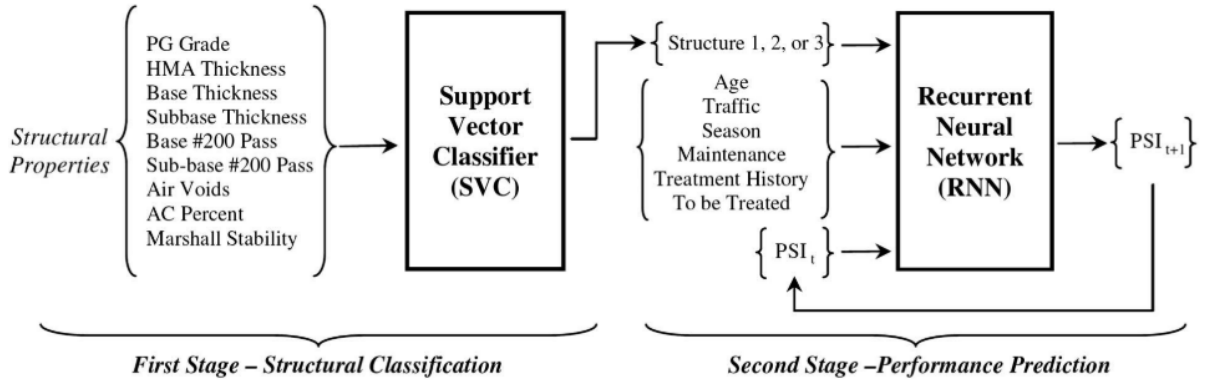

Figure 2-5 Schematic of the SVC-RNN model to predict PSI (Tabatabaee et al., 2013)

This model predicts pavement PSI at an accuracy of $R^2 > 0.95$, but the shortcoming is that the information fed into the model to predict pavement performance is not readily available for network-level PMS. Eventually, the author provided a set of coefficients of variation (COV) for different input variables. It was found that the lowest COV was assigned to Marshall stability, binder content, subbase thickness, and subbase percentage passing the 200 sieve (P200), which leads to the takeaway that the lower pavement layers significantly control pavement performance.

Eldin et al. (*41*) predicted the condition rating of controlled sections in the Oregon DOT pavement network employing a backpropagation (BP) based 17-6-1 MLP model of the neural network. The total training instances were 744 and 1,736 for the two datasets. The outcome and recommendation of the project were that neural networks could predict the condition rating even if there was a certain amount of noise in the data. Also, the rating of the prediction model was more relatable to the pavement condition than the Oregon DOT's prediction model.

Attoh-Okine (*42*) approached the pavement condition rating problem from a different standpoint while investigating the most influential features that control the rating of the pavement. The author developed an NN called a self-organizing map (SOM) to group the most influential features of the components of PCR Rating. The structure of the SOM (*43*) is shown in Figure 2-6.

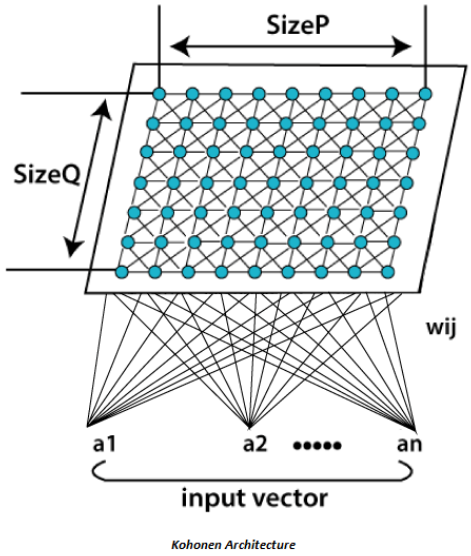

Figure 2-6 Kohonen Self-Organizing feature map (Kohonen,2023)

Using the algorithm, Attoh-Okine was able to group similar types of features in the same group and train the neural network to provide more weightage to the most influential features of the component. On a broader scope, the SOM is not classified as reinforced learning or supervised learning; rather, it is considered unsupervised learning. The major downside of this methodology is that there is no easy, straightforward way to incorporate any engineering judgment and subjective observations in the model. The methodology of neural network implementation in the PMS to assign the correct rehabilitation strategy was summarized by Abambres (*44*), as shown in Figure 2-7. Thus, most NN architectures were comprised of 1 Hidden Layer MLP, Back Propagation Training, Logistic Transfer Function, and Logistic Output Transfer function.

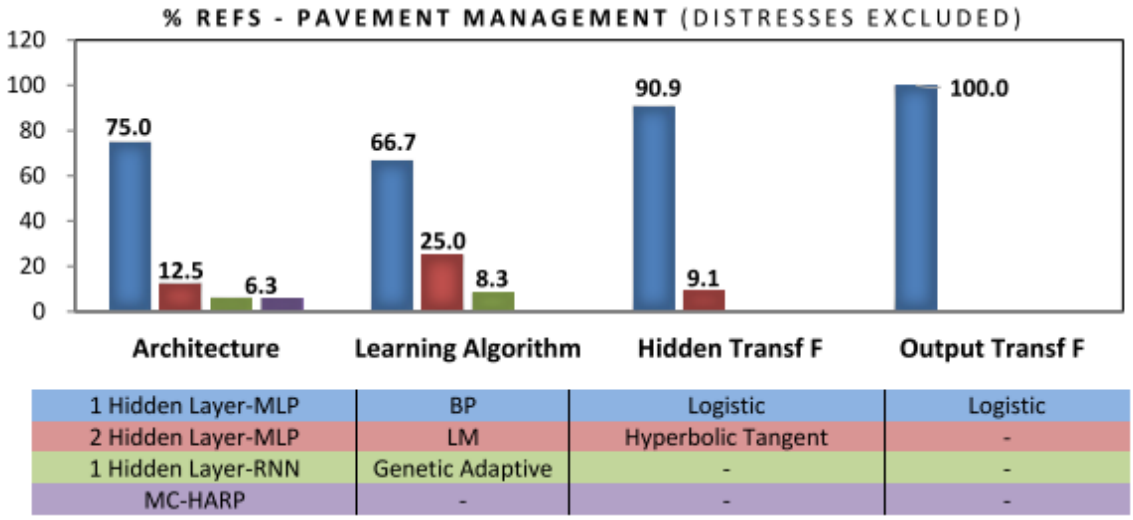

Figure 2-7 Percentage of studies discussing network architecture for different NN-based models for PMS problems (Abambres et al., 2019)

Records indicate that Kaseko et al. (*45*) have pioneered work incorporating NN in crack detection. The authors recommended a multilayer feedforward network (MLFF) to identify the classification of cracks from pavement images. The study reports that a BP-based 5-5-5 MLP was used for this task, and the model could classify the cracks with over 96% accuracy (*45*). Mei et al. (*46*) employed NN to predict crack depth using the following parameters: annual average daily traffic (AADT), percent truck traffic, pavement age, AC layer stiffness, support type, and crack opening geometry. The study also indicated a rise in complexity decision-making with the number of hidden layers and several neurons in each hidden layer. After several sessions of training data, the authors recommended an 8-10-8-1 MLFF network (*47*).

Gajewski et al. (*48*) used a hybrid of NN and finite element (FEM) models to predict crack propagation from structural information such as layer thickness and layer elastic modulus. The study also compares radial basis function (RBF) and multi-layer perceptron (MLP) networks adopted to analyze the data in the experimental setup. An MLP 4-7-2 architecture yields 97.7%

accuracy, whereas RBF 4-5-2 architecture yields 82.3% accuracy in the prediction. The individual model quality information in training, validation, and testing indicates that the MLP 4-7-2 architecture is better than RBF 4-5-2 architecture (*48*). Based on the literature studied, the percentage of area cracked over a pavement length is usually predicted by the NN model comprising a single or, at most, two hidden layers. The model architectures heavily equipped for identifying cracking from the images or convolutional YOLO v3 (a modern-day machine learning algorithm capable of identifying specific objects within an image or video and extracting target properties) algorithms are not included in the preset project literature studies. An extensive literature review by Abambres et al. (5) indicated that most of the studies adopted BP-based two-hidden layer MLP with a sigmoidal activation function, as shown in Figure 2-8.

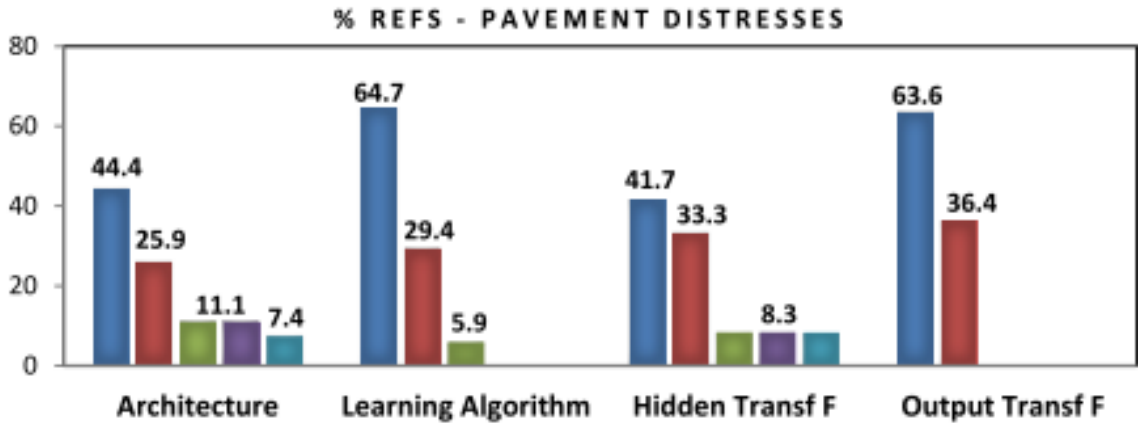

2 Hidden Layer-MLP	BP	Logistic	Linear
1 Hidden Layer-MLP	LM	Hyperbolic Tangent	Logistic
3 Hidden Layer-MLP	Self-Organized	Mexican Hat Wavelet	-
RNN, WNN, Generalized Adaptive	-	Linear	-
1 Hid. Layer-RBFNN	-	Gaussian	-

Figure 2-8 Percentage of studies discussing network architecture for different NN-based models for pavement surface distress prediction, Abambres et al. (2019)

One of the pioneering works from the perspective of pavement roughness and NN was developed by Roberts and Attoh-Okine (*49*). The paper reported several NN architectures to predict pavement roughness: mapping ANNs, recurrent ANNs, temporal ANNs, and hybrid ANNs through three major learning paths: supervised, self-organized, and reinforcement learning. In addition, the authors employed dot product learning (supervised learning with sigmoid transfer function) and quadratic function NN model (a hybrid of supervised and self-organized Learning with linear transfer function). This study recommends a 10-5-1 multi-layer perceptron (MLP) architecture for the prediction. The results indicate that supervised learning offered a correlation coefficient of 0.57 compared to 0.74 for the self-organized learning method. In the initial era of the implementation of NN in pavement performance modeling, the work was groundbreaking yet not free from some limitations: device bias, limited data points, and the presence of random noise where the effect is not yet explored (*49*).

Yildrim and Uzmay (*50*) used vehicle velocity as input to predict pavement roughness employing radial basis function neural network (RBFNN) based on 1-20-3 architecture with 80,000 numbers of training. The paper also indicated the efficiency of the radial basis Gaussian network for fast-tracking errors. Choi et al. (*51*) experimented with several hidden layer nodes (1~15) and hence proposed a backpropagation (BP)-based 6-10-1 MLP network as the most efficient in predicting IRI. The authors also performed sensitivity analyses of IRI values with the change of percentage of fines (P_{200}), binder content, percentage air voids, and pavement AC layer thickness. Finally, Yousefzadeh et al. (*52*) used the accelerometer data to model roughness on the pavement surface. The data model was then validated with the ADAMS software, allowing users to generate a synthetic database of accelerometer readings and road roughness profiles. The model

was an ANN-based feed forward (FF) network with three hidden layers with 6 nodes each. The model provided a variable correlation factor of 0.80 to 0.95 (*52*).

Solhmirzaei et al. (*53*) recommended a newer form of ANN, the wavelet neural network (WNN). The basic difference between WNN and NN is that the WNN adopts a wavelet activation function instead of the MATLAB conventional purelin, logsig or tansig functions. The wavelet function follows an expansion and contraction of the basis function to capture the local and global signals. This study adopted 12 -wavelet nodes and 2 -past inputs at a 0.01 sampling rate to predict the roughness of the road profile from the vehicle accelerometer data from the ADAMS software simulation (*53*). Ngwangwa et al. (*54*) estimated the road roughness from the vehicle dynamic (acceleration) using the autoregressive with exogenous inputs (NARX) network, which is capable of handling nonlinear models with 3-layer multilayer perceptron (MLP). The model architecture was 3-50-50-2 MLP which was trained with 3964 data points. This model can reconstruct road defects within a 20% error with a minimum correlation coefficient of 0.94 (*55*).

Ziari et al. (*56*) studied the prediction model for IRI for both long and short-term prediction employing the NN and group method of data handling (GMDH). The benefit of GMDH is that this method helps model extremely high-order regression-type polynomials leading to a single output. The data source was reported as the Long-Term Pavement Performance (LTPP) database. The NN model was set to several variations with hidden layers (1~3) and the number of neurons (3~100). The findings are impressive: the 9-80-50-30-1 network architecture provides the most accurate short-term prediction, while the 9-8-1 architecture provides the most accurate long-term prediction. The authors also recommended 9-5-1, 9-7-1, 9-20-1, and 9-50-1 architecture for the most precise prediction of IRI to a degree of correlation coefficient greater than 0.90 (*57*). Also, the study recommended a set degree of influence for predicting IRI, as shown in Figure 2-9.

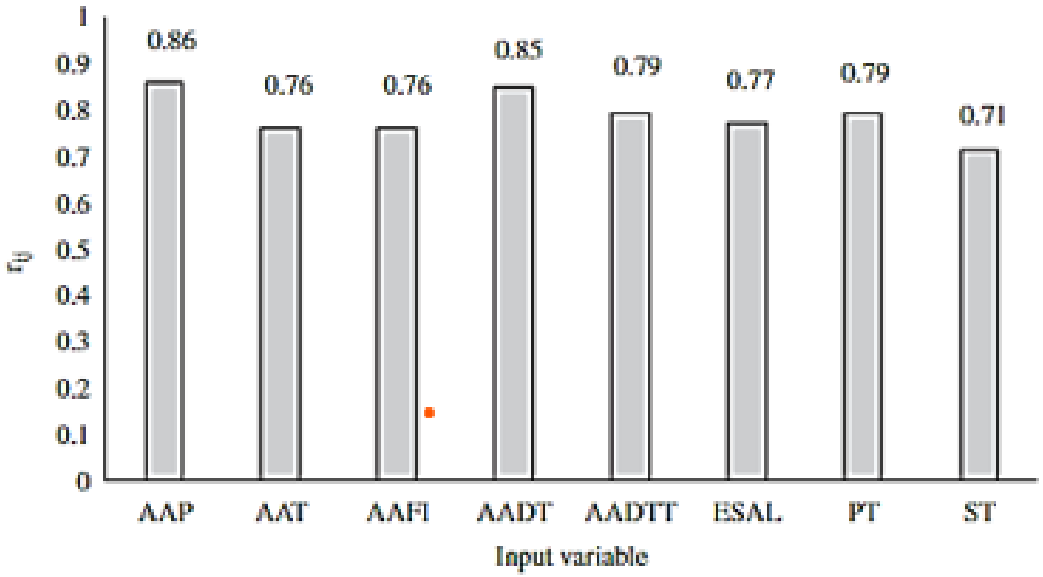

r_{ij} = degree of importance for each variables, AAP= Annual Average Precipitation, AAT = Annual Average Temperature, AAFI = Annual Average Freezing Index, AADT = Annual Average Daily Traffic, AADTT = Annual Average Daily Truck Traffic, ESAL = Equivalent Single Axle Load, PT = Pavement Thickness, ST = Surface Thickness.

Figure 2-9 Degree of importance for the effective variables in IRI prediction (Zairi et al., 2016)

Bashar et al. (*58*) compared different machine learning (ML) algorithms for predicting IRI, such as artificial neural network (ANN), Random Forest (RF), and support vector machine (SVM). The authors also studied the number of hidden layers (1~3), the number of input neurons (1~10+), and the number of neurons in each hidden layer (1~31+). The random forest (RF) reported the most effective IRI prediction at a 0.995 correlation coefficient. NN and SVM also could predict the IRI at a higher than 0.90 correlation coefficient. The author recommended the NN over RF as the level of detail needed for feeding the model may not be a possible case for most of the analysis (*58*). Abambres and Ferreira (*59*), in an extensive literature review of the use of NN in the field of pavement research, reported the widely accepted use of backpropagation (BP) algorithm with logsig transfer function by most of the researchers in the prediction of IRI (*59*).

Several studies have been performed to enrich and provide more accuracy to the nondestructive testing of pavement layers to estimate the backcalculated layer moduli from deflection, structural, and traffic data. The practice of pavement structural condition investigation using NN first started with the prediction or estimation of subgrade reaction modulus, and the research interest has moved to the AC layer moduli in recent years. As asphalt concrete is a viscoelastic material, the computational ability of the computers could not capture most of the phenomenon properly, while the subgrade modulus was comparatively less complex and easier to predict using NN algorithms at convenience. Ceylan et al. (*60*) estimated each pavement layer's stress-dependent moduli. The project's objective was to use NN to evaluate the stress-dependent moduli from the FWD data to aid the mechanistic design of pavements. A BP-based 6-60-60-2 layer architecture was chosen for training the model with 10,000 learning cycles. The backcalculation results were compared, and it was found that the computed and measured strains matched while the stresses did not. The authors explained the potential mismatch as inadequate/ inaccurate materials characterization and error in instrumentation (*60*, *61*).

Sharma et al. (*62*) developed a synthetic database to train the NN to estimate the layer moduli. The study reports a common pattern of neural network architecture consisting of 1~2 hidden layers with 7~20 hidden nodes within each hidden layer for the cases of backcalculating layer moduli. The significant takeaway from the study is that NN can be a useful tool in pavement moduli backcalculation due to reduced computation time and enhanced accuracy (*62*). Gopalakrishnan (*63*) adopted NN to estimate the backcalculated layer moduli from the heavy weight deflectometer (HWD) data from flexible airport pavements. Different NN architectures adopted to predict AC and subgrade modulus are 6-40-40-1 and 8-40-40-1, with an absolute error of 8.2% and 7.6%, respectively. The author also recommends NN-based methodology over

conventional FE-based models. The proposed method counts for the stress-dependency of the unbound granular materials and fine-grained cohesive layers in the subgrade (*63*, *64*).

Solanki et al. (*65*) compared the traditional regression method and neural network to predict the resilient modulus of the subgrade soil (M_R) in Oklahoma. Moisture content, dry density, plasticity index, percent passing the No. 200 sieve, and unconfined compressive strength are the input parameters to predict the M_R value of the 64 soil samples. RBFN and MLP methods in a side-by-side comparison, indicated better results could be achieved with the NN models (*65*). Saltan et al. (*66*) explored using the neural network to predict three target parameters, while it is quite conventional to predict one single parameter. A synthetically developed database was employed to train the model to predict the AC layer moduli, Poisson's ratio, and thickness. The author experimented with 1~3 hidden layers with 7~20 nodes in each hidden layer to find the best fitting where the best architecture was reported 7-15-3. This author also claims the capabilities of the neural network to capture complex nonlinear pavement behavior (*66*). Leiva-Villacorta et al. (*67*, *68*) performed backcalculation of the layer moduli from full-scale test sections at the NCAT Test Track using NN feedforward backpropagation with sigmoid models. The authors backcalculated the layer moduli for two conditions, full slip and full bond (*67*).

Shafabakhsh et al. (*69*) and Plati et al. (*70*) estimated the stress-strain condition of the pavement AC layer. FEM modeling is time-consuming and does not allow many controlling parameters as inputs. On the other hand, both studies used the FWD data from a known pavement structure to estimate the longitudinal strain at the bottom of the AC layer. The required inputs for materials properties are also not extensive: estimated layer thicknesses, elastic moduli, and Poisson's ratio are the common inputs for both studies discussed here (*70*, *71*).

There have been very few studies incorporating the NN methodology in predicting deflection basin parameters such as BDI, BCI or AUPP. Gopalakrishnan (*72*) also proposed the effectiveness of deflection basin parameters from the airport runway in characterizing the structural degradation of the flexible pavement. Pożarycki (*73*) used NN and deflection basin parameters to estimate the AC layer thickness when prerequisite data on the pavement structure is not reliable. The model can estimate the layer thickness of the AC layer using the following inputs: pavement surface temperature, measured deflections at several distances from the center of the load plate, and type of structure. The 5-9-1 MLP yielded the highest value for the Pearson correlation coefficient. The major drawback reported is that the model is only accurate for a known arrangement of geophones(*73*).

One study by Shrestha et al. (*74*) involved traffic speed deflectometer (TSD) measurements for the Virginia Department of Transportation (VDOT) network-level pavement management in 2014. One of the findings from the project discussed how to incorporate the TSD information into the PMS decision-making process. A total of 5,928 miles of TSD data was collected for the study between November 2013 to September 2015. VDOT uses its PMS decision matrices for groups formed based on roadway class, pavement types and cost estimate per mile for repair. Based on VDOT's core treatment categories (do nothing (DN), preventive maintenance (PM), corrective maintenance (CM), rehabilitation maintenance (RM), and reconstruction (RC)), the modification did not change the core but added a layer of validation to the structural condition of the pavement. The flow chart for incorporating structural conditions into the PMS is shown in Figure 2-10.

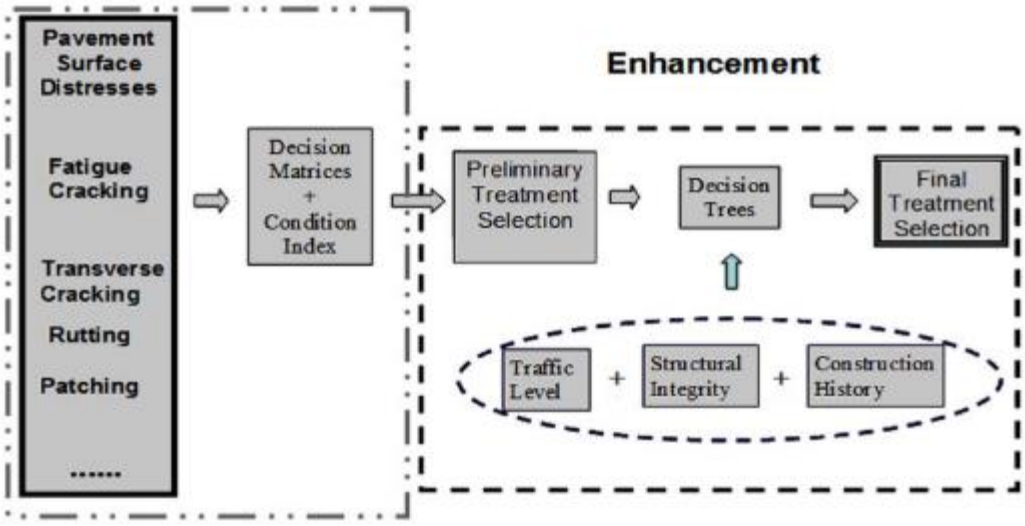

Figure 2-10 Incorporation of structural integrity in PMS decision flow (Shrestha et al. 2018)

In summary, most of the efforts in estimating the structural evaluation of the pavement have focused on assessing the elastic moduli of the individual layers when the layer thicknesses are well documented and estimated accurately. Unfortunately, no study was found that used the NN or conventional FEM to estimate the elastic moduli without the input of layer thickness. Abambres (*44*) summarized the architecture, learning algorithm, hidden layer transfer Function, and output transfer functions for pavement materials and design problems throughout the literature, as shown in Figure 2-11.

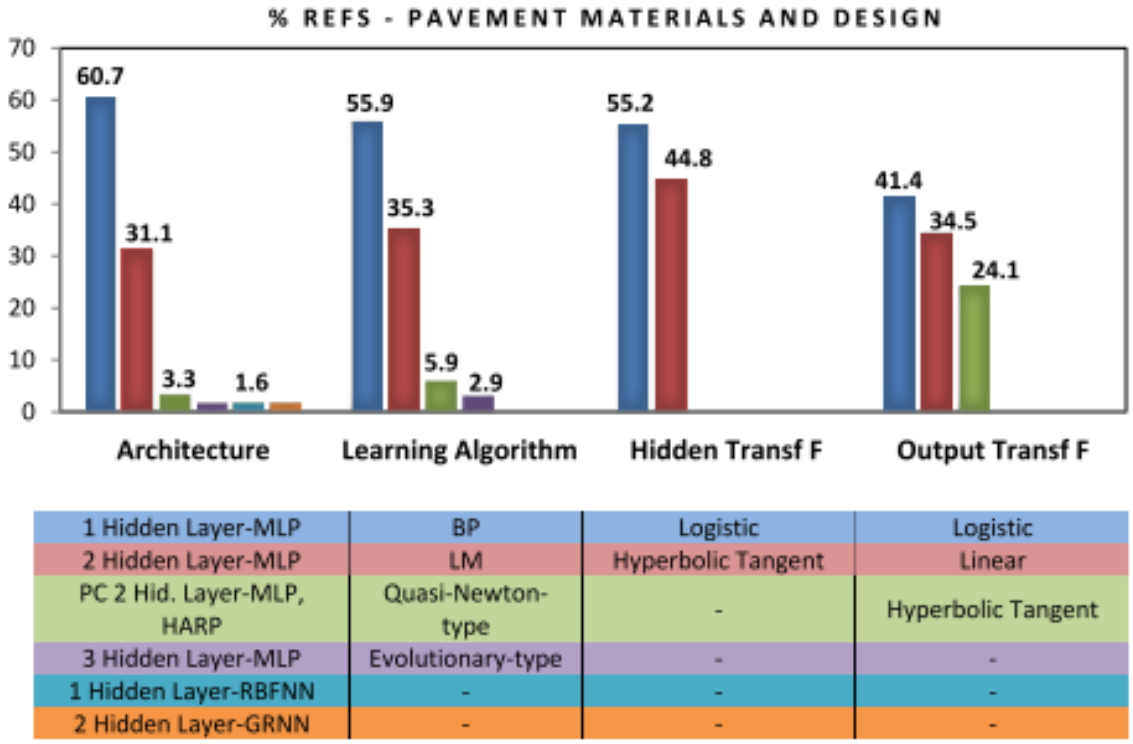

1 Hidden Layer-MLP	BP	Logistic	Logistic
2 Hidden Layer-MLP	LM	Hyperbolic Tangent	Linear
PC 2 Hid. Layer-MLP, HARP	Quasi-Newton-type	-	Hyperbolic Tangent
3 Hidden Layer-MLP	Evolutionary-type	-	-
1 Hidden Layer-RBFNN	-	-	-
2 Hidden Layer-GRNN	-	-	-

Figure 2-11 Percentage of studies discussing network architecture for different NN-based models for pavement materials and design problems, Abambres et al. (2019)

2.5 Relationship Between Functional and Structural Condition

Sollazzo et al. (*75*) used NN to correlate pavement roughness with structural performance. The authors mentioned that structural condition evaluation of the pavement throughout the whole network is expensive and time-consuming. Therefore, the agency needs to develop a method to bypass FWD or HWD testing using functional pavement condition parameters. The study employed total pavement thickness, AC layer thickness, ESALs, AADT, mean annual average temperature (MAAT), standardized temperature (numeric average of annual max and min temperature), the average number of warm days in a year (>32ºC), the average number of cold days in a year (<0ºC), time since first IRI reading was performed, initial IRI on the first

observation, and effective structural number (SNeff) calculated using the AASHTO 1993 equation from the FWD testing data as the training variable. The authors developed three models for predicting SNeff: all-weather, limited weather models (15ºC~25ºC), and no weather input models. The correlation indicates that the limited weather model provides the highest correlation (0.97). The author mentions that the models are limited to local models, and improvement can involve more performance parameters as input during training (*75*). Wang et al. (*76*) attempted to predict IRI using the fuzzy and gray model (FGM) with other functional condition parameters. The authors mentioned that FGM is more suitable for handling partially known information. The inputs were time since major construction, the total length of transverse cracks, rut depth, the total area of fatigue cracking, and length of medium to high severity longitudinal cracking for the asphalt concrete pavement sections within the study.

Finally, Vyas et al. (*77*) presented the prediction of deflection basin parameters from functional condition parameters using the BP-based NN model. The study adopted the log-sigmoid transfer function (logsig) transfer function for the feedforward backpropagation algorithm with four neural net architectures: 8-4-1, 8-8-1, 8-16-1, 8-17-1, 8-4-4-1, 8-8-8-1, 8-16-16-1, and 8-17-17-1. Input variables were AC layer thickness, base layer thickness, total pavement thickness, IRI, California bearing ratio (CBR), maximum dry density of soil, air temperature, and the measured surface temperature at the time of testing. The models predicted the surface curvature index (SCI) and BCI for the study, employing the abovementioned NN architectures and conventional MLR for comparison. Based on the MSE and R^2 values, the 8-8-1 network architecture was proposed by the authors (*78*). One of the major drawbacks of the study was that to eliminate the complication of computation, only the pavement sections which never went through any maintenance and rehabilitation activity were chosen. Thus, the model cannot predict pavement structural conditions

when the section goes through any M&R activity. Also, the study did not account for two other significant functional condition parameters (cracking and rutting).

2.6 Summary of Findings

The use of neural network modeling in the pavement engineering field has been limited mostly to modeling the functional condition of the pavement. Some studies indicate that pavement structural parameters such as layer moduli, pavement stiffness, or estimating the depth of the individual layers should be used. Regarding the health of the pavement, most of the tools developed are strictly focused on project-level investigation. Many of the required features can be extracted from lab testing results, which is difficult and expensive when the methodology is applied to network-level management. No model was found to predict pavement structural conditions without considering pavement layer thickness within the model inputs. Measuring accurate layer thickness is quite difficult for network-level management. The gaps in research on pavement structural condition assessment using the neural network include studies that address the effect of pavement preservation and length of service after the last construction or major rehabilitation activity.

Several models have predicted the critical condition index (CCI) as a measure of pavement structural health, but not all the functional condition parameters were used in the model. Many studies have shown that rougher roads with higher IRI values are positively correlated with poor structural health. However, higher roughness is not always caused by poor structural health but also by poor construction practices, inefficient temperature control of the mix, and the use of a high number of recycled materials. Therefore, IRI should not be considered the only functional condition parameter that can explain the variability in structural health beyond a certain level of

accuracy. To explain the variability in the modeling of structural condition parameters, more functional, climatic, and traffic variables need to be included in the model.

Several instances were found to model the structural condition of the pavement based on a certain set of data points within a shorter span of data collection efforts, such as over a couple of months of continued data collection in maximum instances. Within the small duration of data collection, many of the deterioration effects on the data cannot be captured and modeled. Moreover, no study in the literature collected functional and structural pavement condition data providing equal focus within the same experimental setup. In addition, the length of service life after the last treatment application is a variable that could be employed to explain many unexplained variances from the model.

Finally, in pavement management systems, the structural and functional condition of the pavement is typically not considered in the same framework or process flow. Some instances were found where the pavement structural condition testing is performed before any structural repair to determine the structural need or justify the structural rehabilitation. But in the first place, the decision of structural repair is based on a decision tree where the decision factors are based on functional condition parameters. Therefore, a need for a unified PMS model which considers both functional and structural condition parameters was identified in the literature.

3 METHODOLOGY AND SITE DESCRIPTION

In the Methodology Chapter, the data sources, data collection methods, basics of neural network (NN) architecture and modeling parameters, associated challenges with the implementation of the NN modeling, implementation of the NN modeling via MATLAB® Software, and the pavement condition rating (PCR) by Alabama DOT is discussed and supported by some evidence of the applicability of these methods to achieve the objectives of the dissertation.

3.1 Pavement Preservation Group (PG) Study

Several efforts have investigated the performance of preservation treatments based on functional conditions, acknowledging their life-extending benefits and low-cost alternatives to delay major rehabilitation or reconstruction. Understanding the research need and potential use of pavement preservation treatments in coming decades, the National Center for Asphalt Technology (NCAT) at Auburn University and the Minnesota Department of Transportation Road Research Facility (MnROAD) formed a partnership to investigate the life-extending benefits of preservation treatments under different traffic and climate conditions. The first test sections were constructed in the summer of 2012 on a low traffic volume county road (Lee Road 159) in Auburn, Alabama. These were followed by the construction of high traffic volume test sections on Highway US 280 near Opelika, Alabama, in 2015, and the construction of similar low and high traffic volume test sections in County State Aid Highway 8 (CSAH 8) and Highway US 169 near Pease, Minnesota in 2016. This experimental design provides different traffic (low and high volume) and environmental (cold and warm climate) combinations of test site conditions.

The pavement preservation treatments included in the study range from crack sealing to cold recycled bases surfaced with thin asphalt overlays. A number of treatment combinations and

multi-layer applications are among the test sections. In addition, untreated (control) sections were left in place in each of the locations and are used as a baseline for comparison. A list of treatments and their classification for this research is shown later in Section 3.2.4.

Compared to other State DOT or Long-Term Pavement Performance (LTPP) databases, the PG Study involved more controlled construction methods and more accurate measurement of pavement performance. A few of the major drawbacks of previous State DOT level research are lack of homogeneity in distress measurement methods across different studies, scarce or unavailable construction information, lack of traffic information, and finally, the scarcity of good quality data produced to undertake innovative research demanding a high amount of good quality data. The PG Study eliminates most of the prior drawbacks and has provided good-quality pavement performance data for over 10 years.

3.2 Data Collection and Assignment of Groups

The PG Study collected a variety of pavement functional, structural, construction, and traffic information to quantify the life-extending benefits of the pavement preservation treated sections. In this current section, the types of data collected, collection frequency, pavement structure information, assignment of treatment, and traffic classes are discussed.

3.2.1 Performance Data Collection

As a part of the continued approach to investigate the effectiveness of pavement preservation treatments on the prolonged pavement service life, the PG Study collected pavement performance data over the analysis period discussed in this dissertation. The types of performance data collected for all the test locations are summarized in Table 3-1. A total of 99 treated sections,

along with the Control (Untreated) sections in both Alabama and Minnesota test locations, were tested routinely. In addition, trained personnel from established service providers calibrated the equipment used for testing in both locations, while the routine servicing and calibration information was properly documented. Finally, before updating performance information to the central data server, several steps of QC were performed, including but not limited to removing outliers, filling up missing data and performing basic statistical tests to ensure that the database is suitable for NN training. Also, for US 280, CSAH 8 and US 169, the preconstruction FWD data was not collected. To verify the geometrical information of the pavement structure, several cores from random locations over different test locations were collected, and thicknesses were measured. In addition, the climatic information was collected from the National Oceanic and Atmospheric Administration website for specific test locations and testing dates.

The National Center for Asphalt Technology performs the pavement structural testing of the pavement preservation test segments located on Lee Road 159 and US 280. The Dynatest 8000 device used for the structural testing in this study for the Southern Test Sections is shown in Figure 3-1. A similar type of FWD device is also used for structural testing in the northern sections located in Minnesota.

Figure 3-1 Dynatest 8000 FWD device used for the NCAT MnROAD Study

Table 3-1 Summary of the Available Climatic, Geometry and Performance data

Data Class	Data Title	Lee 159	US 280	CSAH8	US 169
Climate Zone	MAAT (ºF)	62.8	62.8	41.2	41.2
Treatment	# TreatedSection	23	34	22	20
Geometry	AC thickness	5.5	6	7	6.5
	Base Thickness	6	9	6	17
Pre-construction	Precrack	✓	✓	✓	✓
	PreIRI	✓	✓	✓	✓
	PreRut	✓	✓	✓	✓
	PreMacrotexture	✓	×	×	×
	PreFWD	✓	×	×	×
Construction	Treatment details	✓	✓	✓	✓
Postconstruction	FWD	✓	✓	✓	✓
	Crack	✓	✓	✓	✓
	IRI	✓	✓	✓	✓
	Rut	✓	✓	✓	✓
	Macrotexture	✓	×	×	×
	Moisture data	✓	×	×	×
Climate	Air Temp	✓	✓	✓	✓
	Surface Temp	✓	✓	✓	✓
	Precipitation	✓	✓	✓	✓
	Frost Condition	✓	✓	✓	✓
Traffic	Traffic ESALs	✓	✓	✓	✓
Age Since Application (months)		111	75	63	63

3.2.2 Section Information and Traffic Class Assignment

Lee Road 159 (also referred to as "LR159" or "Lee159" in this dissertation) is a two-lane, two-way county road with a dead end that gives access to the Martin Marietta Rock Quarry. Without other major traffic-generating establishment along the road segment, there is a significant amount of truck traffic (approximately 60%). In the inbound lane, the unloaded trailer trucks enter the quarry facility, and in the outbound lane, the loaded trailer trucks exit the road segment. For this reason, the outbound lane is subjected to higher equivalent single axle loads (ESALs) than the inbound lane. The data sharing agreement between the rock quarry and NCAT allowed estimating the traffic ESALs from the weight station information of inbound and outbound truck weight. Since the beginning of the study in the summer of 2012, the outbound lane in Lee Road 159 has experienced a total of 1.5 million accumulated ESALs, while in inbound lane experienced close to 100 thousand accumulated ESALs. Figure 3-2 shows the accumulated ESALs in the inbound and outbound lanes in Lee Road 159. The impact of the different traffic loading conditions also significant affects the functional and structural performance of the pavement. Figure 3-3 shows an overview of the lane condition, traffic direction, and geographic location of the Lee Road 159 study site. In the symbology, the dump trucks with no fill indicate empty trucks, and the trucks with dark fill indicate loaded trailer trucks. Multiple dump trucks on a single lane indicate higher repetition of loads or, in other words, higher ESAL application.

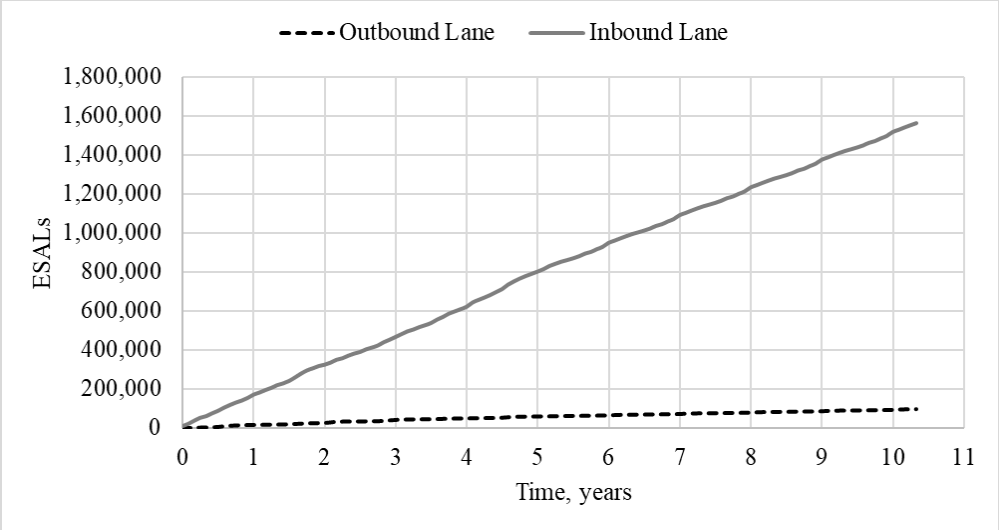

Figure 3-2 Accumulated traffic ESALs in inbound and outbound lanes on Lee Road 159

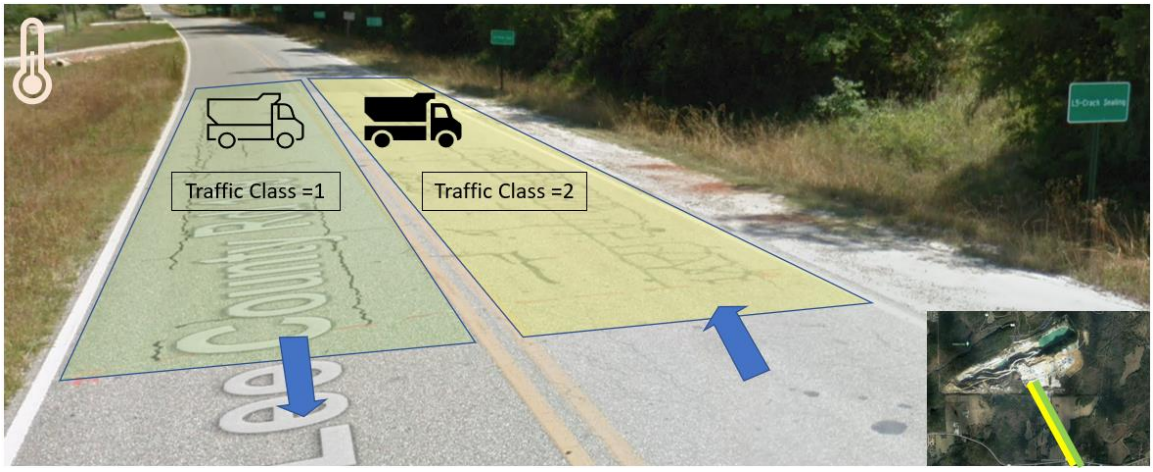

Figure 3-3 Lane configuration and traffic direction in Lee Road 159

US 280 is a four-lane divided highway, and the test sections cover a 4.5-mile segment (each section is 0.1 miles long) along the driving lane in the westbound direction near Opelika, Alabama. The accumulated ESALs since treatment application are approximately 4.5 million, representing a much higher traffic level. Figure 3-4 shows the lane condition, traffic direction, and geographic location of the US 280 test sections.

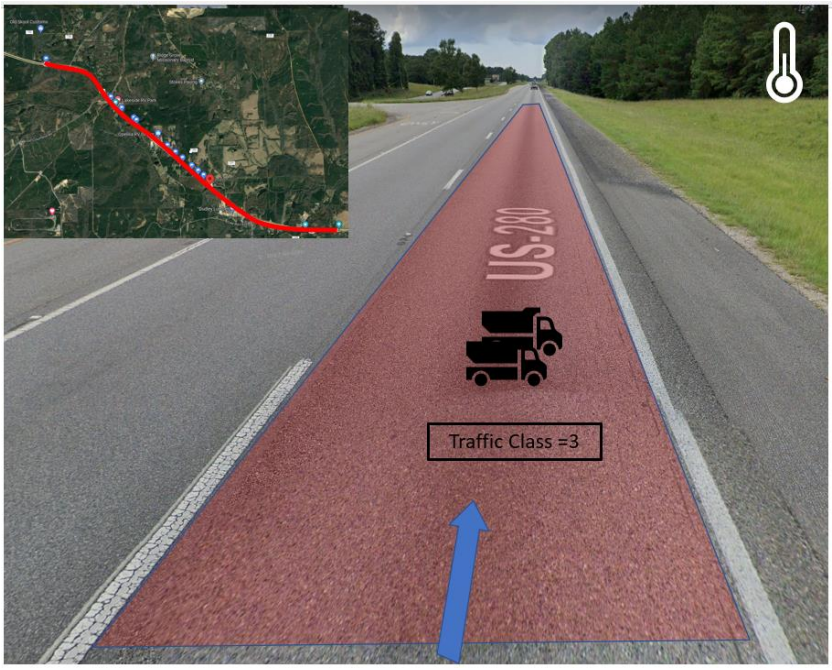

Figure 3-4 Lane configuration and traffic direction in US 280

The test locations in CSAH 8 (similar traffic as Lee Road 159) and US 169 (similar traffic as US 280) are located near Pease, MN, 60 miles north of Minneapolis, MN. CSAH 8 received treatments in both lanes of a two-lane county road while treatments were applied on the driving lane northbound on US 169, a four-lane divided highway. There is no available traffic count or ESAL information for the northern sections, but the traffic count is similar for CSAH 8 and Lee Road 159, the low traffic volume sections within the study. On the other hand, the US 169 and US 280 have been assigned to the same heavy traffic group, as assumed that the traffic count for these locations is similar. Figure 3-5 and Figure 3-6 show the lane configuration and traffic direction at CSAH 8 and US 169, respectively.

Figure 3-5 Lane configuration and traffic Direction in CSAH 8

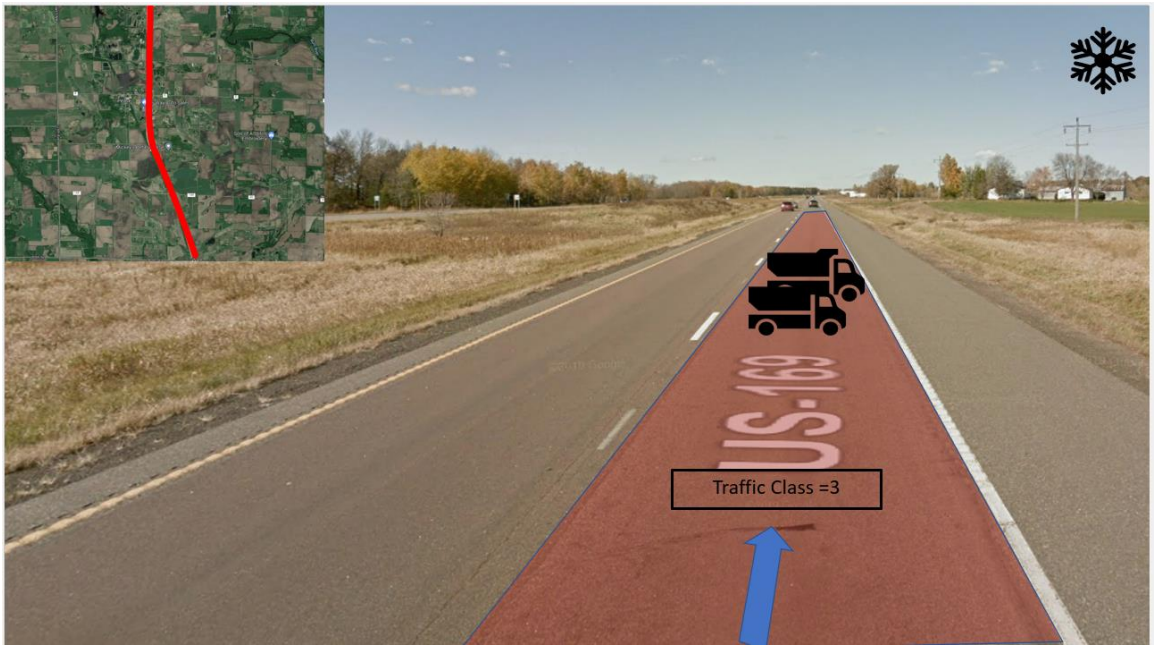

Figure 3-6 Lane configuration and traffic direction in US 169

The traffic class was assigned to identify the traffic conditions where the actual ESAL information is unavailable for the study. Therefore, rather than using ESALs as a continuous variable, the traffic class is used as a categorical variable to implement the impact of traffic in the study analysis. Moreover, the methodology explained in the next chapters targets network-level analysis. Collecting actual ESAL information is difficult compared to the proposed traffic classifications based on the pavement class and traffic volume. In this study, the lane on Lee Road 159, which carries the unloaded trucks, and both lanes on CSAH 8 are classified as "Traffic Class 1". The lane that carries the loaded truck traffic in Lee Road 159 is classified as "Traffic Class 2". All other sections under the study along US 280 and US 169 are classified as "Traffic Class 3". Table 3-2 summarizes the test locations, segment length and assigned traffic classes for the segments included within this study.

Table 3-2 Summary of Test Locations and Treatment Application

Test Site Name	Location	Lat., Long.	Total Length (mile)	Each Section Length (ft)	No Treated Sections	Traffic Class	Age of Pavement when Treated (yrs)
Lee Road 159	Auburn AL	32°32'23.0"N 85°28'29.5"W	0.5	100	22	1 & 2	14
US 280	Opelika AL	32°37'35.4"N 85°16'46.9"W	4.5	528	34	3	9
CSAH 8	Pease MN	45°41'57.6"N 93°38'27.7"W	2.5	528	22	1	11
US 169	Pease MN	45°41'57.6"N 93°38'27.7"W	2.5	528	21	3	6

3.2.3 Data Collection Period

Figure 3-7 indicates the length of data collection (months) after treatment application considered in the development of this dissertation. As shown, pavement ages range from 76 to 124 months, during which data was collected regularly.

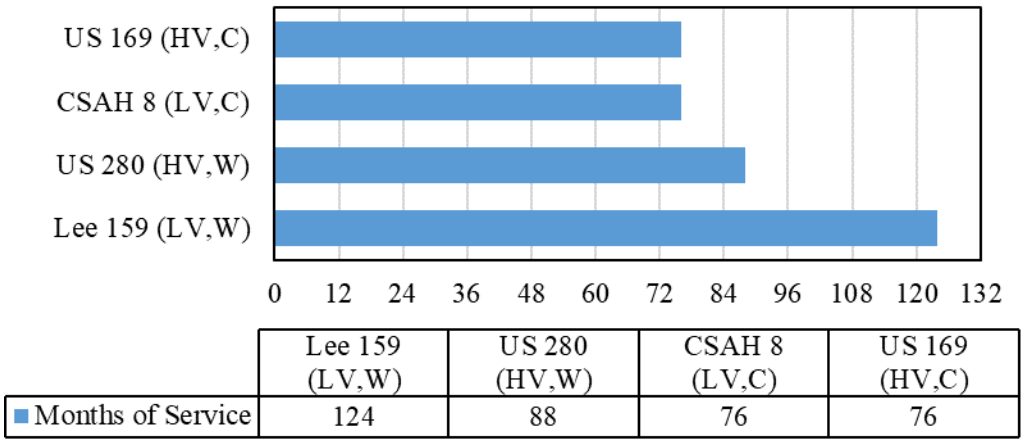

	Lee 159 (LV,W)	US 280 (HV,W)	CSAH 8 (LV,C)	US 169 (HV,C)
Months of Service	124	88	76	76

Figure 3-7 Site specific months of service (LV=Low Traffic Volume, HV= High Traffic Volume, W = Warm Weather, C= Cold Weather)

Pavement deflection data were collected monthly in Lee Road 159 from 2012 to 2018. After closely monitoring the data, it was detected that the condition was not deteriorating significantly over time, and the data collection schedule was modified to quarterly measurements. Quarterly testing was performed in the US 280 test location since treatment application due to the increased traffic control effort required to complete the measurements. The testing schedule is different in the Northern test locations where the winter and early spring months of the year remain under frigid cold with a frozen subgrade. Therefore, pavement deflection data is not collected from November to April until the subgrade is thawed. The US Department of Commerce and NOAA

reported that based on the historic data from 1981-2010, the subgrade remains frozen under 16ºF beginning mid-November to mid-March at 90% Confidence (*79*).

According to Minnesota DOT, a frozen soil profile during the winter season was collected and resembled the NOAA information (*80*). As shown in Figure 3-8, the underlying clay layer remains frozen between mid-November to mid- April. However, in the middle of February, the frost depth goes up to six feet toward the subgrade layer. Therefore, the data collection effort in the Minnesota sections is halted between these times of the year, while the data collection in the Alabama section in not interrupted.

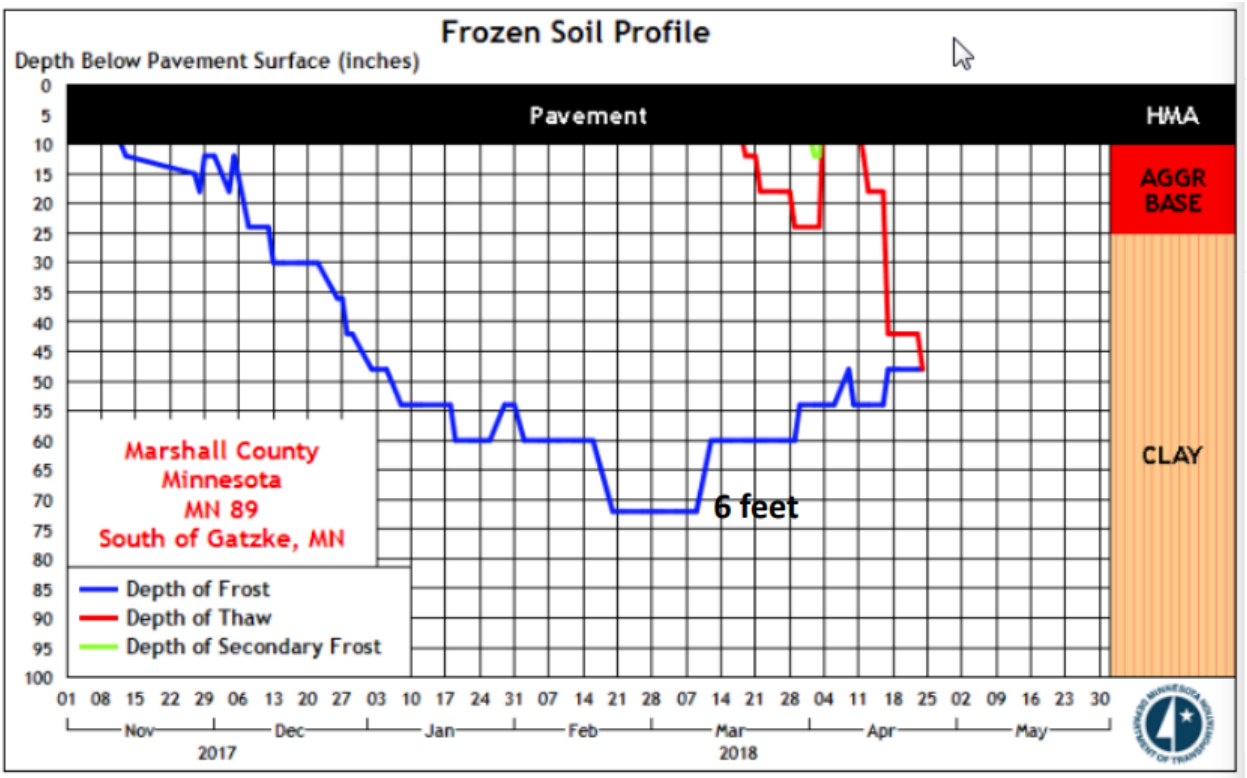

Figure 3-8 Typical soil frost profile in Minnesota pavements (Ulring, 2018)

The functional condition data collected for the PG Study are surface cracking (percent of total area), international roughness index (IRI), average rut depth, and mean texture depth. The

high-resolution cracking images were collected using a vehicle-mounted camera. The images are processed manually to map and measure the percentage of pavement surface with visible cracking. Roughness was measured using an inertial profiler following the ASTM E950 (*81*) methodology. Rutting on the wheel paths was collected from the automatic road analyzer (ARAN) van using high-speed lasers to capture surface deflections on the wheel path according to the AASHTO R48 methodology. The cracking, roughness and rutting data is collected approximately twice a month for the Lee Road 159 and US 280 test locations. As crack mapping is a time-consuming manual process, the crack mapping was performed quarterly with the same frequency as FWD. In the northern region, CSAH 8 and US 169 locations were not tested for any condition during the winter months due to low-temperature limitations for the equipment and snow covering the pavement surface.

3.2.4 Treatments Applied to the Sections under Evaluation

To meet the research needs of the PG Study, various types of preservation treatments were included: crack sealing, fog seals, chip seals, micro surfacing, thin asphalt overlays (thinlays), and cold recycled bases surfaced with thin overlays., Treatment combinations and multiple layer applications were also included. Table 3-3 through Table 3-6 show a complete list of treatments by location and their assigned treatment class. The treatment class represents the treatment feeding into a neural network. For example, the treatment class “0” means no treatment was applied, and the original surface was maintained, while treatment class “6” means the AC was removed and replaced with recycled materials (in situ or in a central plant) and then overlaid with a thin asphalt layer. The treatment class is assigned based on the following considerations: expense in construction, type of equipment needed, the time required for construction, level of complexity in construction, and added life to the pavement surface based on agency and research experience.

Table 3-3 List of Treatments Applied on the Lee Road 159 Site with Treatment Class

Section	Treatment Type	Description	Treatment Class
1	Fog seal	Rejuvenating fog seal	1
2	Chip seal	Single layer chip seal on fiber membrane (Fibermat®)	2
3	Control	Untreated	0
4	Control	Untreated	0
5	Crack seal	Crack sealing	1
6	Chip seal	Single layer chip seal	2
7	Chip seal	Single layer chip seal with crack sealing	3
8	Chip seal	Triple layer chip seal	3
9	Chip seal	Double layer chip seal	3
10	Cape seal	Micro surfacing over single layer chip seal	3
11	Micro surfacing	Single layer micro surfacing	2
12	Micro surfacing	Single layer micro surfacing with crack sealing	3
13	Micro surfacing	Double layer micro surfacing	3
14	Cape seal	Micro surfacing over Fibermat® chip seal	3
15	Cape seal	Micro surfacing over scrub seal	3
16	Scrub seal	Scrub seal	2
17	Chip seal	Single layer chip seal on fiber membrane (Fibermat®)	2
18	Thin overlay	¾” thin overlay over Fibermat® chip seal	4
19	Thin overlay	¾” thin overlay with PG 67-22	4
20	Thin overlay	¾” thin overlay over foamed recycled base	4
21	Thin overlay	¾” thin overlay with PG 76-22	4
22	Thin overlay	Ultra Thin Bonded Wearing Course (UTBWC)	4
23	Thin overlay	¾” thin overlay with 50% reclaimed asphalt pavement (RAP)	4
24	Thin overlay	¾” thin overlay with 5% recycled asphalt shingles (RAS)	4
25	Thin overlay	¾” thin overlay with high polymer-modified (HiMA) binder	4

Table 3-4 List of Treatments Applied on US 280 Location with Treatment Class

Section	Treatment Type	Description	Treatment Class
6	Thin Overlay	¾" thin overlay with PG 76-22	4
7	Micro surfacing	Double micro surfacing	3
8	Crack sealing	Crack sealing	1
9	Micro surfacing	Single layer micro surface with fibers	2
10	Micro surfacing	Single layer high polymer-modified (HiMA) micro surface	2
11	Fog Seal	Rejuvenating Fog Seal	1
12	Fog Seal	Fog Seal	1
13	Control	Untreated	0
14	Chip seal	Single layer chip seal with crack sealing	3
15	Scrub seal	Scrub seal	2
16	Chip seal	Single layer chip seal	2
17	Control	Untreated	0
18	Micro surfacing	Single layer micro surfacing	2
19	Control	Untreated	0
20	Control	Untreated	0
21	Cape seal	Micro surfacing over scrub seal	3
22	Micro surfacing	Single layer micro surfacing with crack sealing	3
23	Cape seal	Micro surfacing over single layer chip seal	3
24	Cape seal	Micro surfacing over Fibermat® chip seal	3
25	Chip seal	Single layer chip seal on fiber membrane	3
26	Chip seal	Triple layer chip seal	3
27	Chip seal	Double layer chip seal	3
28	Micro surfacing	Double layer micro surfacing	3
29	Control	Untreated	0
30	OGFC	Open Graded Friction Course	4
31	OGFC	Open Graded Friction Course	4
32	OGFC	Open Graded Friction Course	4
33	OGFC	Open Graded Friction Course	4
34	OGFC	Open Graded Friction Course	4
35	Thin overlay	¾" thin overlay over scrub seal	5
36	Thin overlay	¾" thin overlay over Fibermat® chip seal	5
37	Thin overlay	¾" thin overlay over chip seal	5
38	Thin overlay	Micro surface over ¾" thin overlay	5
39	Thin overlay	¾" asphalt binder replacement (ABR) thin overlay	4
40	Cold recycling	1" thin overlay over foamed cold central plant recycled (CCPR) base	6
41	Cold recycling	1" thin overlay over emulsion cold central plant recycled (CCPR) base	6
43	Cold recycling	1" thin overlay over emulsion cold in-place recycled (CIR) base	6
44	Cold recycling	1" thin overlay over foamed cold in-place recycled (CIR) base	6
45	Thin overlay	Ultra Thin Bonded Wearing Course (UTBWC)	4
46	Control	Untreated	0

Table 3-5 List of Treatments Applied on CSAH 8 Location with Treatment Class

Section	Treatment Type	Description	Treatment Class
1	Crack seal	Crack sealing	1
2	Chip seal	Single layer chip seal with crack sealing	3
3	Chip seal	Single layer chip seal	2
4	Cape seal	Micro surfacing over single layer chip seal	3
5	Chip seal	Double layer chip seal	3
6	Chip seal	Triple layer chip seal	3
7	Chip seal	Single layer chip seal on fiber membrane	2
8	Cape seal	Micro surfacing over Fibermat® chip seal	3
9	Micro surfacing	Single layer micro surfacing	3
10	Scrub seal	Scrub seal	2
11	Micro surfacing	Single layer micro surfacing with crack sealing	3
12	Micro surfacing	Single layer micro surfacing	2
13	Micro surfacing	Double layer micro surfacing	3
14	Fog seal	Fog Seal	1
15	Fog seal	Rejuvenating Fog Seal	1
16	Thin overlay	¾” thin overlay over Fibermat® chip seal	4
17	Thin overlay	¾” thin overlay over scrub seal	5
18	Thin overlay	¾” thin overlay over chip seal	5
19-22	Control	Untreated	0
23	Thin overlay	¾” virgin thin overlay	4
24	Thin overlay	¾” asphalt binder replacement (ABR) thin overlay	4
25-27	Control	Untreated	0
28	Thin overlay	Ultra Thin Bonded Wearing Course (UTBWC)	4
29	Thin overlay	¾” asphalt binder replacement (ABR) thin overlay with rejuvenator	4
30	Control	Untreated	0

Table 3-6 List of Treatments Applied on US 169 Location with Treatment Class

Section	Treatment Type	Description	Treatment Class
0	Control	Untreated	0
1	Crack seal	Crack sealing	1
2	Chip seal	Single layer chip seal with crack sealing	3
3	Chip seal	Single layer chip seal	2
4	Chip seal	Double layer chip seal	3
5	Chip seal	Single layer chip seal	3
6	Cape seal	Micro surfacing on top of chip seal	3
7	Micro surfacing	Micro surfacing on top of overband technique crack seal	3
8	Micro surfacing	Micro surfacing with Fibers	2
9	Micro surfacing	Double layer micro surfacing	3
10	Chip seal	Single layer chip seal on fiber membrane	2
11	Cape seal	Micro surfacing over Fibermat® chip seal	3
12	Cape seal	Micro surfacing over scrub seal	3
13	Scrub seal	Scrub seal	2
14-16	Control	Untreated	0
17	Fog seal	Rejuvenating Fog Seal	1
18	Control	Untreated	0
19	Fog seal	Fog Seal	1
20	Control	Untreated	0
21	Control	Untreated	0
22	Thin overlay	¾” asphalt binder replacement (ABR) thin overlay with rejuvenator	4
23	Thin overlay	¾” virgin thin overlay	4
24	Thin overlay	Ultra Thin Bonded Wearing Course (UTBWC)	4
25	Thin overlay	¾” thin overlay with high polymer-modified (HiMA) binder	4
26	Thin overlay	¾” asphalt binder replacement (ABR) thin overlay	4
27	Thin overlay	¾” thin overlay over Fibermat® chip seal	5
28	Control	Untreated	0

3.3 Data Cleaning and Training Setup

After completing the database development from all the field performance data, the following steps were performed: duplicate removal, fixing blank cells, filtering outliers, detecting missing entries and performing basic statistics with the data. An example of data cleaning for the pavement and air temperature can be mentioned. The pavement and air temperature during FWD

testing should be in proximity. Exceptionally different observation, as the surface temperature is 87ºF and air temperature 32ºF, is unacceptable. Therefore, the observations with these types of anomalies were checked to see if those were just an instance or a series of occurrences. The average from the previous and next observations was applied with a 10% controlled random noise to allow the data continuity for a missing observation. The final step of the checklist for data QC was performed by basic statistical tests and outlier detection. On the present dataset, around 10% of data was found erroneous in any of the five steps and was removed from the analysis.

The total dataset was split randomly for NN training at 70%, 15% and 15% ratios for training, testing and validation dataset. The training algorithms tested for training in the initial phase of the study were Levenberg-Marquardt (LM) backpropagation and Bayesian Regularization (BR) algorithm. Though training accuracy for both algorithms was acceptable, the training time for the BR algorithm was significantly higher than LM. Also, the literature recommends the LM algorithm for prediction or curve fitting problems of NN, compared to BR algorithms which show better performance in image recognition problems (*82*).

3.4 Training tool (MATLAB® 2021b)

MATLAB® is a computation and programming tool used to compute, model, and solve mathematical and logical problems. For the present study, the MATLAB® Neural Network training tool "2021b" was used for training and prediction of the structural condition of the pavement based on the functional condition parameters, traffic class, treatment class, duration of service after the treatment applied, and pavement and air temperatures.

The MATLAB® Neural Network Training tool has default features that help avoid delayed training time and overfitting. Several methodologies exist to assign data to train, test and validate

datasets: index data division (divideind), random data division (dividerand), block data division (divideblock), and interleaved data division (divideint). Each mechanism has its benefits and packet size; the random data division " dividerand" was employed in the present study. The input data is cycled through the training, validation, and testing database at a desired proportion for this training.

The general workflow for Multilayer Shallow Neural Networks and Backpropagation Training and Modeling followed seven basic steps:

1. Collect Data: Once the database was developed and cleared for QC after removing outliers and missing data, there were more than 200,000 records of FWD data along with the eleven input variables.
2. Create the network structure: The next important step of NN training is selecting the number of neurons in each layer and scoping the number of layers to be run for trial iterations. For example, the first hidden layer consisted of eleven input neurons, and then the number of nodes in each layer was iterated based on two criteria: the number of nodes must be a multiplier of 12 increments, and the number of nodes in the first hidden layer must be higher than the second hidden layer.
3. Configure the network: Iterations were made based on the activation function in each layer. The initial choices of activation functions were: sigmoid, logsig, hyperbolic tangent and purlin. Next, the training algorithms were iterated between the LM and BR algorithms.
4. Initialize the weight and bias: In the first round of feedforward training, the MATLAB default weight and bias were set. Next, the weights and biases were adjusted through the gradient descent method, and the error value at each iteration was fed in the backward direction to adjust the weight and bias to minimize the errors.

5. Train the network: There was no fixed number of iterations that were limited to stop training to prevent overfitting. Rather the slope of the loss function was used to determine the end of the training. The NN training records the weight and bias after each iteration until the loss function curve slope starts going upwards, in other words, the slope becomes positive. In the present study, the code was designed to allow up to three positive slopes after the inflection point.
6. Validate the network: The validation phase is the most important phase of NN training. In this phase, the validation dataset (ranging from 5% to 20%) of the training data is kept separate and fed to the trained model to determine if overfitting occurred. There is no cut-off value for the RMSE or coefficient of determination of the validation dataset, but a good rule of thumb is that a well-trained model validation dataset should show the same accuracy after the training dataset.
7. Use the network: Finally, the model with the same architecture and training algorithm was trained 10 times and saved as MATLAB (.m) files for further use.

Figure 3-9 shows the user interface and training windows for the Multilayer Shallow Neural Networks and Backpropagation Training.

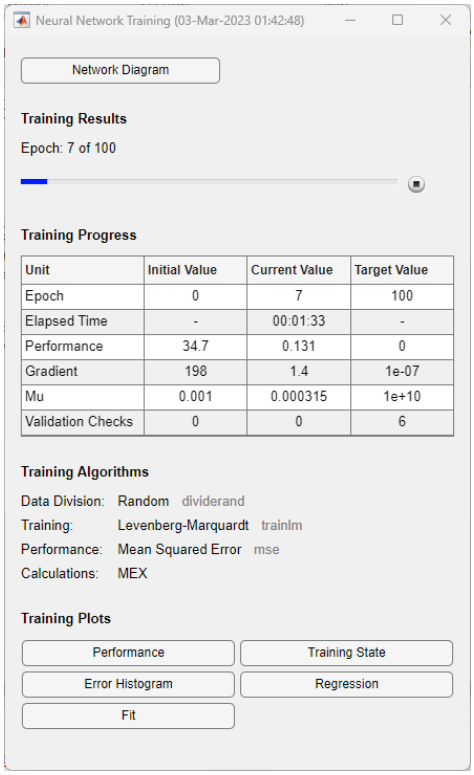

(a)

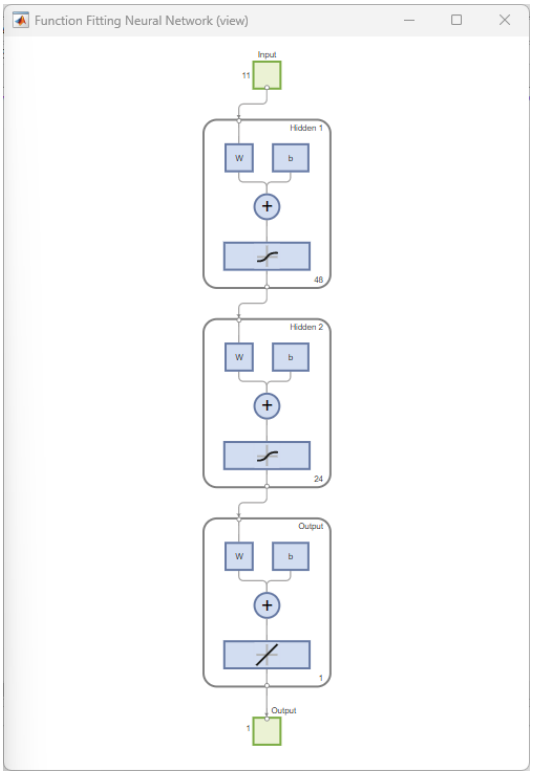

(b)

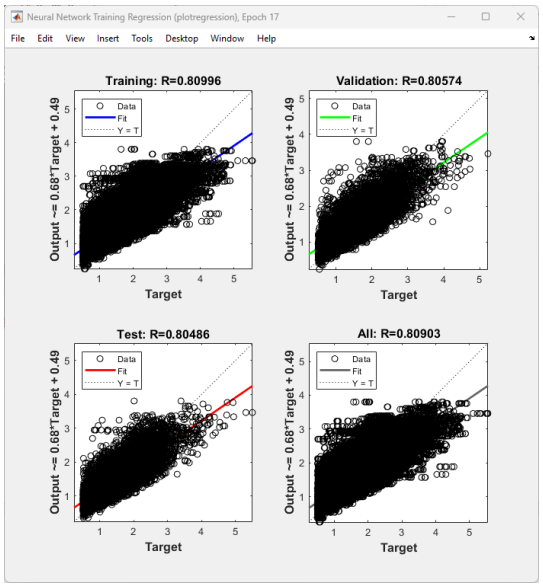

(c)

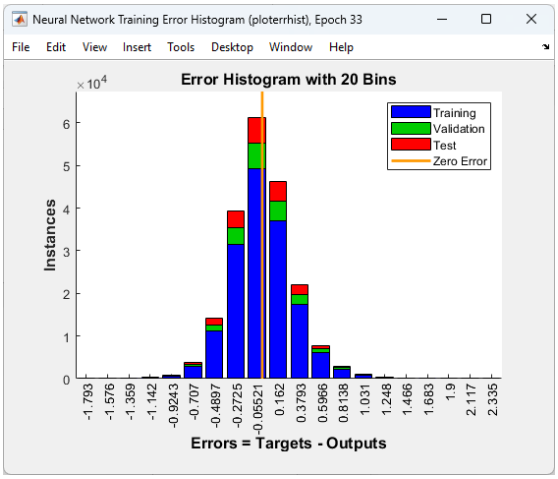

(d)

Figure 3-9 MATLAB® GUI for (a) training GUI, (b) network diagram, (c) regression fit and (d) error histogram

3.5 Pavement Condition Rating (PCR)

The present study adopted the Pavement Condition Rating (PCR) as a way to incorporate functional conditions in the decision-making process, along with structural information. The PCR is a metric developed by the Alabama Department of Transportation (ALDOT) which measures the pavement functional condition based on age, percent of area cracked, roughness, and rutting (*8*). The individual distresses are scored from "0" being "Poor," and "100" is in "good" condition based on MAP-21 criteria (*83*). The "good", "fair," and "poor" classifications for different modes of distresses are shown in Table 3-7 (*6*).

Table 3-7 Distresses classification based on MAP-21 Criteria (WSDOT, 2019)

	Asphalt	Concrete	Good	Fair	Poor
International Roughness Index (IRI) (inches/mile)	✓	✓	< 95	95 - 170	> 170
Cracking (%)	✓	✓	< 5	CRCP: 5 - 10 Jointed: 5-15 Asphalt: 5-20	> 10 > 15 > 20
Rutting (inches)	✓		< 0.20	0.20 - 0.40	> 0.40
Faulting (inches)		✓	< 0.10	0.10 - 0.15	> 0.15
Present Serviceability Rating (PSR^2) (0.0-5.0 value)	✓	✓	<4.0	2.0-4.0	<2.0

For example, if a pavement has less than 5% cracking, the pavement cracking score is assigned 100. On the other hand, a pavement section with more than 20% of the area cracked is assigned a cracking score of 0. The middle range between 5% and 20% cracking is linearly interpolated. The same method was applied for age, IRI, and rutting. To incorporate the "priority" of being selected for a year, the "Age Index" is included in the PCR Calculation. A pavement section that did not receive any maintenance or rehabilitation for more than 16 years receives an

age score of 0, and any newly treated pavement receives an aging index of 100. The equations for calculating the distress indices are shown in Equation 3-1 through Equation 3-12.

$$Index_{age} = 100 \quad \text{age} \leq 0 \text{ years} \quad \text{Equation 3-1}$$

$$Index_{age} = \frac{16 - \text{age}}{16 - 0} \times 100 \quad 0 < \text{age} \leq 16 \text{ years} \quad \text{Equation 3-2}$$

$$Index_{age} = 0 \quad \text{age} > 16 \text{ years} \quad \text{Equation 3-3}$$

$$Index_{cracking} = 100 \quad \%\, Cracking \leq 5\% \quad \text{Equation 3-4}$$

$$Index_{cracking} = \frac{20 - (\%\ \text{Cracking})}{20 - 5} \times 100 \quad 5\% < \%\, Cracking \leq 20\% \quad \text{Equation 3-5}$$

$$Index_{cracking} = 0 \quad \%\, Cracking > 20\% \quad \text{Equation 3-6}$$

$$Index_{rutting} = 100 \quad Rut \leq 0.20\ in \quad \text{Equation 3-7}$$

$$Index_{rutting} = \frac{0.40 - RUT}{0.40 - 0.20} \times 100 \quad 0.20\ in < Rut \leq 0.40\ in \quad \text{Equation 3-8}$$

$$Index_{rutting} = 0 \quad Rut > 0.40\ in \quad \text{Equation 3-9}$$

$$Index_{IRI} = 100 \quad IRI \leq 95\ in/mile \quad \text{Equation 3-10}$$

$$Index_{IRI} = \frac{170 - IRI}{170 - 95} \times 100 \quad 50\ in/mile < IRI \leq 170\ in/mile \quad \text{Equation 3-11}$$

$$Index_{IRI} = 0 \quad IRI > 170\ in/mile \quad \text{Equation 3-12}$$

Figure 3-10 (a) through (d) shows the Distress index for the different extent of distress types based on the ALDOT-inspired PCR Rating. It is important to mention that the cracking index was modified for the present study to reflect the data collection procedure followed in the PG Study. The cracking percentage is calculated based on the entire pavement width rather than just the wheel paths.

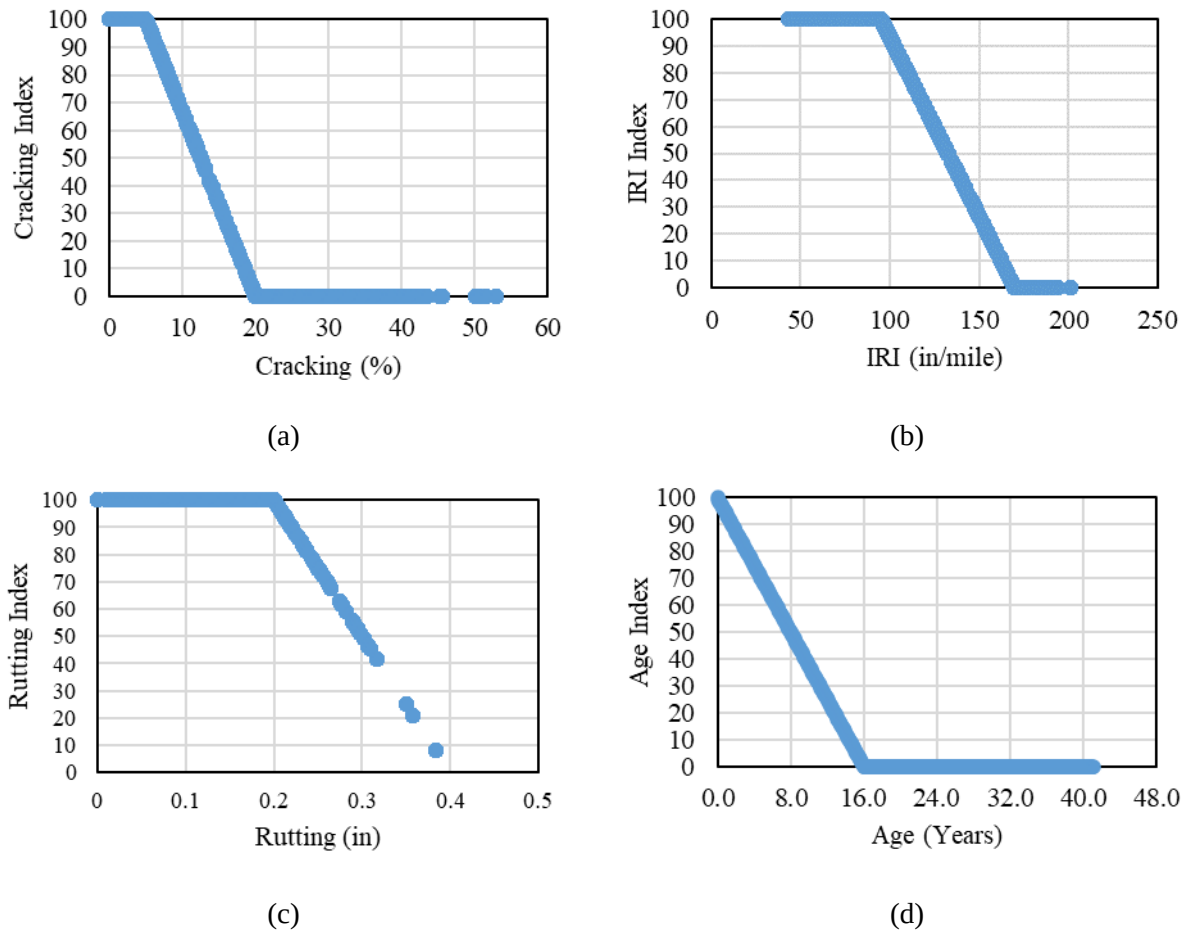

Figure 3-10 Distress Index for different distress amounts for Lee Road 159 (a) Cracking, (b) IRI, (c) Rutting, (d) Age

Once the individual distress index is calculated, the PCR is calculated as a numerical average of the four indices. Equation 3-13 shows the PCR calculation from individual distress indices.

$$PCR = \frac{(cracking\ index + IRI\ index + rutting\ index + age\ index)}{4} \qquad \text{Equation 3-13}$$

ALDOT's Transportation Asset Management Plan (TAMP) also provides the classification of the pavement condition based on the PCR value reported. This is a 3- tier system that reports only "good", "Fair," and "poor" classes (*8*). The PCR classes are shown in Table 3-8.

Table 3-8 PCR Classification Based on the ALDOT TAMP 2019

PCR Range	PCR Class
$PCR \geq 70$	Good
$55 < PCR \leq 70$	Fair
$PCR > 70$	Poor

The PCR reporting allows the management to classify the pavement functional conditions quickly and effectively. However, there is no straightforward way to indicate which distress is dominant, and there is no incorporation of the structural condition of the pavement in this condition-reporting methodology.

3.6 Summary

Pavement structures are complicated, and many features control their performance. Therefore, neural networks can be very useful tools for the problem statement in this dissertation. However, proper methods, careful data validation, and monitoring testing performance are necessary to achieve the objectives. This chapter discussed the data collection procedure, collection frequency, collected data QC and development of the NN training database, and the associated shortcomings of the study methodology. Then the MATLAB NN training parameters and parameters tuning were discussed towards developing models to predict the structural condition of preservation treated HMA pavements.

4 IMPLEMENTATION OF NEURAL NETWORKS IN PAVEMENT STRUCTURAL CONDITION PREDICTION

4.1 Prediction of Structural Condition Index from Multiple Linear Regression (MLR)

One of the most ancient and effective regression problem solutions is multiple linear regression (MLR). The two major benefits of MLR are: (i) the relative weight for each variable can be compared, and (ii) the outliers can be easily identified. On the other hand, the major disadvantage of MLR is that the model provides biased prediction based on the data used to fit the regression model. To predict the BDI and BCI values, a multiple linear regression was initially performed based on the type of treatment (slab), the surface temperature at the time of testing (Surface), air temperature at the time of testing (Air), months elapsed after treatment application (CumMonth), PreCracking (OreCrk), Pre roughness index (PreIRI), Pre Rutting (PreRut), traffic conditions (TrafficClass), current cracking (cracking), current roughness (IRI), and current rutting (rut). The analysis was conducted using the Minitab statistical software.

4.1.1 Prediction of BDI using MLR

Equation 4-1 shows the MLR equation for the prediction of BDI. The model yielded R^2 and $Adj\ R^2$ values of 24.84% and 24.83%, respectively.

$$\begin{aligned}\text{BDI} = {} & 3.1192 + 0.00394\ \text{Slab} - 0.003292\ \text{Air} - 0.000017\ \text{Surface} + 0.000199\ \text{CumMonth} \\ & + 0.020760\ \text{Cracking} + 0.002000\text{IRI} - 1.7975\ \text{Rutting} + 0.037842\ \text{PreCrk} + 0.000062\ \text{PreIRI} \\ & + 5.1964\ \text{PreRut} - 0.48953\ \text{TrafficClass}\end{aligned}$$

Equation 4-1

The Variance Inflation Factor (VIF) measures multicollinearity within the model. Higher VIF leads to a wider confidence interval and lower model predictive performance. VIF between 1 and 5 means the variables are moderately correlated, and 5 to 10 means the variables are highly correlated. As seen from Table 4-1, the VIF is higher for air temperature, surface temperature, and PreIRI. Also, the RMSE Value is 1.149, where RMSE between 0.2 and 0.5 is the acceptable range for proper prediction.

Table 4-1 MLR Model Summary of the BDI Prediction Model

Term	Coef	SE Coef	95% CI	T-Value	P-Value	VIF
Constant	3.1192	0.0223	(3.0755, 3.1629)	139.88	0.000	
Slab	0.00394	0.00194	(0.00014, 0.00775)	2.03	0.042	1.73
Air	**-0.003292**	**0.000341**	**(-0.003961, -0.002624)**	**-9.65**	**0.000**	**6.26**
Surface	**-0.000017**	**0.000258**	**(-0.000523, 0.000490)**	**-0.06**	**0.949**	**5.48**
CumMonth	0.000199	0.000150	(-0.000095, 0.000493)	1.33	0.185	1.93
Cracking	0.020760	0.000318	(0.020136, 0.021383)	65.26	0.000	2.03
IRI	0.002000	0.000144	(0.001718, 0.002282)	13.91	0.000	2.33
Rutting	-1.7975	0.0469	(-1.8894, -1.7055)	-38.32	0.000	1.41
PreCrk	0.037842	0.000469	(0.036923, 0.038761)	80.69	0.000	1.28
PreIRI	**0.000062**	**0.000181**	**(-0.000294, 0.000418)**	**0.34**	**0.732**	**2.48**
PreRut	5.1964	0.0571	(5.0846, 5.3082)	91.07	0.000	1.25
TrafficClass	-0.48953	0.00409	(-0.49755, -0.48151)	-119.66	0.000	1.34

RMSE	R-sq	Adj R-sq	PRESS	R-sq(pred)	AICc	BIC
1.14913	24.84%	24.84%	264370	24.83%	623781.47	623914.16

Figure 4-1 shows the model fit plot for the BDI Prediction MLR model. The observed BDI value ranged from 0.2 to 12 mils, and the predicted BDI values ranged from 1.75 to 6 mils. The red dotted lines along the observed and predicted BDI values indicate BDI=8 mils, which is the threshold where the BDI value changes from "good" to "fair". As the predicted model shows, no BDI value falls within the "fair" region where observations fall within the "fair" region.

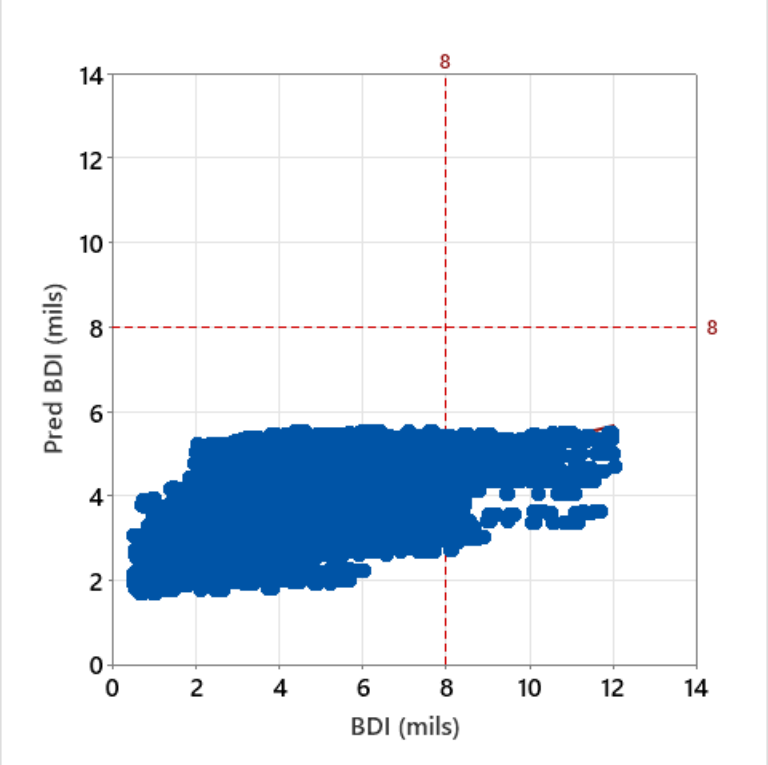

Figure 4-1 Predicted vs. observed BDI based on the MLR fitting

Figure 4-2 indicates the residual plots for the BDI prediction model. It was observed that the residual distribution is skewed to the right. Also, the residual vs. fitted values plot indicated no correlation or trend.

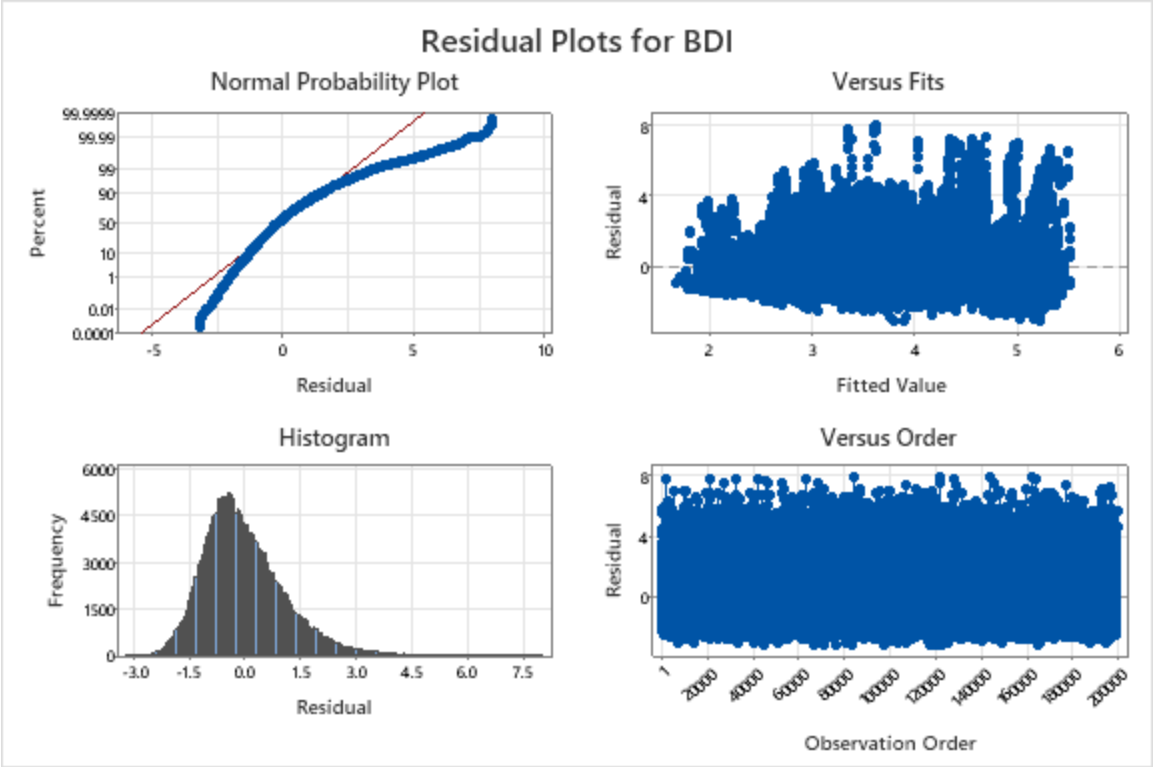

Figure 4-2 Residual plot for the BDI MLR prediction model

4.1.2 Prediction of BCI using MLR

Equation 4-2 shows the MLR equation for the prediction of BCI. The model yielded R^2 and Adj R^2 values of 34.17% and 34.16%, respectively.

$$\begin{aligned}\text{BCl} = {} & 2.80064 - 0.026757\ \text{Slab} - 0.010771\ \text{Air} - 0.003110\ \text{Surface} - 0.002137\ \text{CumMonth} \\ & + 0.005735\ \text{Cracking} - 0.001649\text{IRI} + 0.3931\ \text{Rutting} + 0.004803\ \text{PreCrk} + 0.005244\ \text{PrelRI} \\ & - 1.7005\ \text{PreRut} - 0.12961\ \text{TrafficClass}\end{aligned}$$

Equation 4-2

As seen from Table 4-2, the VIF is higher for air temperature, surface temperature and PreIRI. Also, the RMSE value is 0.462, which is within the acceptable range for proper prediction.

Table 4-2 MLR Model Summary of the BCI Prediction Model

Term	Coef	SE Coef	95% CI	T-Value	P-Value	VIF
Constant	2.80064	0.00897	(2.78306, 2.81823)	312.10	0.000	
Slab	-0.026757	0.000782	(-0.028290, -0.025225)	-34.23	0.000	1.73
Air	**-0.010771**	**0.000137**	**(-0.011040, -0.010502)**	**-78.46**	**0.000**	**6.26**
Surface	**-0.003110**	**0.000104**	**(-0.003313, -0.002906)**	**-29.93**	**0.000**	**5.48**
CumMonth	-0.002137	0.000060	(-0.002256, -0.002019)	-35.36	0.000	1.93
Cracking	0.005735	0.000128	(0.005484, 0.005986)	44.80	0.000	2.03
IRI	-0.001649	0.000058	(-0.001763, -0.001536)	-28.51	0.000	2.33
Rutting	0.3931	0.0189	(0.3561, 0.4301)	20.83	0.000	1.41
PreCrk	0.004803	0.000189	(0.004433, 0.005173)	25.45	0.000	1.28
PreIRI	**0.005244**	**0.000073**	**(0.005101, 0.005387)**	**71.81**	**0.000**	**2.48**
PreRut	-1.7005	0.0230	(-1.7455, -1.6555)	-74.06	0.000	1.25
TrafficClass	-0.12961	0.00165	(-0.13284, -0.12638)	-78.73	0.000	1.34

RMSE	R-sq	Adj R-sq	PRESS	R-sq(pred)	AICc	BIC
0.462426	34.17%	34.16%	42811.2	34.16%	259326.90	259459.58

Figure 4-3 shows the model fit plot for the BCI Prediction MLR model. The observed BDI values range from 0.5 to 5.75 mils, and the predicted BCI values range from 0.5 to 3 mils. The red dotted lines along the observed and predicted BCI values indicate BCI=4 mils, which is the

threshold where the BCI value changes from “good” to “fair”. As the predicted model shows, no BCI value falls within the “fair” region, where observations fall within the “fair” region.

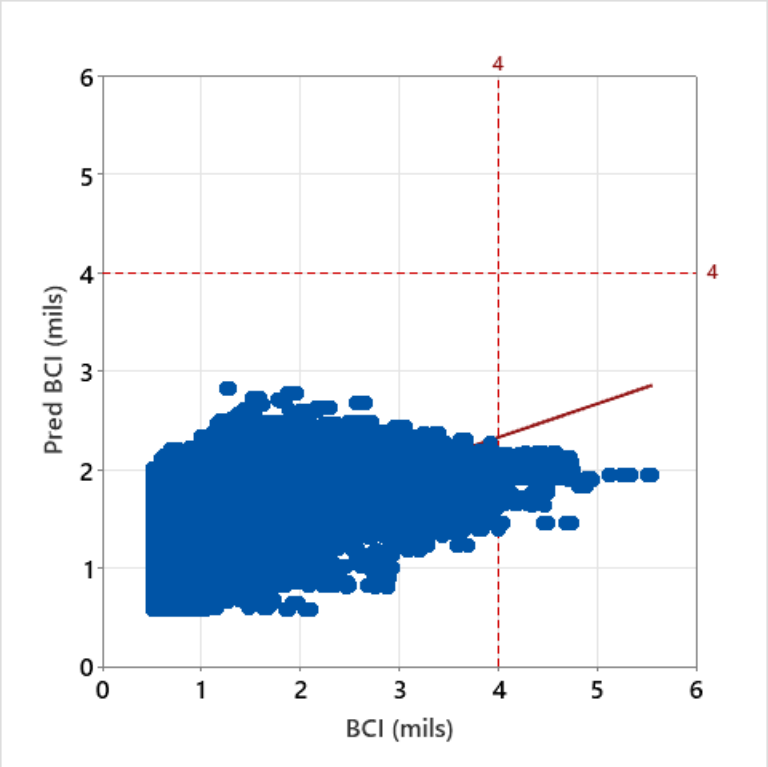

Figure 4-3 Predicted vs. observed BCI based on the MLR fitting

Figure 4-4 indicates the residual plots for the BCI prediction model. This is observed that the residual distribution is skewed to the right. Also, the residual vs. fitted values plot indicates no correlation or trend.

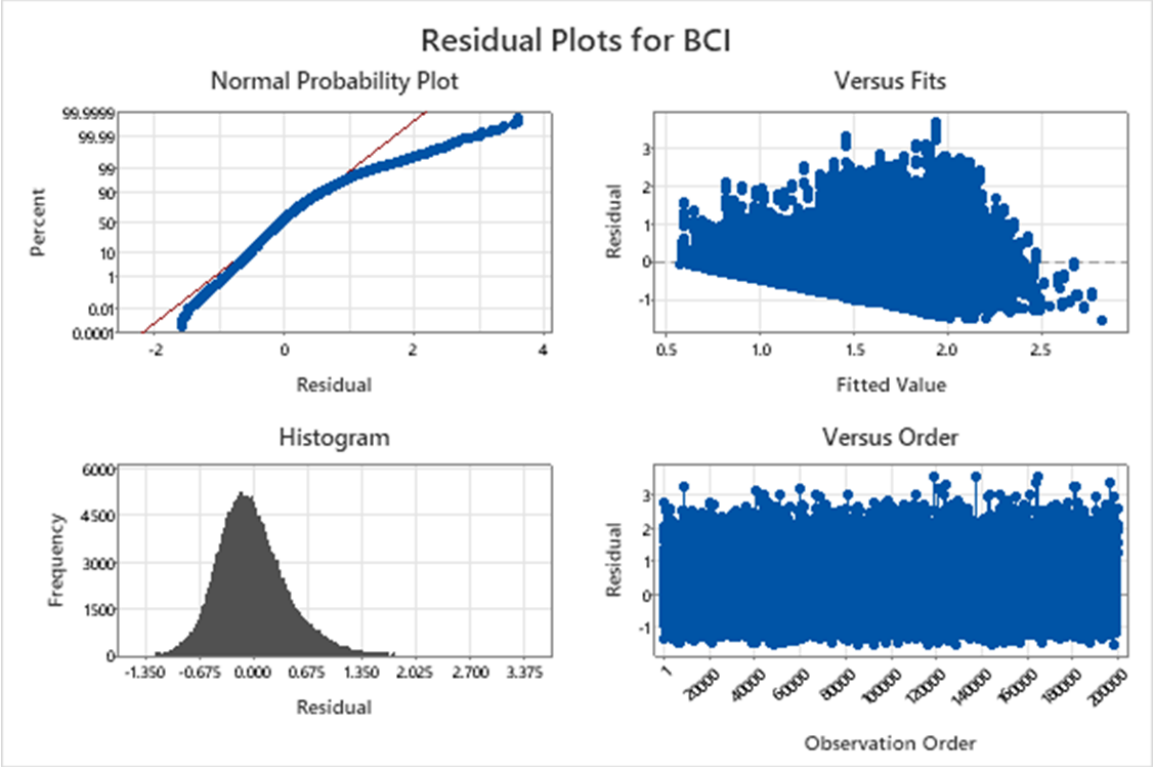

Figure 4-4 Residual plot for the BCI MLR prediction model

Based on the observations from Section 4.1.1 and Section 4.1.2, the multiple linear regression models could not produce enough accuracy in predicting the BDI and BCI values. Therefore, to capture the more complex structural behavior of the pavement, a more powerful, accurate, and repeatable model development procedure is needed.

4.2 Model Development and Effect of Features on Model Performance

In the current section, the processes of BDI and BCI prediction modeling using NN are discussed, which includes the variable selection criteria, hidden layer size assignment, size of hidden layers, choice of activation functions and prevention of overfitting. In addition, there are more processes to fit a regression model using NN to achieve more accuracy and generalization power, but for the present study, the following actions were taken to fit the NN prediction model.

4.2.1 Selection of Input Variables

For the present study, the target variables are BDI and BCI, continuous variables, and the input variables are a combination of categorical and continuous variables. The following input variables were initially chosen for the neural network:

1. Treatment Class (0~6, classification variable according to Table 3-3 through Table 3-6)
2. Air Temperature (°F, continuous variable)
3. Surface Temperature (°F, continuous variable)
4. Time of Service after application (months)
5. Precipitation (inch.)
6. Surface Cracking (percent of total area cracked)
7. IRI (inch/mile)
8. Rutting (inch)
9. Pre-Cracking (percent of total area cracked)
10. Pre-IRI (in/mile)
11. Pre-Rutting (inch)
12. AC Layer thickness (inch.)
13. Base Layer thickness (inch.)
14. Traffic Class (1~3, categorical variable according to section 3.2.2)
15. Frost Condition (1~0, binary classification, 1= Frost, 0 = No frost)

Determining feature weights using a diagonal adaptation of neighborhood component analysis (NCA) was the most efficient and reliable method (*84–88*). Using the "fsrnca" (*89*) tool in MATLAB R2022b., the feature weights were selected by implemented diagonal application of

NCA. This algorithm is widely accepted for the feature selection of continuous output variables. Moreover, the algorithm allows supervised learning using the pairwise distance between the observations to predict the responses. For the present study, there were 20 independent iterations for the whole training dataset to calculate the feature weights. Figure 4-5 shows the relative feature weights of the input variables for predicting the BDI. The higher the feature weight is, the higher the impact of the predictor variable on the predicted value. As the weights are relative, there is no cut-off or standard for choosing the variables to keep or drop from the training dataset. As there were 20 independent iterations and no user-selected assignment of training data and validation data, the algorithm prepared the random datasets consisting of 70% training data, 15% testing data, and 5% validation data at each iteration. As shown in Figure 4-5, some input variables (i.e., treatment class, air temperature at the time of testing, pre-cracking condition, and traffic class) consistently received higher weightage, while the rest showed a spread in the weightage value.

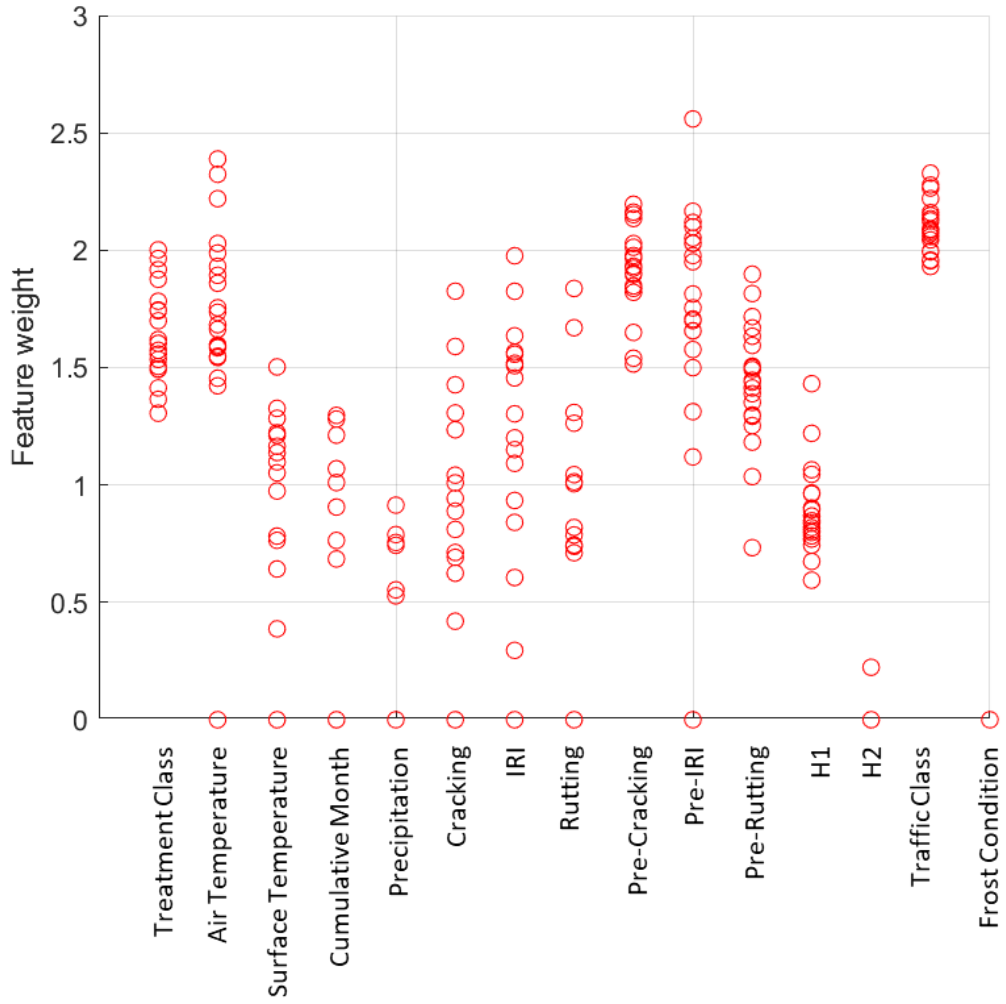

Figure 4-5 Feature weights based on feature selection using neighborhood component analysis for regression (fsrnca)

Based on the findings from the feature weight for different variables and backed up by engineering knowledge and judgment, more variables were dropped from the training dataset. The variables that were dropped are as follows:

- Precipitation: The weightage values from the fsrnca feature selection algorithm indicate a lower contribution of the feature to the model output. Moreover, in a network-level

analysis, it is quite tedious to assign the precipitation amount to the specific zone of treatment application. Therefore, the precipitation variable was dropped from the analysis.

- Asphalt concrete and base layer thickness: Accurate pavement thickness measurement is quite challenging for network-level analysis, even in project-level analyses in some cases where there is not much opportunity for drilling cores or using other tools such as ground penetrating radars (GPR). In most cases, collecting historical construction information about the lift thicknesses or depth of the base layer is much more challenging for different agencies. For this reason, the thickness information was not included in the training database.
- Frost condition: The sections in Minnesota experience a freeze/thaw cycle each year, which is responsible for damage to the top AC and underlying pavement layers. Deflections are not measured when the subgrade is frozen, and the data collection process is resumed every spring or summer. By the time the deflection testing is resumed, the subgrade is already thawed, and the frosting parameter was the least effective in the training dataset and thus removed.

After removing the variables, the fsrnca tool was rerun to measure the weightage of the variables. Then, the contribution of each variable to the prediction was calculated based on their relative weightage compared to the other variables. Figure 4-6 shows each feature's contribution percentage to the output variable.

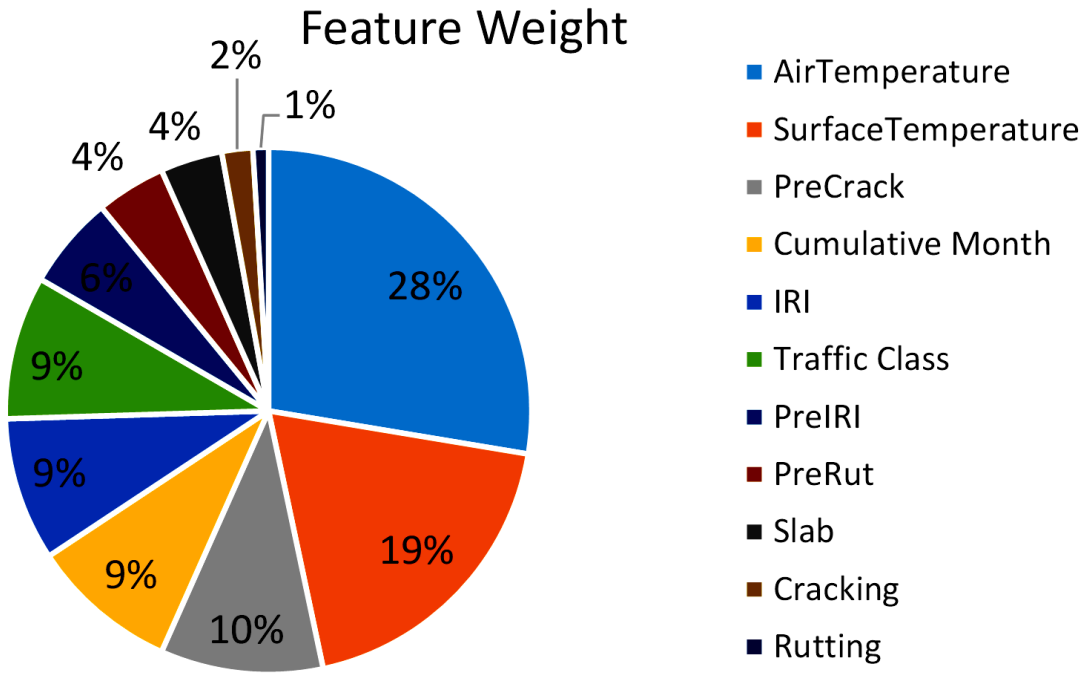

Figure 4-6 Contribution of each variable to the model output

These proportions indicate that combined air and surface temperature at a given test time contributes to up to 47% of the output variable. Pre-cracking, cumulative month (months of service after treatment), IRI, traffic class, and Pre-IRI each contribute to the model by roughly 10% individually.

4.2.2 Effect of Hidden Layer Number on the Model Performance

The NN architecture greatly depends on the number of hidden neurons and layers between input and output. For more complicated analyses such as image recognition, classification, or behavioral science, a greater number of hidden layers increases the predictability power of the trained network. On the other hand, the major downsides of occupying a larger number of layers

are higher computational power requirements, longer training time, and the need for a larger dataset with more variables. In addition, the associated risk of implementing more than two hidden layers includes but is not limited to the risk of overfitting, challenges in the reproducibility of the model, and difficulties in implementation without the use of sophisticated software tools designed for neural network modeling (*32*).

There is no fixed conclusion or rule for the number of hidden layers and shape of the hidden layers. The shape of the hidden layers is decided upon several iterations considering how complicated the model is, the number of predicting features and the number of predictor features (variables). The rule of thumb is to use 2 hidden layers maximum for a shallow neural network. Therefore, the number of hidden layers has been limited to two due to a limited number of predictor variables available and to maintain model simplicity and reproducibility. The number of hidden nodes in each layer was decided based on multiple iterations. Based on the literature, it is also recommended in many studies to change the number of neurons in a hidden layer as a multiple of the number of input variables. If the number of input variables is n, the number of nodes in a hidden layer should be between $n\ and\ 4n$ at an increment of n. Therefore, the number of hidden nodes was iterated based on the product of the number of input features in the present study.

Several iterations were performed to capture the model efficiency as trial model performances were evaluated. BDI and BCI predictor models were developed for both 2-layered and 3-layered architectures, and some of the model efficiency parameters, such as root mean square error (RMSE), mean average error (MAE), R-train, R-test, R-validation and R-overall are compared. Figure 4-7 shows the comparative model accuracy for BDI and BCI for both 3-layered and 2-layered models. Results indicated that the RMSE value for both architectures is of the same magnitude for both cases of BCI and BDI. However, the average error (AE) for all the neural

network prediction models indicated that the 3-layered models yield a lower magnitude of average error overall. Also, the R-train, R-test and R-validation values for both architecture models did not show any added benefit to the model prediction accuracy.

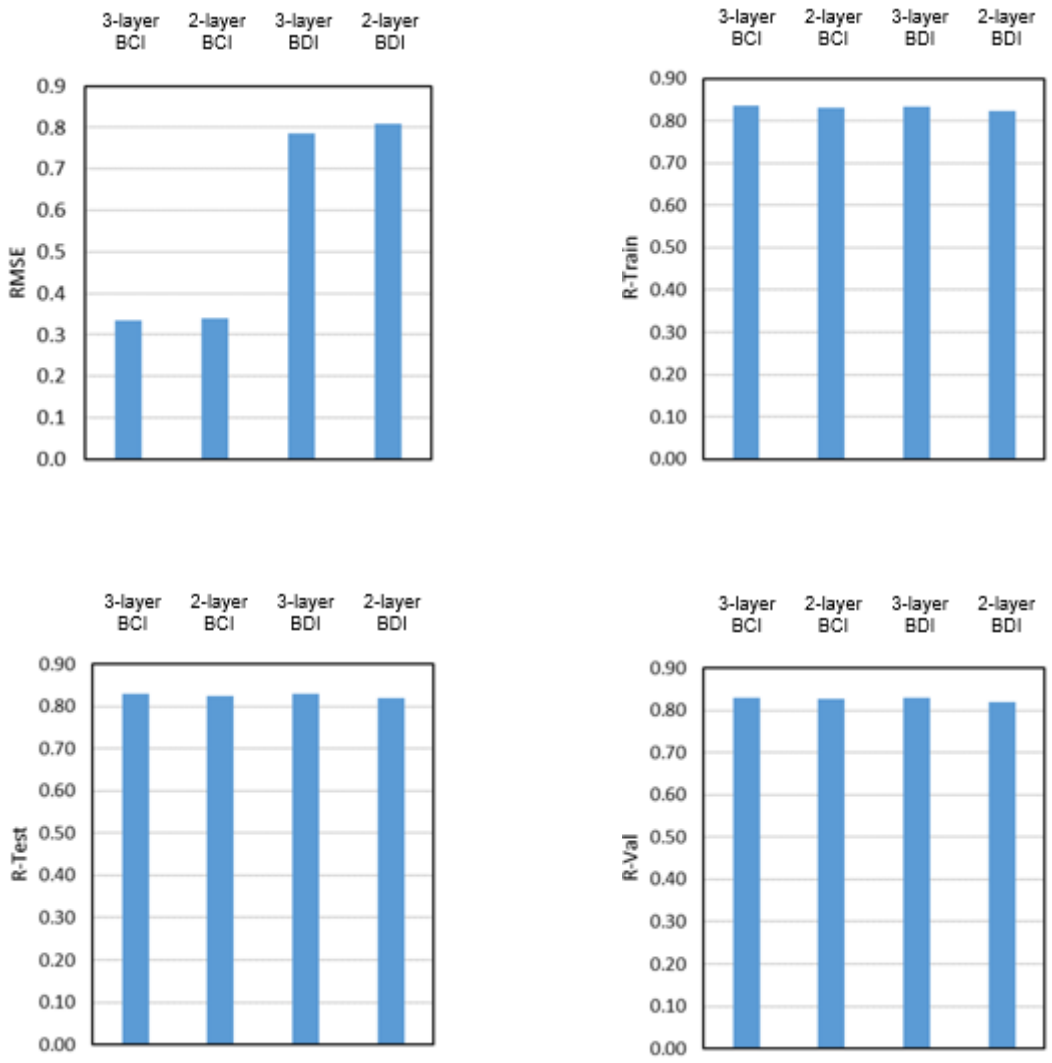

Figure 4-7 Comparison of model performance accuracy measurement parameters

Aside from the average magnitude, the model efficiency parameters were compared by t-test. P-values for one-tail and two-tail tests indicate that two-layer and three-layer model architectures do not differ significantly (p-value >0.05). Existing literature and data science practices indicate that

the RMSE and R-validation are the most acceptable and effective parameters to compare among all the testing efficiency parameters. Table 4-3 indicates that all the p-value comparing the difference of means in the accuracy parameters for different training architectures are greater than 0.05, which means the model efficiency is not statistically significant on the model performance for predicting BCI and BDI.

Table 4-3 Summary of t-Test Results for NN Architectures for BCI and BDI

Prediction	BCI				BDI			
Parameter	RMSE		R-Val		RMSE		R-Val	
Architecture	3-Layer	2-Layer	3-Layer	2-Layer	3-Layer	2-Layer	3-Layer	2-Layer
Mean	0.33	0.34	0.83	0.83	0.78	0.81	0.82	0.81
Variance	0.00	0.00	0.00	0.00	0.00	0.00	0.00	0.00
Observations	76	72	76	72	104	84	76	72
df	146		146		186		186	
t Stat	-0.97		0.66		-1.71		1.65	
P(T<=t) one-tail	0.17		0.25		0.08		0.06	
t Critical one-tail	1.66		1.66		1.66		1.66	
P(T<=t) two-tail	0.33		0.51		0.09		0.10	
t Critical two-tail	1.99		1.99		1.98		1.99	
Hypothesized Mean difference = 0; Tested for both One-tail and Two-tail								

4.2.3 Effect of Number of Nodes in Hidden Layers

During the iterations, the number of nodes in each hidden layer was incremented at 12 nodes per iteration, starting from 12 to 48 (such as $I-12-12-O, I-24-12-O, \ldots, I-48-36-O$, $where\ I = Number\ of\ Input\ Variables, O = Number\ of\ Output\ Variables$). One of the methodologies followed during the model architecture design is maintaining an equal or lower number of hidden nodes in the next layer than the previous one. Model weight (W) is the value that signifies the number of hidden nodes and connected neurons between the nodes. The higher the weight, the more the prediction capability; the higher the training time, the higher the risk of overfitting (*32*, *44*, *90*, *91*). For example, an $11-12-12-1$ model architecture has a model weight of 313, and an $11-48-36-1$ model architecture has a model weight of 2,377. The plots in Figure 4-8 show that for all the prediction model architectures, an increase in model weight increases the model's prediction accuracy by lowering the RMSE value or increasing the Adj R-sq or R-Val value. The plots indicate that for all the BCI and BDI prediction architectures, models with a weight of more than 2,000 yield Adj-R sq and R-Val roughly over 0.75 and 0.85, respectively.

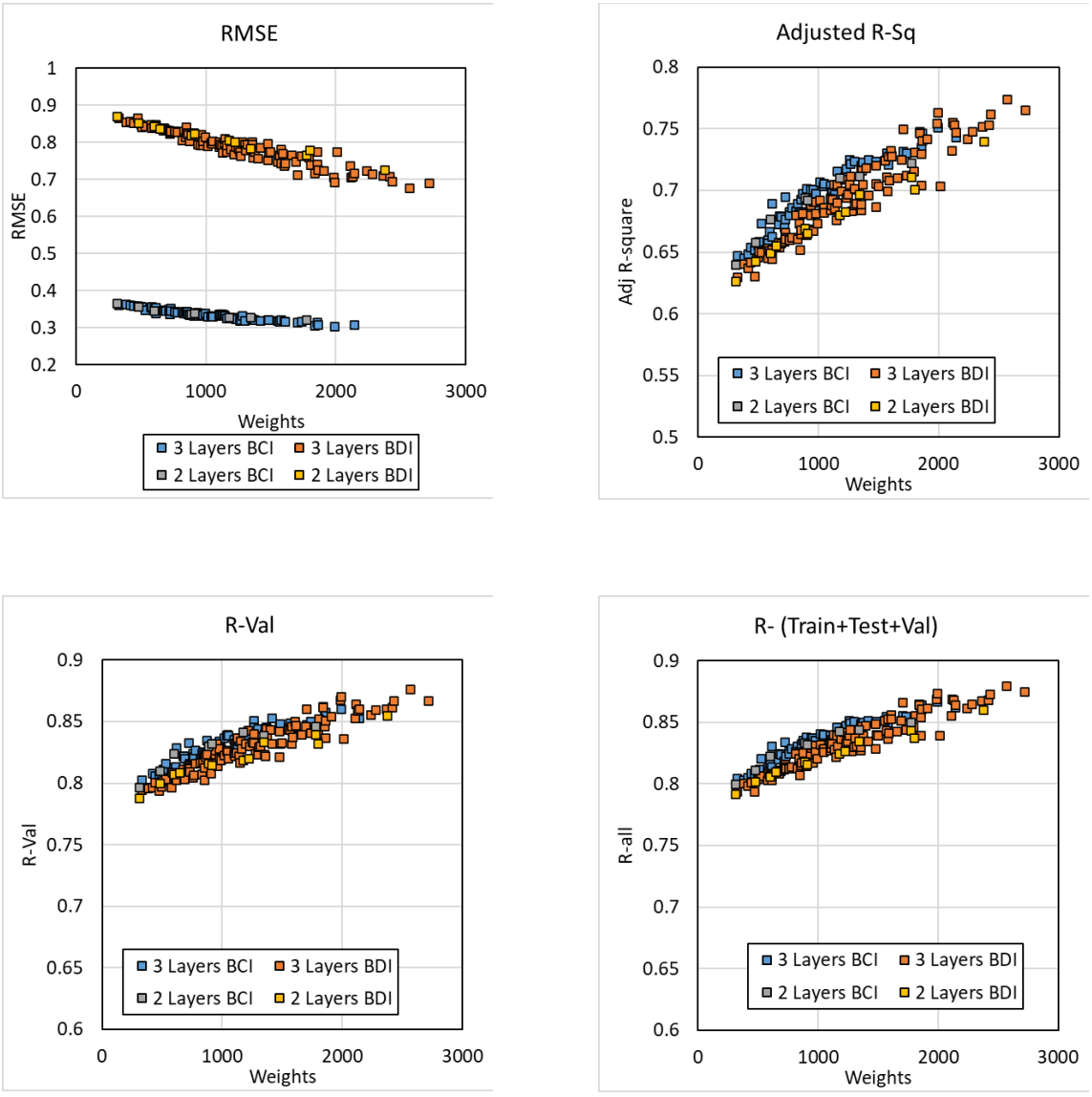

Figure 4-8 Effect of model weights on prediction RMSE, Adj R-Sq, R-Val, R-All

4.2.4 Effect of Activation Function on Model Performance

The effect of different activation functions on the overall model performance was investigated by running iterative models occupying three top activation functions in neural network regression models: log-sigmoid (logsig), tan-sigmoid (tansig), and pure linear (purlin). Although more complex convolutional networks employ other activation functions, only the

abovementioned activation functions are used considering the problem statement and simplicity. Therefore, iterations were set up so that all the combinations of these three activation functions are used for the hidden layers of the model. As there are three activation functions with two hidden layers, the number of combinations was found to be 2^3=8. Figure 4-9 and Figure 4-10 indicate model R-values for different combinations of activation layers in the model architecture. It is evident that for both BDI and BCI modeling, using the purlin activation function reduced the overall model accuracy. For this reason, the purlin activation function was dropped from consideration.

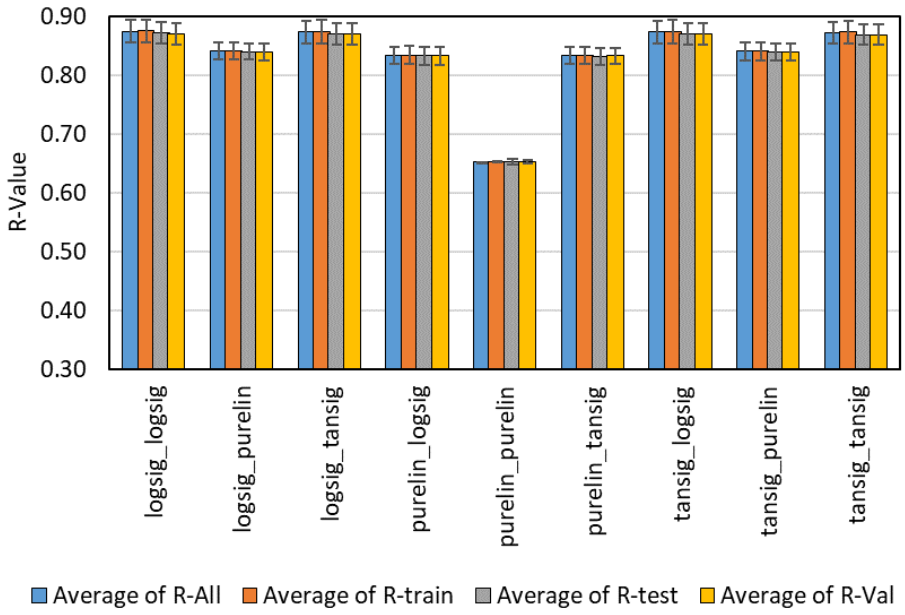

Figure 4-9 Effect of different activation functions on BDI prediction model R-Values

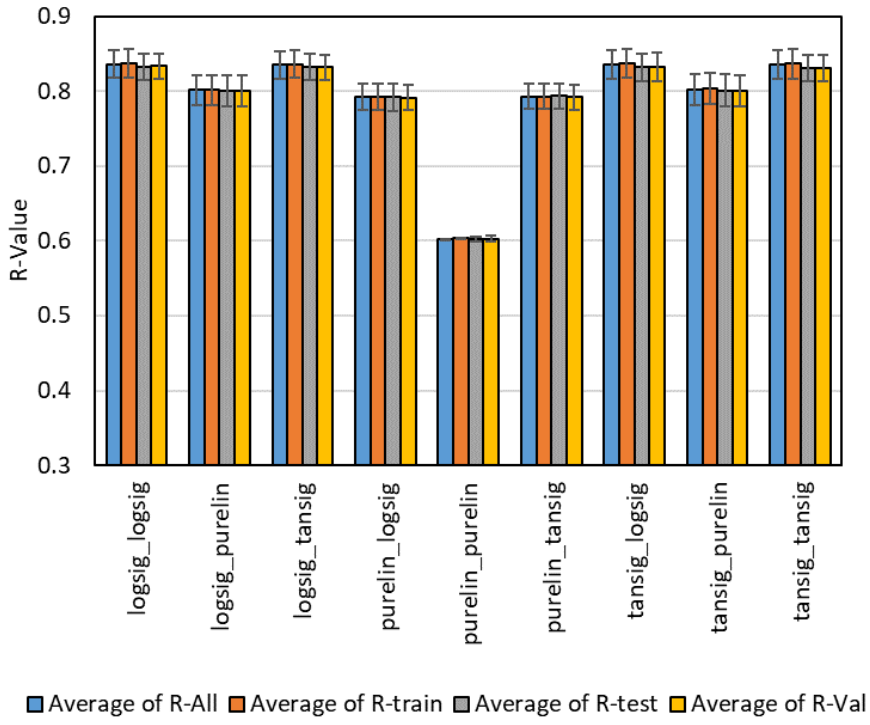

Figure 4-10 Effect of different activation functions on BCI prediction model R-Values

Aside from the magnitude of the R-Value for different combinations of activation functions, the hypothesis of "model efficiency for all the activation function combinations is the same" is to be tested if the difference in mean efficiency for different activation function pairs is statistically different. If the ANOVA results indicate a p-value less than 0.05, it means at least a pair of model efficiency parameters are different. Table 4-4 and Table 4-5 indicate a p-value less than 0.05, meaning that at least a pair of the efficiency parameters for different activation functions are different for BDI and BCI prediction models.

Table 4-4 ANOVA Results for BDI Prediction Model RMSE of Activation Functions

Groups	Observation Count	Sum (RMSE)	Average (RMSE)	Variance (RMSE)
logsig_logsig	4	3.291	0.823	$4.83E-06$
logsig_purelin	4	3.161	0.790	$6.56E-07$
logsig_tansig	4	3.287	0.822	$4.87E-06$
purelin_logsig	4	3.133	0.783	$4.98E-07$
purelin_purelin	4	2.409	0.602	$1.90E-08$
purelin_tansig	4	3.132	0.783	$7.75E-07$
tansig_logsig	4	3.286	0.822	$5.89E-06$
tansig_purelin	4	3.159	0.790	$5.52E-07$
tansig_tansig	4	3.283	0.821	$6.25E-06$

ANOVA

Source of Variation	SS	df	MS	F	P-value	F crit
Between Groups	0.1549	8	0.0193	7154.78	$\mathbf{7.62E-43}$	2.305
Within Groups	$7.30E-05$	27	$2.70E-06$			
Total	0.155	35				

Table 4-5 ANOVA Results for BCI Prediction Model Efficiency of Activation Functions

Groups	Observation Count	Sum (RMSE)	Average (RMSE)	Variance (RMSE)
logsig_logsig	4	3.339	0.834	$4.76E-06$
logsig_purelin	4	3.204	0.801	$3.38E-07$
logsig_tansig	4	3.336	0.834	$4.66E-06$
purelin_logsig	4	3.168	0.792	$2.47E-07$
purelin_purelin	4	2.411	0.602	$1.14E-07$
purelin_tansig	4	3.172	0.793	$5.72E-07$
tansig_logsig	4	3.338	0.834	$7.43E-06$
tansig_purelin	4	3.208	0.802	$1.3E-06$
tansig_tansig	4	3.335	0.833	$6.83E-06$

ANOVA

Source of Variation	SS	df	MS	F	P-value	F crit
Between Groups	0.172	8	0.0215	7390.006	$\mathbf{4.93E-43}$	2.305
Within Groups	$7.874E-05$	27	$2.92E-06$			
Total	0.172	35				

It is evident that the combinations of different activation functions statistically affect the model efficiency parameter. Therefore, the terminology "model efficiency" is widespread, involving different model evaluation parameters based on the model requirement. The present study aims to fit the regression model for the BDI and BCI; therefore, the R-Value (R-train, R-Val, and R-Test) is considered an efficiency parameter for the model.

4.2.5 Effect of Activation Functions on Model Training Time

The training time required to train the model is also significant when replicating the methodology or retraining the model with more information. During the iteration process, the training time for each activation function pair was recorded, and the average training time for different activation function sets is plotted in Figure 4-11. The plots indicate that the purlin-purlin combination of activation functions completes the training at a significantly lower time than other combinations. However, the prediction accuracy was substantially lower than the other combinations of activation functions, as discussed in Section 4.2.4 in this document.

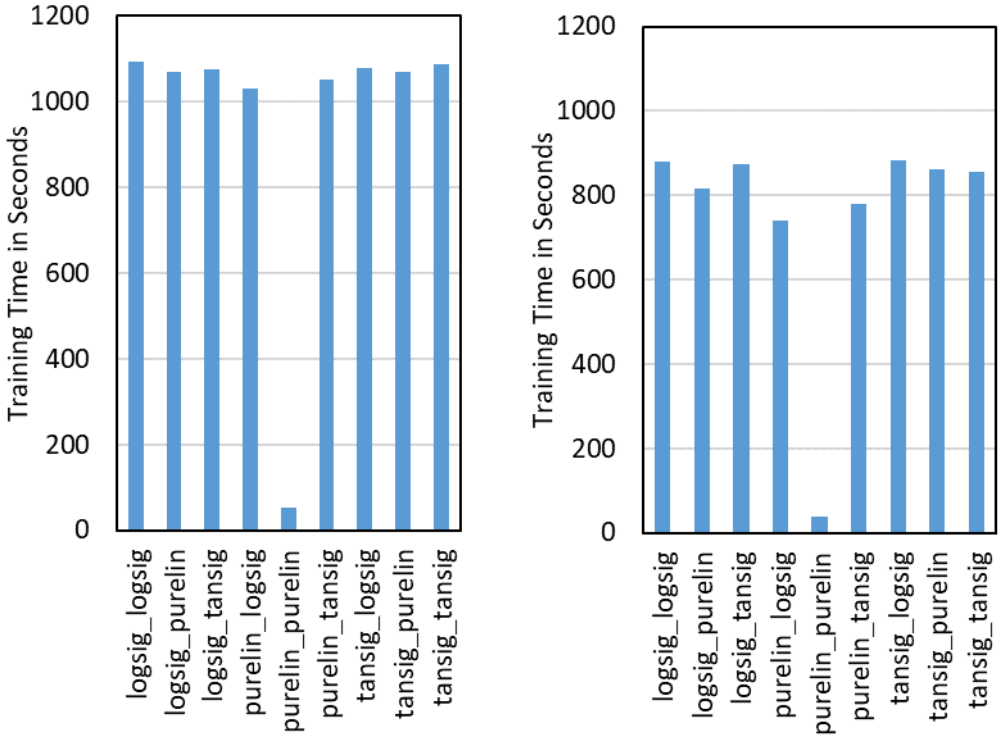

(a) (b)

Figure 4-11 Average training time in seconds for training models with different sets of activation functions (a) BDI prediction model (b) BCI prediction model

To summarize the results in Section 4.2.4 and Section 4.2.5, it was concluded that the purlin activation function should not be selected as the regression model in a similar research problem statement in pavement engineering. Still, the choice between "logsig" and "tansig" activation functions can be made based on the range of data being fed to the model through the activation function. The "logsig" activation function only transmits positive values through the feedforward neural network nodes, while the "tansig" covers both positive and negative values of the variables. In the present study, all the variables that are set to be input variables for the model are positive real numbers; therefore, the choice of "tansig" as an activation function would underutilize the activation function capability, as the half of the curve that has negative values would never be used. Therefore, for the present study, when the word activation function is mentioned in any analysis results, it refers to the "logsig" activation function in all hidden layers of the model.

4.2.6 Model Overfitting and Regularization Parameter

Overfitting of the model occurs when the model's bias is lowest, and the variance is higher. Simply put, the model explains all the training data variability but exhibits poor performance for the testing dataset. The MATLAB Neural Network Training Tool stops the training when the model validation dataset error value exceeds the training dataset error. The default trigger difference in error is 2×10^{-5} in set by default in MATLAB. The present study investigated if the model was overfitting, and the probable regularization parameter lambda (λ) was tested for both BCI and BDI prediction models. The types of regularization and methods are discussed in the methodology chapter. The present study's regularization method is Ridge Regression Regularization (L2), which works by adding the penalty equivalent to the sum of squares (SS) of the magnitude of the coefficient. Figure 4-12 shows the λ value for different training models for BDI (top) and BCI (bottom). At a different number of iterations, the best weight of the penalty is

chosen based on the lowest MSE. Based on iterations, the best λ value for BDI is 7.5205×10^{-6} and 0 for the BCI prediction model. The λ value depends on the amount of training data. Regularization is commonly used for more complicated architecture for convolutional neural networks, image recognition, genetic algorithm (GA) based deep learning, or AI-based BPNN architectures where the data scientist does not determine the number of required variables. This regularization helps reduce the number of variables implemented in the model by penalizing overfitting (*92–97*). Based on the existing problem statement of this research project, the number of available predictor variables is well described, and there is not any statistically redundant variable, so the use of regularization parameter is not considered in the proposed methodology,

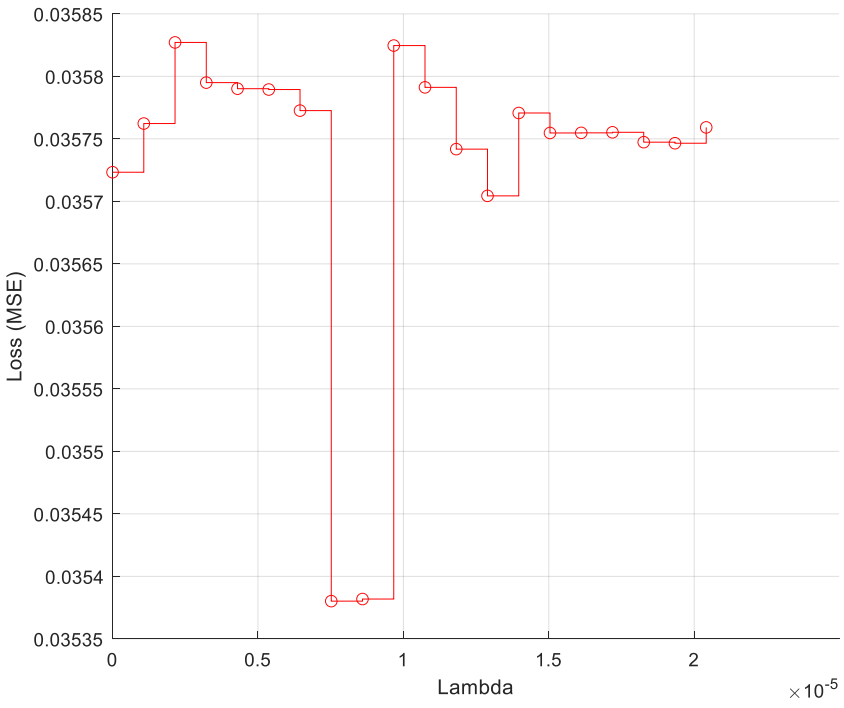

(a)

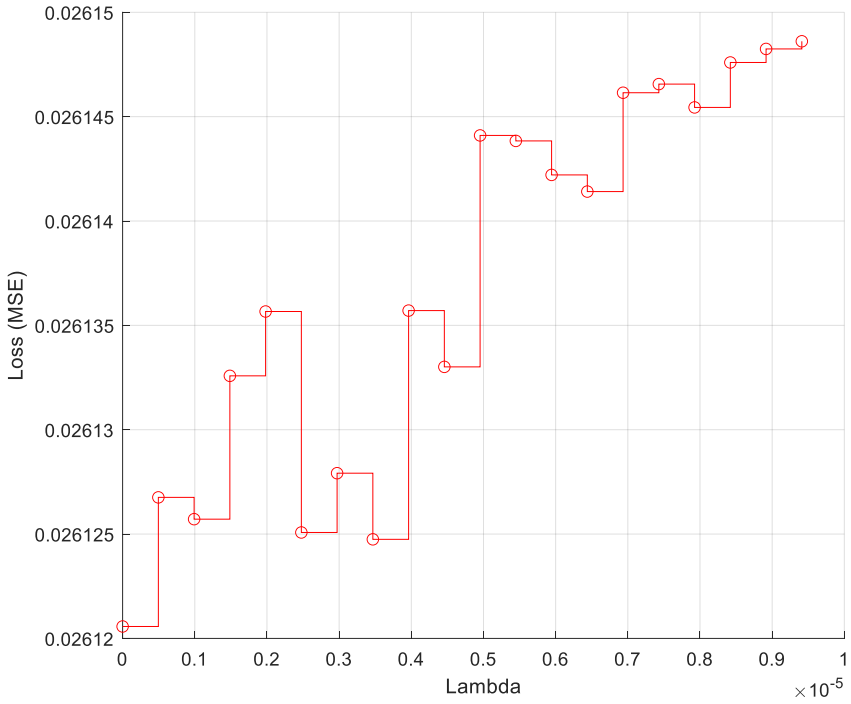

(b)

Figure 4-12 Regularization parameter Lambda for BDI model (a) and BCI model (b)

In the present study, based on the results from the regularization and early stopping iterations from the model development phase, both choices of regularization and early stopping have been applied for BDI, and only early stopping was applied for BCI as the regularization parameter as shown in Figure 4-12 (b) is close to zero.

4.3 Model Errors

Model error is the difference between the observed value and model predicted output. Error value provides the initial measurement of prediction capability, the goodness of fit and departure from the normality assumptions in conventional regression analysis. In NN methodology, the model error value is equally useful for the measurement of the RMSE of the model.

4.3.1 Effect of Activation Function on Model Errors

Iteration was performed for the different activation function combinations and layer sizes; in simple words, different model architectures were put in trial and model performance parameters RMSE, Adj R-sq, R-train, R-test, R-validation, R-all, and mean absolute error were populated. Finally, the summary of the models is shown in Table 4-6 and Table 4-7. The green highlighted cells indicate the top five R-values for Adj R-sq, R-train, R-test, R-val and R-all, and the bottom five values for RMSE and MAE for BDI and BCI prediction models, respectively. All other model accuracy results from other combinations are presented in Appendix A of this dissertation.

Table 4-6 Summary of BDI Prediction Model Architecture and Performance

Layer 1 Activation	Layer 2 Activation	Layer1 Nodes	Layer2 Nodes	RMSE	Adj R-sq	R-train	R-test	R-Val	R-All	MAE
logsig	logsig	48	24	0.77	0.76	0.90	0.89	0.89	0.89	0.56
			36	0.74	0.79	0.91	0.90	0.90	0.91	0.54
	purelin	48	24	0.85	0.70	0.86	0.85	0.85	0.86	0.61
			36	0.85	0.70	0.86	0.85	0.85	0.86	0.61
	tansig	48	24	0.77	0.76	0.89	0.89	0.89	0.89	0.56
			36	0.74	0.78	0.91	0.90	0.90	0.91	0.54
purelin	logsig	48	24	0.88	0.67	0.84	0.84	0.84	0.84	0.64
			36	0.86	0.69	0.85	0.85	0.85	0.85	0.63
	purelin	48	24	1.14	0.41	0.65	0.65	0.65	0.65	0.86
			36	1.14	0.41	0.65	0.65	0.65	0.65	0.86
	tansig	48	24	0.88	0.67	0.84	0.84	0.84	0.84	0.64
			36	0.87	0.68	0.85	0.85	0.84	0.85	0.63
tansig	logsig	48	24	0.76	0.76	0.90	0.89	0.89	0.90	0.56
			36	0.73	0.79	0.91	0.90	0.90	0.91	0.54
	purelin	48	24	0.85	0.70	0.86	0.85	0.85	0.86	0.61
			36	0.85	0.70	0.86	0.86	0.85	0.86	0.61
	tansig	48	24	0.77	0.76	0.89	0.89	0.89	0.89	0.56
			36	0.74	0.78	0.91	0.90	0.90	0.91	0.54

Table 4-7 Summary of BCI Prediction Model Architecture and Performance

Layer 1 Activation	Layer 2 Activation	Layer1 Nodes	Layer2 Nodes	RMSE	Adj R-sq	R-train	R-test	R-Val	R-All	MAE
logsig	logsig	48	24	0.32	0.73	0.91	0.90	0.90	0.91	0.24
			36	0.31	0.75	0.92	0.91	0.91	0.92	0.23
	purelin	48	24	0.35	0.68	0.88	0.87	0.87	0.88	0.26
			36	0.35	0.68	0.87	0.88	0.88	0.87	0.26
	tansig	48	24	0.32	0.74	0.91	0.90	0.90	0.91	0.24
			36	0.31	0.75	0.92	0.91	0.91	0.91	0.23
purelin	logsig	48	24	0.37	0.64	0.85	0.85	0.85	0.85	0.27
			36	0.35	0.68	0.87	0.87	0.87	0.87	0.26
	purelin	48	24	0.49	0.36	0.65	0.65	0.65	0.65	0.37
			36	0.49	0.36	0.65	0.65	0.65	0.65	0.37
	tansig	48	24	0.37	0.65	0.85	0.85	0.85	0.85	0.27
			36	0.36	0.67	0.87	0.87	0.86	0.87	0.26
tansig	logsig	48	24	0.32	0.74	0.91	0.91	0.91	0.91	0.24
			36	0.31	0.75	0.92	0.92	0.91	0.92	0.23
	purelin	48	24	0.35	0.68	0.87	0.87	0.87	0.87	0.26
			36	0.35	0.68	0.87	0.87	0.87	0.87	0.26
	tansig	48	24	0.32	0.74	0.91	0.90	0.90	0.91	0.24
			36	0.31	0.75	0.92	0.91	0.91	0.92	0.23

The results indicate that the models with logsig or tansig activation functions with a higher number of nodes yield more R-value and the least model errors for both BDI and BCI prediction neural network models. The choice between logsig and tansig activation functions can be determined from the range of values the functions can handle as input. Figure 4-13 shows the different architectures of the activation functions (*98*). Therefore, in the onward discussion and results in this dissertation, all the results indicated and architectures discussed would have "logsig" as the activation function in all the hidden layers.

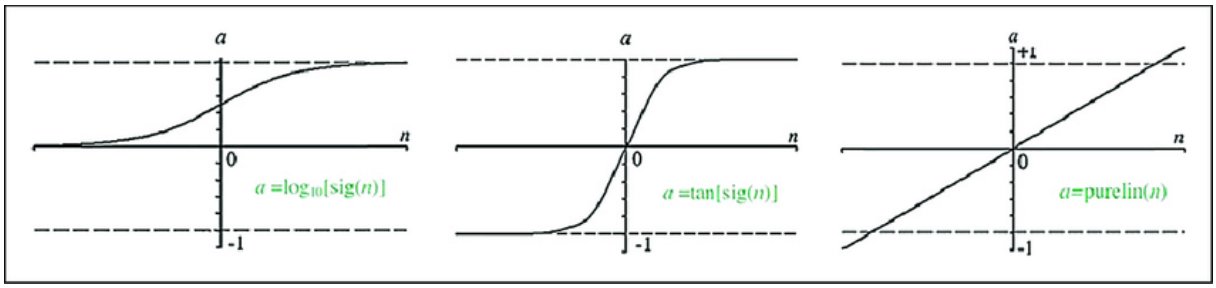

Figure 4-13 Activation functions (Left) Logsig, (Middle) Tansig, and (Right) Purlin (*98*)

4.3.2 Regression Results and Error Histogram

The MATLAB Neural Network Tool provides a model training condition and fitting performance through GUI throughout the training session and the model performance matrices after the training are complete. Figure 4-14 through Figure 4-16 indicate, respectively, the model fit, error by epoch and error histogram for the BDI prediction model with an architecture of 11-48-36-1 with a maximum epoch set to 25 for demonstration purposes. The following sections explain the detailed effect on the epoch and attain more accurate outputs. Figure 4-14 indicates an overall model fit R-value of 0.83 for model training, validation and testing. Figure 4-15 indicates a final MSE of 0.617 at the end of 25 epochs. It is important to mention that the higher the number of epochs, the lesser the MSE until the validation MSE increases again and the model overfits. The

demerit of reaching an overfitting model is that the model predicts well for the input ranges in the training data but produces erroneous results for the validation dataset. There is no magic number for the number of epochs to reach; this is mostly decided by the type of data received and the level of accuracy expected. Figure 4-16 shows the error histogram for the same prediction model and architecture. The error range is between -3.25 and +3.5, which is wider than the expected accuracy, but stopping at 25 epochs indicates the necessity of adding more epochs while training.

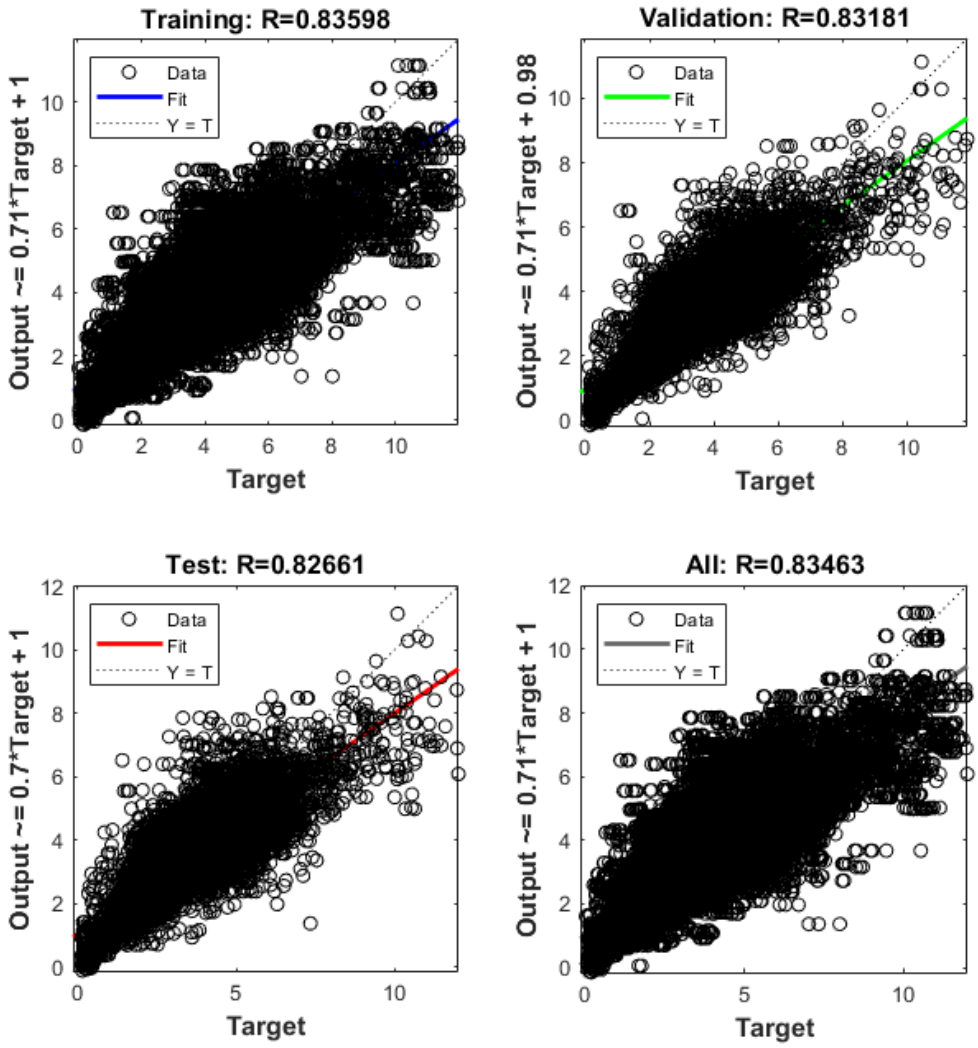

Figure 4-14 Model fit plots for BDI prediction model architecture 11-48-36-1

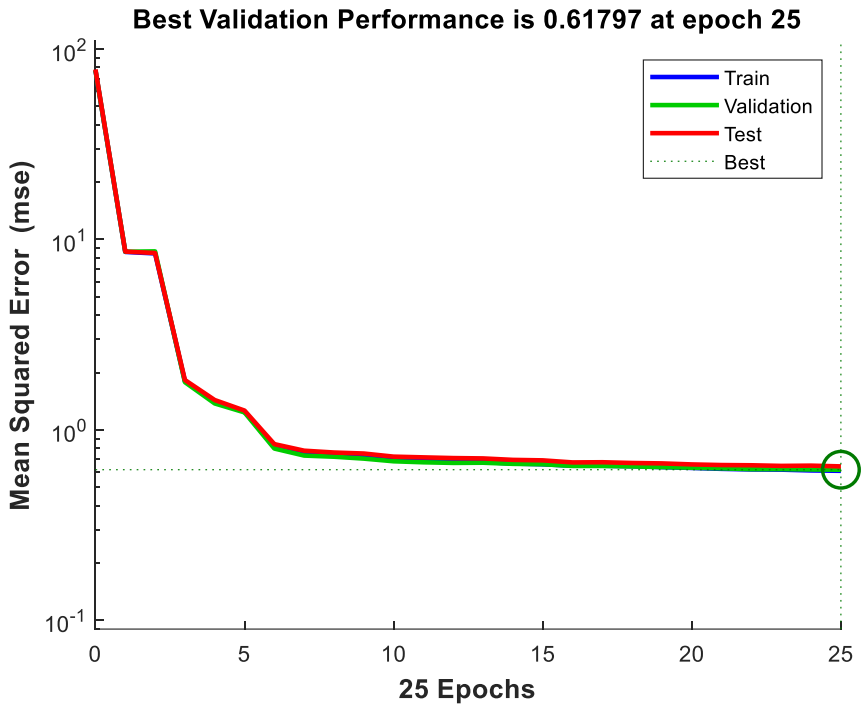

Figure 4-15 MSE per epochs plot BDI prediction model architecture 11-48-36-1

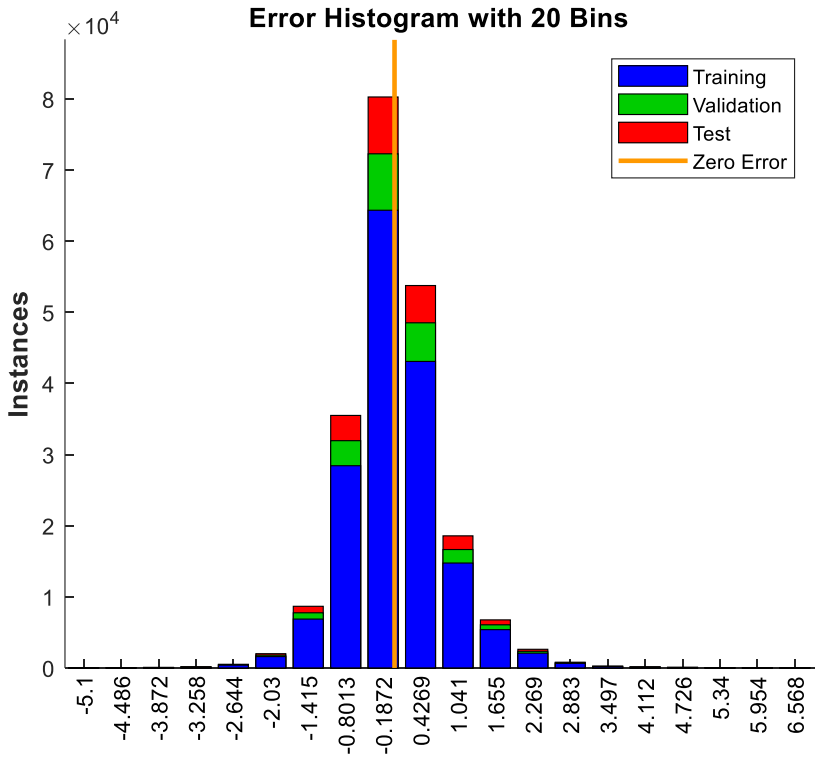

Figure 4-16 Error histogram for BDI prediction model architecture 11-48-36-1

Figure 4-17 through Figure 4-19 show the model fit, error by epoch, and error histogram for the BCI prediction model, respectively, with an architecture of 11-48-36-1 with a maximum epoch set to 25 for demonstration purposes. Figure 4-17 shows an overall R-Value for model training, testing, and validation of approximately 0.85. Figure 4-18 indicates the training model's final MSE of 0.11 for the BCI training model up to 25 epochs. Figure 4-19 shows the error histogram of the BCI training model of the architecture of 11-48-36-1. The error range lies between -1.2 and +1.3, which can be narrowed down if the number of epochs increases.

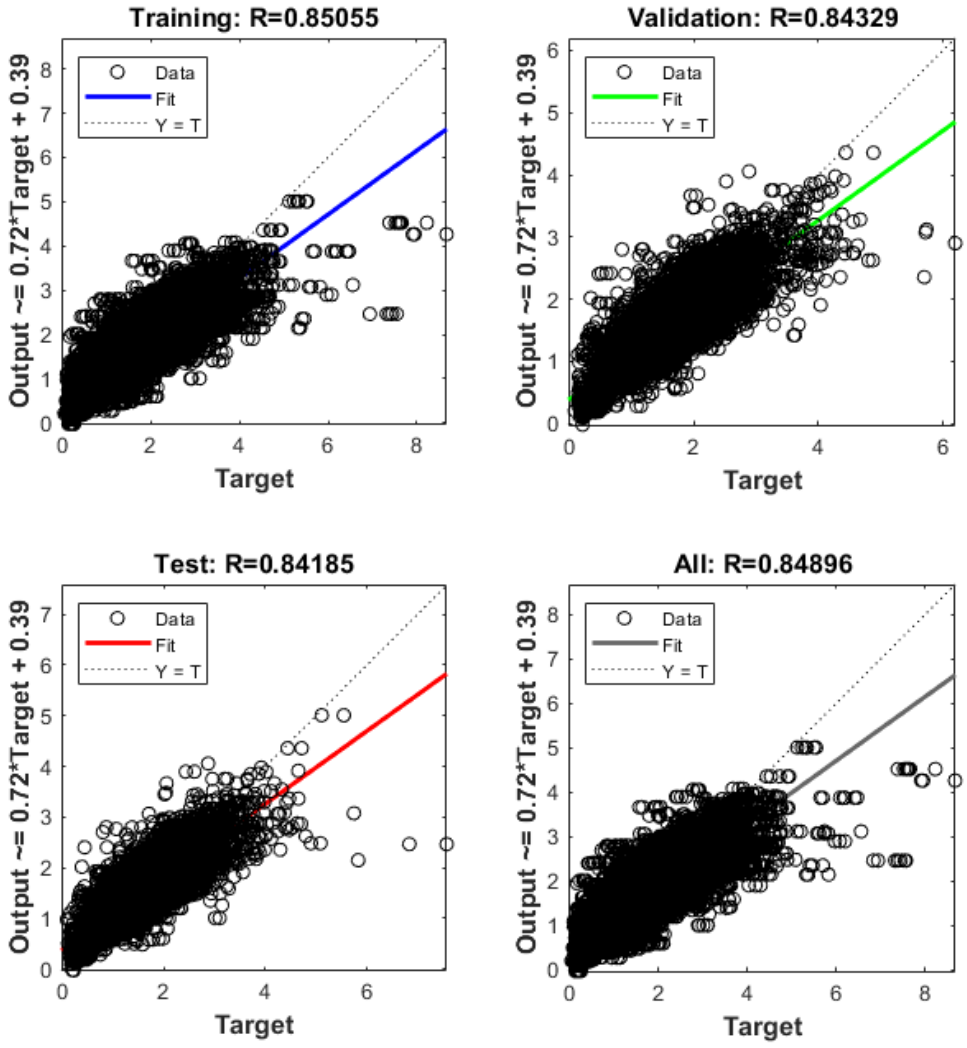

Figure 4-17 Model fit plots for BCI prediction model architecture 11-48-24-1

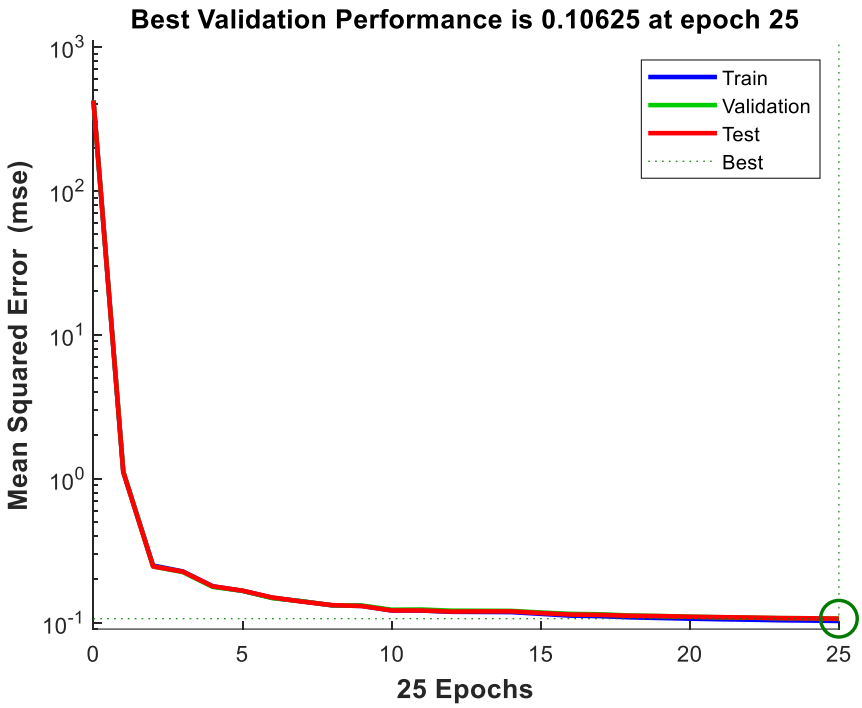

Figure 4-18 MSE per epochs plot BCI prediction model architecture 11-48-24-1

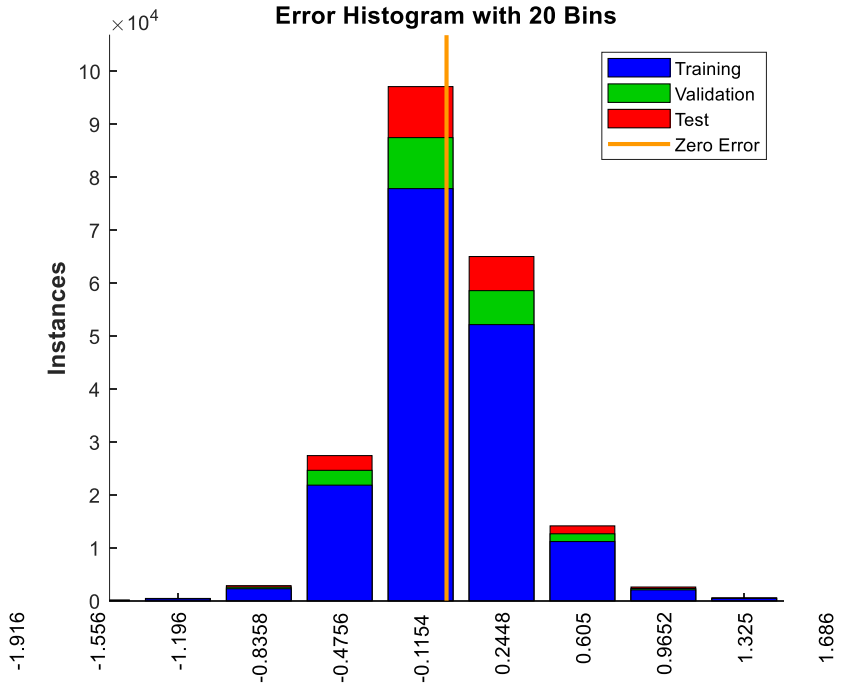

Figure 4-19 Error histogram for BCI prediction model architecture 11-48-24-1

4.3.3 Effect of Number of Epochs on the Error Distribution

The total number of epochs signifies the complete cycle of reassignments and adjustments of weight and bias while training the network. Adjusting the weights and bias values helps the network learn the regression or pattern from the training dataset. In previous sections, it was observed that the error histogram spread was higher, making the model less reliable from the perspective of the model's capability to predict. To understand the effect of the number of total epochs on the model prediction capability, an attempt is made to train the models with different epochs to inspect if the error histogram gets narrower. The BDI and BCI prediction 11-48-24-1 architecture model was trained at 20, 40,60,80 and 100 epochs, and error histograms were plotted. The model training time should allow a minimum number of back-and-forth iterations to adjust the weights and bias of the model to reduce the MSE to the lowest while ensuring the model does not start overfitting by increasing the MSE of the validation dataset. Figure 4-20 shows the model MSE per epoch for different cut-off MSE values between 20 and 100 epochs at 20 epoch increments. Figure 4-20(a) shows the model MSE values for BDI, and Figure 4-20(b) shows the model MSE values for BCI. During the training, it was observed that the best MSE values are not the lowest when the cut-off epoch is as low as 40. The MSE does not change significantly between 60 and 80 epochs as the epoch increases. It was observed that when the cut-off epochs were set to 100, the training stopped between 90-95 epochs as the model training started overfitting, and the difference in training and validation MSE values started to increase. Based on the type of problem statement and available training data, the optimum number of epochs for this study was set to 80.

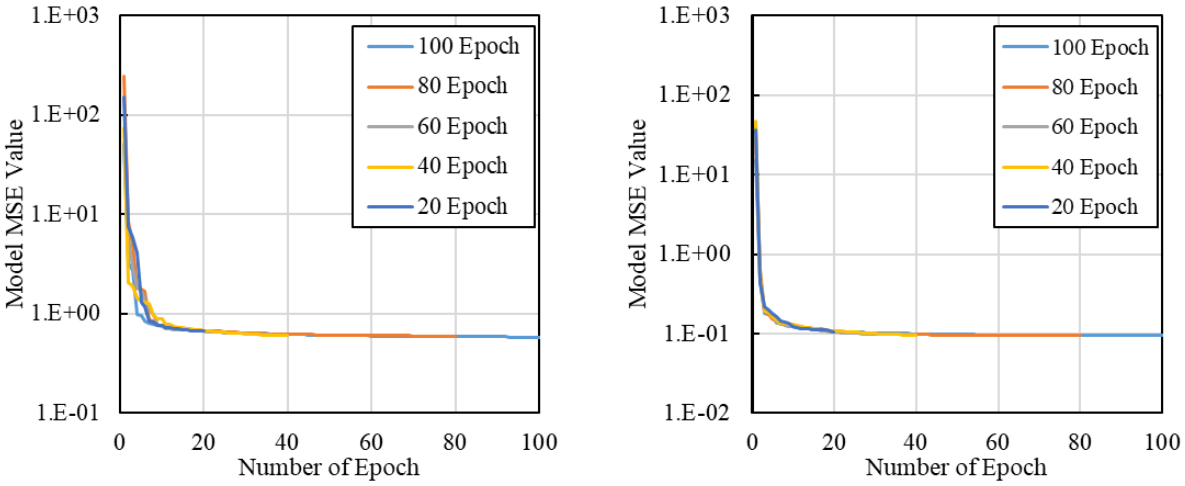

(a) (b)

Figure 4-20 The model training MSE plot by epoch (a) BDI and (b) BCI

It is also important to study the error histogram of the model to capture the range of errors and understand their distribution. Figure 4-21 shows the error histogram for BDI and BCI prediction models trained up to 80 epochs. The error histogram has more spread for BDI than the error histogram of BCI, which can be explained by the BDI being representative of the base layer closer to the pavement's surface layer. Many pavement construction variables affect the base layer, including but not limited to the type of AC layer, age of AC layer, type of compaction method applied, aggregate used in the base layer construction, health of the AC layer, etc. Also, the base layer being immediately under the AC layer, is subjected to traffic damage, and the number of ESALs is an important parameter to measure the accumulated damage in either the AC or the base layer of the pavement. As further research continues, more variables can be added to the model, while the neural network can capture and explain some of the variability in the prediction model.

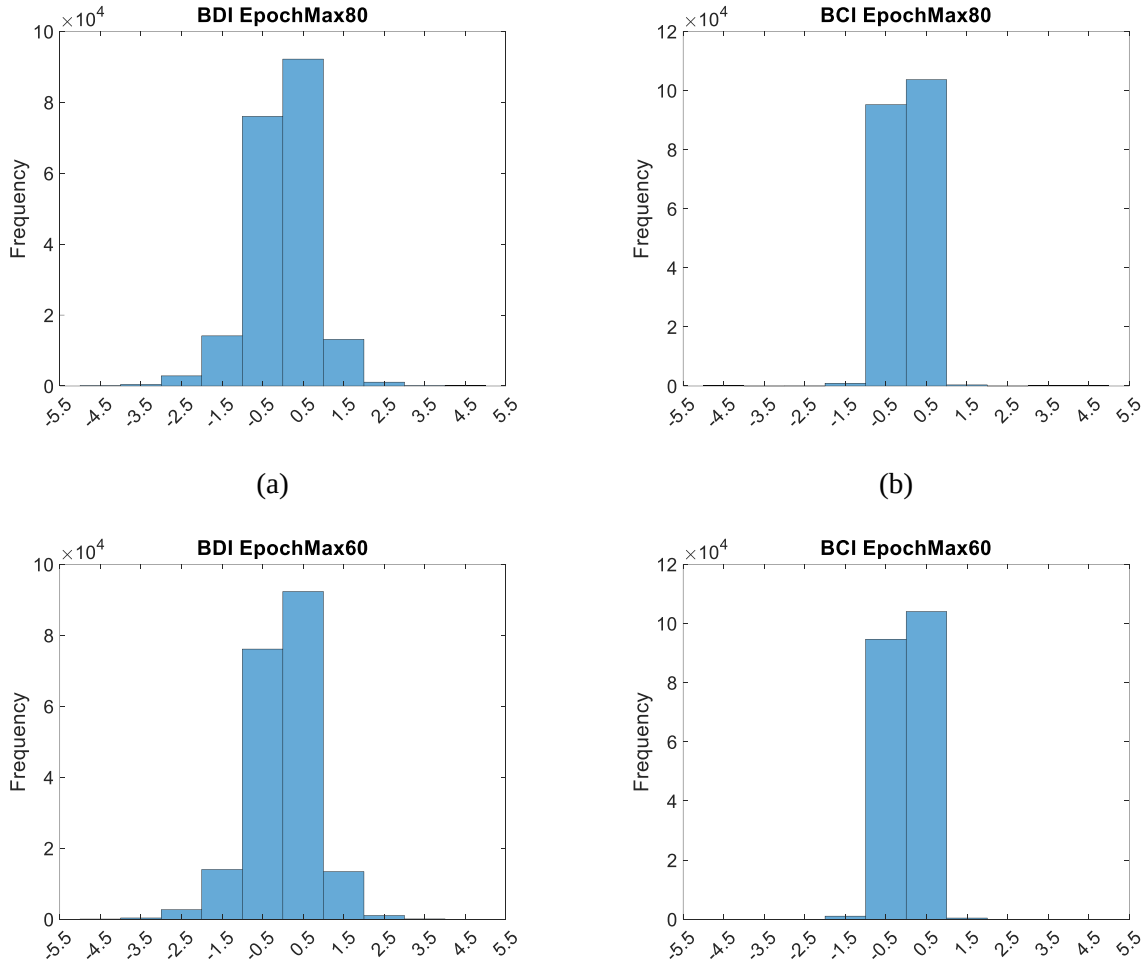

Figure 4-21 Error histogram for (a) BDI and (b) BCI for the model trained at 80 Epochs (c) BDI and (d) BCI for the model trained at 60 Epochs

Based on the discussion in Sections 4.2 and 4.3, the BDI and BCI prediction models shown in Table 4-8 Recommended Models for Prediction of BDI and BCI were found to be the best fit for further data analysis in this dissertation.

Table 4-8 Recommended Models for Prediction of BDI and BCI

Prediction	Hidden Layer 1 Neuron	Hidden Layer 2 Neuron	Activation Function	Training Epochs	Training method
BDI	48	36	logsig	80	LM
BCI	48	24	logsig	80	LM

4.4 Model Fit Results for Traffic Class

The trained models were tested for correlation by subdividing the training dataset into several groups based on the traffic conditions and treatments applied so that the accuracy of each combination could be determined.

4.4.1 Model Fit for Base Damage Index (BDI)

In continuation of the result discussion from Section 4.3, the trained models are used to verify if the predictions are accurate for different traffic classes and treatment types. The observed and predicted BDI values from the trained models are compared in Figure 4-22. The R-Value for low (Class 1), moderate (Class 2), and heavy (Class 3) traffic conditions, the model prediction value, and the observed value yielded a correlation R-value of 0.76, 0.90, and 0.83, respectively.

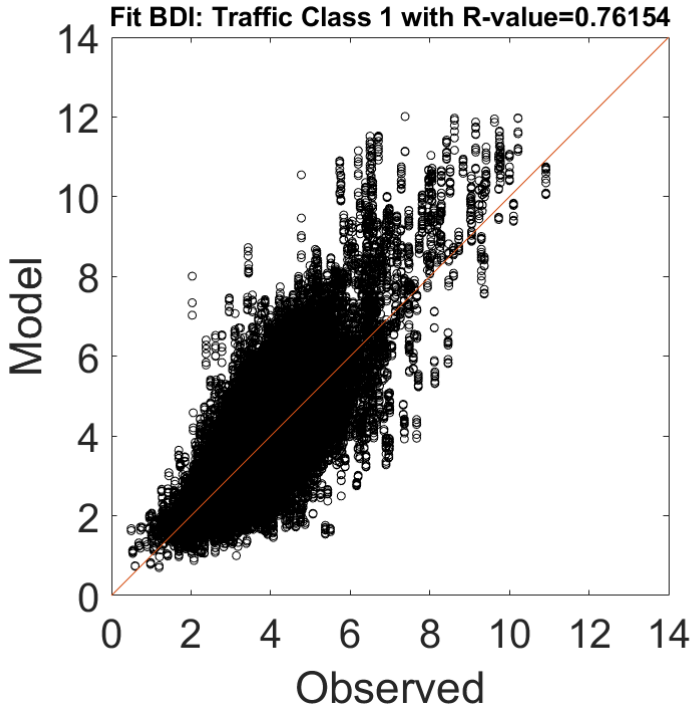
Fit BDI: Traffic Class 1 with R-value=0.76154
Model
Observed
0
2
4
6
8
10
12
14

(a)

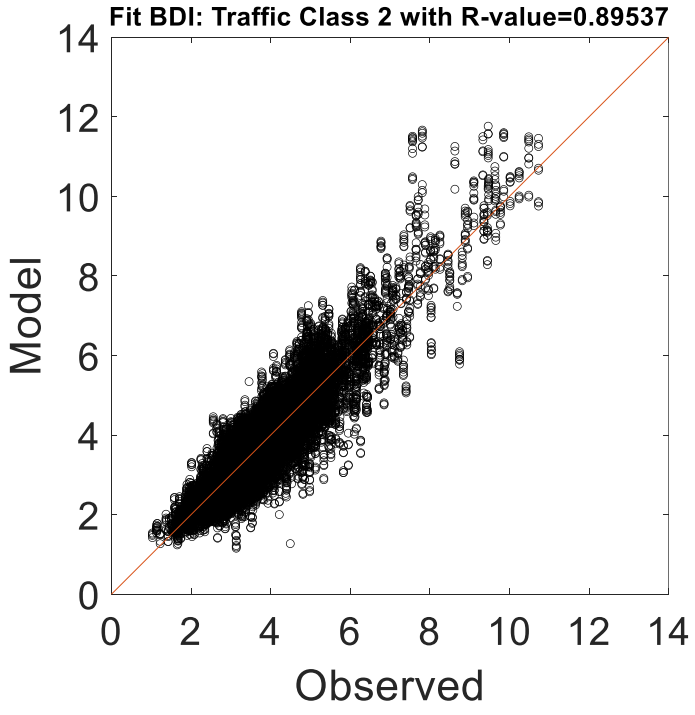
Fit BDI: Traffic Class 2 with R-value=0.89537
Model
Observed
0
2
4
6
8
10
12
14

(b)

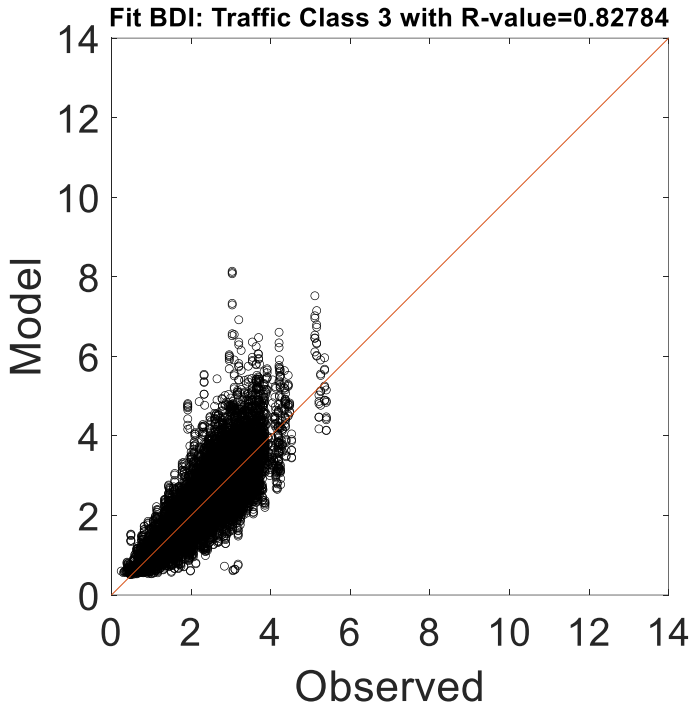

(c)

Figure 4-22 BDI prediction model fit for (a) low traffic, (b) moderate traffic, (c) heavy traffic conditions

A summary of the model fit R-Values for BDI Prediction models for different traffic conditions is shown in Table 4-9.

Table 4-9 Model Fit Summary for BDI Prediction at Different Traffic Conditions

Traffic Condition	Test Segment	Model Fit R-Value
Class 1	Inbound Lane Lee Road 159. Both Lanes CSAH 8	0.76
Class 2	Outbound Lane Lee Road 159	0.89
Class 3	US 280 and US 169	0.83

4.4.2 Model Fit for Base Curvature Index (BCI)

The observed vs. the predicted BCI values for the models are compared for the three traffic conditions based on the R-Value of the model fit. Figure 4-23 indicates that the model fit R-Values for low, moderate and high traffic conditions are 0.83, 0.85, and 0.86, respectively.

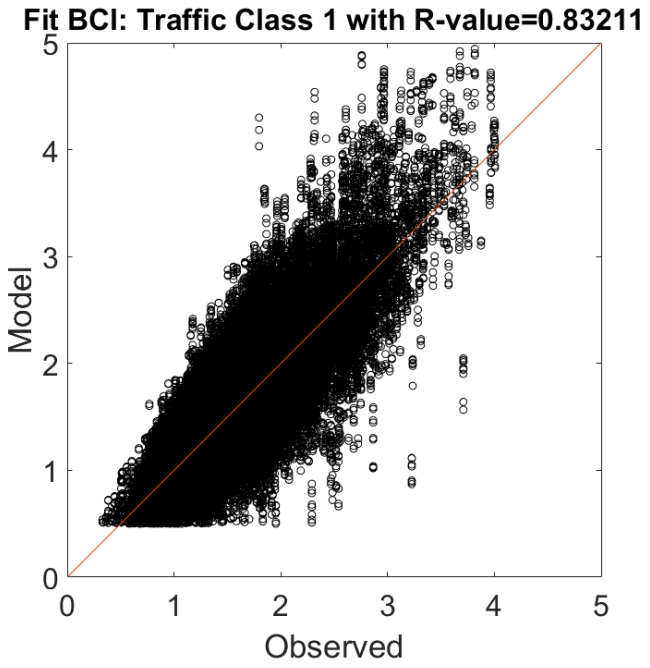

(a)

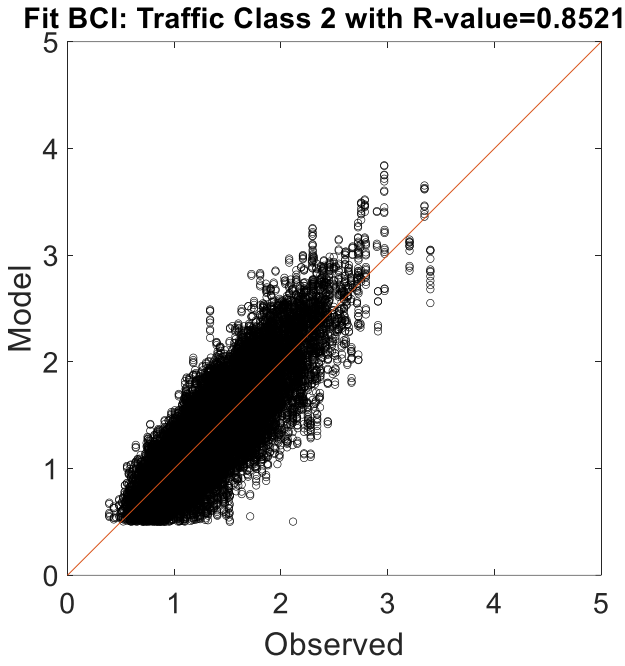

(b)

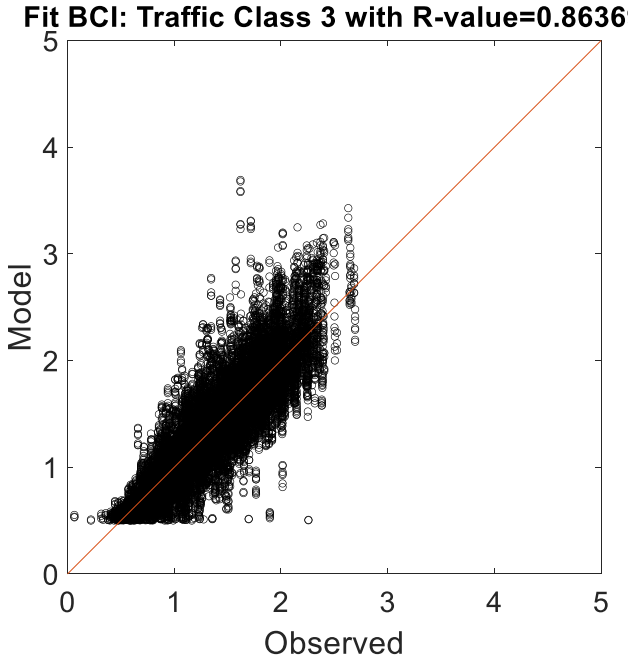

(c)

Figure 4-23 BCI prediction model fit for (a) low traffic, (b) moderate traffic, (c) heavy traffic conditions

A summary of the model fit R- Values for BCI Prediction models for different traffic conditions is shown in Table 4-10.

Table 4-10 Model Fit Summary for BCI Prediction at Different Traffic Conditions

Traffic Condition	Test Segment	Model Fit R-Value
Class 1	Inbound Lane Lee Road 159. Both Lanes CSAH 8	0.73
Class 2	Outbound Lane Lee Road 159	0.85
Class 3	US 280 and US 169	0.86

4.5 Model Fit Results for Treatment Groups

The prediction capability of the NN models is compared based on different treatment groups in the study. The primary objective of the groupwise fitting is to validate if the values predicted by the models are accurate enough for any specific treatment group.

4.5.1 Model Fit for Base Damage Index (BDI)

The observed vs. model BDI values per treatment group are compared to investigate the model's capability and sensitivity to different treatments. The treatment groups were divided into seven groups designated 0 to 6, as previously discussed. Figure 4-24 shows the BDI prediction model fit for different treatment groups. Each treatment group model fit exhibits the overall fit for all traffic and weather conditions.

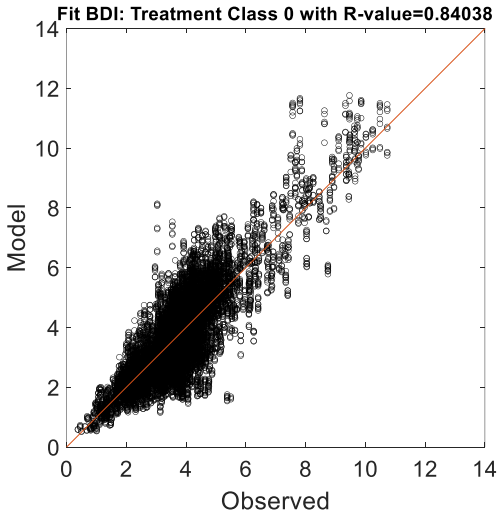
Fit BDI: Treatment Class 0 with R-value=0.84038
Model
Observed
0
2
4
6
8
10
12
14

(a)

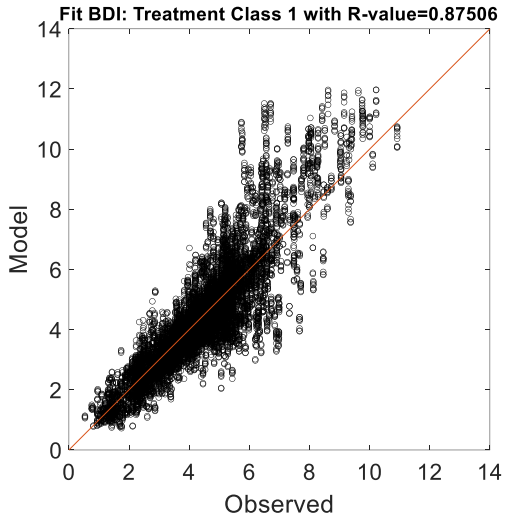
Fit BDI: Treatment Class 1 with R-value=0.87506
Model
Observed
0
2
4
6
8
10
12
14

(b)

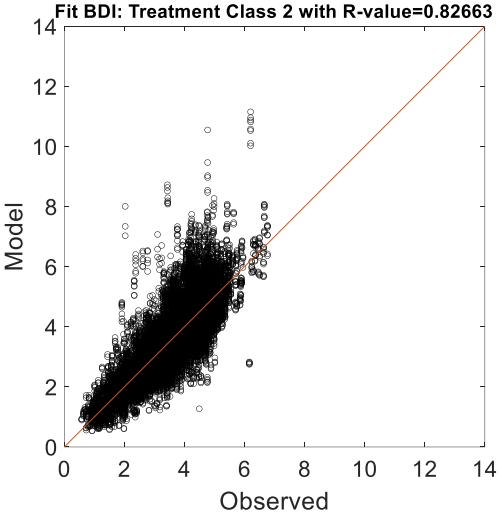
Fit BDI: Treatment Class 2 with R-value=0.82663
Model
Observed
0
2
4
6
8
10
12
14

(c)

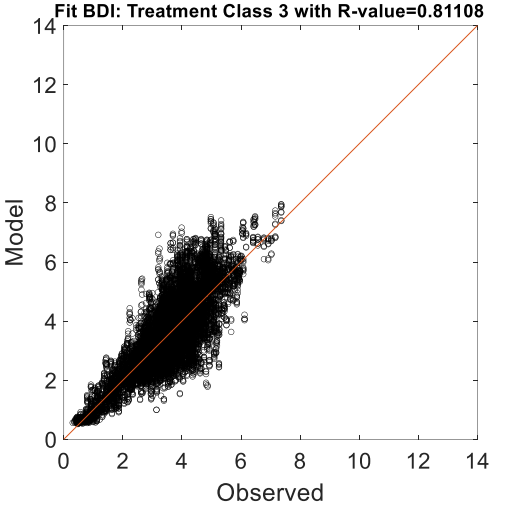
Fit BDI: Treatment Class 3 with R-value=0.81108
Model
Observed
0
2
4
6
8
10
12
14

(d)

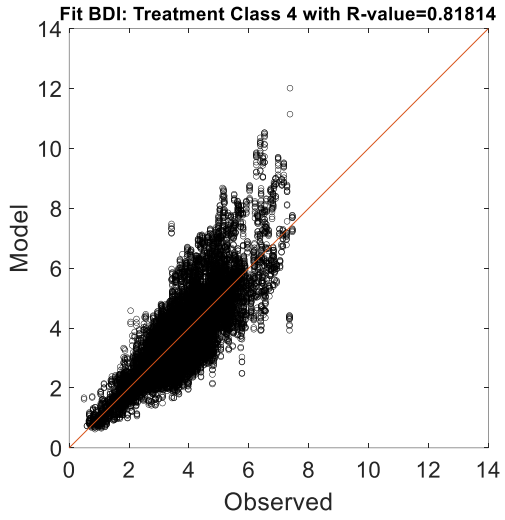

(e)

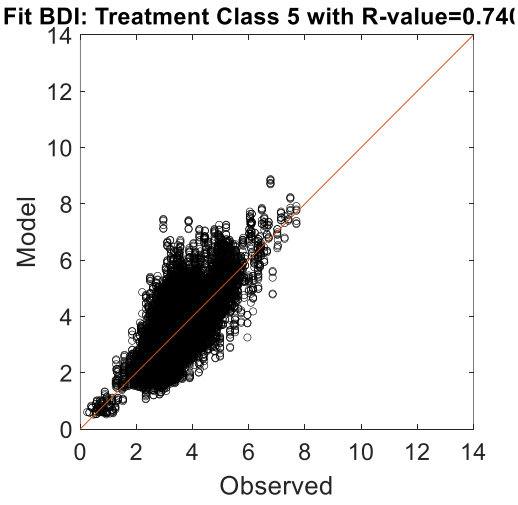

(f)

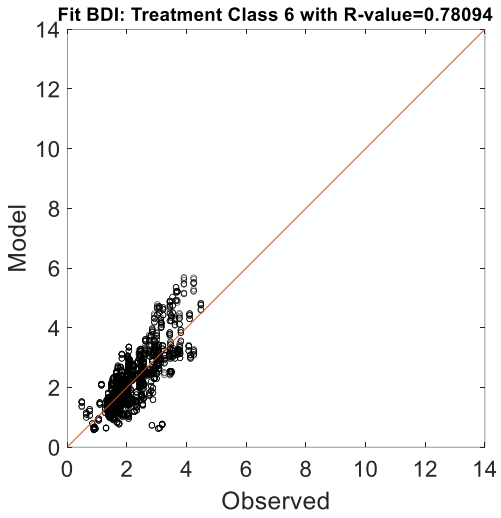

(g)

Figure 4-24 BDI prediction fit for different treatment groups

Table 4-11 summarizes the BDI prediction model fit for different treatment groups. It can be observed that the model fit R-Value ranges from 0.74 to 0.88. The reason for comparatively lower accuracy for treatment groups 5 and 6 is the unexplained variation in the dataset. The performance of thinlays largely depends on the quality of the aggregate, type of binder, source of

binder, use of recycled materials, type of paver, mat density, and other construction-related variables. Those variables are not included in the model predictor variables. The models for groups 5 and 6 could be substantially improved if those variables were included. In contrast, the model prediction capability for lighter treatments such as crack seal/ fog seal, chip seal, slurry seal, micro surfacing, and the combination of treatments was significant.

Table 4-11 Summary of the BDI Prediction Model Fit by Different Treatment Groups

Treatment Group	Description	Model Fit R-Value
0	Untreated Control	0.84
1	Crack Seal/ Fog Seal	0.88
2	Chip Seal/ Micro surfacing	0.83
3	Cape Seal (Chip Seal + Micro surfacing)	0.81
4	Conventional Thinlays/OGFC	0.82
5	Thinlays Combined with Chip Seal/ Micro Surfacing	0.74
6	CCPR/CIR	0.78

4.5.2 Model Fit for Base Curvature Index (BCI)

The BCI value corresponds to the condition of the subgrade, which is protected by the base and AC layers above it, making it less susceptible to traffic-induced damage. Also, the BCI values are more susceptible to change due to climatic impacts than BDI, where the type of treatment applied, existing traffic conditions, and quality of the construction influence the BDI value. Figure 4-25 shows the BCI prediction model fit for different treatment groups combining all traffic condition data in each treatment category. The model fit data indicates that treatment groups 5 and

6 have lower model accuracy than other treatments. Still, the magnitude of the BCI values is also lower for both observed and predicted values. The heavy and robust treatment applications, despite having some undefined contributing factors, help extend the life of the pavement by keeping the subgrade in good structural condition.

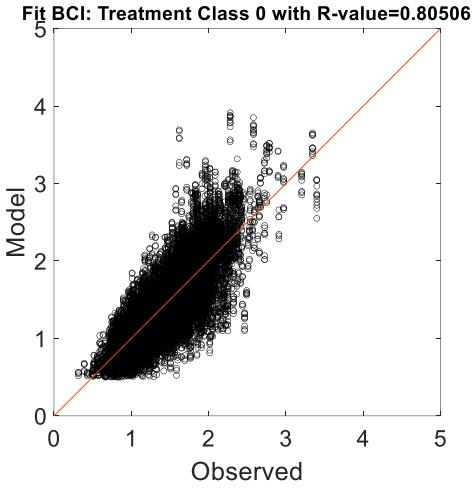

(a)

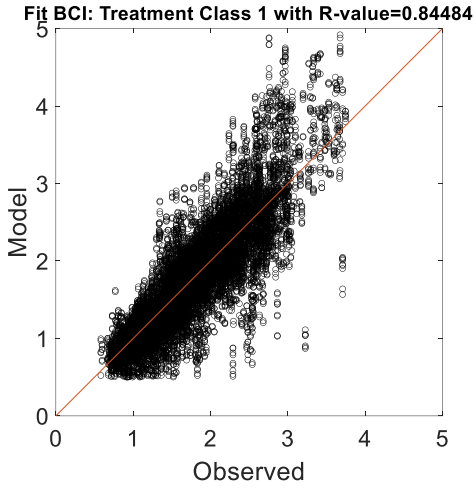

(b)

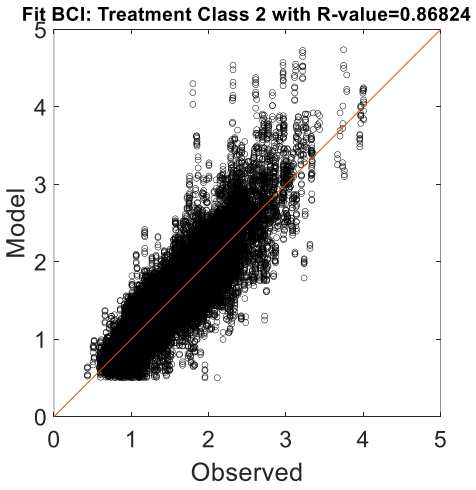

(c)

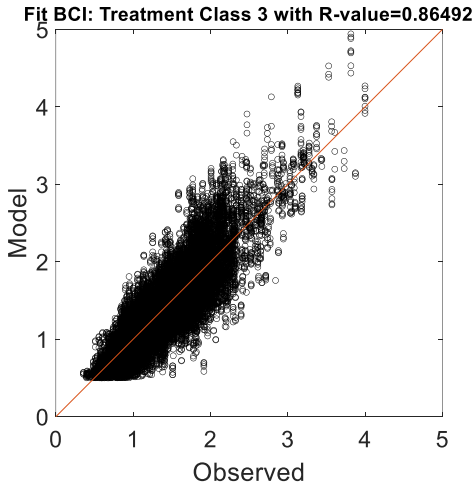

(d)

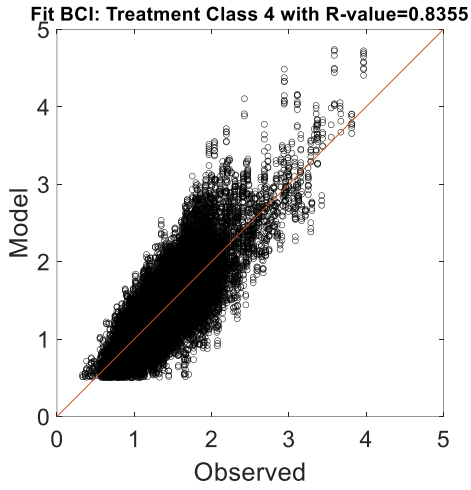

(e)

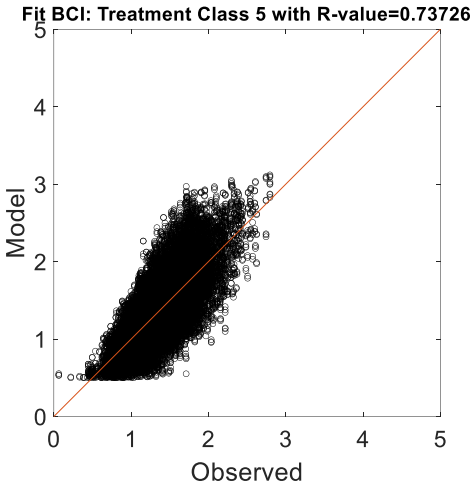

(f)

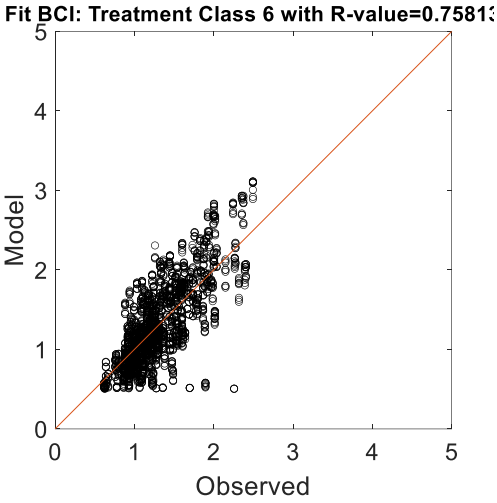

(g)

Figure 4-25 BCI prediction fit for different treatment groups

Table 4-12 summarizes the BCI Prediction model fit data for all treatment groups. The obtained BCI model fit R-Value ranges from 0.74 to 0.87. The model fit results for a more robust type of treatment showed a comparatively lower prediction capability than the lighter treatments.

Therefore, the recommendations from Section 4.4.2 can be adopted for better prediction capability for heavier treatment groups.

Table 4-12 Summary of the BCI Prediction Model Fit by Different Treatment Groups

Treatment Group	Description	Model Fit R-Value
0	Untreated Control	0.81
1	Crack Seal/ Fog Seal	0.84
2	Chip Seal/ Micro surfacing	0.87
3	Cape Seal (Chip Seal + Micro surfacing)	0.87
4	Conventional Thinlays	0.84
5	Thinlays Combined with Chip Seal/ Micro	0.74
6	CCPR/CIR	0.76

4.6 Chapter Summary

This Chapter demonstrated the processes involved with model selection, the effect of the controlling component of model fine-tuning, and prediction capabilities for both BDI and BCI models for different traffic conditions and treatment groups. The choice of the model is quite subjective, depending on the desired accuracy, availability of good quality data, the number of related variables, computational power, etc. The process flow and results indicated in this Chapter are unique for predicting the structural health of treated pavement sections where layer thickness data is unavailable. As a result, the FWD testing requirement for the overall network could be eliminated, saving significant agency resources. The results shown in this Chapter apply to the network-level management for small to medium size pavement networks focusing on planning pavement rehabilitation projects.

5 LIMITATIONS OF THE EXISTING STRUCTURAL CONDITION INDEX BENCHMARKING AND RECOMMENDED MODIFICATIONS

5.1 Existing Pavement Condition Benchmarking based on Deflection Basin Parameters

The use of deflection basin parameters for the structural condition assessment has been found useful when there is no thickness information available to backcalculate the layer moduli (*20*, *23*, *24*, *99*, *99–102*). Also, the backcalculation of the layer moduli requires specialized engineering judgment and access to specialized backcalculation software. Therefore, for the instances when limited thickness information is available, DBP benchmarking for the classification is helpful. Ullidtz et al. (*103*) and Horak et al. (*100*) have developed benchmarking systems which can be adjusted based on the required sensitivity. Pavement preservation treatments, by definition, are not intended to improve the structural condition of the pavement but rather to sustain the existing structural condition. The changes in the structural condition of the preservation-treated sections are very subtle in the early stage of application, but the effect can be significant over a long period of service life to reach the next condition category. The existing structural condition benchmarking systems are spread over a wide range of BDI and BCI values where the effect of pavement preservation treatments cannot be effectively captured from the structural condition standpoint. FHWA recommends a 3-tier scale for BDI and BCI (*102*), as shown in Figure 5-1. The recommended benchmark values were based on the study by Horak et al. (*24*), where no study was found to validate or evaluate the effectiveness of the present FHWA recommended benchmark values.

Figure 5-1 BDI and BCI benchmarking based on FHWA guideline

Pavement preservation treatments are applied to surfaces in "good" to "fair" condition. In contrast, surfaces in "poor" condition are subjected to the removal of the AC layer, which classifies as "pavement rehabilitation" (*104*). Figure 5-2 compares the Pavement Condition Rating (PCR) and the BDI for the Lee Road 159 test location. It is observed from the plot that over 75% of the observations remain in the "good" BDI region while the PCR rating ranges from 20 to 100. Therefore, any structural rehabilitation applied on a good pavement with "poor" PCR will overuse resources. On the other hand, not applying a rehabilitation activity to a weak pavement based on the PCR rating will lead to irreversible structural damage to the pavement. Based on the current rating classification of the structural health of pavement, it is very difficult to capture the classification of the exact structural condition. The requirement of a modified benchmarking method for BDI and BCI values is discussed in this chapter.

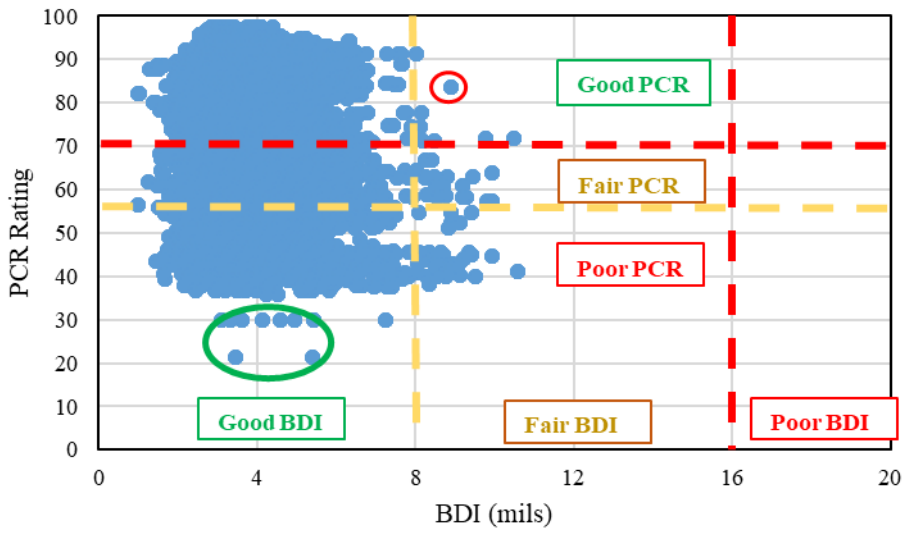

Figure 5-2 Pavement Condition Rating (PCR) vs. BDI plot for the Lee Road 159 test location

As shown in Figure 5-2, the observation identified by the red circle indicates a set of observations where the pavement is functionally in "good" condition but structurally in "fair" condition. On the other hand, observations within the green ellipse indicate "poor" functional condition but structurally "good" condition. Therefore, failing to apply rehabilitation activity in the first case will lead to more expensive repairs later on caused by structural damage. The latter case can lead to a misuse of resources as the functional condition of the pavement might be poor, but the structural condition is good. Therefore, any heavy rehabilitation or reconstruction performed based on the PCR rating would not be beneficial but rather a waste of valuable taxpayer money. Therefore, the need for a modified structural condition index classification can indicate that approaching the "fair" or "poor" condition of the pavement structure is identified.

5.2 Study DBP Results Based on Existing Benchmarking

The present study consists of deflection testing results from different test locations with up to 10 years of continuous deflection testing data. In addition, the study limited the treatment applied to the sections with “good” to “fair” structural conditions. No section in the “poor” condition received treatment. The BDI and BCI percentile plots for the entire length of the study are shown in Figure 5-3, where it is seen that more than 99% of the BDI and BCI values recorded in the study fall under the “good” category for both BDI and BCI. It is important to discuss that the scope of the study has been set to reform the benchmarking values for the structural condition parameters for the pavement structure, which can be restored or rehabilitated by applying pavement preservation or light rehabilitation treatments. Any observations beyond the “fair” region are subjected to major rehabilitation or reconstruction.

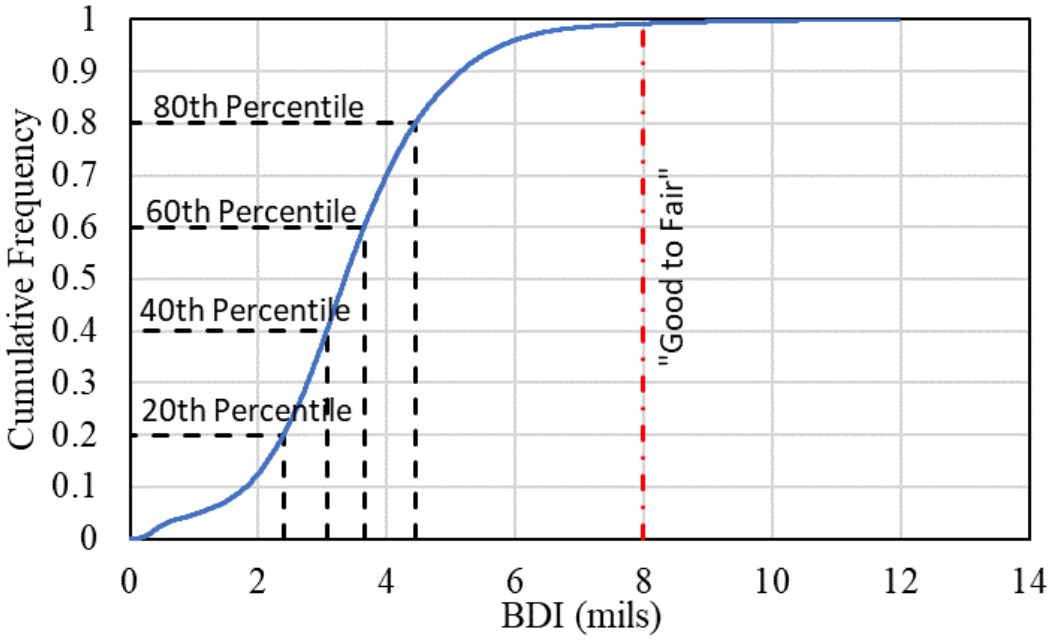

(a)

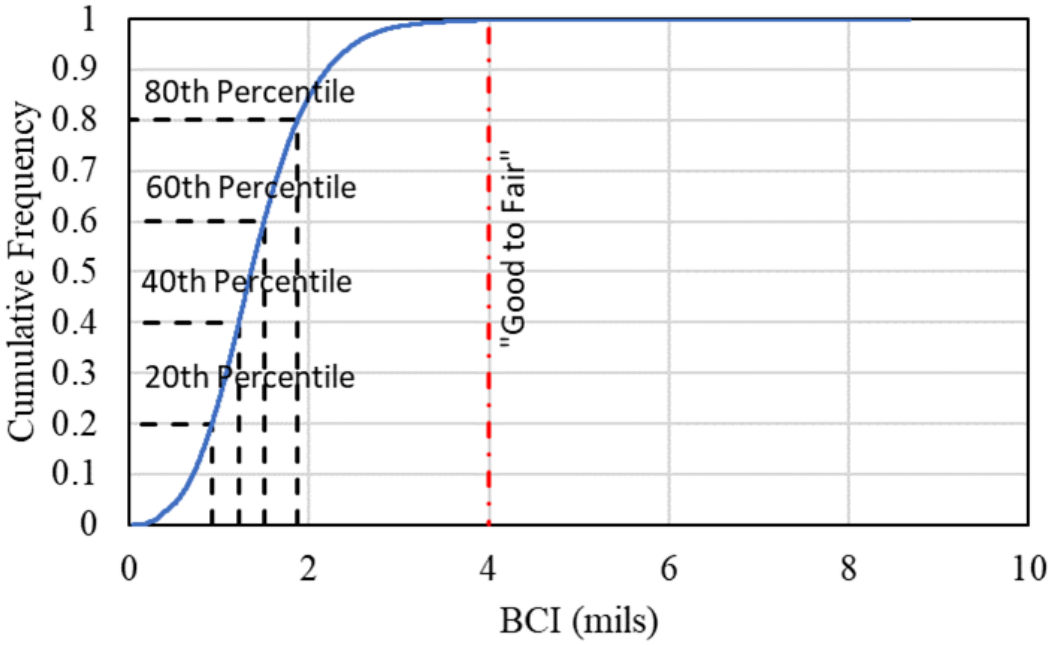

(b)

Figure 5-3 Study dataset cumulative frequency plot (a) BDI and (b) BCI

In network-level management, the surface and structural conditions should be harmonious to some degree to make overall decision-making easier and simpler. Further refinement of the DBPs benchmarking was found to be required as other condition parameters such as cracking, IRI, and rutting ranged across the “good”, “fair”, and “poor” condition categories.

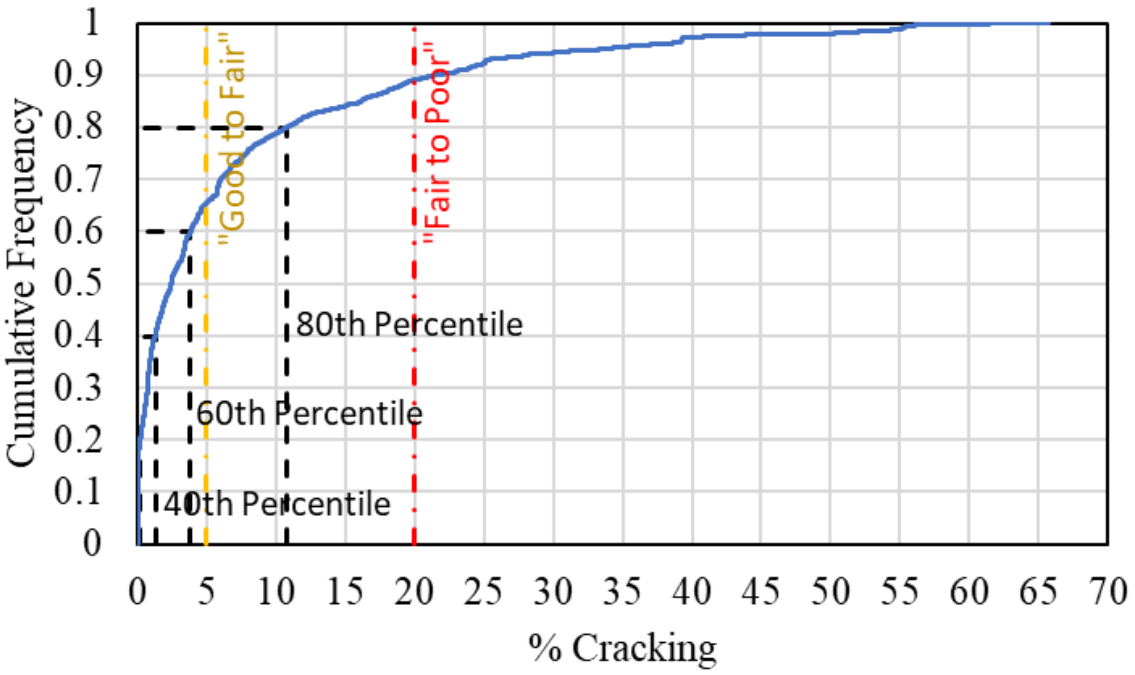
Cumulative Frequency
1
0.9
0.8
0.7
0.6
0.5
0.4
0.3
0.2
0.1
0
"Good to Fair"
"Fair to Poor"
80th Percentile
60th Percentile
40th Percentile
0 5 10 15 20 25 30 35 40 45 50 55 60 65 70
% Cracking

(a)

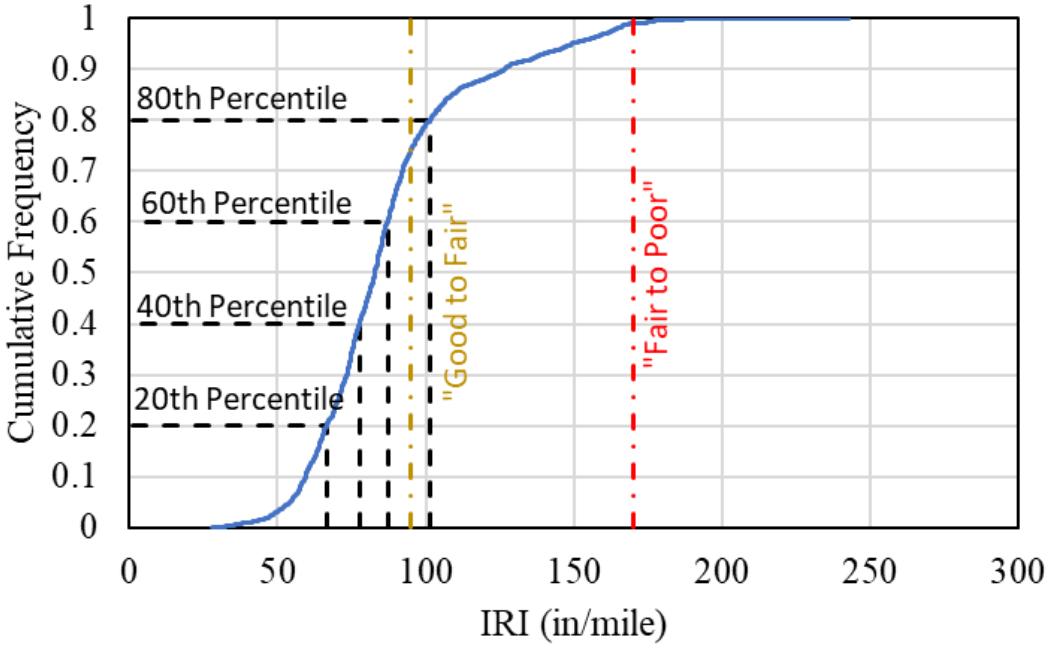
Cumulative Frequency
1
0.9
0.8
0.7
0.6
0.5
0.4
0.3
0.2
0.1
0
80th Percentile
60th Percentile
40th Percentile
20th Percentile
"Good to Fair"
"Fair to Poor"
0 50 100 150 200 250 300
IRI (in/mile)

(b)

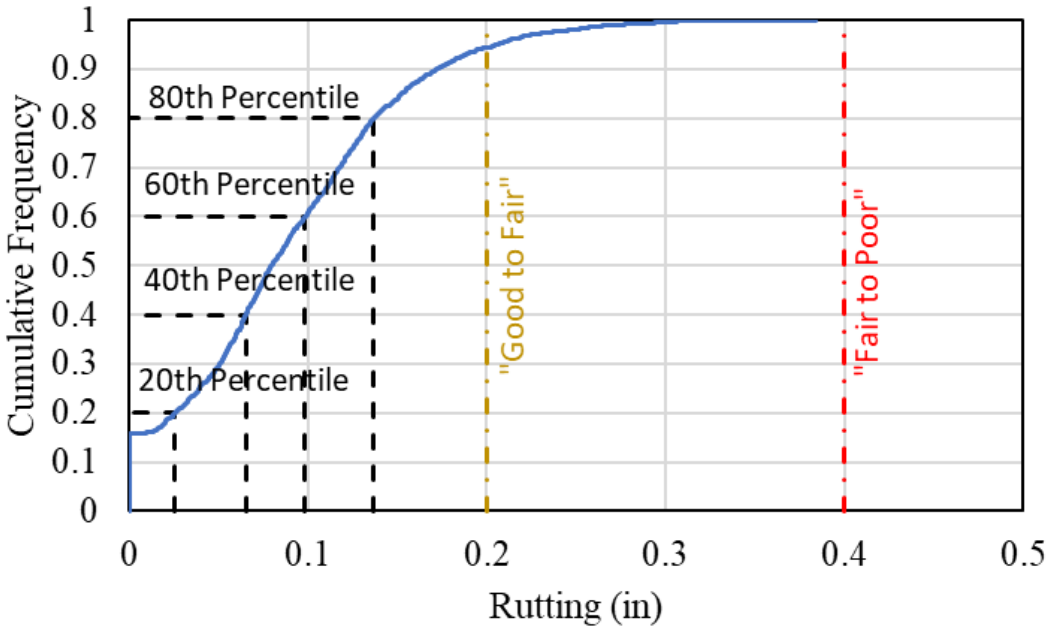

(c)

Figure 5-4 Cumulative frequency plot for (a) cracking, (b) IRI, and (c) rutting data included in the study and the FHWA designated benchmark values

Figure 5-4 indicates the percent cracking, IRI, and rutting values over the collected dataset range from “good”, “fair,” and “poor” categories of their respective benchmark values. A benchmarking system that is not sensitive enough to capture the effect of pavement preservation or too wide to assign all roads to the same class would not help the agency identify the roads that need structural repair or more robust preservation treatments. Establishing new benchmark values may be necessary to integrate pavement structural conditions into network-level management.

The BDI and BCI values for different traffic conditions were studied to determine if the reported BDI and BCI values follow a similar trend and fall into a similar range of classification based on the existing benchmarking. Figure 5-5 shows that over 95% of the observed BDI and BCI values are within the “good” region, while the other surface condition parameters have

reached the respective “fair” or “poor” conditions, as shown in Figure 5-4. This justifies the need for establishing new DBP benchmarks.

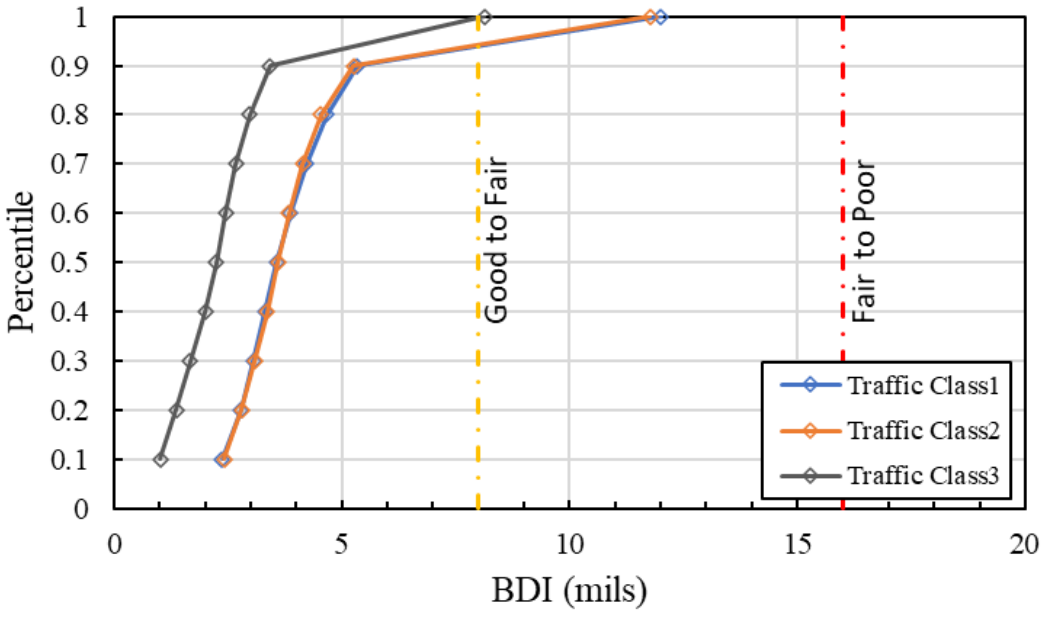

(a)

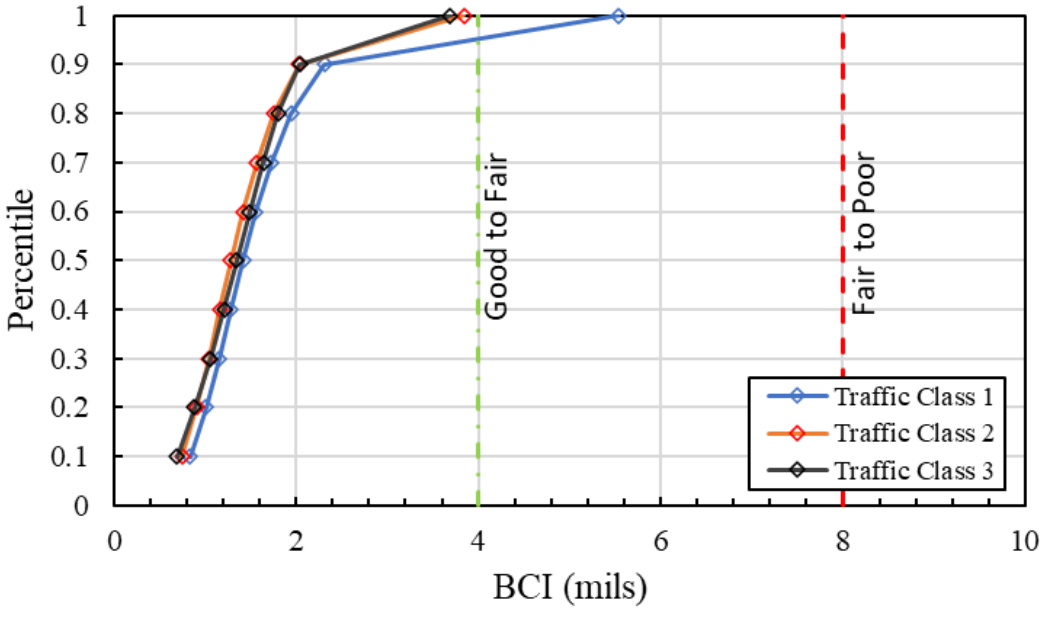

(b)

Figure 5-5 BDI and BCI percentile values for different traffic conditions

Based on the plots shown in Figure 5-4 and Figure 5-5, it is concluded that the surface condition index benchmarking and deflection basin parameter benchmarking are not synergetic. Therefore, to implement structural condition parameters in network-level management, the deflection basin parameters require modified benchmarking, sensitive to more subtle structural condition changes due to the application of preservation treatments.

5.3 Comparison of Surface Conditions vs. DBP for Different Traffic Conditions

This section compares the surface condition classification for cracking, IRI, and rutting to the structural condition classification. The term “initial traffic” indicates the pavement condition after treatment application, before a significant traffic load has been applied. On the other hand, the “post-traffic” condition indicates the pavement condition as of the last available data point of December 2021. The summary of the changes is shown in Figure 5-6. The color-coded bar charts indicate the “good”, “fair”, and “poor” conditions of the pavements for surface and structural condition parameters at different times for variable traffic conditions. It is worth mentioning that the benchmarking rules followed to generate the plots are the established benchmarking for cracking, IRI, rutting, BDI, and BCI. All the surface condition parameters throughout the study period changed the classes to reflect the deterioration due to applying traffic load, freeze-thaw cycles, and pavement aging. However, the DBP (BDI and BCI) values did not change their classes during the 10 years of service, with only an insignificant (<1%) amount of data indicating that the pavement structure deteriorated from “good” to “fair”. The comparison shown in Figure 5-6 establishes the lack of synergy between the benchmarking across the condition variables and reinforces the claim of reorganizing the present benchmarking method for BDI and BCI.

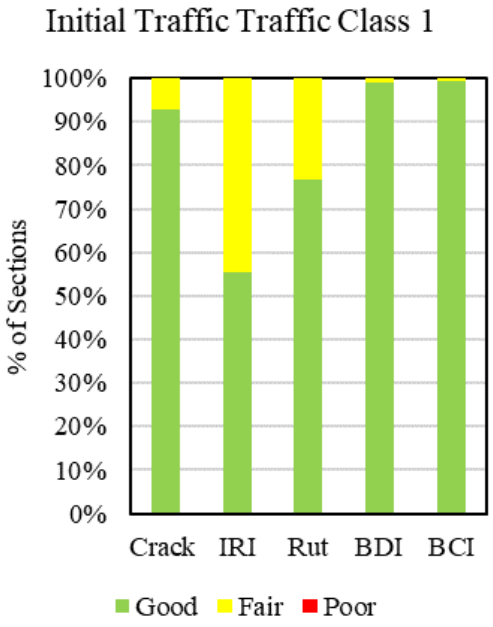
Initial Traffic Traffic Class 1
% of Sections
100%
90%
80%
70%
60%
50%
40%
30%
20%
10%
0%
Crack
IRI
Rut
BDI
BCI
Good
Fair
Poor

(a)

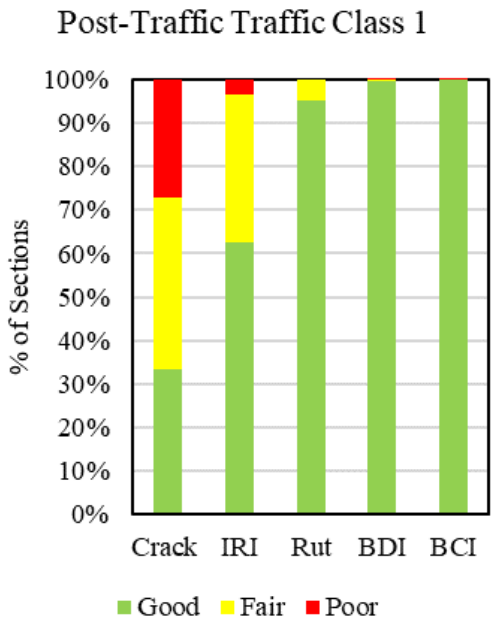
Post-Traffic Traffic Class 1
% of Sections
100%
90%
80%
70%
60%
50%
40%
30%
20%
10%
0%
Crack
IRI
Rut
BDI
BCI
Good
Fair
Poor

(b)

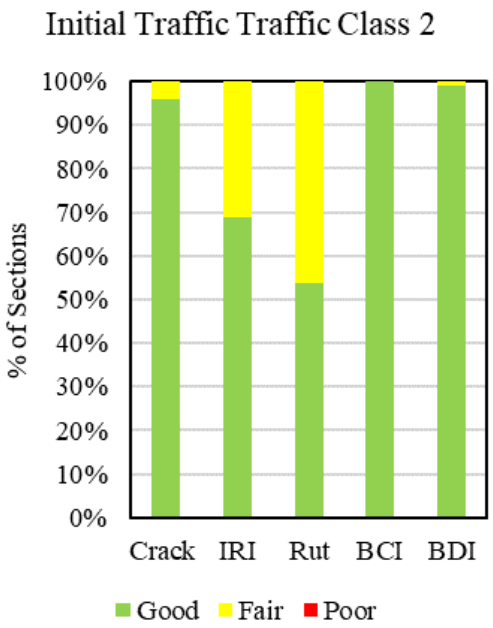
Initial Traffic Traffic Class 2
% of Sections
100%
90%
80%
70%
60%
50%
40%
30%
20%
10%
0%
Crack
IRI
Rut
BCI
BDI
Good
Fair
Poor

(c)

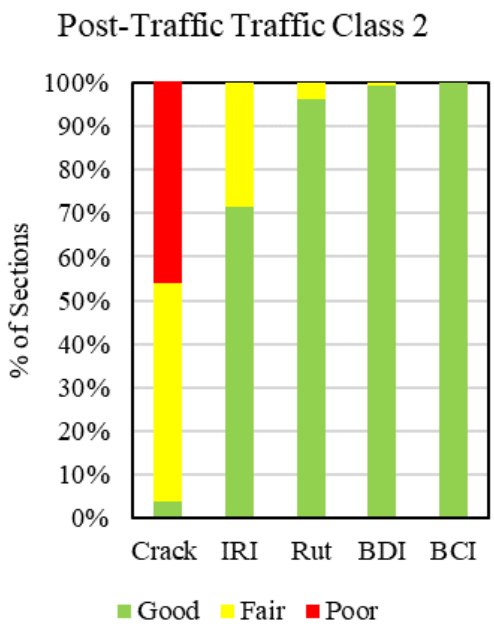
Post-Traffic Traffic Class 2
% of Sections
100%
90%
80%
70%
60%
50%
40%
30%
20%
10%
0%
Crack
IRI
Rut
BDI
BCI
Good
Fair
Poor

(d)

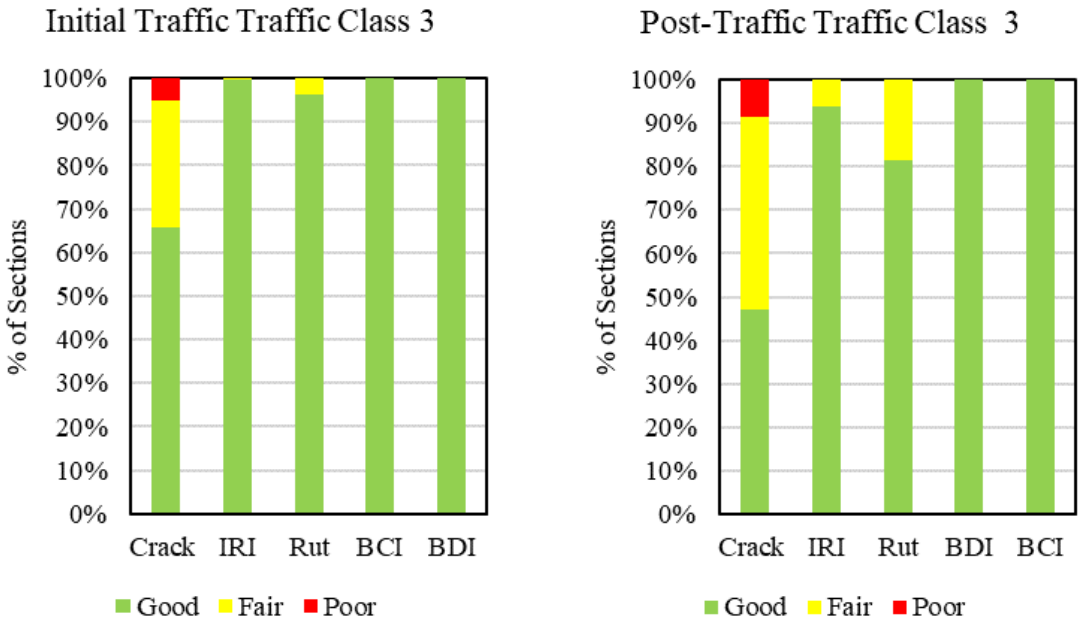

(e) (f)

Figure 5-6 Comparison of pavement condition parameters at a variable time and traffic conditions

Figure 5-7 shows the changes in surface conditions over the data collection period for heavy traffic conditions, where the deterioration is faster than in the other two traffic locations. Also, the effect of treatment type on the deterioration is inspected and compared. It is observed in Figure 5-7(a) and (b) that for the light treatments, initially, 72% of the sections were in the "good" cracking category, while in the post-traffic condition, 12% were in the "poor" category and 50% in the "fair" category. In addition, 20% of the sections changed the rutting condition from "good" to "fair". In contrast with the cracking, IRI, and rutting conditions, the DBPs did not exhibit category changes based on the existing benchmarking system. Also, a similar conclusion can be made in Figure 5-7 (c) and (d), where cracking and rutting conditions were observed in the sections treated with heavy and robust treatments such as thinlays and recycled bases. 35% of the sections

changed from “good” to “fair” cracking category and 5% of the sections changed their cracking class from “fair” to “poor” cracking category. Rutting was reduced from 55% in “good” category to 95% in “good” category after 9 years of traffic application. Meanwhile, the DBPs remained in the same condition category despite such changes.

After investigating the changes in the functional condition parameters, it can be summarized that the structural condition benchmarking is insensitive to the changes in the functional condition, and the benchmarking method needs to be modified.

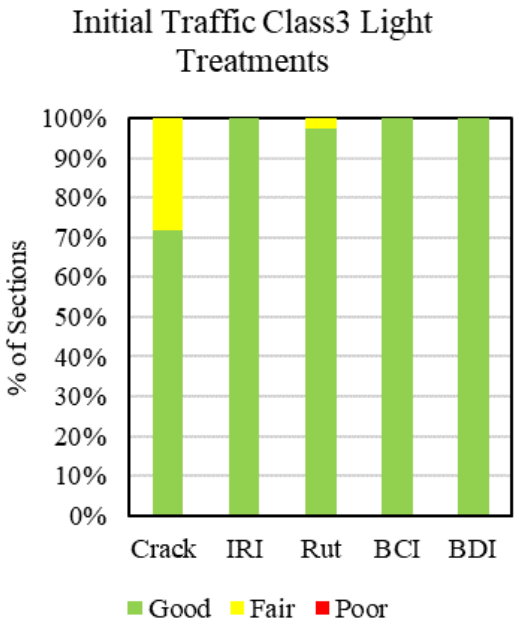

(a)

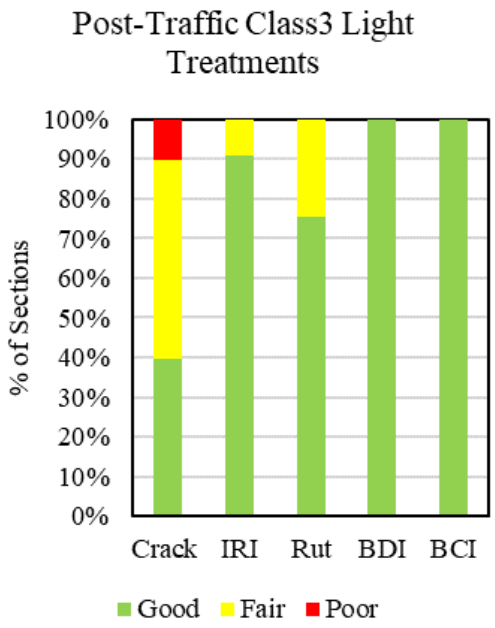

(b)

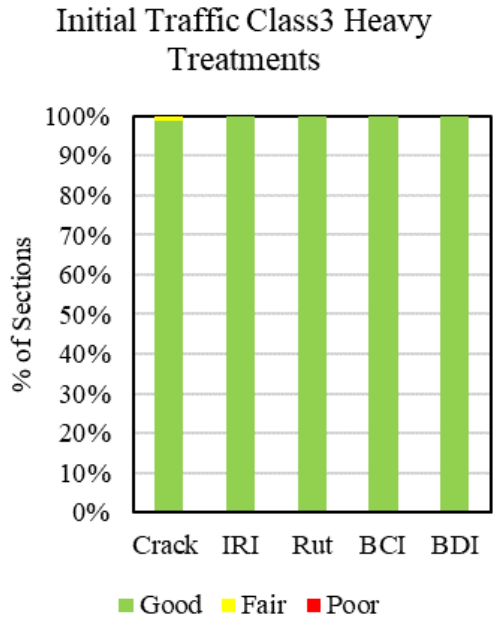

(c)

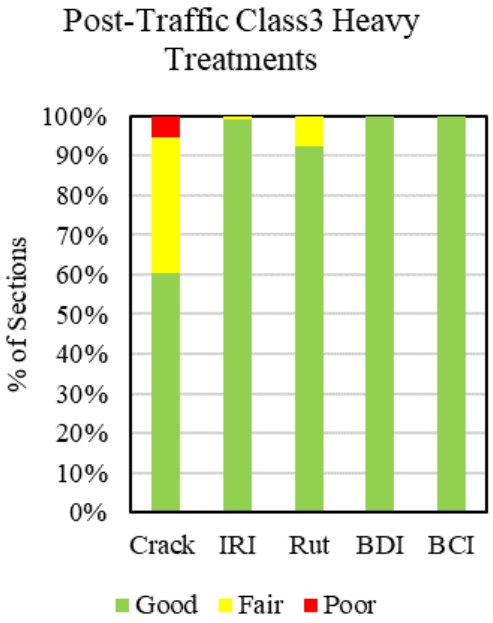

(d)

Figure 5-7 Comparison of initial and present condition classes for light and heavy treatments (heavy traffic conditions only)

5.4 Effect of Preservation Treatments on Surface Condition Parameters

Before adjusting the DBP benchmarking, it is important to verify if the changes in other condition parameters were significant over the study period to determine what percentage of sections or observations changed from "good" to "fair", "fair" to "poor", or "good" to "poor" condition. For example, Figure 5-8 shows the difference in cracking, IRI, and rutting values in pre-application, immediately after application, and over the service period after treatment application. The cracking plots in Figure 5-8 (a) indicate that over 50% of the sections were in the "good" region when the treatments were applied. After treatment application, 92% of the sections were in "good" condition at the end of the first year of service. Currently, 60% of the sections are in "good" condition, and 15% have reached the "poor" region. To summarize, over the service life

in this study, the cracking distribution of the sections (including the control sections) has indicated that 85% of the observations of cracking measurement were still lower than the pre-treatment condition.

For the IRI plots in Figure 5-8 (b), it was observed that IRI distribution has not changed from the first year of treatment to the end of data collection as of this date. The 90th percentile IRI value at Pre-treatment, end of the first year of service, and end of the analysis period are 103.83 in/mile, 120.66 in/mile and 127.76 in/mile, respectively. Figure 5-8(c) indicates the rutting percentile plots at different time stamps of the study period. After the treatments were applied, the rutting percentile curve shifted to the left, which indicates improvement in the rutting condition due to the treatment application. Throughout the study, the rutting percentile plot did not shift to the right indicating a rise in the rutting value on the treated sections. Observed values indicated no sections in "poor" rutting conditions during the study.

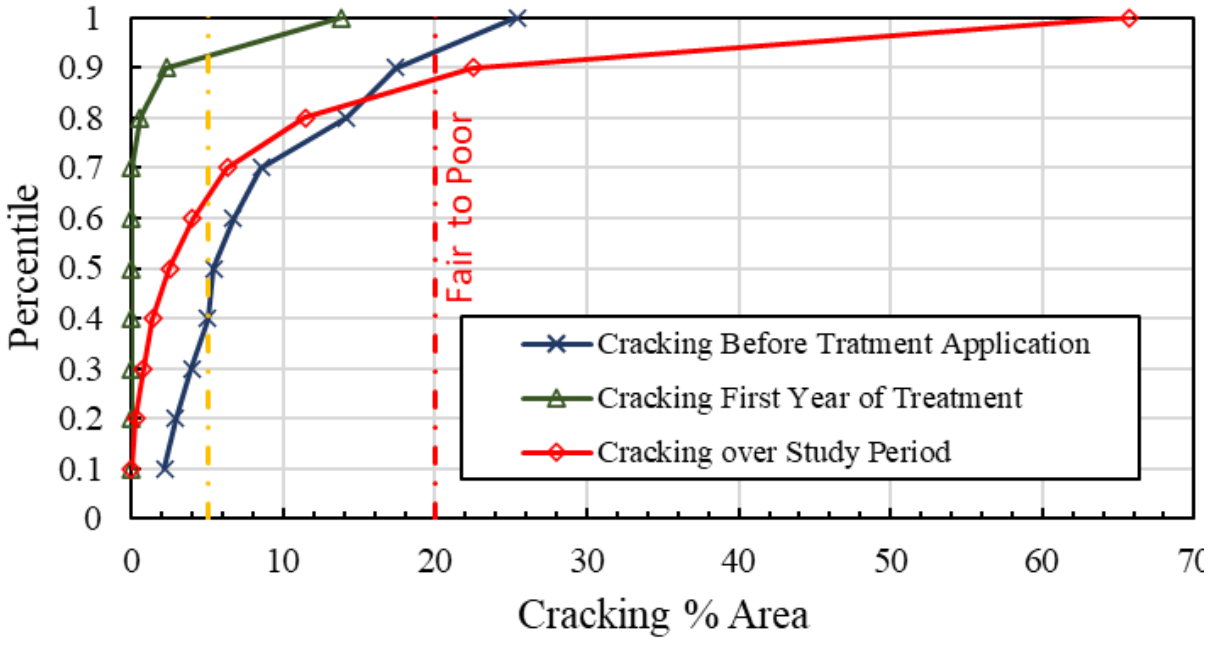

(a)

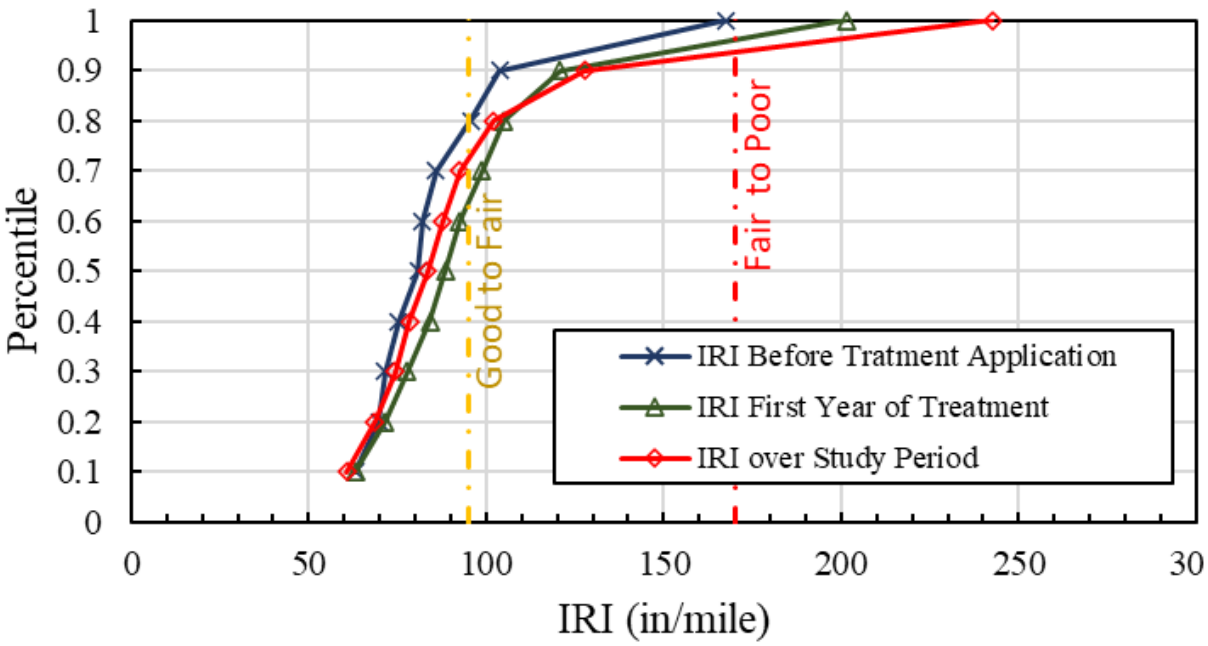

(b)

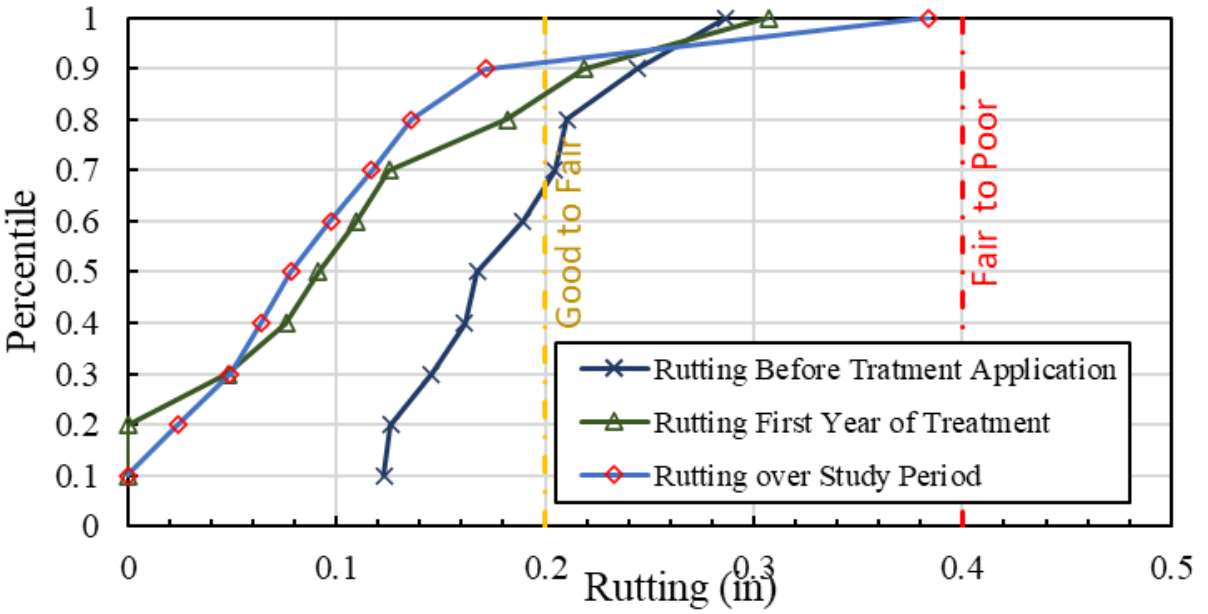

(c)

Figure 5-8 Cumulative frequency plot for (a) cracking, (b) IRI, and (c) rutting for pre-application, post-application and over the study period

5.5 Recommendation of New Benchmarking Values

Based on the discussion of results in the previous sections, it is understood that the FHWA recommended BDI and BCI benchmarking classes are not exhibiting any sensitivity to the changes due to the slight improvement of the pavement structure. In addition, as discussed in the background, the preservation treatments do not add to the structural capacity of the pavement structure, but the sealing of cracks and correcting minor distress lead to a slower rate of structural deterioration. Therefore, the FHWA recommended benchmarking value for BDI and BCI needs to be reclassified to capture any structural benefit due to the slowing of the structural deterioration resulting from the application of preservation treatments.

5.5.1 Modified Benchmarking System for BDI

Based on the data employed in the neural network model training and the percentile values shown in Figure 5-3 (a) and (b), intermediate or transitioning benchmark ranges are proposed in the present study. To benchmark the BDI values, intermediate ranges are proposed to split the existing ranges into several more ranges. For example, in contrast with the existing classification, the proposed benchmarking of BDI recommends splitting the "good" BDI region into "excellent", "very good," and "fair". The remaining benchmark classification of BDI for "warning" and "poor" remains the same. Side-by-side comparisons of the existing and recommended benchmarking are shown in Figure 5-9. The proposed 5-tier classification for BDI would help classify subtle changes within the range of BDI values, including identifying and incorporating the changes in structural conditions due to the application of preservation treatments. The proposed changes provide more sensitivity to the benchmarking system than the existing one. The present study collected pavement condition information from over 10 years of in-service under live traffic load in low-volume and

high-volume traffic conditions. Moreover, the sections are located in both warm and cold weather regions. Therefore, the performance data analyzed in the present study represents a broad range of weather and traffic conditions in the United States.

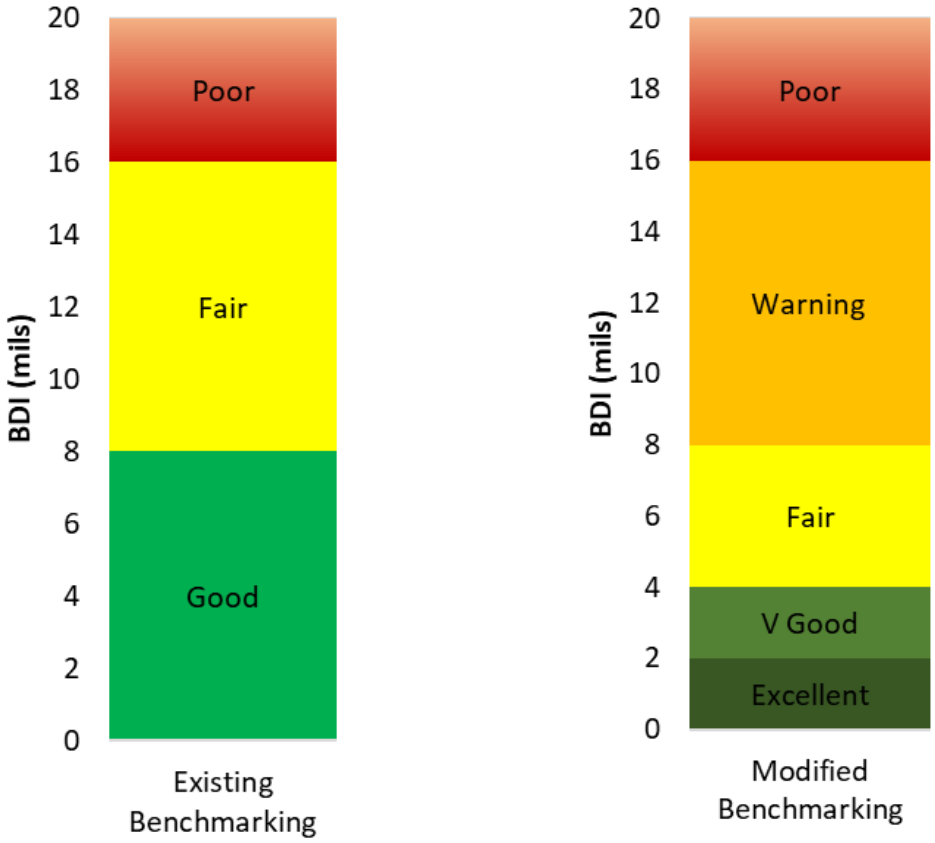

Figure 5-9 Existing and proposed benchmarking of Base Damage Index (BDI)

As shown in Figure 5-9, the "good", "fair," and "poor" regions of the existing benchmarking system got split into several subranges in the proposed benchmarking system. Eventually, the broader range of values is similar to the existing benchmark recommended by FHWA. The "warning" region starts at 8 mils in the modified benchmarking systems, while the "poor" region also starts at 16 mils for the existing and proposed benchmarking. Figure 5-10 compares the observed and modeled BDI values distribution based on (a) current and (b) modified

benchmarking. It is observed from the plot that 100% of the observed and model-predicted BDI values fall within the "good" BDI region based on the current benchmarking system. While comparing with the modified benchmarking system, the "excellent", "very good," and "fair" classes contain respectively 8%, 60% and 30% of the observation and model BDI values.

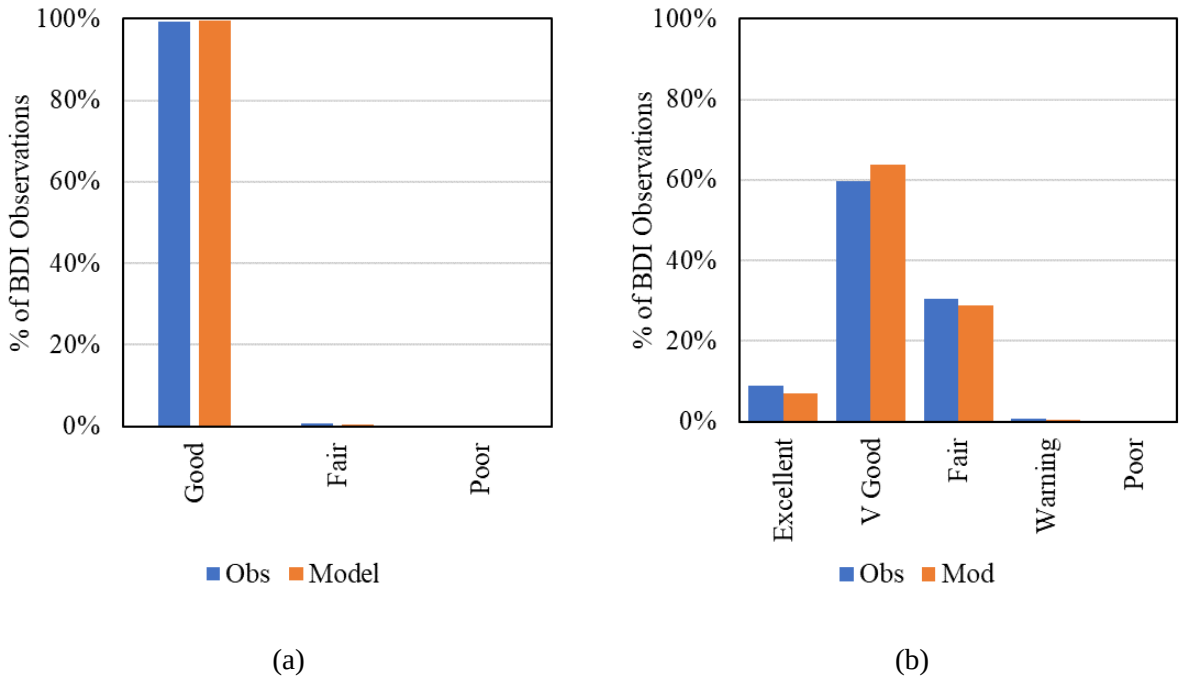

(a) (b)

Figure 5-10 Comparison of distribution for BDI observation and model values based on the (a) Current benchmarking, (b) Modified benchmarking system

As shown in Figure 5-10, the modified benchmarking system allows more separation of the BDI values to capture the base layer structural health of the pavement. Further refinement can be possible to capture more ranges of BDI values for severely distressed pavements which fall within the "warning" and "poor" regions. As the present scope of the study is limited to pavement preservation, the target pavement structure for treatment application was targeted for the sections either in "good" or "fair" condition.

5.5.2 Modified Benchmarking System for BCI

A similar approach was taken for the BCI benchmarking; the broader ranges of "good", "fair", and "poor" remain identical to the existing benchmarking, and a few intermediate ranges were introduced. Figure 5-11 shows the side-by-side comparison of the existing and proposed benchmarks for the BCI. As discussed, the "fair" regions start at 4 mils for both benchmarking systems, and the "poor" region starts at 8 mils. The 4-tier proposed benchmarking for BCI allows for capturing subtle changes in the subgrade condition.

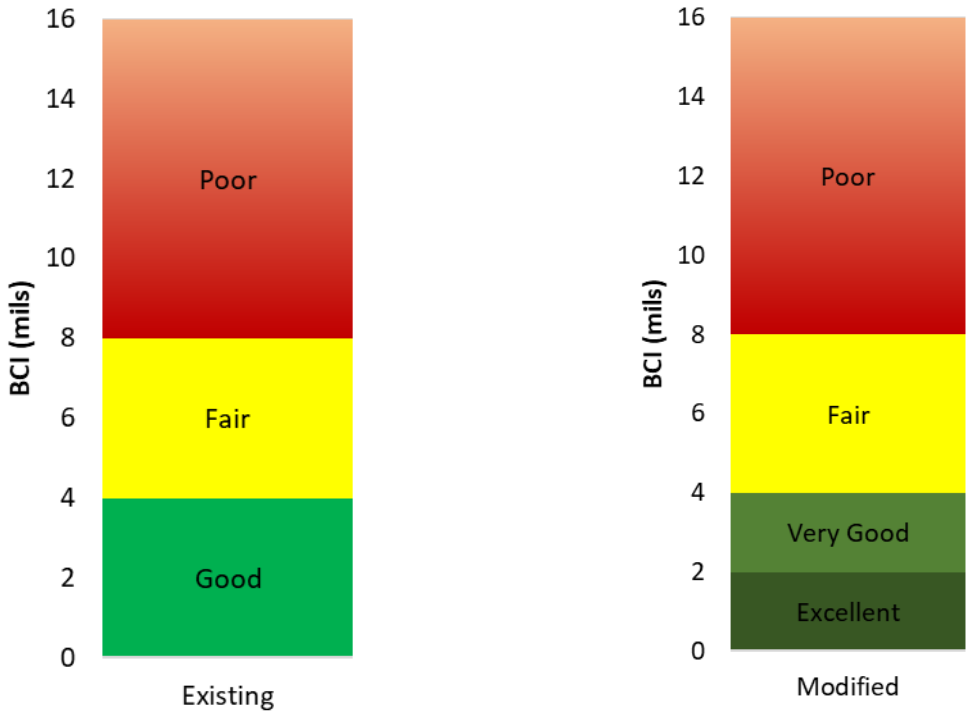

Figure 5-11 Existing and proposed benchmarking of Base Curvature Index (BCI)

The comparison of BCI distribution of the observed and model-predicted BCI values based on the (a) current and (b) modified benchmarking of BCI are shown in Figure 5-12 – a similar segregation of the BCI classes was observed in Figure 5-10 for BDI values. A 100% "good" BCI

value was split between 82% of "excellent" and 17% of "very good" classes based on the modified benchmarking system.

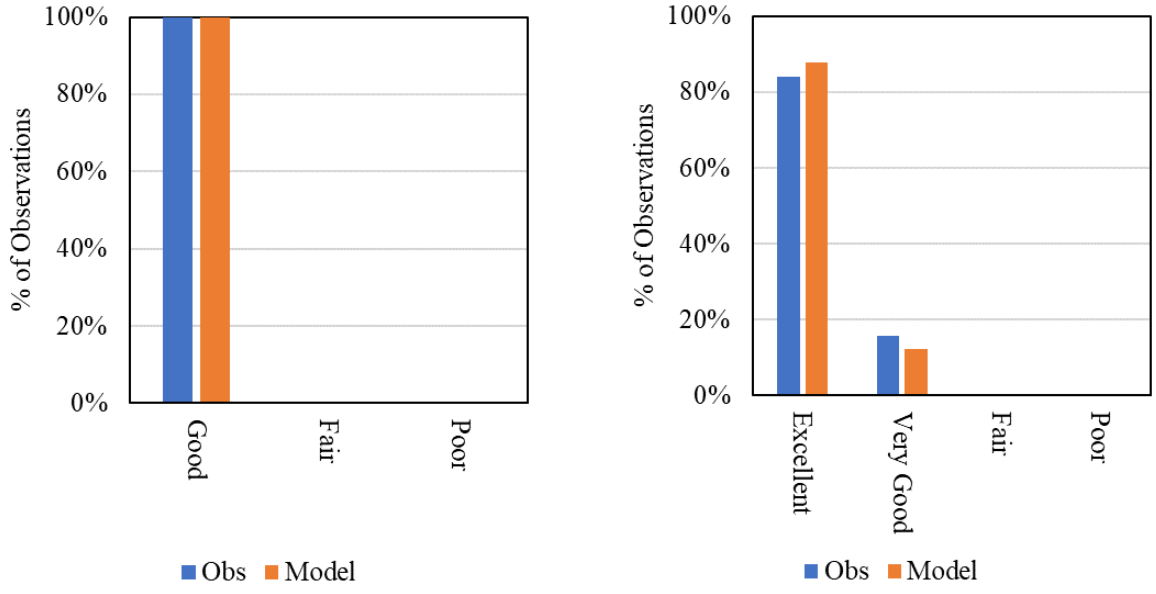

(a) (b)

Figure 5-12 Comparison of distribution for BCI observation and model values based on the (a) current benchmarking, (b) modified benchmarking system

The modified benchmarking system allows the network management planning to incorporate specific types of treatment for a specific range of structural conditions compared to the current benchmarking, which implies "one condition category for all sections" from the present study.

5.5.3 Unified BDI and BCI Benchmarks "Combined Structural Health"

Once the structural condition of the base layer is based on BDI and subgrade based on the BCI while implementing the classes into a PMS, a unified benchmark or ranking is much needed to determine a single input class that represents both the health of the base and subgrade layer. The

goal was achieved by summing up the BDI and BCI values at an equal weightage. The assumption between equal weightage for BDI and BCI is that if the pavement is in worsening base layer condition, the load distribution on the subgrade will be concentrated, leading to premature structural deterioration. A relationship between BDI and BCI is shown in Figure 5-13 and Figure 5-14. The thin layered pavement is considered those with a total pavement thickness of less than 12" on top of the subgrade. Any pavement structure with a cross-section thicker than 12" is considered thick layered pavement.

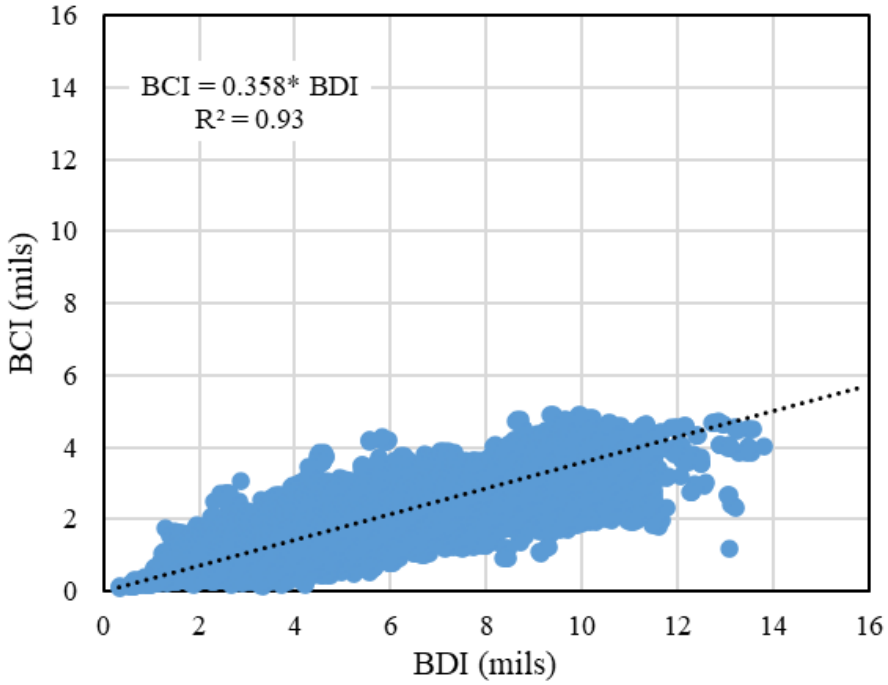

Figure 5-13 Relationship between BDI and BCI for thin layered pavements

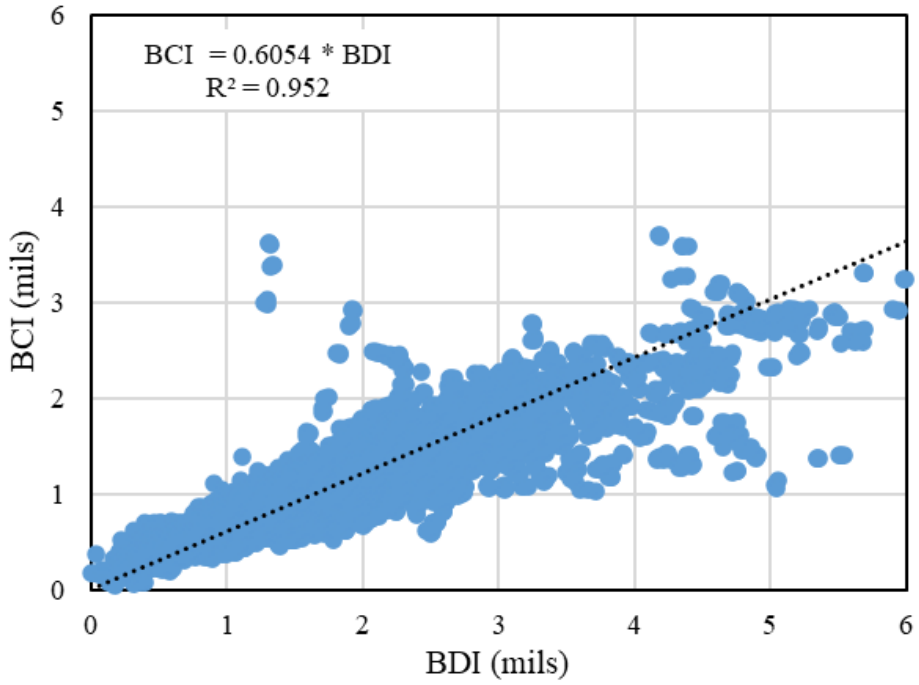

Figure 5-14 Relationship between BDI and BCI for thick layered pavements

As shown in Figure 5-13and Figure 5-14, the BDI and BCI values are well correlated with R^2 value of 0.93 and 0.95 respectively for thin and thick layered pavements. As they are highly correlated numerically, it can be assumed that any pavement with worsening base layers condition also shows a higher tendency to exhibit worsening subgrade layer condition. To establish a unified benchmarking scale for the overall structural health of the pavement, equal weightage for the BDI and BCI is applied. Thus, the combined structural health score is shown in Figure 5-15.

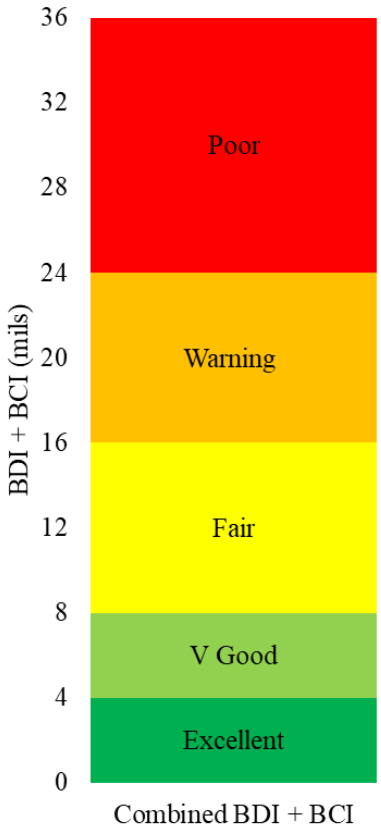

Figure 5-15 Combined benchmarking for BDI and BCI for structural condition

A unified score allows the incorporation of the overall structural health into one benchmarking unit. The combined structural health benchmarking can be implemented into a PMS as a deciding factor for the structural condition of the pavement.

5.6 Application of NN Prediction Methodology on Proposed Benchmarking

The previous chapter discusses the application and accuracy of neural network methodology in predicting BDI and BCI values. The results indicated that trained neural networks can predict the BDI and BCI values with over 80% accuracy. The present section investigates if splitting benchmarking categories for BDI and BCI from the proposed benchmarking system adversely affects the modeled output classification. For example, the “excellent” category ranges

from 0 to 2 mils for the BDI and BCI for the modified benchmarking. If the model prediction tolerance is more than 2 mils, some of the "Excellent" class observations will be predicted as a "very good" class by the model, which increases the percentage of misclassification and leads to a failure in the PMS decision tree. The observed and predicted value tolerance should lie within the narrowest classification group of the benchmarking system (2 mils). Figure 5-16 shows the percentile plots for training and model output for BDI and BCI.

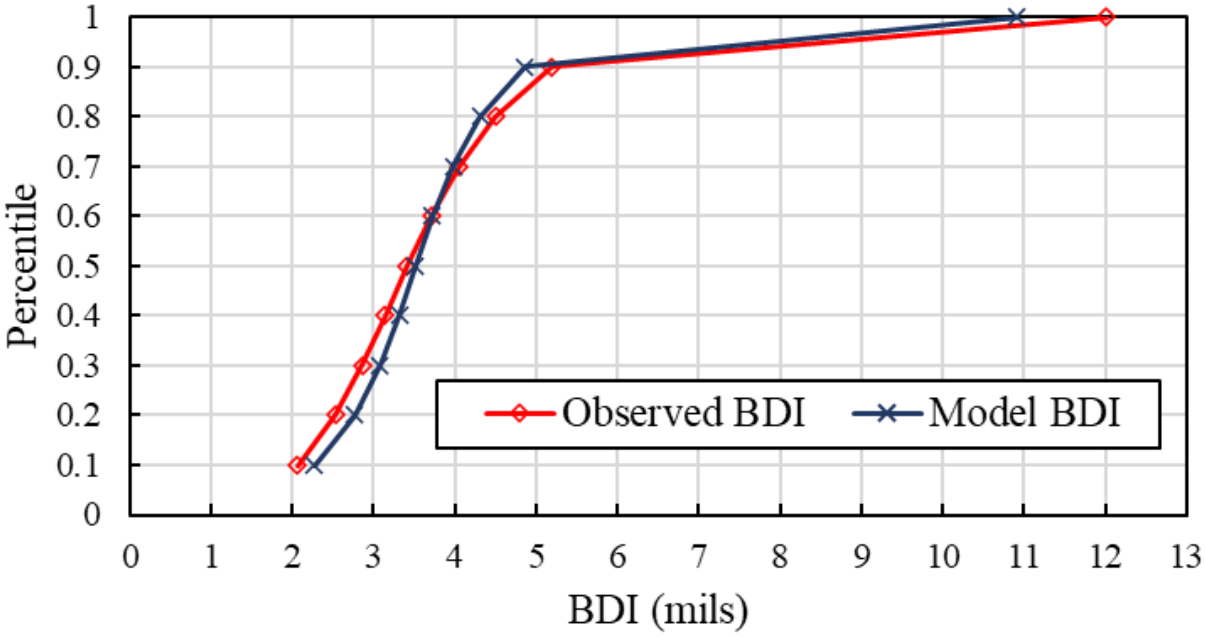

(a)

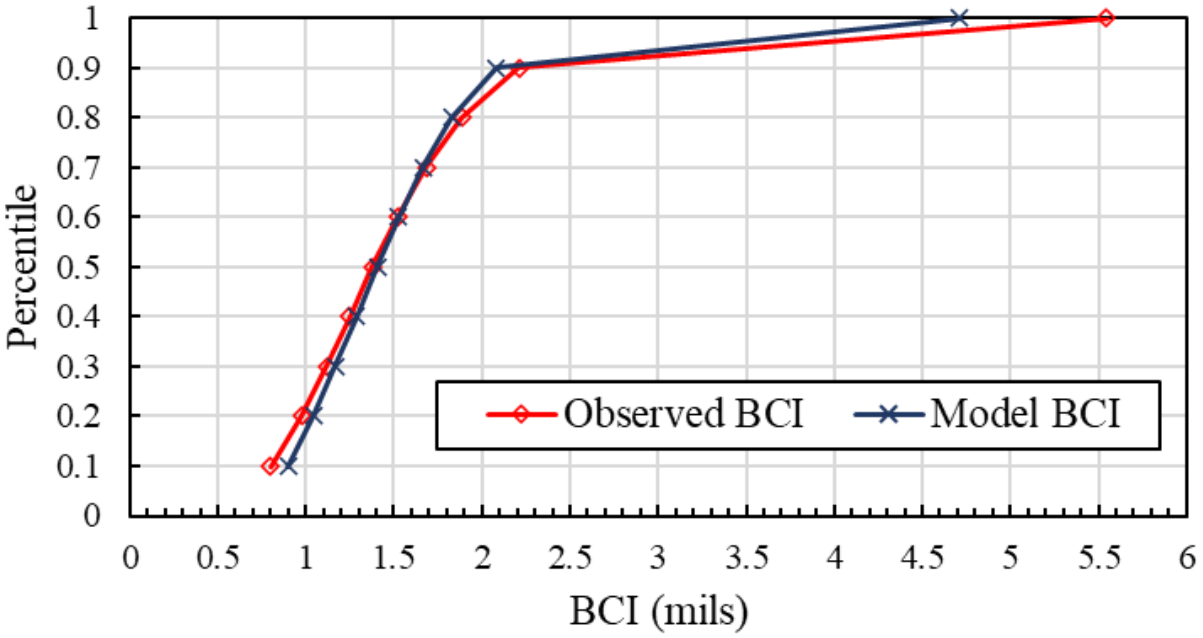

(b)

Figure 5-16 Percentile plot for (a) BDI and (b) BCI comparing observed and trained model outputs

As shown in Figure 5-16, the percentile plots for the observed and predicted values lie within the narrowest classification range (2 mils). Therefore, the observed and predicted values distribution should be as close as possible but not compromise the risk of overfitting. The objective is to combine the model prediction values and proposed benchmarks to detect the percentage of observations that the neural network trained model misclassified. It is important to mention that no segment was within the "poor" region in the existing classification for both BDI and BCI. Therefore, the prediction and classification accuracy within the "poor" classification is difficult to conclude at this data collection stage. Furthermore, the cracking performance of some of the test segments reached "poor" conditions at the end of the analysis period while the structural condition of those treated sections was still in "good" or "fair" condition, which means the issue is from the surface of the pavement but leading to structural damage to the pavement structure by letting

moisture get into the pavement structure through the cracks. Previous research based on ARIMA models developed for the same test sections (*9, 10*) predicted that the age when the BDI and BCI are expected to reach the "poor" classification is beyond 10 years old, which is over the expected life expectancy of the preservation treatments (*105*).

5.6.1 Classification Results for BDI

The classification matrix comparing the observed and model BDI values were populated using all the training data (200,189 data points) of observed and predicted outputs. Results indicated that the neural network model could accurately capture over 80%, 80%, 72% and 87% of the classification for the "excellent", "very good", "fair," and "warning" regions, respectively. Figure 5-17 shows the classification matrix for the BDI prediction model, a simple representation of the confusion matrix used for neural network classification problems.

Observed / Model	Excellent	V Good	Fair	Warning	Poor
Excellent	80%	5%	0%	0%	0%
V Good	20%	80%	26%	0%	0%
Fair	0%	15%	72%	13%	0%
Warning	0%	0%	2%	87%	0%
Poor	0%	0%	0%	0%	0%

Figure 5-17 Class prediction matrix for BDI based on proposed benchmarking

5.6.2 Classification Results for BCI

The classification matrix comparing the observed and predicted BCI values were also populated using all the training data of observed and model outputs. Results indicated that the neural network model could accurately capture over 92%, 72% and 83% of the classification for the "excellent", "very good," and "warning" regions. Also, there is no data point in the "poor" classification within the matrix as in the training dataset, as there was no BCI observation to reach the "poor" condition in the classification. The misclassification matrix for the BCI values based on the new BCI benchmarking is shown in Figure 5-18.

Observed / Model	Excellent	Very Good	Warning	Poor
Excellent	92%	27%	0%	0%
Very Good	8%	72%	17%	0%
Warning	0%	1%	83%	0%
Poor	0%	0%	0%	0%

Figure 5-18 Class prediction matrix for BCI based on proposed benchmarking

Regarding the misclassifications in Figure 5-17 and Figure 5-18, there is some misclassification where a percentage of observations were assigned to the upper or lower class in the model compared to the observed class. There is no tool to achieve 100% accuracy unless the model is heavily over-trained. One downside of over-training is the failure to predict numbers

based on unseen feature values. The misclassification results from a trade-off between bias and generalization in neural network modeling.

5.7 Summary of the Chapter

A revised and more sensitive classification system targeting the preservation treatments is required to integrate the structural condition parameter in network-level management. This methodology is a demonstration of how the objective can be achieved. Based on the available dataset, no section reached the “poor” condition of the existing or proposed classification system. Therefore, the proposed classification and neural network could identify the correct classification with an accuracy of 75% and 88% for BDI and BCI, respectively.

6 INCORPORATION OF STRUCTURAL CONDITION INTO THE PAVEMENT MANAGEMENT DECISION TREE

The final objective of the present study is to validate the functional and structural benefits of pavement preservation treatments and incorporate the benefits into the PMS decision tree. The key components driving the decision are the PCR score and the structural condition index. The functional and structural benefits are captured during the study period as individual treatments, and the treatment class is mentioned in section 3.2.4. The present chapter discusses the effectiveness of the preservation treatments towards a certain mode of distress, quantifying the life extension benefit and, finally, incorporation of the structural and functional condition of the pavement into the PMS decision tree.

6.1 Functional Benefit Validation

The Pavement Condition Rating (PCR) discussed in Section 3.5 has been adopted in the present study to identify the overall functional condition of the pavement. If the PCR is over 90, it means the overall functional condition of the pavement is adequate and can be recommended for the “Do Nothing” class. In the next step, it is checked if any of the indices within the PCR rating is below 55. Then the index with the lowest value is assumed to be the dominant distress for that section. This methodology identifies if any specific type of treatment is less effective or inefficient in mitigating any specific type of distress. Figure 6-1 shows the process flow diagram to identify the dominant distresses based on the PCR value.

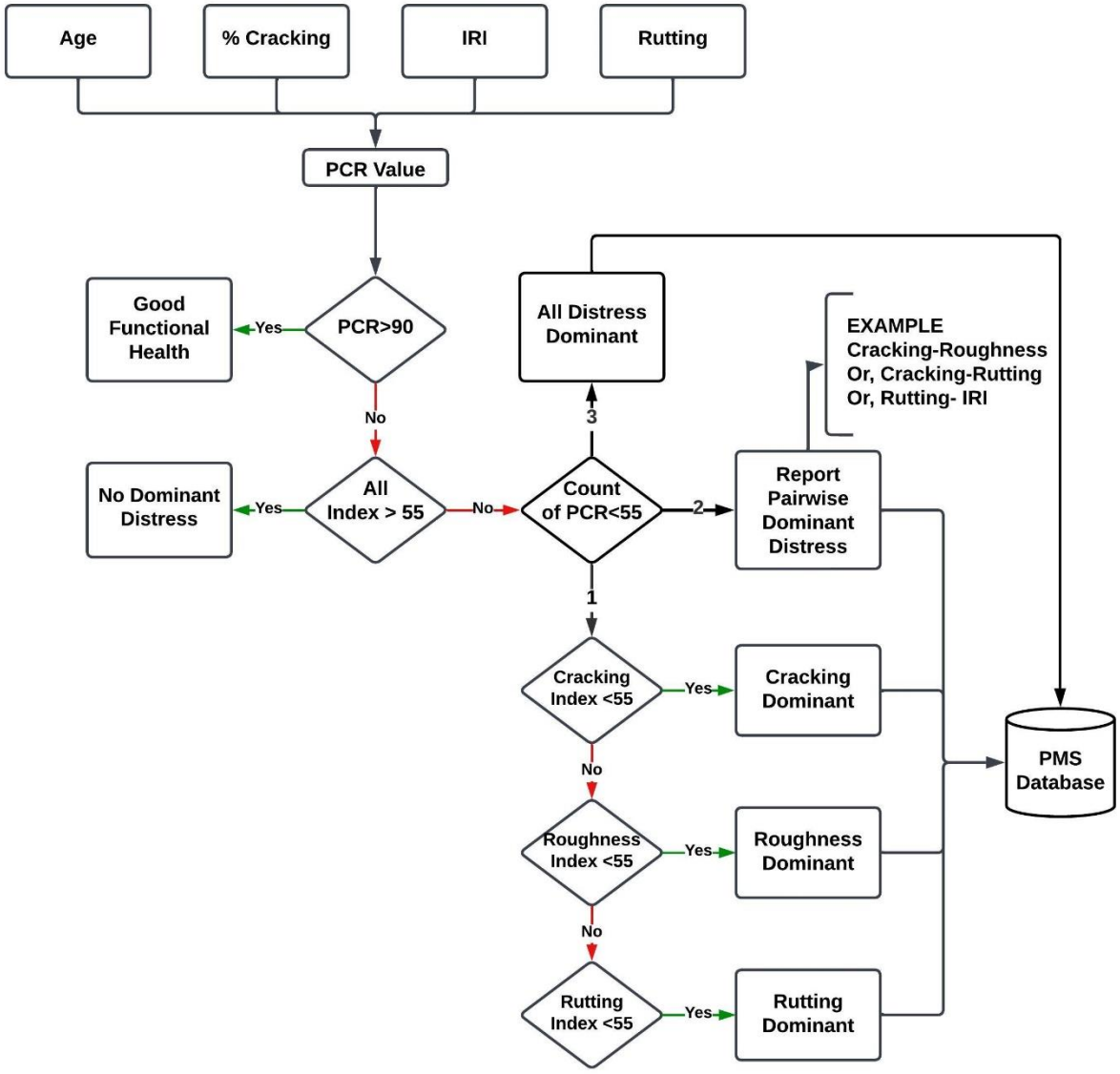

Figure 6-1 Process of determining dominant distress in pavement based on PCR

The dominant distress was identified for all the treatment locations throughout the analysis period. The percentage of sections containing dominant functional distress and also the percentage of sections in good condition are shown in Figure 6-2.

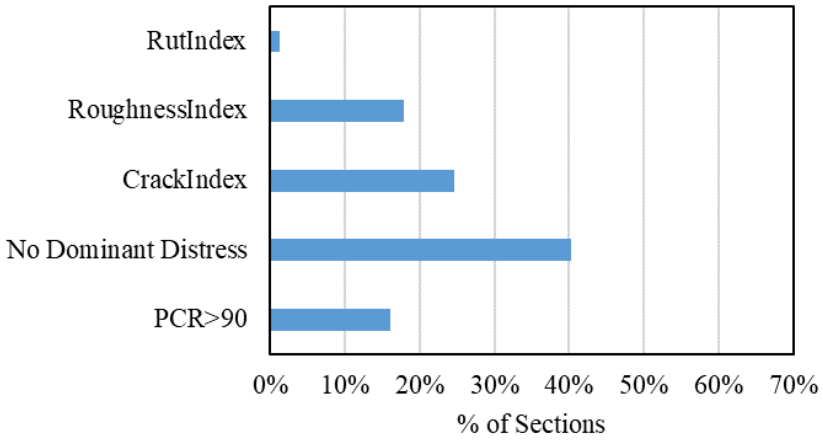
RutIndex
RoughnessIndex
CrackIndex
No Dominant Distress
PCR>90
0%
10%
20%
30%
40%
50%
60%
70%
% of Sections

(a)

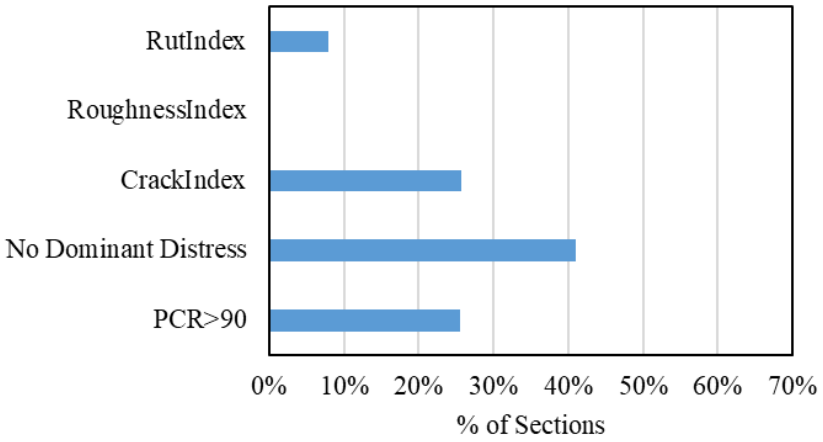
RutIndex
RoughnessIndex
CrackIndex
No Dominant Distress
PCR>90
0%
10%
20%
30%
40%
50%
60%
70%
% of Sections

(b)

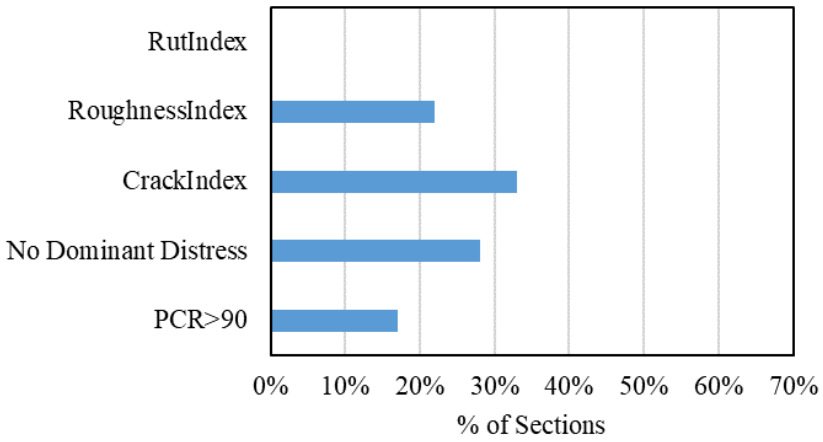
RutIndex
RoughnessIndex
CrackIndex
No Dominant Distress
PCR>90
0%
10%
20%
30%
40%
50%
60%
70%
% of Sections

(c)

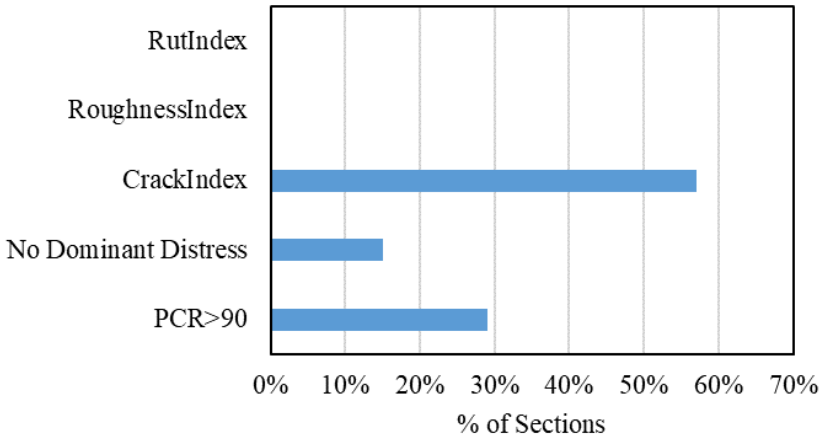

(d)

Figure 6-2 Percentage of sections with dominant distresses for (a) Lee Road 159, (b) US 280, (c) CSAH8 and (d) US 169

As shown in Figure 6-2, Lee Road 159, a warm weather, low traffic volume thin cross-section road, has exhibited all the dominant distress with 16% of the sections with a PCR greater than 90. US 280, warm weather, high traffic volume road thick cross-section, has exhibited all dominant distress except roughness, with 25% of the sections with PCR greater than 90. CSAH 8, a cold weather, low traffic volume, thin cross-section road, has not exhibited rutting as a dominant distress, with 17% of the sections with a PCR greater than 90. Finally, US 169, cold weather, high traffic volume thick cross-section road, has not exhibited rutting or roughness as dominant distresses but has a significantly higher amount of dominant cracking distress (57%), with a 29% of the sections remaining in service with a PCR greater than 90. Based on the dominant distresses, it can be concluded that pavement roughness is less dominant in thick cross-section pavements, while rutting is less dominant in cold weather conditions. The finding also supports the assumption that the thick layers of pavement, especially the thick AC layer, can spread the wheel load through a wider stress cone preventing any permanent roughness-causing deformation in the subgrade

layer. In cold weather conditions, the top AC layer wearing course shows higher stiffness and can resist more traffic impact without significantly higher strains in the AC layer.

6.2 PCR Condition over the Study Period

PCR or any other condition index that combines individual surface distresses and converts them to one single value representing the overall functional condition can be a significant parameter in the PMS implementation and decision tree. The change of PCR for different treatment classes for different test locations is shown in Figure 6-3. As discussed earlier, the control (untreated) sections are assigned to the treatment group "0".

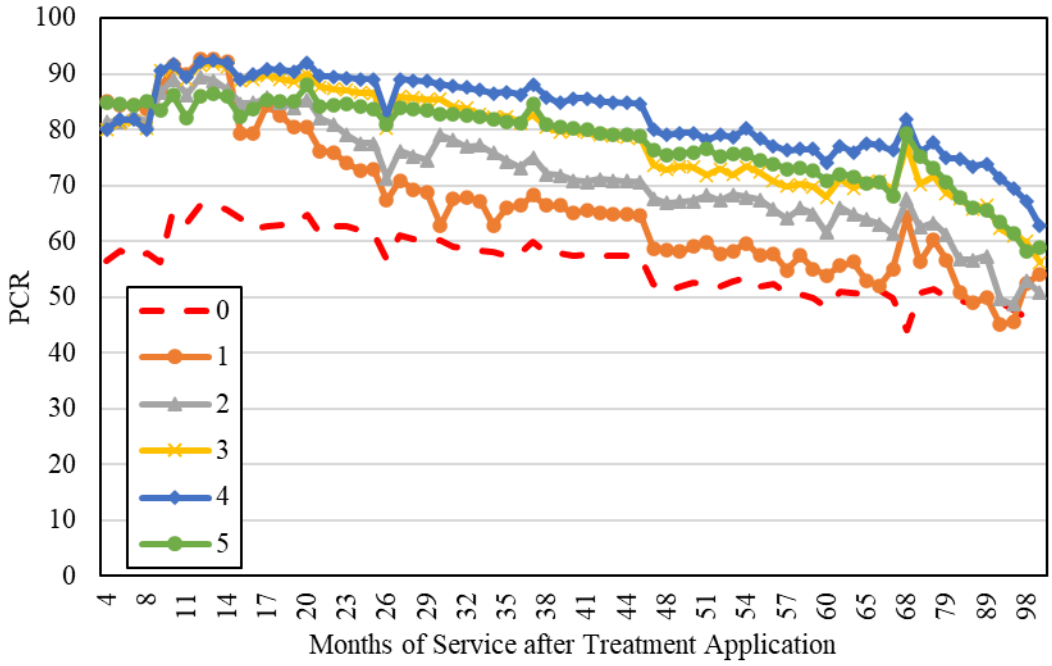

(a)

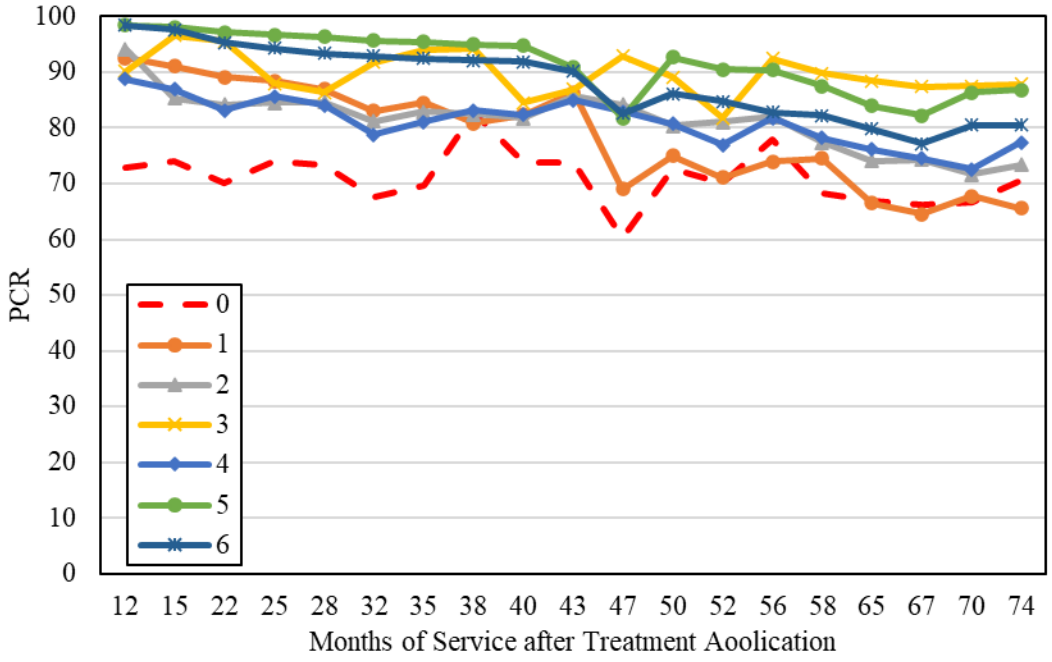
100
90
80
70
60
50
40
30
20
10
0
PCR
0
1
2
3
4
5
6
12 15 22 25 28 32 35 38 40 43 47 50 52 56 58 65 67 70 74
Months of Service after Treatment Aoolication

(b)

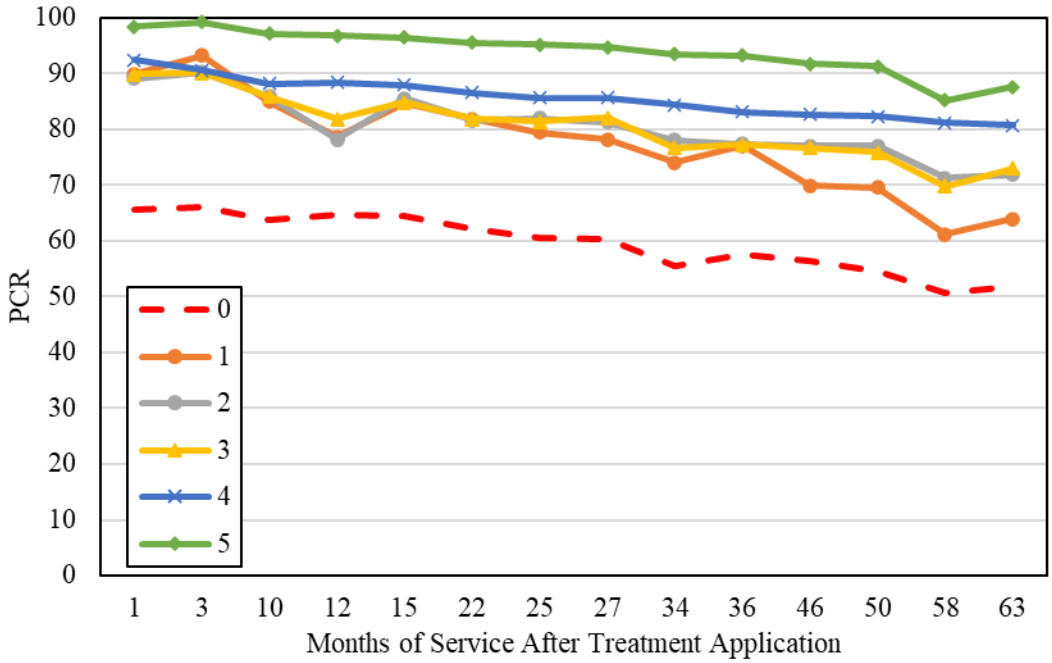
100
90
80
70
60
50
40
30
20
10
0
PCR
0
1
2
3
4
5
1 3 10 12 15 22 25 27 34 36 46 50 58 63
Months of Service After Treatment Application

(c)

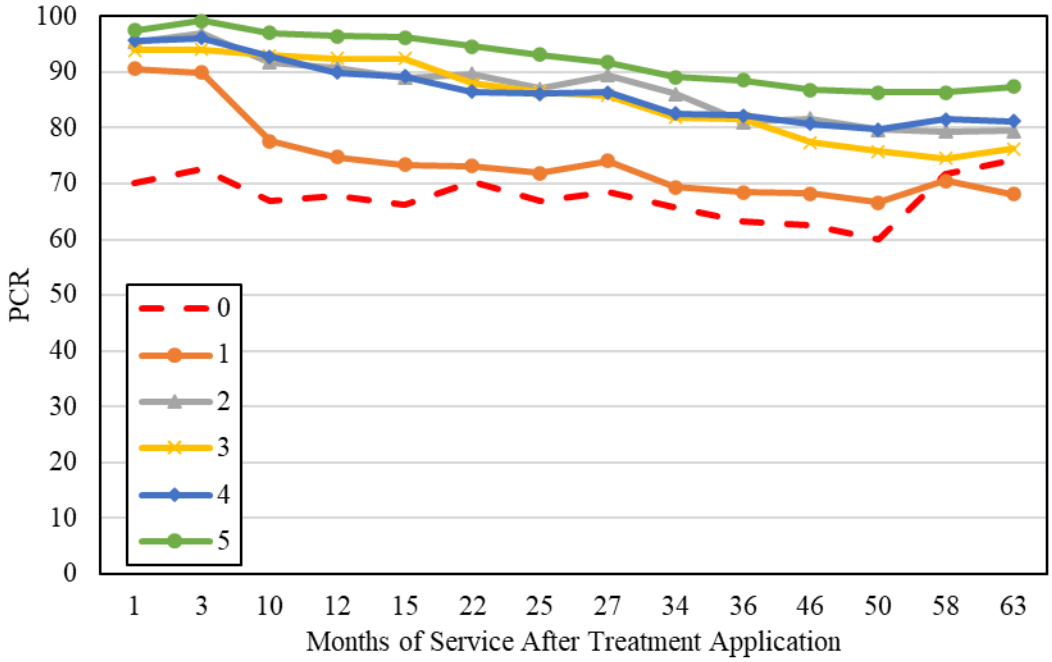

(d)

Figure 6-3 PCR over the study period for different treatment classes for (a) Lee Road 159, (b) US 280, (c) CSAH 8, (d) US 169

As shown in Figure 6-3, the treatments within the higher treatment group indicate that the average PCR stays in, the higher PCR range over the analysis period. At the beginning of the analysis period, the control or untreated sections were several years old, so the age index was already reduced. However, the age index of the treated sections was restored to 100 following treatment application. The age of the pavement when the treatment was applied at each test location is shown in Table 6-1. Simply put, the age is calculated as the time elapsed since the last maintenance or rehabilitation activity.

Table 6-1 Age of Pavement Surface and Age Index of the Treatment Section Since the Last Recorded Rehabilitation/ Construction

Test Location	Age of Pavement at the Time of Treatment Application(years)	Age Index at the Time of Treatment Application (0~100)
Lee Road 159	14	13
US 280	6	63
CSAH 8	11	31
US 169	7	57

Once the treatments were applied to the test sections, the age index was restored to 100 while the untreated sections continued to age, starting with the age index indicated in Table 6-1.

6.3 Area Under Pavement Condition Rating (AUPCR) Curve

To measure how long a pavement has remained in good condition, the difference between the initial and final value at the end of the analysis period can be a good practice, but how long it has sustained good condition is also important to calculate the overall functional benefit provided to the pavement due to the application of the treatment. To estimate the amount of functional benefit reached by the pavement, the Area Under Pavement Condition Rating (AUPCR) was introduced. The idea of AUPCR is inspired by the deflection basin parameter AUPP. The equation for AUPCR is shown in Equation 6-1.

$$AUPCR = 0.5 \times \sum_{t=0}^{t=n} (PCR_{t+p} - PCR_t) \times (t + p - t) \quad \text{Equation 6-1}$$

$AUPCR =$ Area Under PCR, t = time (months), p= time increment, $n =$ total month of service under the PCR curve. AUPCR can also be compared to the sum of the area under the PCR curve over the life of the pavement during the analysis time window.

Once the AUPCR and difference in PCR ($Final\ PCR - Initial\ PCR$) are calculated, both measurements are ranked. The step-by-step procedure for ranking the treatments and pass/fail criteria are explained in the next steps:

- Individual ranking based on the BDI and BCI score achieved by the treatment section is summed up. The summed-up rank indicates that the lower the rank sum, the higher the functional benefit received from the treatment.
- Then the rank sums are rated between 0 for untreated to the maximum number of treatment groups for the specific test location. For example, for Lee Road 159, CSAH 8 and US 169, the total number of the treatment group is six (0~5), and for US 280, the total number of the treatment group is seven (0~6). The ranks are converted to a scaled matrix from 0~5 for the first group and 0~6 for the second group.
- If the "assigned treatment group" in Section 3.2.4 and "observed treatment group" is the same or the "observed treatment group" is higher than the "assigned treatment group", it indicates the treatment has met the expectation of functional service.
- Conversely, if the "assigned treatment group" is higher than the "observed treatment group", the treatment has not met the expectation of functional service.

- Finally, the Structural Condition Index is compared between the values at the end of the analysis period and the first observation after the treatment application. If either or both functional and structural condition criteria are met, the overall performance of the treatment is considered acceptable to be implemented in the PMS. However, if both conditions are not reaching expectations, those treatments are forwarded for further investigation. The summary of the example of the calculation for the Lee Road 159 site is shown in Table 6-2.

Table 6-2 Summary Table for the Overall Benefit from the Preservation Treatment in Lee Road 159 Test Location

Treatment	Treatment Group	Final PCR	PrePCR	Difference (- ve Detr. + ve	Rank by Difference	Rank By AUPCRC	Combined Score	Score [0-5]	Func. Expect Y/N	Structural Health Y/N	Overall (Stuct.+ Func.)
Untreated	0	42	65	-23	24	24	48	0	Y	Y	Y
Untreated	0	41	46	-6	18	25	43	1	Y	Y	Y
Rejuvenating fog seal	1	57	64	-7	20	20	40	1	Y	Y	Y
Crack sealing	1	51	40	11	4	21	25	3	Y	N	Y
Fibermat® chip seal	2	51	66	-14	22	18	40	1	N	Y	Y
Single layer chip seal	2	56	70	-14	21	9	30	2	Y	N	Y
Single layer micro surfacing	2	45	52	-7	19	23	42	1	N	Y	Y
Fibermat® chip seal	2	49	49	0	13	15	28	2	Y	N	Y
Single layer chip seal with crack sealing	3	51	46	5	10	11	21	3	Y	Y	Y
Double layer chip seal	3	61	63	-1	16	10	26	2	Y	Y	Y
Single layer micro surfacing with crack sealing	3	47	37	10	7	19	26	2	Y	Y	Y
Micro surfacing over Fibermat® chip seal	3	66	55	11	5	7	12	4	Y	Y	Y
Triple layer chip seal	3	65	58	7	9	8	17	3	Y	N	Y
Micro surfacing over chip seal	3	66	66	1	12	4	16	3	Y	Y	Y
Double layer micro surfacing	3	52	42	10	6	12	18	3	Y	Y	Y
Micro surfacing over scrub seal	3	68	61	7	8	2	10	4	Y	N	Y
Scrub seal	3	62	63	-1	14	5	19	3	Y	N	Y
Thin overlay over Fibermat® chip seal	4	76	58	17	2	3	5	5	Y	Y	Y
Virgin thin overlay	4	72	45	27	1	1	2	5	Y	N	Y
Virgin thin overlay on foamed recycle base	4	60	56	5	11	14	25	3	N	Y	Y
Virgin thin overlay	4	63	64	-1	15	6	21	3	N	N	N
Ultra thin bonded wearing course	4	39	63	-23	25	22	47	0	N	Y	Y
50% RAP thin overlay	4	50	66	-16	23	16	39	1	N	N	N
5% RAS thin overlay	4	54	56	-2	17	13	30	2	N	N	N
HiMA thin overlay	4	56	40	16	3	17	20	3	N	Y	Y

As shown in Table 6-2, all treatments except one of the virgin thinlays, 50% RAP thinlay, and 5% RAS thinlay showed the expected performance. The location of these treatment sections is near the south end of the test location, where there is an intersection where loaded trailer trucks slow down as they approach. This may cause the impact of traffic load to be more damaging. In addition, the 50% RAP and 5% RAS thinlay sections contained a high amount of recycled asphalt binder, resulting in stiffer mixes with high cracking susceptibility. The summary of the performance tables for US 280, CSAH 8 and US 169 are shown in Appendix C.

Based on the performance summary from all the test locations, it was evident that the pavement preservation-treated sections performed better than the control sections in all testing locations.

6.4 Measurement of Service Life in Good Condition

An investigation was performed to estimate the duration of service for the treated sections while the PCR value remained at 70 or above, which is considered a “good” condition on the PCR scale. Despite excess tire loading and braking at the intersection, the 5% RAS and 50% RAP thinlay remained in the good PCR range for over 48 months. Some of the best-performing treatments based on sustained PCR rating for more than 7 years of service are variations of chip seal and cape seal treatments. Also, the remainder of the treatments indicated equal or more than the expected service life discussed in the literature (*7*). The summary bar chart showing the duration of service with a PCR of 70 or greater for the preservation-treated sections is shown in Figure 6-4.

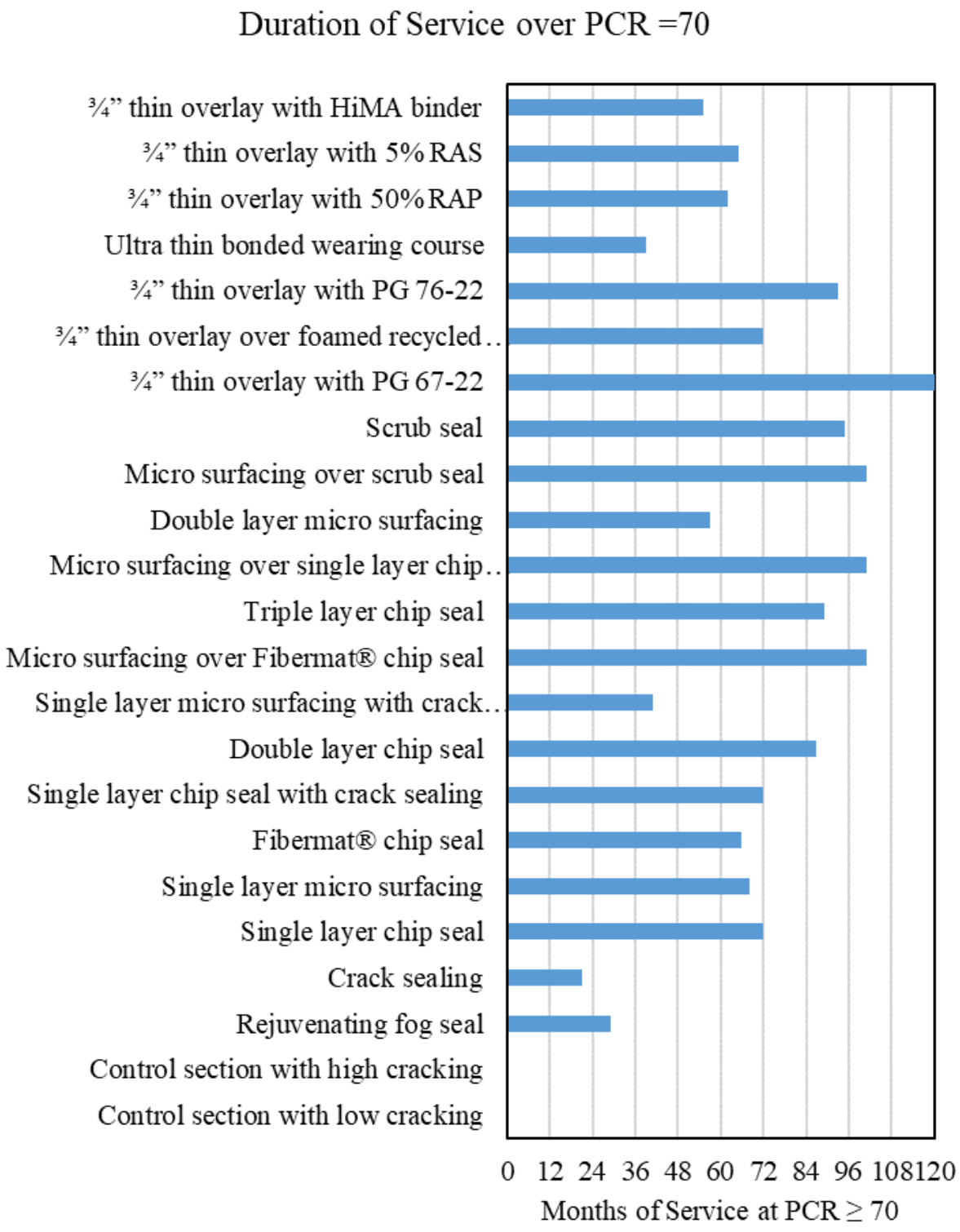

Figure 6-4 Duration of service at PCR ≥70 for Lee Road 159 treatment sections

For the US 280 sections, the same methodology was applied to extract the duration of service for different treatment sections. Combining the condition rating score and the duration of "good" PCR condition over the service life, all the treatment sections met the expected performance. Figure 6-5 summarizes the observed "good" PCR condition duration for different treatments in the US 280 test location.

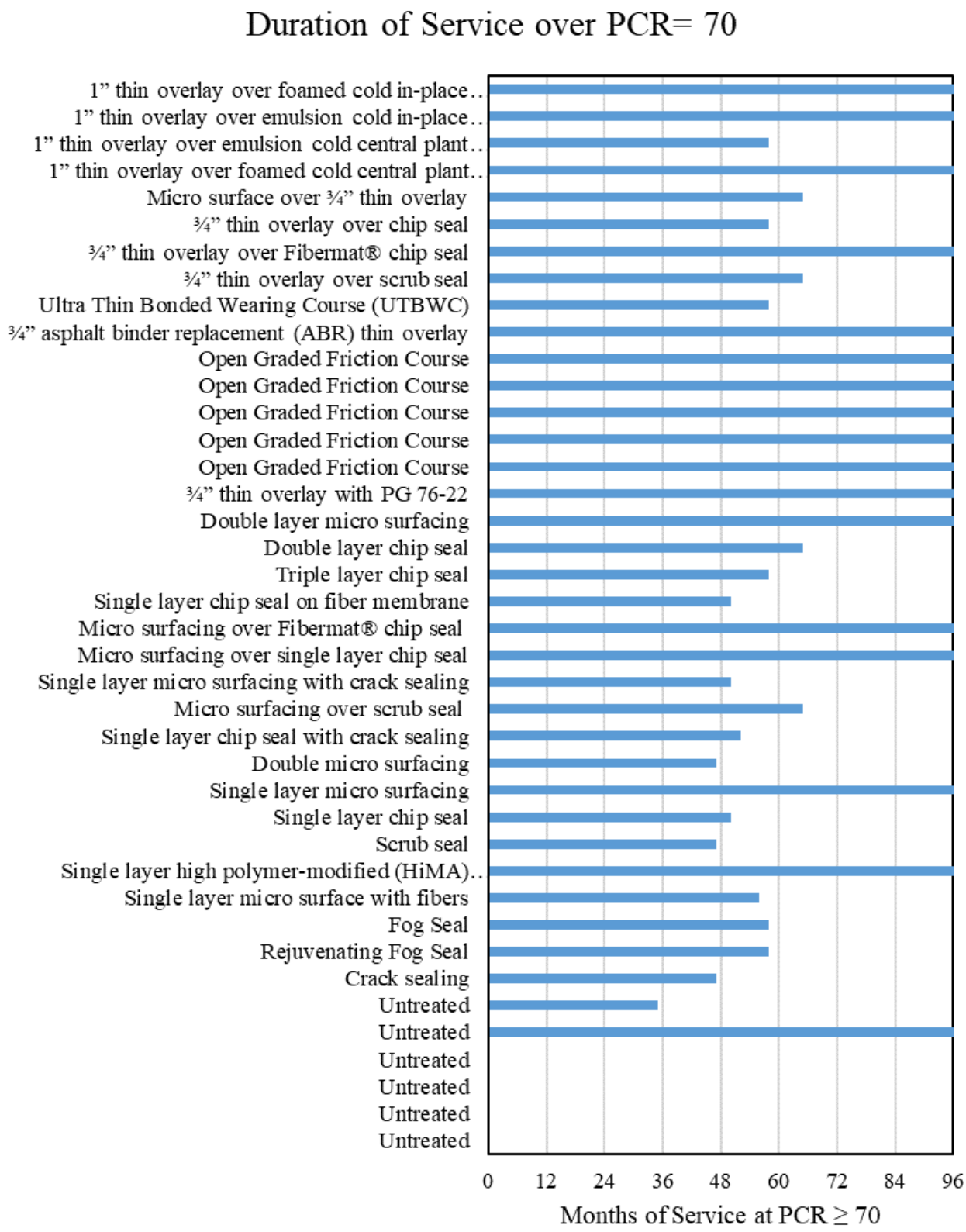

Figure 6-5 Duration of service at PCR ≥70 for US 280 treatment sections

For the other test locations, CSAH 8 and US 169, only six years of data were available. Furthermore, the data collection for these cold weather sections is less frequent, providing fewer data points to conclude the duration of service life with a PCR of 70 and above. Therefore, the results for observed service life duration are not presented in the study, but the same methodology could be applied once enough data become available.

6.5 Proposed Pavement Management Decision Tree

Based on the performance evaluation of each treatment discussed in Section 6.1 through Section 6.4, no treatment exhibited worse functional and structural conditions than the control section. Thus, all the preservation treatments within this study can be applied to effectively extend pavement life. The proposed decision tree shown in Figure 6-6 incorporates the structural condition class developed in Section 5.5. The flowchart combines pavement PCR and structural conditions while assigning rehabilitation types. The rehabilitation assignment is performed based on the PCR deterioration curve only. Some agencies apply Structural Condition Index in the final stage of rehabilitation as a final check before any heavy rehabilitation work is assigned for a pavement section.

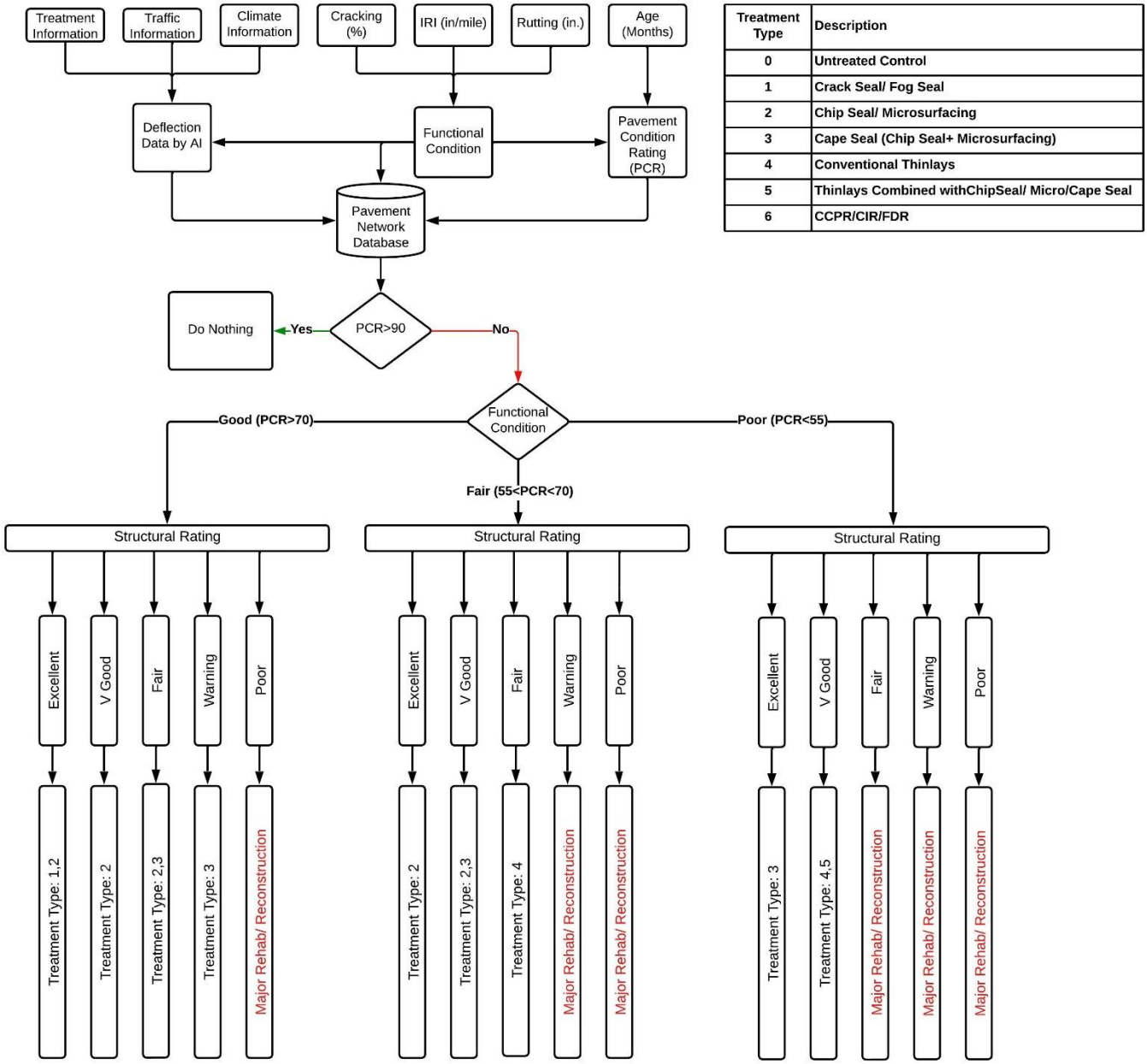

Treatment Type	Description
0	Untreated Control
1	Crack Seal/ Fog Seal
2	Chip Seal/ Microsurfacing
3	Cape Seal (Chip Seal+ Microsurfacing)
4	Conventional Thinlays
5	Thinlays Combined withChipSeal/ Micro/Cape Seal
6	CCPR/CIR/FDR

Figure 6-6 Proposed decision tree for PMS for low and high-volume roads

6.6 Chapter Summary

An effort is made to establish an integrated pavement management decision tree incorporating pavement functional class and structural condition. To aid proper and distinguished classification of the pavement's functional and structural conditions, the PCR classification and

modified structural benchmarking in Section 3.5 and Section 5.6 allow the incorporation of the unified decision-making process more easily without involving any complicated mathematical modeling. In addition, Section 6.1 discusses the methodology to identify any specific distress that is dominant on the pavement surface layer in a comparative method. This process allows the PMS to assign any specific type of solution to a pavement surface based on the dominant distresses alongside the structural condition. Section 6.2 indicated that the pavement preservation-treated sections exhibited higher PCR values over the analysis period than the untreated sections. Treatment-wise PCR benefit, expressed by Area Under the PCR Curve (AUPCRC), is the measurement of functional benefit over the service life of each treatment. Finally, Section 6.5 provides a complete framework for the PMS to effectively incorporate pavement structural and functional conditions. It is advised that PMS administrators assign a specific type of treatment within an assigned treatment group based on the budget needs, site conditions, and expected duration of post-application service.

7 CONCLUSION AND RECOMMENDATIONS

7.1 Summary of Findings

In this chapter, the summary of the findings from Chapter 4 through Chapter 6 is discussed to provide a summary of the dissertation. The neural network models developed in Chapter 3.6 allow the agency to predict pavement structural conditions based on functional data without the need for deflection testing. Furthermore, for the agencies where pavement preservation plays a great role in the sustainable long service life of the pavement, the deflection basin parameters (DBPs) benchmarking designed by the FHWA were modified to capture the effect of pavement preservation in terms of the long-term structural benefit. The modified benchmarking method is shown in Chapter 5 of this dissertation. Finally, as the agency users have the structural condition information and modified benchmarking to capture pavement preservation benefits, Chapter 6 incorporates the structural condition into the PMS alongside an overall functional condition rating.

7.1.1 Use of Neural Network

Based on the literature, it was found that neural networks can capture and model complicated pavement behaviors such as rutting, roughness, remaining service life, etc. In this dissertation, the DBPs were modeled using neural networks incorporating functional condition data, traffic data, and climatic information. Over 200,000 data points from the functional condition and structural condition data from full-scale test sections were used to train the NN model. Several iterations were performed for different network breadth, depth, activation function, stopping time, and training algorithms. Also, to restrict the over-fitting of the data, regularization and early stopping mechanisms were applied to prepare the model to predict when unseen data is fed through the model efficiently. Finally, a 2- layered NN model with 48 nodes in the first hidden layer and

36 nodes in the second layer was found, yielding the lowest RMSE and highest R^2 (0.83) value for BDI. On the other hand, the model for BCI had 48 hidden nodes in layer 1 and 24 hidden nodes in layer 2. For both models, the activation function was logsig, and the training algorithm was Levenberg-Marquardt (LM). The LM algorithm has the steepest descent method, which allows faster convergence and the lowest training time with desirable accuracy. For all the training, fitting, and prediction works, the MATLAB® Neural Network training tool was used.

7.1.2 Modified Benchmarking of the Deflection Basin Parameter

Based on the FHWA benchmarking of BDI and BCI classification, the "good" condition ranges from 0 to 8 mils for BDI and 0 to 4 mils for BCI. The training data showed that more than 99.7% of the structural condition data falls within the FHWA-assigned "good" condition. However, the results indicate that when the ranges were developed, a small amount of improvement of structural condition (<2mils) due to the long time structural benefit resulting from the preservation treatments not being accounted for. Therefore, the present study focuses on a very small improvement in structural health which can be significant throughout service life. The distribution of BDI and BCI classification at different times of service are compared, and it was observed that the modified benchmarking method allows for capturing the change of classification along the duration of service. Based on the FHWA classification, the BDI and BCI classifications in the study do not change over time. The new benchmarking system splits the higher class of BDI or BCI into two main classes, such as "good" from the existing benchmark class being split into "excellent" and "very good". On the other hand, the modified benchmarking shows that 20% of the BDI Values from the sections within the study changed from a "very good" class to a "fair" class after 97 months of service. Therefore, the modified benchmarking can provide higher sensitivity of the BDI and BCI benchmark classification.

7.1.3 Incorporation of Structural Condition into the PMS Decision Tree

A modified decision tree was developed to capture the functional and structural condition of the pavement. The modified decision tree collects all pavement performance data but can provide a more accurate rehabilitation strategy based on the existing structural condition of the pavement. In conventional practice, structural testing would be used to verify the need for structural rehabilitation or reconstruction in pavements with a higher degree of deterioration. The proposed decision tree allows structural condition input at any PCR range.

7.2 Conclusion

Based on the outcome of the current dissertation, the following conclusions can be reached:

1. Neural Network applications can be implemented to predict structural condition indicators based on surface condition data with an accuracy of over 85%. The higher computational ability required for this methodology is not required for modeling the training of a Shallow Neural Network. This approach can potentially allow agencies to incorporate structural condition at network-level pavement management without requiring a significant amount of additional time or resources.
2. Although pavement preservation is not intended to improve the structural capacity of pavements, pavements that receive preservation treatments were found to have better structural performance than similar untreated pavements. Therefore, accounting for the effect of pavement preservation on functional and structural conditions in a PMS can improve the system's efficiency and lead to better planning and selection of pavement sections and treatments.

3. The models developed in this study can account for the contribution of various pavement preservation treatment categories to the structural performance of the pavement. An agency can use this information, along with monetary and non-monetary factors, during the decision-making process to select appropriate treatments. The large number or treatments considered in this study resulted in a model robust enough for network-level pavement management based on general treatment categories.
4. The modified benchmarking of the BDI and BCI allows the agency to capture changes when the pavement is in overall "good" or "fair" condition. This modification especially aids the quantification of structural benefits obtained from the preservation treatments over the service life and provides additional detail that can be used during treatment selection.
5. The proposed framework for developing a decision tree for PMS allows the agency to make more educated decisions and more optimized budgeting over the pavement service life. Incorporating structural condition along with functional condition can minimize the risk of misclassifying the type of M&R needed during network-level analysis.

7.3 Recommendations and Future Improvements

One of the major shortcomings of the present study is the limited availability of the cold region data for training the model. Adding more training data from the cold weather region can improve the model in terms of accuracy. In addition, there are other limitations of the study, such as the limited computational ability to work with deep neural networks. Deeper networks can achieve more accuracy and better predict pavement structural condition in a controlled training environment.

Recommendations for future work and implementation are as follows:

- The data used in the development of this research was limited to four locations with extreme differences in climate and traffic condition that encompass a large portion of possible scenarios within the United States. Incorporating a wider range of climatic and regional data into the model can help improve its general applicability.
- Local calibration parameters are needed to make a model available to a particular agency. A user can utilize the general model as a starting point and based on its own dataset and PMS feedback, calibrate and improve the model. The basic statistics, distributions, weight, and bias for the trained model are provided in Appendix A so that the user can identify how accurately the model would predict structural condition based on the particular dataset.
- This dissertation used the PCR as an example of a condition rating based on functional parameters. It is common for agencies to develop custom indices or ratings to evaluate pavement conditions. These can be incorporated following the same methodology described in this dissertation but would require additional adjustments to reflect the agency's pavement management practices (for example, adjusting the threshold values that define the different condition categories).

In a conclusive summary, the methodology developed can be recommended for evaluation of the structural condition of preservation treated pavements based on functional condition data. The modified benchmarking allows capturing the structural benefits for the application of preservation treatments over the service life of the treated pavements. The proposed decision tree provides guidelines for the agency and user groups to implement the methodology on their networks upon local calibration and adjustment to the models and decisions.

8 REFERENCES

1. Hicks, R. G., A. L. Simpson, and J. L. Groeger. Pavement Management Practices in State Highway Agencies: Madison, Wisconsin Peer Exchange Results. 2011.

2. Hudson, W. R., R. Haas, and R. D. Pedigo. *Pavement Management System Development.* 1979.

3. Vitillo, N. Optimising Long Life Low Noise Porous Asphalt. *Asphalt Pavements*, 2014, pp. 245–254. https://doi.org/10.1201/b17219-35.

4. Zimmerman, K. A., M. Grogg, P. Ram, O. Smadi, D. Peshkin, B. Allen, L. Pierce, and M. Yapp. Pavement Management Roadmap. No. September, 2022.

5. Corley-Lay, J., J. O'Doherty, J. Hooks, L. Scofield, A. Iowa State University, and F. H. Administration. *Federal Highway Administration (FHWA) Pavement Preservation Research Roadmap*. 2020.

6. WSDOT. MAP-21 and Washington State. *WSDOT*, No. February 2019, 2019, pp. 2–3. https://doi.org/10.1093/acref/9780195301731.013.46323.

7. Sustainable, T., P. Systems, and P. Treatments. Chapter 7 . Maintenance and Preservation Treatments To Improve Sustainability. 2005.

8. ALDOT, D. Arkle, and G. Conner. *Transportation Asset Management Plan (TAMP) Final Report*. 2020.

9. Rahman, M., and A. Vargas-Nordcbeck. Effect of Thin Overlays on the Structural Performance of Cold Recycled Bases for High Traffic Volume Roads. 2019.

10. Rahman, M., and A. Vargas-Nordcbeck. Structural Performance of Sections Treated with Thin Overlays for Pavement Preservation. *Transportation Research Record*, Vol. 2675, No. 8, 2021, pp. 382–393. https://doi.org/10.1177/0361198121997816.

11. Buchanan, B. G. A Brief History of Artificial Intelligence. *American Association for Artificial Intelligence*, Vol. 26, No. 11, 2006, pp. 1059–1067. https://doi.org/10.1051/medsci/2020189.

12. Samer W. Katicha, S. Ercisli, P. D. Gerardo W. Flintsch, Ph.D., P.E., James M. Bryce, and P. E. Brian K. Diefenderfer, Ph.D. Development of Enhanced Pavement Deterioration Curves. 2015, pp. 1–83.

13. Bryce, J., S. Katicha, G. Flintsch, N. Sivaneswaran, and J. Santos. Probabilistic Life-Cycle Assessment as Network-Level Evaluation Tool for Use and Maintenance Phases of Pavements. *Transportation Research Record*, Vol. 2455, 2014, pp. 44–53. https://doi.org/10.3141/2455-06.

14. Haider, S. W., R. J. Eisma, K. Chatti, G. Ireland, and N. McDonald. Impact of Site Factors on the Effectiveness of Flexible Pavement Preservation Treatments. Vol. 4, 2015, pp. 593–604.

15. Smith, K. D., J. E. Bruinsma, M. J. Wade, K. Chatti, J. M. Vandenbossche, and H. T. Yu. Using Falling Weight Deflectometer Data with Mechanistic-Empirical Design and Analysis, Volume I: Final Report. *Report No. FHWA-HRT-16-009. Federal Highway Administration*, Vol. I, No. March, 2017. https://doi.org/10.1520/STP104445.

16. ASTM. Standard Guide for General Pavement Deflection Measurements. https://www.astm.org/d4695-03r20.html. Accessed Oct. 24, 2022.

17. ASTM. Standard Test Method for Deflections with a Falling-Weight-Type Impulse Load Device. https://www.astm.org/d4694-09r20.html. Accessed Oct. 24, 2022.

18. Irwin, L. H., Yang, W. S., and Stubstad, R. N. Deflection Reading Accuracy and Layer Thickness Accuracy in Backcalculation of Pavement Layer Moduli. *American Society for Testing and Materials*, 1989.

19. Jung, F., and F. E. D. Stolle. *Nondestructive Deflection Testing and Backcalculation for Pavements*. 1992.

20. Hossain, A. S. M. M., and J. P. Zaniewski. Characterization of Falling Weight Deflectometer Deflection Basin. *Transportation Research Record: Journal of the Transportation Research Board*, No. 1293, 1991.

21. Kim, Y. R., and H. Park. Use of Falling Weight Deflectometer Multi-Load Data for Pavement Strength Estimation. No. June, 2002.

22. Thompson, M. R. Area Under the Pavement Profile to Predict Strain. 1989.

23. Horak, E., A. Hefer, S. Emery, and J. Maina. Flexible Road Pavement Structural Condition Benchmark Methodology Incorporating Structural Condition Indices Derived from Falling Weight Deflectometer Deflection Bowls. *Journal of Civil engineering and Construction*, Vol. 4, No. 1, 2015, pp. 1–14.

24. Horak, E. Surface Moduli Determined with the Falling Weight Deflectometer Used as Benchmarking Tool. *SATC 2007 - 26th Annual Southern African Transport Conference: The Challenges of Implementing Policy*, No. July, 2007, pp. 284–293.

25. Talvik, O. FWD Mõõtmistulemuste Alusel Arvutatud Parameetrite SCI, BDI Ja BCI Kasutamine Teekatendi Seisukorra Hindamisel (Use of FWD Deflection Basin Parameters (SCI, BDI, BCI) for Pavement Condition Assessment). *Magistritöö. Tallinn: TTÜ teedeinstituut*, 2007.

26. Xu, B., Ranji Ranjithan, and Y. R. Kim. New Condition Assessment Procedure for Asphalt Pavement Layers, Using Falling Weight Deflectometer Deflections. Vol. 7, No. 02, 2002, pp. 57–69.

27. Kim, Y. R., and H. Park. Use of FWD Multi-Load Data for Pavement Strength Estimation. *North Carolina Department of Transportation*, No. June, 2002, p. 192.

28. Seo, J. W., S. Il Kim, J. S. Choi, and D. W. Park. Evaluation of Layer Properties of Flexible Pavement Using a Pseudo-Static Analysis Procedure of Falling Weight Deflectometer. *Construction and Building Materials*, Vol. 23, No. 10, 2009, pp. 3206–3213. https://doi.org/10.1016/j.conbuildmat.2009.06.009.

29. Pierce, L. M., McGovern, and K. A. Zimmerman. *Practical Guide for Quality Management of Pavement Condition Data Collection*. 2013.

30. Hubel, D. H., and T. N. WoeselL. Receptive Fields of Single Neurons in the Cat's Striate Cortex. *The Journal of Physiology*, 1959, pp. 574–591.

31. Ren, S., K. He, R. Girshick, and J. Sun. Faster R-CNN: Towards Real-Time Object Detection with Region Proposal Networks. *IEEE Transactions on Pattern Analysis and Machine Intelligence*, Vol. 39, No. 6, 2017, pp. 1137–1149. https://doi.org/10.1109/TPAMI.2016.2577031.

32. Samarasinghe. Neural Networks for Applied Sciences and Engineering. *Journal of applied physiology*, Vol. 29, No. 3, 2006, p. 395.

33. Aggarwal, C. C. *Neural Networks and Deep Learning*. 2021.

34. Zhang, G., B. Eddy Patuwo, and M. Y. Hu. Forecasting with Artificial Neural Networks: The State of the Art. *International Journal of Forecasting*, Vol. 14, No. 1, 1998, pp. 35–62. https://doi.org/10.1016/S0169-2070(97)00044-7.

35. Banan, M. R., & Hjelmstad, K. D. Neural Networks and AASHO Road Test. Journal of Transportation Engineering. *Journal of Transportation Engineering, 122(5), 358-366*, 1996.

36. Kumar, R., S. K. Suman, and G. Prakash. Evaluation of Pavement Condition Index Using Artificial Neural Network Approach. *Transportation in Developing Economies*, Vol. 7, No. 2, 2021, pp. 1–15. https://doi.org/10.1007/s40890-021-00130-7.

37. Yang, J., J. J. Lu, M. Gunaratne, and Q. Xiang. Forecasting Overall Pavement Condition with Neural Networks: Application on Florida Highway Network. *Transportation Research Record*, No. 1853, 2003, pp. 3–12. https://doi.org/10.3141/1853-01.

38. Terzi, S. Modeling the Pavement Present Serviceability Index of Flexible Highway Pavements Using Data Mining. *Journal of Applied Sciences*, Vol. 6, No. 1, 2006, pp. 193–197. https://doi.org/10.3923/jas.2006.193.197.

39. Domitrović, J., H. Dragovan, T. Rukavina, and S. Dimter. Application of an Artificial Neural Network in Pavement Management System. *Tehnicki Vjesnik*, Vol. 25, 2018, pp. 466–473. https://doi.org/10.17559/TV-20150608121810.

40. Tabatabaee, N., M. Ziyadi, and Y. Shafahi. Two-Stage Support Vector Classifier and Recurrent Neural Network Predictor for Pavement Performance Modeling. *Journal of Infrastructure Systems*, Vol. 19, No. 3, 2013, pp. 266–274. https://doi.org/10.1061/(asce)is.1943-555x.0000132.

41. Eldin, N. N., and A. B. Senouci. A Pavement Condition-Rating Model Using Backpropagation Neural Networks. *Computer-Aided Civil and Infrastructure Engineering*, Vol. 10, No. 6, 1995.

42. Attoh-Okine, N. O. Grouping Pavement Condition Variables for Performance Modeling Using Self-Organizing Maps. *Computer-Aided Civil and Infrastructure Engineering*, Vol. 16, No. 2, 2001.

43. https://www.javatpoint.com/. Kohonen Self- Organizing Feature Map. https://www.javatpoint.com/artificial-neural-network-kohonen-self-rganizing-feature-map. Accessed Apr. 3, 2023.

44. Abambres, M., and A. Ferreira. Application of ANN in Pavement Engineering: State-of-Art. *SSRN Electronic Journal*, 2019, pp. 1–61. https://doi.org/10.2139/ssrn.3351973.

45. Kaseko, M. S., and S. G. Ritchie. A Neural Network-Based Methodology for Pavement Crack Detection and Classification. *Transportation Research Part C*, Vol. 1, No. 4, 1993, pp. 275–291. https://doi.org/10.1016/0968-090X(93)90002-W.

46. Mei, X., M. Gunaratne, J. Lu, and B. Dietrich. Neural Network for Rapid Depth Evaluation of Shallow Cracks in Asphalt Pavements. *Computer-Aided Civil and Infrastructure Engineering*, Vol. 19, 2004, pp. 223–230. https://doi.org/10.1111/j.1467-8667.2004.00350.x.

47. Mei, X., M. Gunaratne, J. Lu, and B. Dietrich. Neural Network for Rapid Depth Evaluation of Shallow Cracks in Asphalt Pavements. *Computer-Aided Civil and Infrastructure Engineering*, Vol. 19, 2004, pp. 223–230. https://doi.org/10.1111/j.1467-8667.2004.00350.x.

48. Gajewski, J., and T. Sadowski. Sensitivity Analysis of Crack Propagation in Pavement Bituminous Layered Structures Using a Hybrid System Integrating Artificial Neural Networks and Finite Element Method. *Computational Materials Science*, Vol. 82, 2014, pp. 114–117. https://doi.org/10.1016/j.commatsci.2013.09.025.

49. Roberts, C. A., and N. O. Attoh-Okine. A Comparative Analysis of Two Artificial Neural Networks Using Pavement Performance Prediction. *Computer-Aided Civil and Infrastructure Engineering*, Vol. 13, No. 5, 1998, pp. 339–348. https://doi.org/10.1111/0885-9507.00112.

50. Yildirim, Ş., and I. Uzmay. Statistical Analysis of Vehicles' Vibration Due to Road Roughness Using Radial Basis Artificial Neural Network. *Applied Artificial Intelligence*. 4. Volume 15, 419–427.

51. Choi, J.-H., T. M. Adams, and H. U. Bahia. Pavement Roughness Modeling Using Back-Propagation Neural Networks. *Computer-Aided Civil and Infrastructure Engineering*, 2004.

52. Yousefzadeh, M., S. Azadi, and A. Soltani. Road Profile Estimation Using Neural Network Algorithm. *Journal of Mechanical Science and Technology*, Vol. 24, No. 3, 2010, pp. 743–754. https://doi.org/10.1007/s12206-010-0113-1.

53. Solhmirzaei, A., S. Azadi, and R. Kazemi. Road Profile Estimation Using Wavelet Neural Network and 7-DOF Vehicle Dynamic Systems. *Journal of Mechanical Science and Technology*, Vol. 26, No. 10, 2012, pp. 3029–3036. https://doi.org/10.1007/s12206-012-0812-x.

54. Ngwangwa, H. M., S. Heyns, H. G. A. Breytenbach, and S. Els. Reconstruction of Road Defects and Road Roughness Classification Using Artificial Neural Networks Simulation and Vehicle Dynamic Responses: Application to Experimental Data. *Journal of Terramechanics*, Vol. 53, 2014, pp. 1–18. https://doi.org/10.1016/j.jterra.2014.03.002.

55. Ngwangwa, H. M., P. S. Heyns, F. J. J. Labuschagne, and G. K. Kululanga. Reconstruction of Road Defects and Road Roughness Classification Using Vehicle Responses with Artificial Neural Networks Simulation. *Journal of Terramechanics*, Vol. 47, No. 2, 2010, pp. 97–111. https://doi.org/10.1016/j.jterra.2009.08.007.

56. Ziari, H., J. Sobhani, J. Ayoubinejad, and T. Hartmann. Analysing the Accuracy of Pavement Performance Models in the Short and Long Terms: GMDH and ANFIS Methods. *Road Materials and Pavement Design*, Vol. 17, No. 3, 2016, pp. 619–637. https://doi.org/10.1080/14680629.2015.1108218.

57. Ziari, H., J. Sobhani, J. Ayoubinejad, and T. Hartmann. Prediction of IRI in Short and Long Terms for Flexible Pavements: ANN and GMDH Methods. *International Journal of Pavement Engineering*, Vol. 17, No. 9, 2015, pp. 776–788. https://doi.org/10.1080/10298436.2015.1019498.

58. Bashar, M. Z., and C. Torres-Machi. Performance of Machine Learning Algorithms in Predicting the Pavement International Roughness Index. *Transportation Research Record*, Vol. 2675, No. 5, 2021, pp. 226–237. https://doi.org/10.1177/0361198120986171.

59. Abambres, M., and A. Ferreira. Application of ANN in Pavement Engineering: State-of-Art. *SSRN Electronic Journal*, 2019, pp. 0–61. https://doi.org/10.2139/ssrn.3351973.

60. Ceylan, H., K. Gopalakrishnan, and A. Guclu. Advanced Approaches to Characterizing Nonlinear Pavement System Responses. *Transportation Research Record*, No. 2005, 2007, pp. 86–94. https://doi.org/10.3141/2005-10.

61. Ceylan, H., and A. Guclu. Use of Artificial Neural Networks for Backcalculation of Pavement Layer Moduli. *Urbana*, No. March, 2004.

62. Sharma, S., and A. Das. Backcalculation of Pavement Layer Moduli from Falling Weight

Deflectometer Data Using an Artificial Neural Network. *Canadian Journal of Civil Engineering*, Vol. 35, No. 1, 2008, pp. 57–66. https://doi.org/10.1139/L07-083.

63. Gopalakrishnan, K. Evaluation of Accelerated Deterioration in NAPTF Flexible Test Pavements. *Journal of Zhejiang University: Science A*, Vol. 9, No. 9, 2008, pp. 1157–1166. https://doi.org/10.1631/jzus.A0720153.

64. Gopalakrishnan, K., and H. Ceylan. Stiffness Characterisation of Full-Scale Airfield Test Pavements Using Computational Intelligence Techniques. *The IES Journal Part A: Civil & Structural Engineering*, Vol. 1, No. 4, 2008, pp. 280–290. https://doi.org/10.1080/19373260802217892.

65. Solanki, P., M. Zaman, and A. Ebrahimi. Regression and Artificial Neural Network Modeling of Resilient Modulus of Subgrade Soils for Pavement Design Applications BT - Intelligent and Soft Computing in Infrastructure Systems Engineering: Recent Advances. In (K. Gopalakrishnan, H. Ceylan, and N. O. Attoh-Okine, eds.), Springer Berlin Heidelberg, Berlin, Heidelberg, pp. 269–304.

66. Saltan, M., V. E. Uz, and B. Aktas. Artificial Neural Networks–Based Backcalculation of the Structural Properties of a Typical Flexible Pavement. *Neural Computing and Applications*, Vol. 23, No. 6, 2013, pp. 1703–1710. https://doi.org/10.1007/s00521-012-1131-y.

67. Leiva-Villacorta, F., A. Vargas-Nordcbeck, and D. H. Timm. Non-Destructive Evaluation of Sustainable Pavement Technologies Using Artificial Neural Networks. *International Journal of Pavement Research and Technology*, Vol. 10, No. 2, 2017, pp. 139–147. https://doi.org/10.1016/j.ijprt.2016.11.006.

68. Leiva-Villacorta, F. *Advanced Computing Techniques in Structural Evaluation of Flexible Pavements Using the Falling Weight Deflectometer*. 2012.

69. Shafabakhsh, G. A., M. Talebsafa, M. Motamedi, and S. K. Badroodi. Analytical Evaluation of Load Movement on Flexible Pavement and Selection of Optimum Neural Network Algorithm. *KSCE Journal of Civil Engineering*, Vol. 19, No. 6, 2015, pp. 1738–1746. https://doi.org/10.1007/s12205-014-0585-0.

70. Plati, C., P. Georgiou, and V. Papavasiliou. Simulating Pavement Structural Condition Using Artificial Neural Networks. *Structure and Infrastructure Engineering*, Vol. 12, No. 9, 2016, pp. 1127–1136. https://doi.org/10.1080/15732479.2015.1086384.

71. Shafabakhsh, G., M. Talebsafa, M. Motamedi, and S. K. Badroodi. Analytical Evaluation of Load Movement on Flexible Pavement and Selection of Optimum Neural Network Algorithm. *KSCE Journal of Civil Engineering*, Vol. 19, No. 6, 2015, pp. 1738–1746. https://doi.org/10.1007/s12205-014-0585-0.

72. Gopalakrishnan, K., and M. R. Thompson. GSP 130 Advances in Pavement Engineering. *GSP 130 Advances in Pavement Engineering*, 2005, pp. 1–15.

73. Pożarycki, A. Pavement Diagnosis Accuracy with Controlled Application of Artifical Neural Network. *Baltic Journal of Road and Bridge Engineering*, Vol. 10, No. 4, 2015, pp. 355–364. https://doi.org/10.3846/bjrbe.2015.45.

74. Shrestha, S., S. W. Katicha, G. W. Flintsch, and S. Thyagarajan. Application of Traffic Speed Deflectometer for Network-Level Pavement Management. *Transportation Research Record*, Vol. 2672, No. 40, 2018, pp. 348–359. https://doi.org/10.1177/0361198118758675.

75. Sollazzo, G., T. F. Fwa, and G. Bosurgi. An ANN Model to Correlate Roughness and Structural Performance in Asphalt Pavements. *Construction and Building Materials*, Vol. 134, 2017, pp. 684–693. https://doi.org/10.1016/j.conbuildmat.2016.12.186.

76. Wang, W., X. Yan, H. Huang, X. Chu, and M. Abdel-Aty. Design and Verification of a Laser Based Device for Pavement Macrotexture Measurement. *Transportation Research Part C: Emerging Technologies*, Vol. 19, No. 4, 2011, pp. 682–694. https://doi.org/10.1016/j.trc.2010.12.001.

77. Vyas, V., A. P. Singh, and A. Srivastava. Prediction of Asphalt Pavement Condition Using FWD Deflection Basin Parameters and Artificial Neural Networks. *Road Materials and Pavement Design*, Vol. 0, No. 0, 2020, pp. 1–19. https://doi.org/10.1080/14680629.2020.1797855.

78. Vyas, V., A. P. Singh, and A. Srivastava. Prediction of Asphalt Pavement Condition Using FWD Deflection Basin Parameters and Artificial Neural Networks. *Road Materials and Pavement Design*, Vol. 0, No. 0, 2020, pp. 1–19. https://doi.org/10.1080/14680629.2020.1797855.

79. NOAA. Final Spring/First Fall Freeze & Frost Date Probabilities | Minnesota DNR. *https://www.dnr.state.mn.us/*. https://www.dnr.state.mn.us/climate/summaries_and_publications/freeze_date.html. Accessed Oct. 15, 2022.

80. Ulring, J. MnROAD/NCAT Partnership. 2018.

81. ASTM. Standard Test Method for Measuring the Longitudinal Profile of Traveled Surfaces with an Accelerometer-Established Inertial Profiling Reference, , 2022.

82. Yu, H., and Bogdan M. Wilamowski. Levenberg–Marquardt Training. *Physics of the Solid State*, Vol. 46, No. 8, 2004, pp. 1404–1409. https://doi.org/10.1134/1.1788770.

83. Geiger, D. R. Memo: Pavement Preservation Definitions - Pavement Preservation - Design & Analysis - Pavements - Federal Highway Administration. https://www.fhwa.dot.gov/pavement/preservation/091205.cfm. Accessed Jul. 30, 2020.

84. Guyon, I., and A. M. De. An Introduction to Variable and Feature Selection André Elisseeff. *Journal of Machine Learning Research*, Vol. 3, 2003, pp. 1157–1182.

85. Mathworks. Introduction to Feature Selection - MATLAB & Simulink.

https://www.mathworks.com/help/stats/feature-selection.html. Accessed Oct. 6, 2022.

86. UCI. UCI Machine Learning Repository. https://archive.ics.uci.edu/ml/index.php. Accessed Oct. 5, 2022.

87. Mathworks. Feature Selection Using Neighborhood Component Analysis for Regression - MATLAB Fsrnca. https://www.mathworks.com/help/stats/fsrnca.html. Accessed Oct. 5, 2022.

88. Collier, P., and S. Waugh. Characteristics of Data Suitable for Learning with Connectionist and Symbolic Methods. *https://www.semanticscholar.org/*, 1994.

89. MATHWORKS. Feature Selection Using Neighborhood Component Analysis for Regression - MATLAB Fsrnca. https://www.mathworks.com/help/stats/fsrnca.html. Accessed Oct. 6, 2022.

90. Samarasinghe. Neural Networks for Applied. *Journal of applied physiology*, Vol. 29, No. 3, 1970, p. 395.

91. Hopfield, J. J. *Artificial Neural Networks*. 1988.

92. Zhuang, L., C. H. Lin, M. A. T. Figueiredo, and J. M. Bioucas-Dias. Regularization Parameter Selection in Minimum Volume Hyperspectral Unmixing. *IEEE Transactions on Geoscience and Remote Sensing*, Vol. 57, No. 12, 2019, pp. 9858–9877. https://doi.org/10.1109/TGRS.2019.2929776.

93. Ye, J., J. Chen, and S. Ji. Discriminant Kernel and Regularization Parameter Learning via Semidefinite Programming. *ACM International Conference Proceeding Series*, Vol. 227, 2007, pp. 1095–1102. https://doi.org/10.1145/1273496.1273634.

94. Huang, X.-L., & X. Ma, F. Hu, Z. Li, J. Chen, Y. Fu, G. Hu, Z. Pan, and L. Zhang. Editorial: Machine Learning and Intelligent Communications. *Mobile Networks and Applications 2017 23:1*, Vol. 23, No. 1, 2017, pp. 68–70. https://doi.org/10.1007/S11036-017-0962-2.

95. Okser, S., T. Pahikkala, A. Airola, T. Salakoski, S. Ripatti, and T. Aittokallio. Regularized Machine Learning in the Genetic Prediction of Complex Traits. *PLOS Genetics*, Vol. 10, No. 11, 2014, p. e1004754. https://doi.org/10.1371/JOURNAL.PGEN.1004754.

96. Rooklin, D. W., M. Lu, and Y. Zhang. Revelation of a Catalytic Calcium-Binding Site Elucidates Unusual Metal Dependence of a Human Apyrase. *Journal of the American Chemical Society*, Vol. 134, No. 37, 2012, pp. 15595–15603. https://doi.org/10.1021/JA307267Y.

97. Ahmed, E.-K., C. Kyung-Hwan, and K. Dae-Ki. Regularization Parameter Tuning Optimization Approach in Logistic Regression | IEEE Conference Publication | IEEE Xplore. *International Conference on Advanced Communications Technology (ICACT)*. https://ieeexplore.ieee.org/abstract/document/6488130?casa_token=Y__bg0N74s0AAAAA:gnR2O82dIHFTafFj8nGZPABMgi9a56fukc_CHPEovLrX_7piVA2WHQ42SZIZelSVe

yyd8l9R6w. Accessed Oct. 13, 2022.

98. Park, B. H., J. A. Laska, H. B. Klasky, A. Boone, O. Ozmen, R. Karthik, A. Advani, C. A. Cox, M. G. Pleszkoch, and E. Begoli. A Practical Guide to Neural Nets. 1991. https://doi.org/10.2172/1515683.

99. Horak, E., J. Maina, and A. Hefer. Structural Number Determined with the Falling Weight Deflectometer and Used as Benchmark Methodology. *Conference Paper*, No. December, 2014, p. 13. https://doi.org/10.13140/2.1.1459.6165.

100. Horak, E. Benchmarking the Structural Condition of Flexible Pavements With Deflection Bowl Parameters. *Journal of the South African Institution of Civil Engineering*, Vol. 50, No. 2, 2008, pp. 2–9.

101. Rabbi, M. F., and D. Mishra. Using FWD Deflection Basin Parameters for Network-Level Assessment of Flexible Pavements. *International Journal of Pavement Engineering*, Vol. 22, No. 2, 2021, pp. 147–161. https://doi.org/10.1080/10298436.2019.1580366.

102. Pierce, L. M., J. E. Bruinsma, D. S. Kurt, K. Chatti, and J. M. Vandenbossche. Using Falling Weight Deflectometer Data with Mechanistic-Empirical Design and Analysis, Volume 2. Vol. 2, No. November, 2017.

103. Ullidtz, P. *Pavement Analysis. Developments in Civil Engineering, 19*. 1987.

104. Peshkin, D. G., K. L. Smith, and L. M. Pierce. *Consideration of Preservation in Pavement Design and Analysis Procedures*. National Academies Press, 2015.

105. Jalali, F. Quantifying Pavement Preservation Performance Using Probablistic Deterioration Modeling. *Dissertation*, 2020, pp. 1–9.

APPENDIX A: STATISTICAL TEST OF THE TRAINING DATA

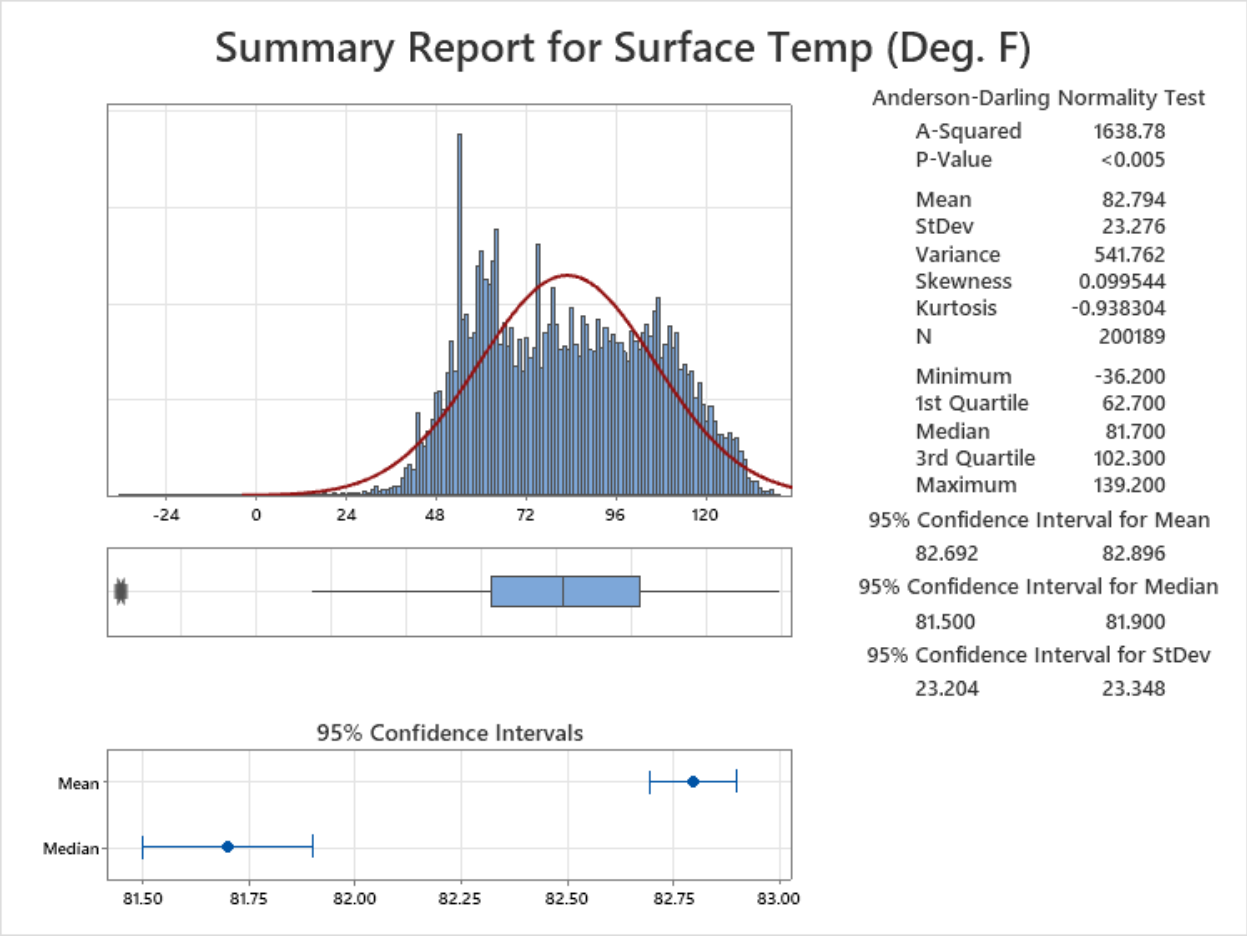

Figure A-1: Summary of training surface temperature (Degree F)

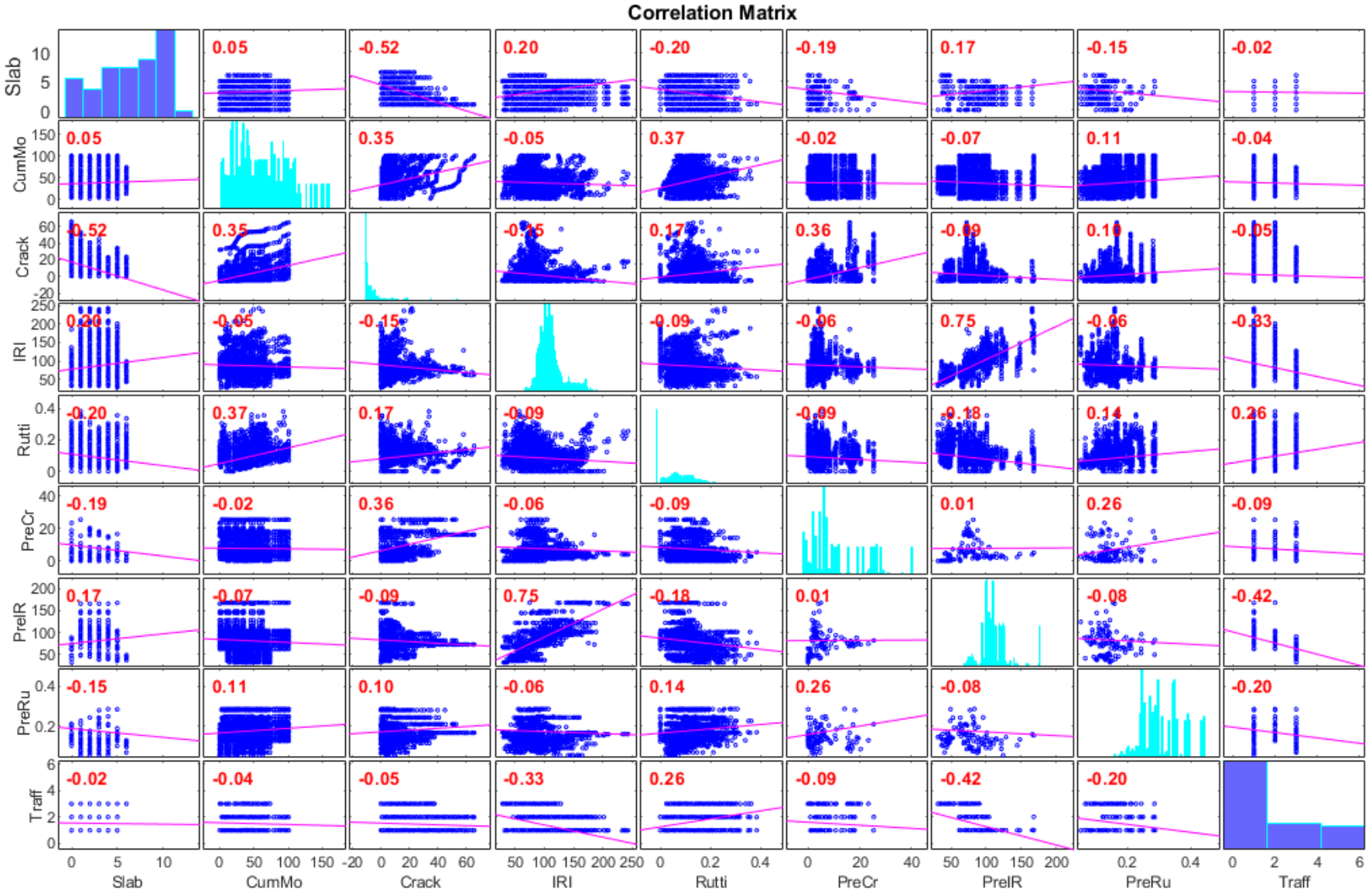

Figure A-2 Correlation matrix for training variables

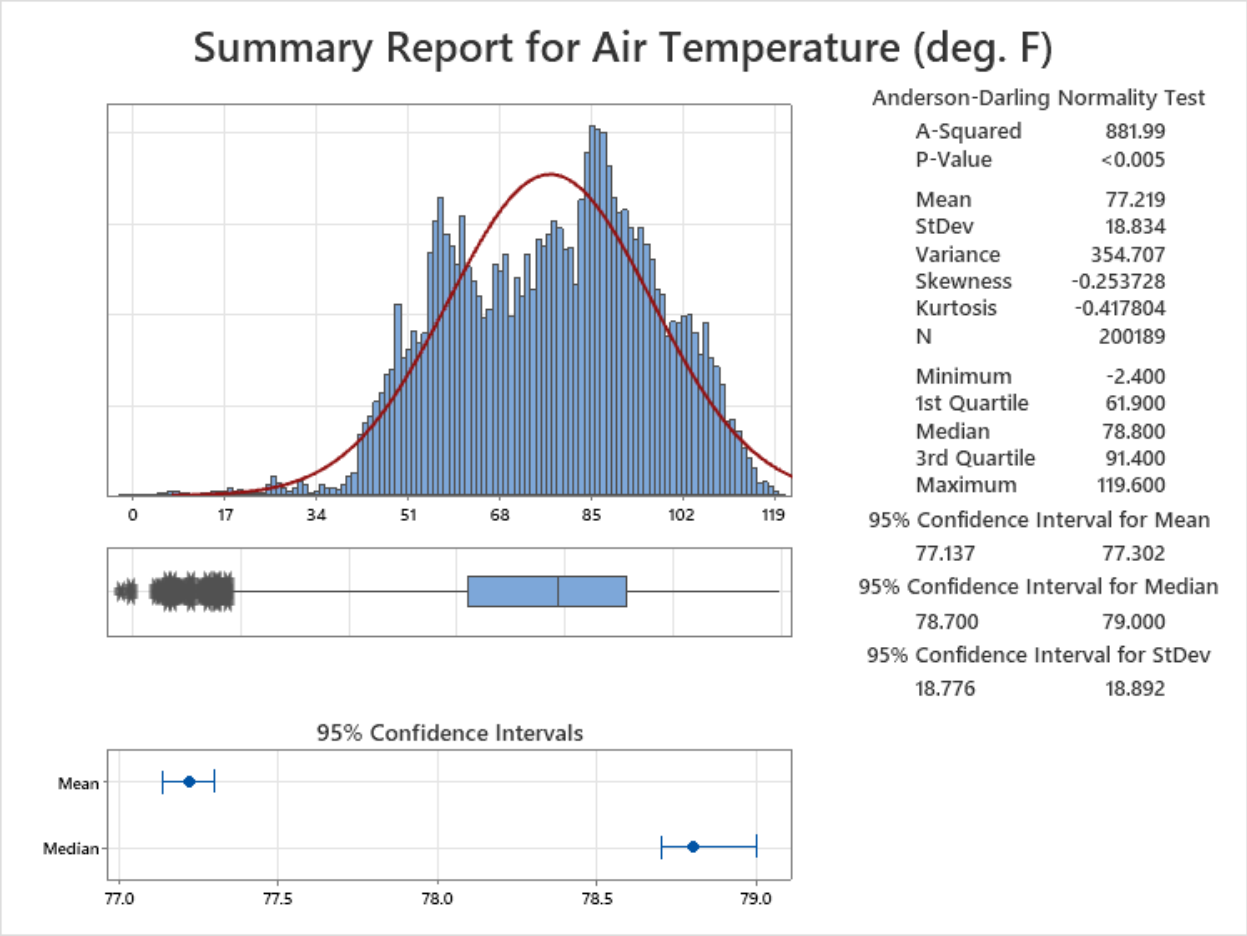

Figure A-3 Summary of training air temperature (Degree F)

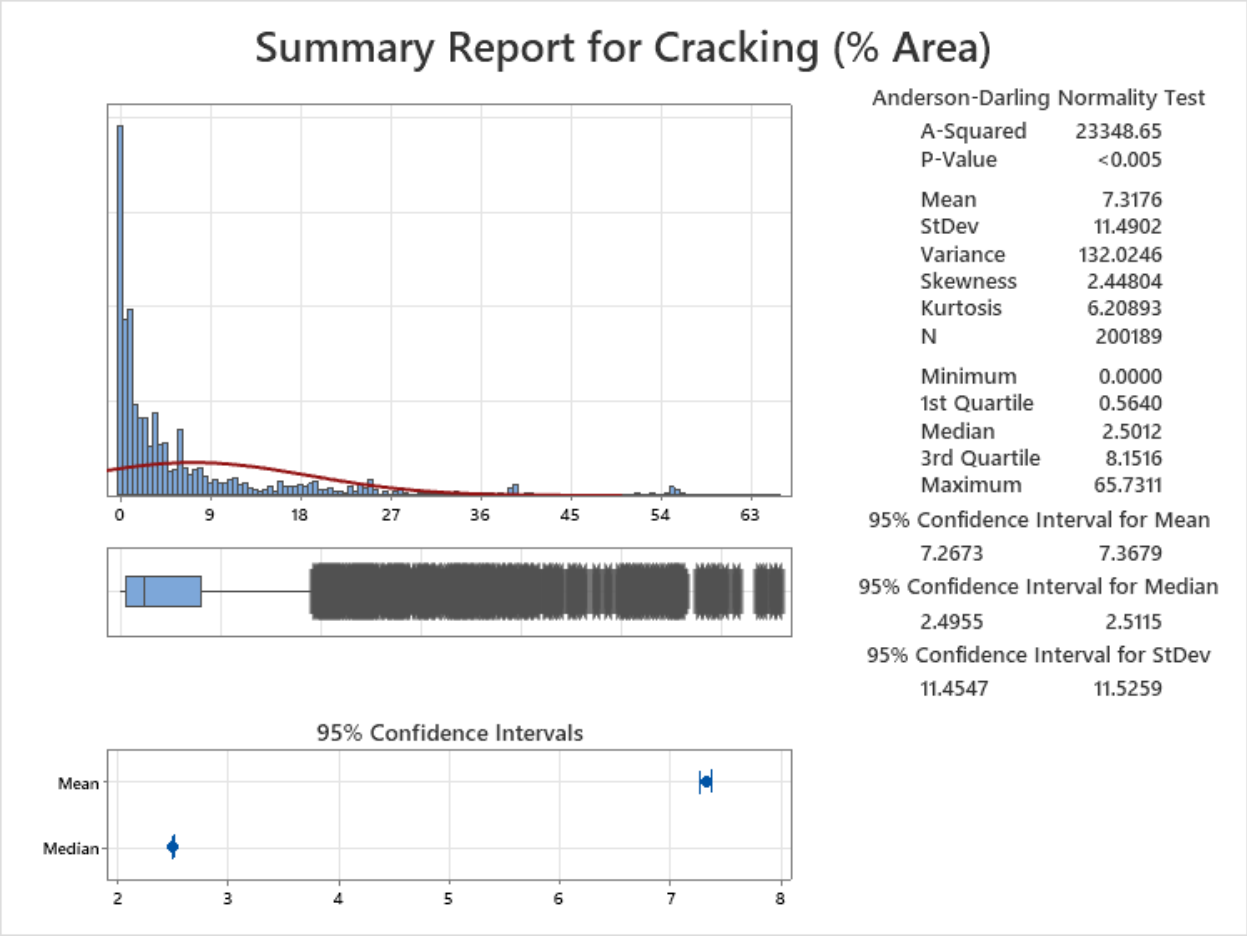

Figure A-4 Summary of training cracking (% area)

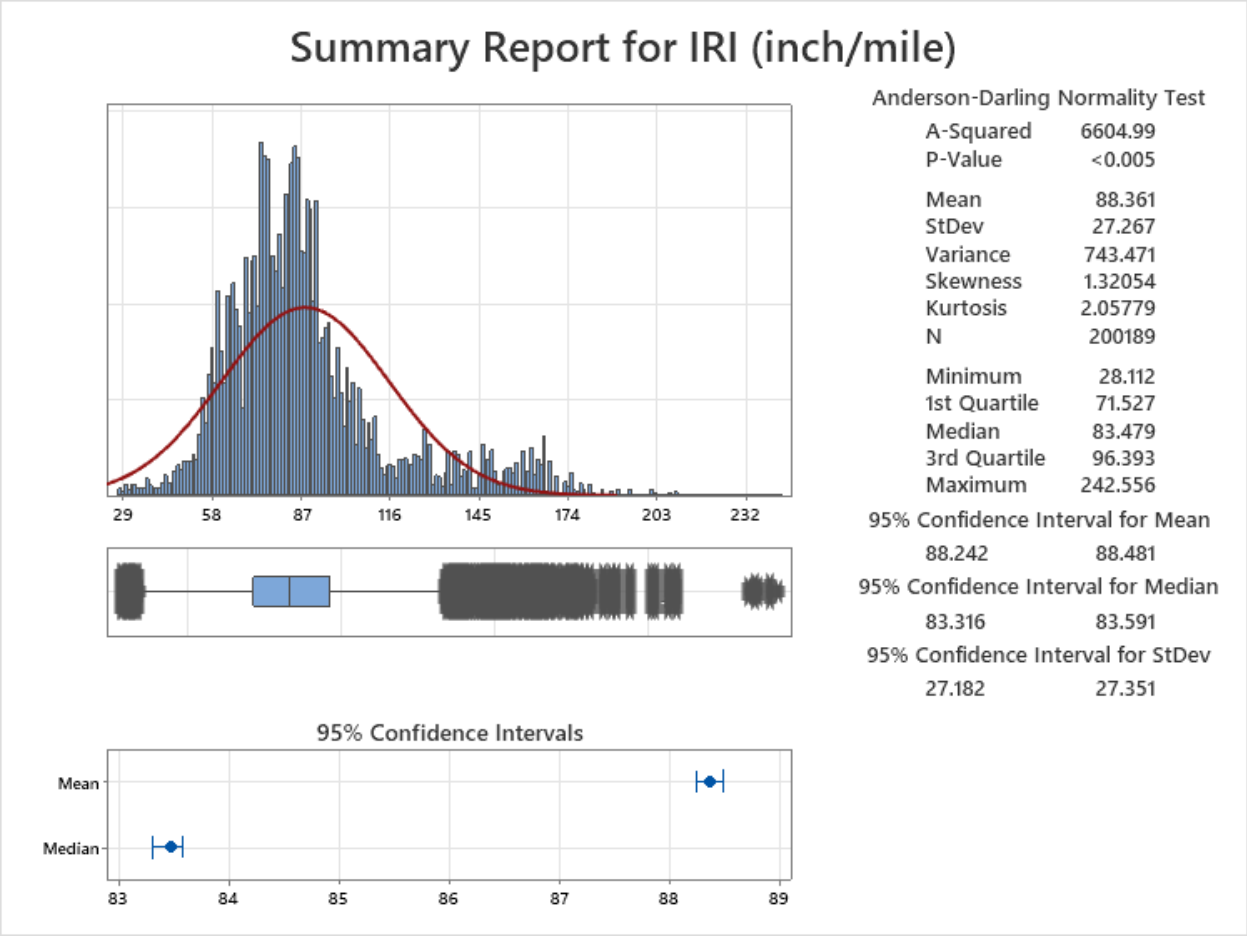

Figure A-5 Summary of training IRI (inch/mile)

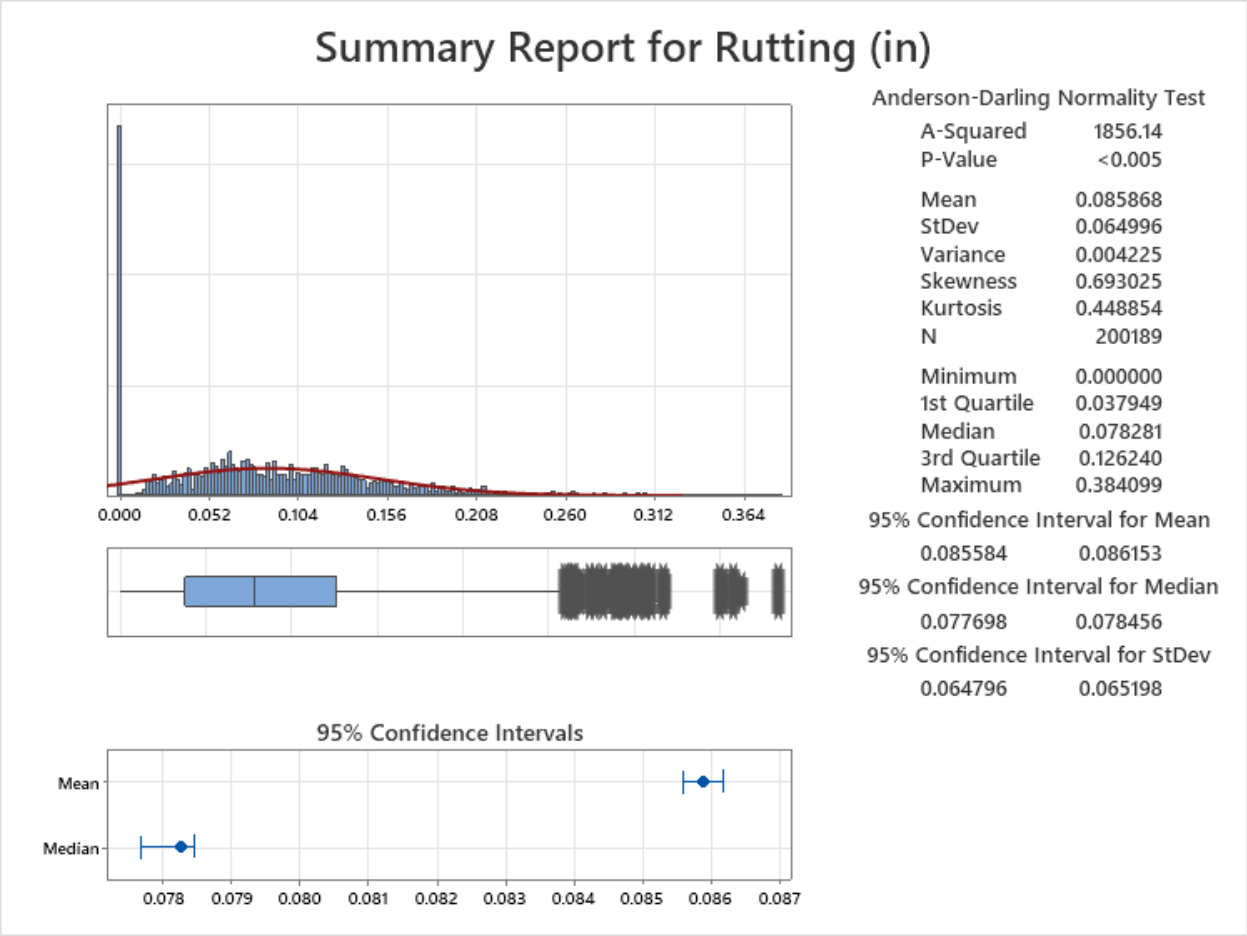

Figure A-6 Summary of training rutting (in)

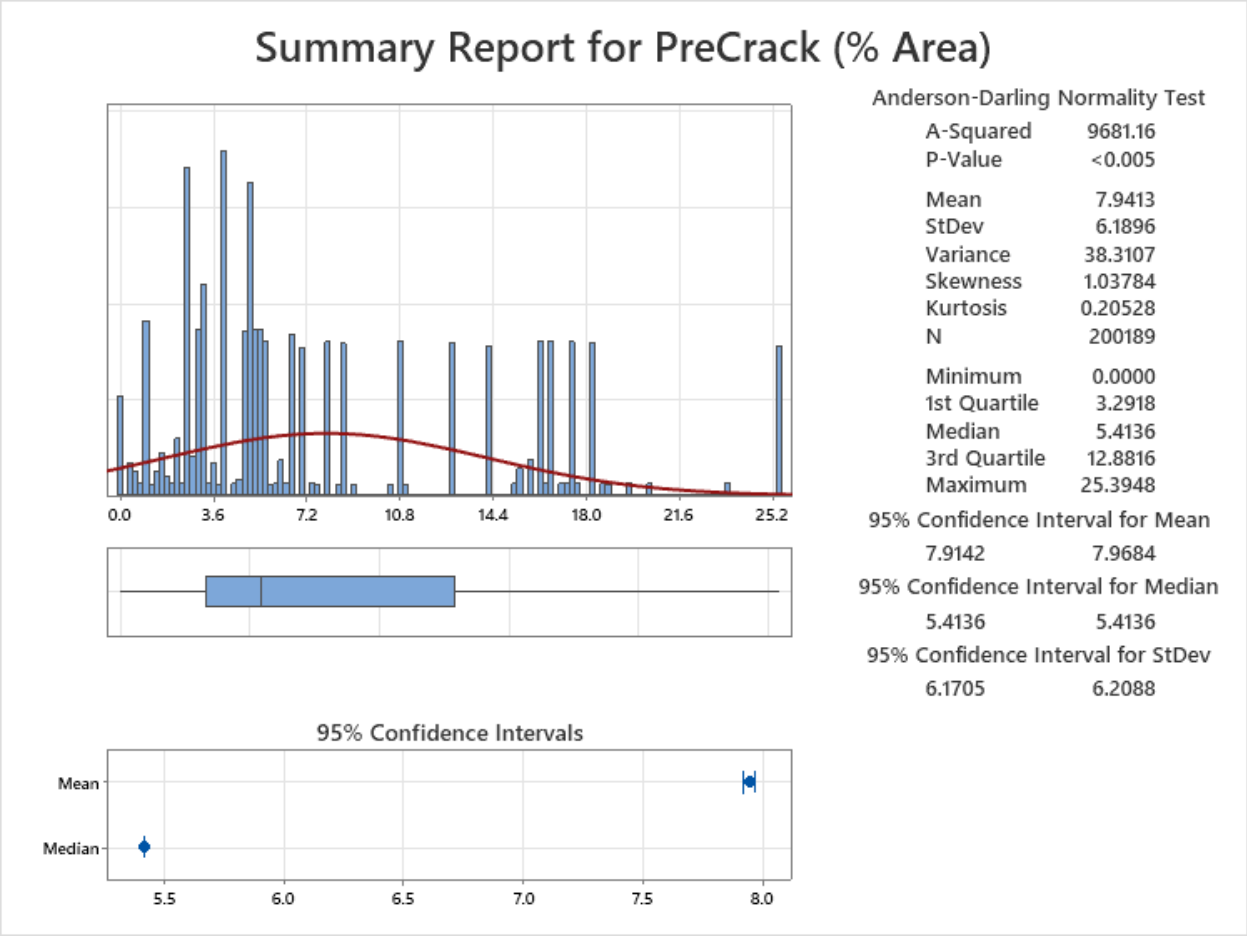

Figure A-7 Summary of training PreCracking (% Area)

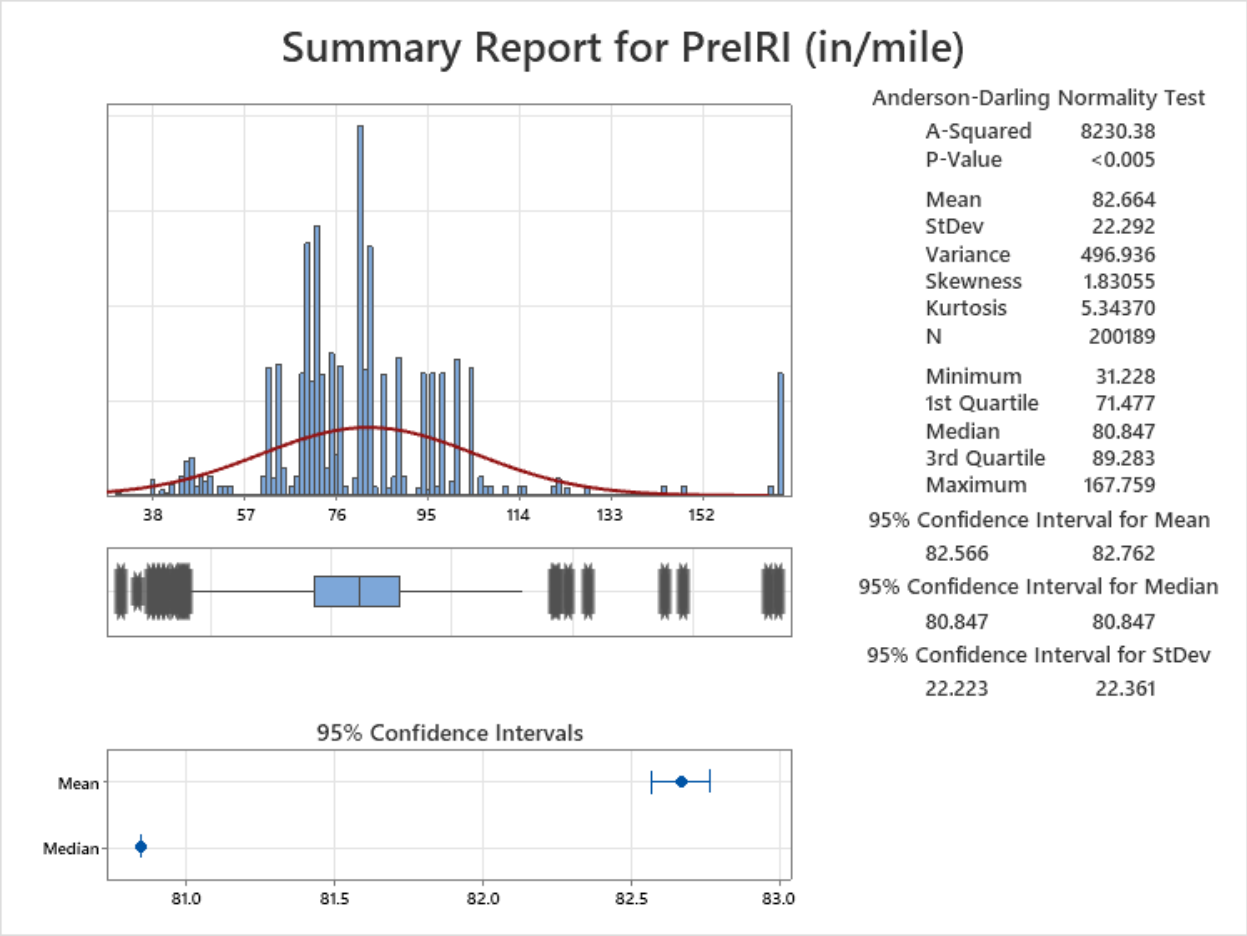

Figure A-8 Summary of training PreIRI (in/mile)

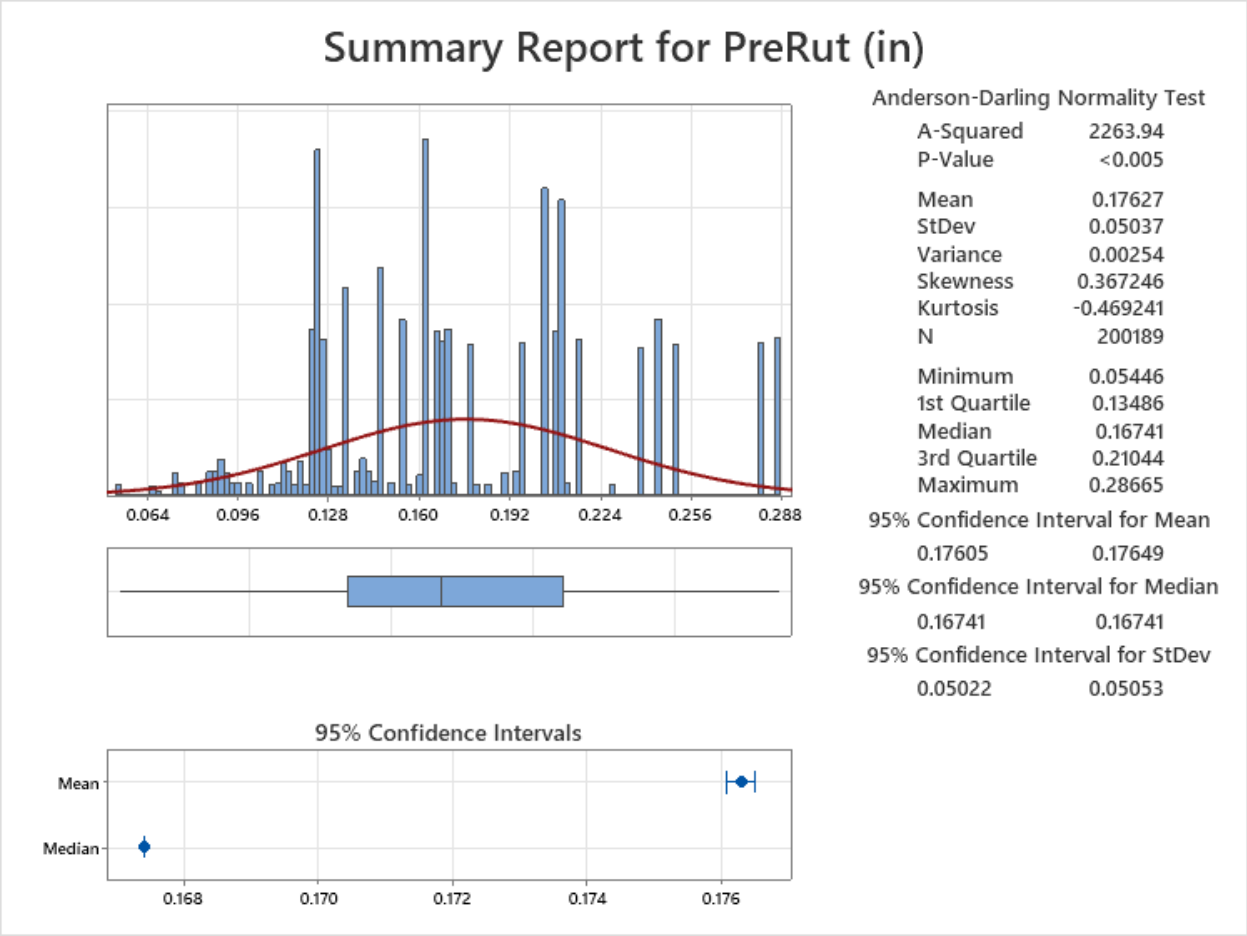

Figure A-9 Summary of training PreRut (in)

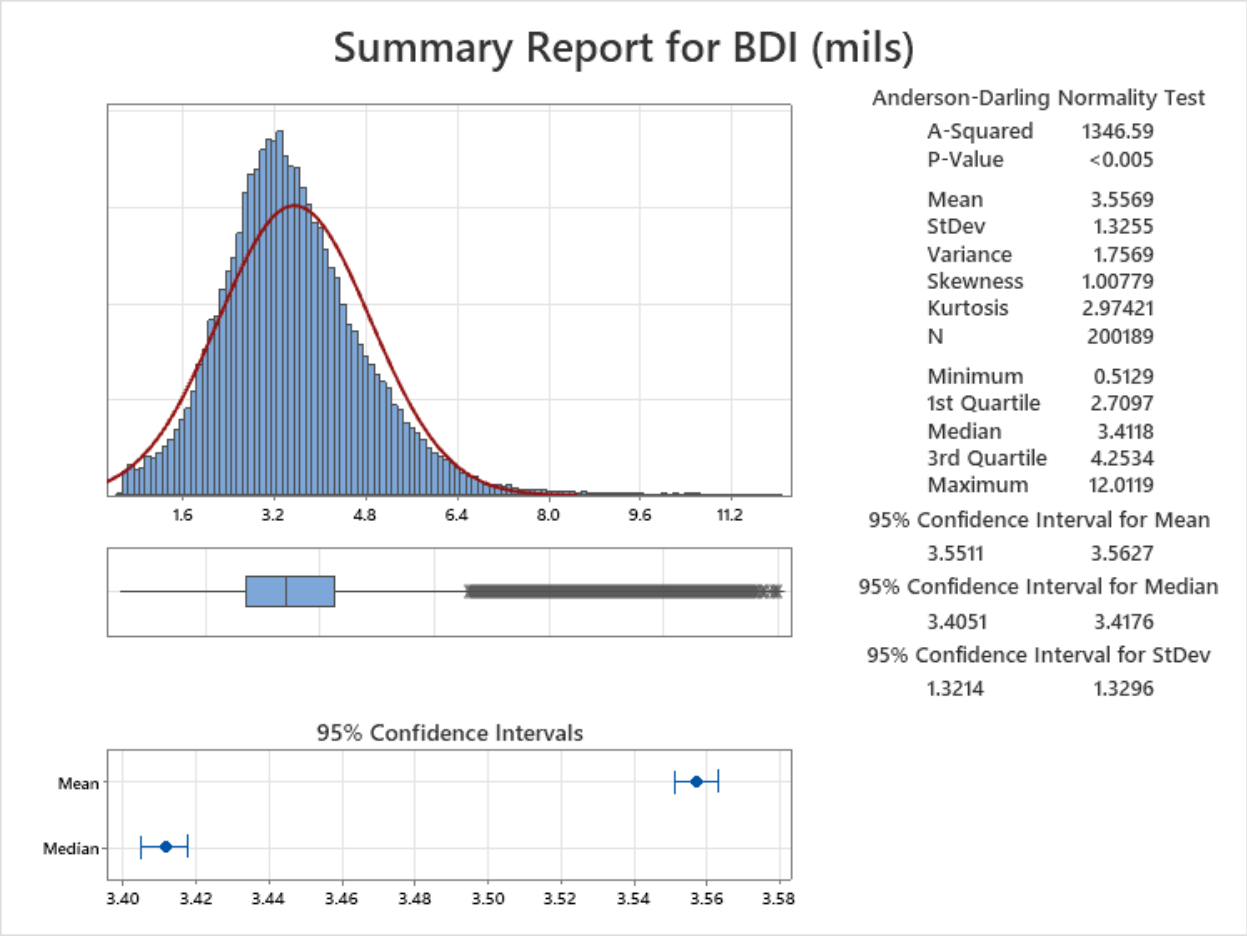

Figure A-10 Summary of training BDI (mils)

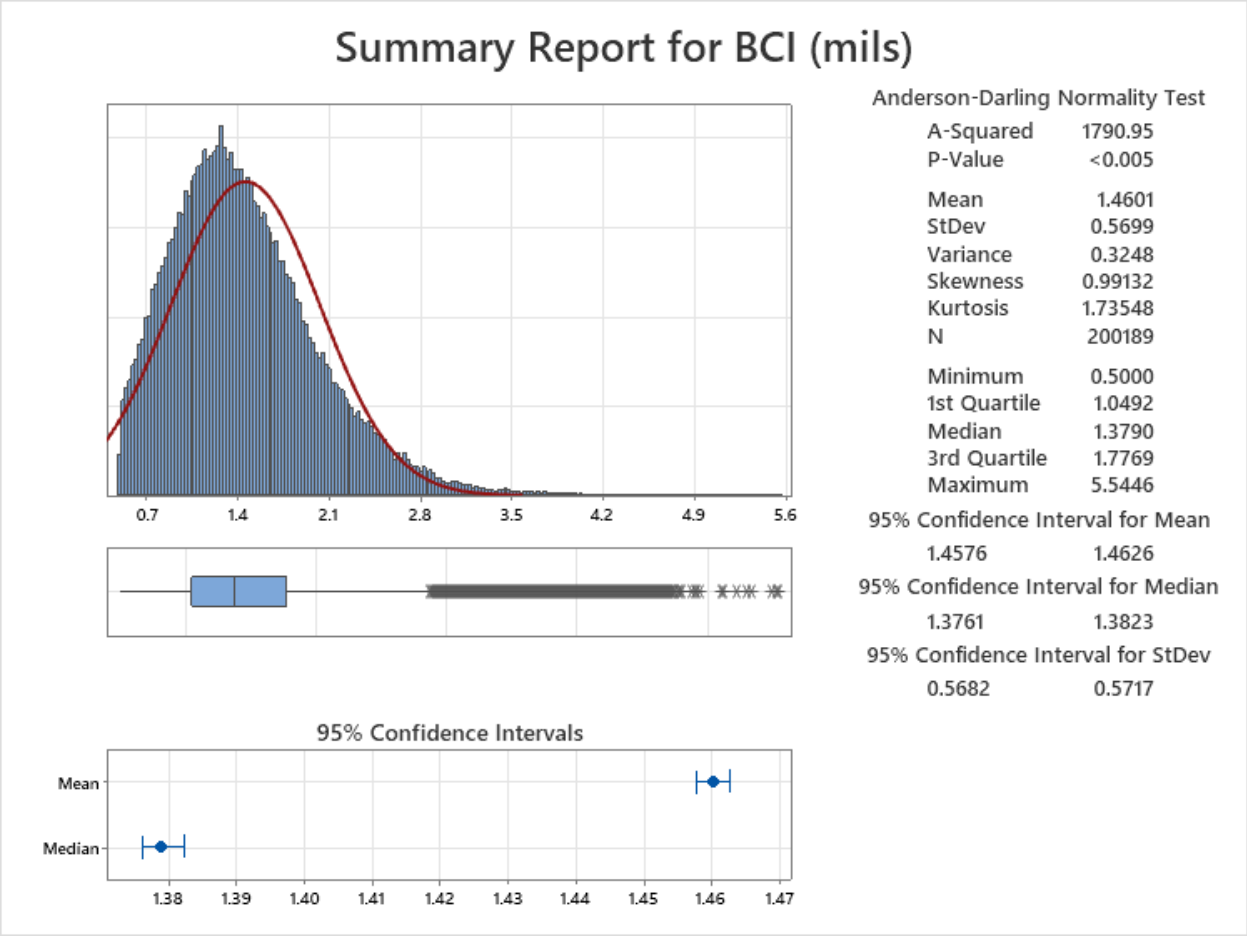

Figure A-11 Summary of training BCI (mils)

Descriptive Statistics

Sample	N	Mean	StDev	SE Mean
BDI	200189	3.55692	1.32547	0.00296
Pred BDI	200189	3.55692	0.66064	0.00148

Estimation for Paired Difference

Mean	StDev	SE Mean	95% CI for μ_difference
-0.00000	1.14910	0.00257	(-0.00503, 0.00503)

μ_difference: population mean of (BDI - Pred BDI)

Test

Null hypothesis H_0: μ_difference = 0

Alternative hypothesis H_1: μ_difference ≠ 0

T-Value	P-Value
-0.00	1.000

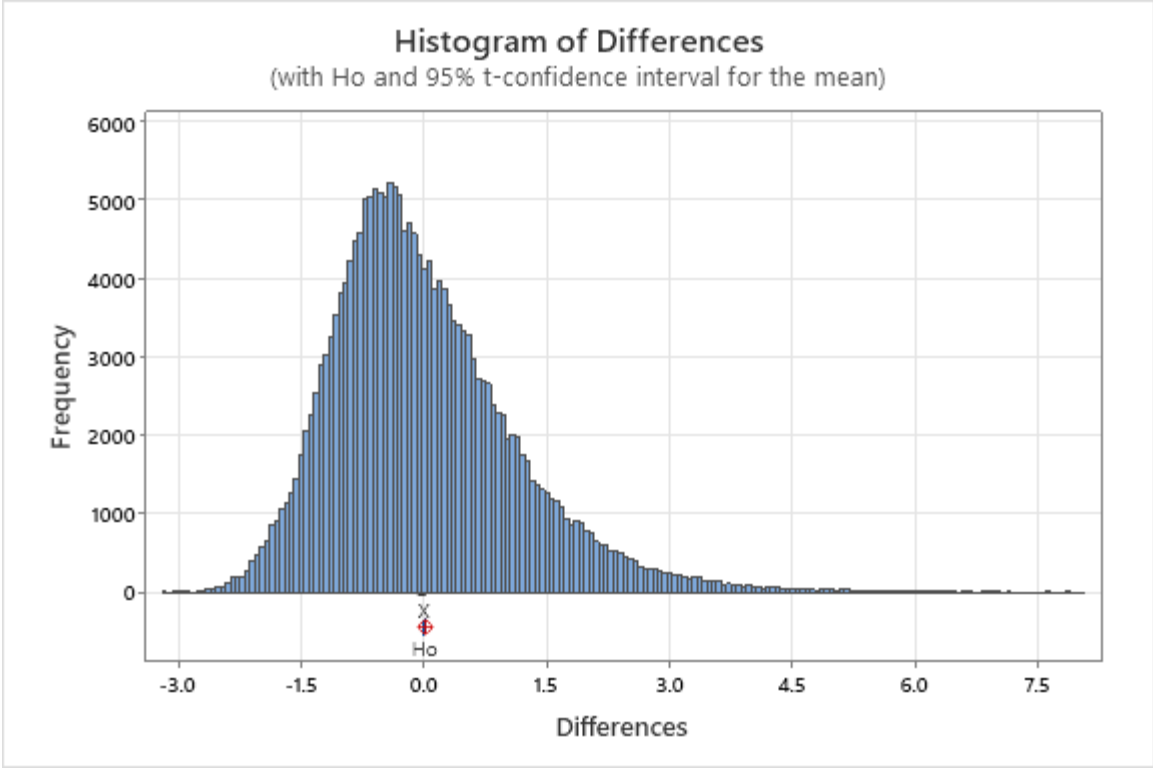

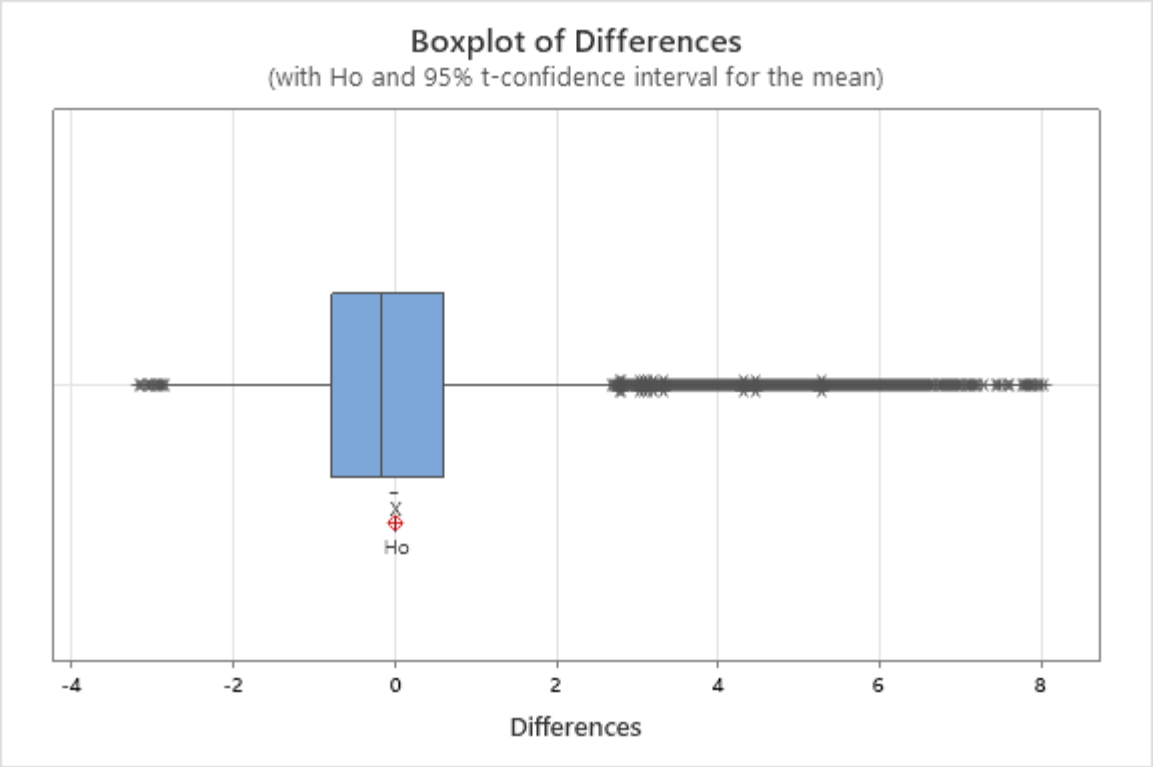

Figure A-12 Comparison of observed and model BDI values from MLR

Descriptive Statistics

Sample	N	Mean	StDev	SE Mean
BCI	200189	1.46007	0.56992	0.00127
Pred BCI	200189	1.46007	0.33314	0.00074

Estimation for Paired Difference

Mean	StDev	SE Mean	95% CI for μ_difference
0.00000	0.46241	0.00103	(-0.00203, 0.00203)

μ_difference: population mean of (BCI - Pred BCI)

Test

Null hypothesis H_0: μ_difference = 0

Alternative hypothesis H_1: μ_difference ≠ 0

T-Value	P-Value
0.00	1.000

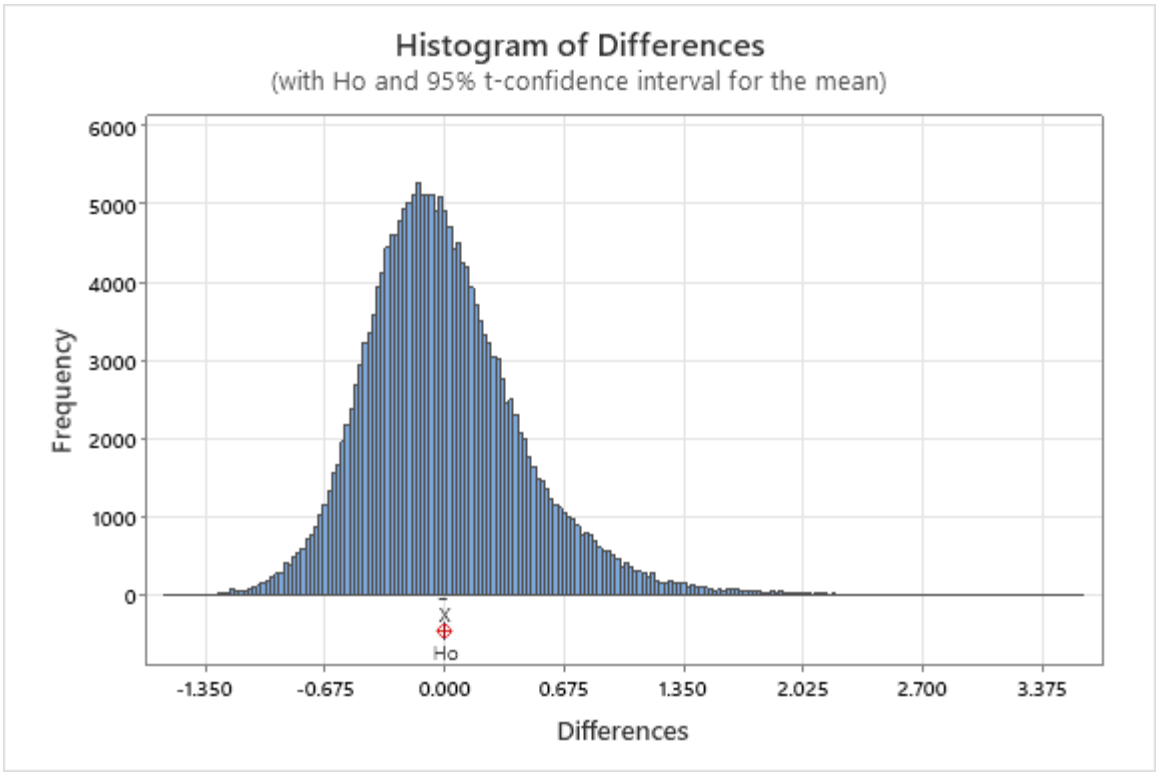

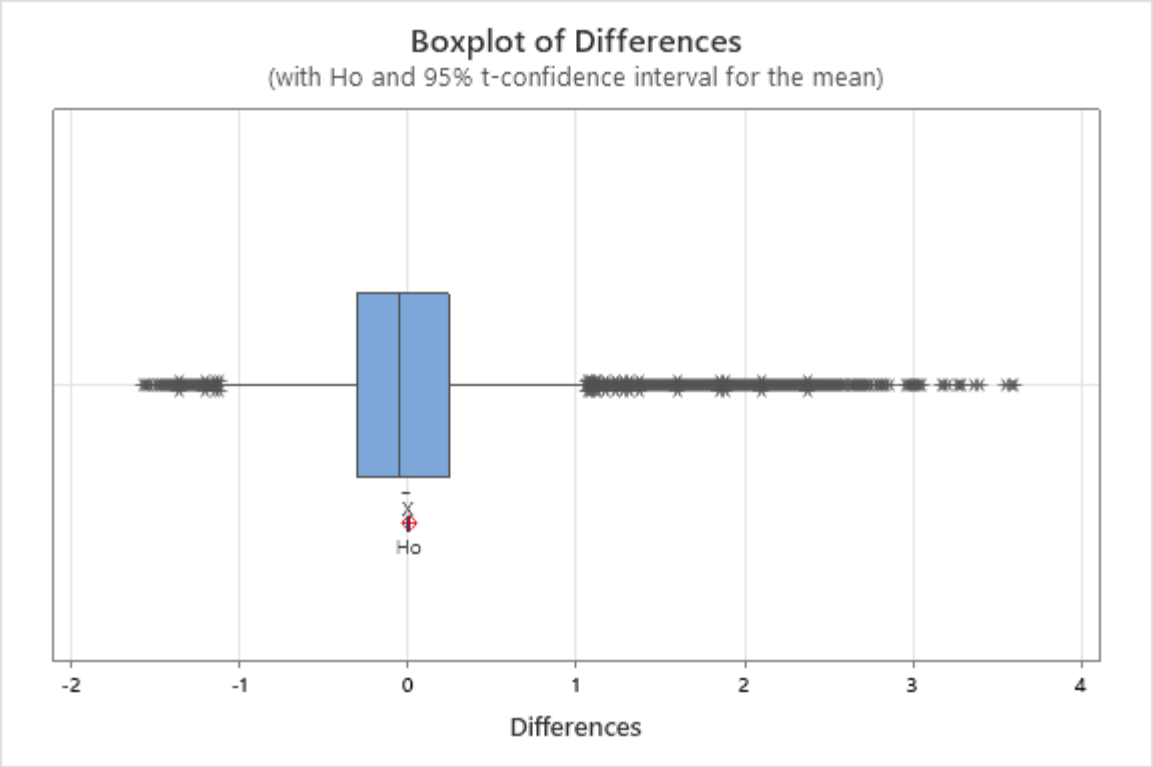

Figure A-13 Comparison of observed and model BCI values from MLR

APPENDIX B: MATLAB CODE FOR NN TRAINING

```
file = readtable('C:\Users\ko2to\OneDrive - Auburn University\Research\01 Project
Works\Project 2- FWD Analysis\08 Experimental Setup\MATLAB\ANN\ANN Models Nov 2021
Proposal\Databank_2\0_all_Drops_Corrected.csv');
data = table2array(file);
output = data(:,13);
input = data(:,1:11);
input_t=input';
output_t=output';
 %%

p=12:12:48;
q=12:12:36;
for i=1:1
    for j=1:length(p)
        for k=1:length(q)
tic
net = fitnet([p(j),q(k)]);
net.divideParam.trainRatio = 80/100;
net.divideParam.valRatio = 10/100;
net.divideParam.testRatio = 10/100;
net.trainParam.mu_dec = 0.8;
net.trainParam.mu_inc = 1.5;
% net.trainParam.showWindow=0;
net.trainParam.epochs=100;
[net,tr] = train(net, input_t, output_t);
yTrain= net(input_t(:,tr.trainInd));
yTrainTrue = output_t(tr.trainInd);
cyt = corrcoef(yTrain,yTrainTrue);
RTrain= (cyt(2,1))^2;

yTest =net(input_t(:,tr.testInd));
yTestTrue= output_t(tr.testInd);
cyt2= corrcoef(yTest,yTestTrue);
% RTest=(cyt2(2,1))^2;

yVal=net(input_t(:,tr.valInd));
yValTrue=output_t(:,tr.valInd);
cyt3 = corrcoef(yVal,yValTrue);
% RVal= (cyt3(2,1))^2;

yAll=net(input_t(:,:));
yAllTrue=output_t(:,:);
cyt4 = corrcoef(yAll,yAllTrue);
% RAll= (cyt4(2,1))^2;

resid= abs(yAll-yAllTrue);
CountVars= numel(data(:,1));
MAE=sum(resid)/CountVars;
AE= sum(yAll-yAllTrue)/CountVars;
MAPE=100*sum((yAll-yAllTrue)/yAllTrue)/CountVars;
E=yAll-yAllTrue;
SQE=E.^2;
```

```
MSE=mean(SQE(:));
RMSE = sqrt(MSE);
A=size(input);
AdjRsq = 1-((1-((cyt4(2,1))^2))*(CountVars-1)/(CountVars-A(:,2)));

[r,m,b] = regression(yAll,yAllTrue);
Nepochs = tr.num_epochs;
toc

timeElapsed=toc;
y = [p(j) q(k) i cyt(2,1) cyt2(2,1) cyt3(2,1) cyt4(2,1) AdjRsq MAE AE MAPE RMSE r m b
timeElapsed Nepochs];
% performdata = [performdata;y];
writematrix(y,['PerformanceBDI',num2str(p(j)),'_',num2str(q(k)),'_',num2str(i),'.csv'
]) ;

netname=['netBDI_',num2str(p(j)),'_',num2str(q(k)),'_',num2str(i),'.m'];
genFunction(net,netname);
%%

FigP= figure;
plot(yTrainTrue,yTrain,'x');
xlim([0 14]);
ylim([0 14]);
daspect([1 1 1]);
title(['netBDI|',num2str(p(j)),'|',num2str(q(k)),'|',num2str(i)]);
xlabel('Observed BDI');
ylabel('Model BDI');
hold on;

plot(yValTrue,yVal,'o');
hold on;

plot(yTestTrue,yTest,'square');
hold on;

plot(0:20,0:20);
hold on;

savefig(FigP,['netBDI_',num2str(p(j)),'_',num2str(q(k)),'_',num2str(i)]);
hold off ;

FigN = plotperform(tr);
title(['Performance_BDI|',num2str(p(j)),'|',num2str(q(k)),'|',num2str(i)]);
% xlim([0 100]);
ylim([0.1 1000]);
%
saveas(FigN,sprintf(['PerformancePlot_',num2str(p(j)),'_',num2str(q(k)),'_',num2str(i
),'.png']))
savefig(FigN,['PerformancePlotBDI_',num2str(p(j)),'_',num2str(q(k)),'_',num2str(i)]);
        end
    end
end

% save('performance.mat',"performdata");
```

```
file = readtable('C:\Users\ko2to\OneDrive - Auburn University\Research\01 Project
Works\Project 2- FWD Analysis\08 Experimental Setup\MATLAB\ANN\ANN Models Nov 2021
Proposal\Databank_2\0_all_Drops_Corrected.csv');
data = table2array(file);
output = data(:,12);
input = data(:,1:11);
input_t=input';
output_t=output';

p=12:12:48;
q=12:12:24;
for i=1:1
    for j=1:length(p)
        for k=1:length(q)
tic
net = fitnet([p(j),q(k)]);
net.divideParam.trainRatio = 80/100;
net.divideParam.valRatio = 10/100;
net.divideParam.testRatio = 10/100;
net.trainParam.mu_dec = 0.8;
net.trainParam.mu_inc = 1.5;
net.trainParam.showWindow=0;
net.trainParam.epochs=100;
[net,tr] = train(net, input_t, output_t);
yTrain= net(input_t(:,tr.trainInd));
yTrainTrue = output_t(tr.trainInd);
cyt = corrcoef(yTrain,yTrainTrue);
RTrain= (cyt(2,1))^2;

yTest =net(input_t(:,tr.testInd));
yTestTrue= output_t(tr.testInd);
cyt2= corrcoef(yTest,yTestTrue);
% RTest=(cyt2(2,1))^2;

yVal=net(input_t(:,tr.valInd));
yValTrue=output_t(:,tr.valInd);
cyt3 = corrcoef(yVal,yValTrue);
% RVal= (cyt3(2,1))^2;

yAll=net(input_t(:,:));
yAllTrue=output_t(:,:);
cyt4 = corrcoef(yAll,yAllTrue);
% RAll= (cyt4(2,1))^2;

resid= abs(yAll-yAllTrue);
CountVars= numel(data(:,1));
MAE=sum(resid)/CountVars;
AE= sum(yAll-yAllTrue)/CountVars;
MAPE=100*sum((yAll-yAllTrue)/yAllTrue)/CountVars;
E=yAll-yAllTrue;
SQE=E.^2;
MSE=mean(SQE(:));
RMSE = sqrt(MSE);
A=size(input);
AdjRsq = 1-((1-((cyt4(2,1))^2))*(CountVars-1)/(CountVars-A(:,2)));
```

```
[r,m,b] = regression(yAll,yAllTrue);
Nepochs = tr.num_epochs;
toc

timeElapsed=toc;
y = [p(j) q(k) i cyt(2,1) cyt2(2,1) cyt3(2,1) cyt4(2,1) AdjRsq MAE AE MAPE RMSE r m b
timeElapsed Nepochs];
% performdata = [performdata;y];
writematrix(y,['PerformanceBCI',num2str(p(j)),'_',num2str(q(k)),'_',num2str(i),'.csv'
]) ;

netname=['netBCI_',num2str(p(j)),'_',num2str(q(k)),'_',num2str(i),'.m'];
genFunction(net,netname);
%%

FigP= figure;
plot(yTrainTrue,yTrain,'x');
xlim([0 14]);
ylim([0 14]);
daspect([1 1 1]);
title(['netBCI|',num2str(p(j)),'|',num2str(q(k)),'|',num2str(i)]);
xlabel('Observed BCI');
ylabel('Model BCI');
hold on;

plot(yValTrue,yVal,'o');
hold on;

plot(yTestTrue,yTest,'square');
hold on;

plot(0:20,0:20);
hold on;

savefig(FigP,['netBCI_',num2str(p(j)),'_',num2str(q(k)),'_',num2str(i)]);
hold off ;

FigN = plotperform(tr);
title(['Performance_BCI|',num2str(p(j)),'|',num2str(q(k)),'|',num2str(i)]);
% xlim([0 100]);
ylim([0.1 1000]);
%
saveas(FigN,sprintf(['PerformancePlot_',num2str(p(j)),'_',num2str(q(k)),'_',num2str(i
),'.png']))
savefig(FigN,['PerformancePlotBCI_',num2str(p(j)),'_',num2str(q(k)),'_',num2str(i)]);
        end
    end
end

% save('performance.mat',"performdata");
```

APPENDIX C: SUMMARY OF PERFORMANCE TABLES FROM TEST LOCATIONS: US 280, CSAH8 AND US 169

Table C-1 Summary of the Performance for US 280 Location

Treatment	Corresponding Treatment Group	Area Under PCR Curve	Final PCR	PrePCR	Difference (- ve Detr. + ve Imprv)	Rank by Difference	Rank By AUPCRC	Combined Score	Score [0-6]	Reached Expectations? Y	Life (PCR>70)
Virgin Thinlay Control	5	5274	79	75	4	1	5	6	6	Y	74+
Double Micro Surface	3	4368	60	75	-15	16	29	45	3	Y	47
Crack Sealing	1	4347	66	79	-14	14	30	44	3	Y	47
Micro Surface with Fibers	2	4410	49	77	-29	30	27	57	2	Y	56
HiMA Micro Surface	2	4806	71	84	-13	13	17	30	4	Y	74+
Rejuvenating Fog Seal	1	4789	60	86	-26	27	18	45	3	Y	58
Fog Seal	1	4764	63	84	-22	22	21	43	3	Y	58
High Rutting CONTROL	0	3113	42	78	-36	37	39	76	0	Y	
Chip Seal with Crack Sealing	3	4497	62	81	-19	19	26	45	3	Y	52
Scrub Seal	3	4728	65	86	-20	21	22	43	3	Y	65
Chip Seal	2	4339	54	86	-32	33	31	64	1	Y	47
High Texture CONTROL	0	3536	45	88	-43	38	37	75	0	Y	

Micro Surface	2	4116	48	78	-30	31	33	64	1	Y	50
High IRI CONTROL	0	2716	36	80	-44	39	40	79	0	Y	
High Cracking CONTROL	0	3289	39	84	-45	40	38	78	0	Y	
Scrub Cape Seal	4	3966	48	81	-33	35	36	71	1	N	50
Micro Surface with Crack Sealing	3	4094	51	86	-34	36	34	70	1	N	50
Cape Seal (Micro on chip seal)	4	4382	62	87	-25	26	28	54	2	N	58
FiberMat Cape Seal (Micro on Fibermat)	4	4622	58	85	-27	29	24	53	2	N	65
FiberMat Chip Seal	2	4969	73	83	-10	9	15	24	4	Y	74+
Triple Chip Seal	4	4995	77	84	-7	6	14	20	5	Y	74+
Double Chip Seal	3	5333	88	87	1	2	4	6	6	Y	74+
Double Micro Surface	3	5560	86	86	0	3	2	5	6	Y	74+
Low Rutting CONTROL	0	4268	71	89	-18	18	32	50	2	Y	74+
OGFC w/Spray paver (eTac)	5	5229	75	86	-10	10	7	17	5	Y	74+
OGFC w/Trackless Tack	5	5175	72	85	-13	12	10	22	5	Y	74+
OGFC w/ AC30 (PG 67)	5	5492	83	87	-4	5	3	8	6	Y	74+
OGFC w/UltraFuse	5	5628	87	89	-2	4	1	5	6	Y	74+
OGFC w/eTac	5	5112	78	87	-9	8	12	20	5	Y	74+
Thinlay Scrub Cape	6	4777	58	91	-32	34	19	53	2	N	74+

Thinlay FiberMat Cape	6	5137	65	89	-24	24	11	35	4	N	58
Thinlay Cape	6	4727	56	87	-31	32	23	55	2	N	65
Micro Surface on Thinlay	6	5219	76	87	-11	11	8	19	5	N	74+
ABR Thinlay Control	6	5206	62	88	-26	28	9	37	3	N	58
Thinlay on Foamed CCPR	6	4772	62	87	-25	25	20	45	3	N	65
Thinlay on Emulsion CCPR	6	5101	71	89	-18	17	13	30	4	N	74+
Thinlay on Emulsion CIR	6	4615	66	89	-22	23	25	48	3	N	58
Thinlay on Foamed CIR	6	4811	72	87	-15	15	16	31	4	N	74+
Ultra Thin Bonded Surface	6	5259	80	88	-7	7	6	13	5	Y	74+
L IRI, LCrack, L Texture CONTROL	0	4026	66	85	-19	20	35	55	2	Y	35

Treatment	Area Under PCR Curve	Final PCR	PrePCR	Difference (- ve Detr. + ve Imprv)	Rank by Difference	Rank By AUPCRC	Combined Score	Score [0-5]	Reached Expectations? Y
Crack seal / Transverse mastic	4535	64	68	-4	17	16	33	2	Y
Single chip seal with crack seal	4693	71	64	7	8	13	21	3	Y
Single chip seal	4362	64	62	2	13	19	32	2	Y
Cape seal	4550	66	69	-3	16	15	31	3	Y
Double chip seal	4724	73	71	2	12	10	22	3	Y
Triple chip seal	4706	76	71	5	10	12	22	3	Y
Fibermat chip seal	4692	72	69	3	11	14	25	3	Y
Fibermat cape seal	5015	81	75	6	9	8	17	4	Y
Scrub cape seal	5194	77	76	1	14	6	20	3	Y
Scrub seal	4712	67	71	-4	18	11	29	3	Y
Micro surface with crack seal	4524	60	68	-8	20	17	37	2	N
Micro surface	4334	58	65	-8	19	20	39	2	Y
Double micro surface	4474	61	61	0	15	18	33	2	Y
Conventional fog seal	3872	46	66	-19	24	22	46	1	Y
Rejuvenating fog seal	2680	28	52	-24	27	30	57	0	Y

HMA Fibermat cape seal	4935	67	58	9	5	9	14	4	Y
HMA scrub cape seal	5381	78	67	11	4	4	8	5	Y
HMA cape seal	5158	77	69	8	7	7	14	4	Y
Control	3212	42	66	-25	28	27	55	0	Y
Control	3740	54	73	-19	23	24	47	1	Y
Control	2976	37	65	-27	30	29	59	0	Y
Control	3562	51	72	-21	25	25	50	1	Y
Virgin thinlay	5732	87	75	12	3	2	5	5	Y
ABR Thinlay	5789	88	74	14	2	1	3	5	Y
Control	3193	50	67	-18	22	28	50	1	Y
Control	4128	60	75	-15	21	21	42	2	Y
Control	3538	46	70	-24	26	26	52	1	Y
Ultra thin bonded wearing course	5389	78	61	17	1	3	4	5	Y
ABR Thinlay with Delta S	5226	75	67	8	6	5	11	4	Y
Control	3856	50	76	-26	29	23	52	1	Y

Treatment	Area Under PCR Curve	Final PCR	PrePCR	Difference (- ve Detr. + ve Imprv)	Rank by Difference	Rank By AUPCRC	Combined Score	Score [0-5]	Reached Expectations? Y
Control	3103	47	33	14	16	28	44	1	Y
Crack seal / Transverse mastic	3834	45	41	4	23	23	46	1	Y
Single chip seal with crack seal	5277	75	35	40	2	4	6	5	Y
Single chip seal	4486	70	39	31	11	18	29	3	Y
Double chip seal	5046	73	39	34	8	14	22	3	Y
Triple chip seal	5101	77	40	37	7	12	19	4	Y
Cape seal	5181	75	41	34	10	9	19	4	Y
Micro surface with crack seal	5142	67	42	25	12	11	23	3	Y
Micro surface	4965	71	37	34	9	15	24	3	Y
Double micro surface	4604	76	38	38	5	17	22	3	Y
Fibermat chip seal	4920	76	39	38	6	16	22	3	Y
Fibermat cape seal	5148	81	42	39	4	10	14	4	Y
Scrub cape seal	5257	81	42	40	3	6	9	5	Y
Scrub seal	5198	80	34	45	1	7	8	5	Y

Control	3288	50	34	16	15	26	41	1	Y
Control	2971	68	58	10	20	29	49	0	Y
Control	3280	74	67	8	21	27	48	1	Y
Rejuvenating fog seal	3999	55	56	-1	25	21	46	1	Y
Control	3670	59	48	10	19	24	43	1	Y
Conventional fog seal	4431	68	51	17	14	19	33	2	Y
Control	3948	65	80	-14	29	22	51	0	Y
Control	4074	67	77	-10	27	20	47	1	Y
ABR Thinlay with Delta S	5580	81	70	11	18	2	20	4	N
Virgin thinlay	5637	87	70	17	13	1	14	4	Y
Ultra thin bonded wearing course	5579	86	72	14	17	3	20	4	N
HiMA thinlay	5198	73	70	3	24	8	32	2	N
ABR Thinlay	5270	76	71	5	22	5	27	3	N
HMA cape seal (thinlay over chip seal)	5060	72	75	-3	26	13	39	1	N
Control	3553	64	74	-11	28	25	53	0	Y

APPENDIX D: WEIGHT ABD BIAS FOR NN MODEL

Table D-1 Weights for the Input Layer for BDI Model

0.9299	0.3978	0.0997	0.8154	0.1108	-0.0582	-0.3925	-0.7633	-1.0195	-0.5638	-1.0763
-0.8713	2.0427	1.2278	-0.0665	0.0447	-0.6028	1.5304	-2.0100	1.1069	-1.9176	-1.0640
0.6148	0.1585	1.0661	0.6294	0.1230	0.0183	-1.0829	-1.5516	-0.3671	-0.0850	0.0013
-0.8084	0.4963	-1.0431	1.1500	-2.5023	-0.1085	0.6040	0.7839	-0.3449	-1.3646	1.0855
-1.5312	0.1408	-0.5615	0.0615	-0.4255	1.0886	0.4998	0.3828	-0.6762	-1.1958	1.1029
-1.2100	-0.3567	1.2203	-0.1899	1.0856	0.5238	-0.1373	1.0834	0.1723	1.1585	0.5397
0.7307	1.0237	0.5043	-0.7845	0.8268	1.1776	-0.2335	0.5546	-0.6879	-2.1708	-1.0458
1.5897	0.5017	-0.2406	-0.2047	1.1943	0.1687	-0.1163	0.6176	0.3345	2.3789	-0.6427
-0.9933	0.6610	0.4987	-0.0933	-0.0183	-0.8161	0.3454	0.4138	1.4307	-1.0609	0.0001
0.5919	0.5202	0.1820	-0.5302	-1.2244	0.5714	-0.7293	0.7284	-0.0275	0.8096	0.4227
1.9883	-0.0730	0.7915	-0.9212	1.2626	0.4703	-0.8206	0.9645	2.7993	-0.3451	-1.7072
-0.1194	-1.4590	-1.4076	-1.6454	1.7892	-0.3917	1.7585	0.9986	0.3638	0.3209	1.9972
0.7053	0.4468	-2.0879	-0.6492	0.3152	1.9315	0.2337	0.9239	-0.3160	1.8449	-0.1155
-2.1243	-1.4222	-0.8326	0.7026	-0.4641	0.1078	-0.5571	0.9106	-0.0896	0.8031	-2.1979
0.3327	-1.3790	-0.8388	0.8122	0.5066	0.0008	1.2296	0.0113	0.3488	-1.0364	-0.0919
0.6986	-0.3192	0.2225	0.9116	-0.8660	-0.1925	0.2001	0.3058	0.9779	0.1676	0.7426
-0.4694	-3.9795	4.5703	-0.5365	0.6638	-0.0191	-0.0772	-0.0927	-2.1706	2.1136	0.5182
-0.9559	0.1419	0.7994	-0.7326	0.0104	0.4773	-0.2038	0.0394	-1.1944	1.6456	1.0054
0.4753	-0.3997	0.7936	0.5361	1.4067	-0.0181	0.0517	0.5215	-1.8204	-1.4999	-2.1121
-0.6606	2.1273	2.5147	-0.9447	-0.4012	-0.8833	-0.5712	-0.5224	1.4126	-0.6560	0.1117
-0.0674	-0.1265	-0.1836	0.7136	-0.9508	-1.3589	-0.0949	-1.2082	1.5998	1.7831	1.8181
1.2195	0.2398	0.1022	0.1978	-0.7956	-1.1606	-0.1336	-1.3136	0.5248	-2.0284	1.0966
-0.0548	0.7464	1.5623	-1.0773	0.7862	0.9963	1.0346	-0.4926	-1.2861	-1.3232	-0.6120
-0.0166	1.5837	-0.0810	1.1161	0.7972	-1.1487	-1.1318	-0.0101	-0.4616	-0.0131	0.3022
-0.0987	-1.6300	0.1664	0.7948	0.8889	1.7746	-0.6232	-0.7569	-1.7878	0.6843	0.1253
-0.2103	3.7875	-0.5717	-0.0575	-2.3497	0.4021	-0.3749	0.2570	1.0984	1.4837	-0.0340
-0.6082	-0.6857	-2.2050	0.4123	0.1669	-0.3628	-0.2596	0.1316	0.5561	-2.3388	-0.6624
-1.0863	0.5416	1.7283	-0.9148	-1.4957	1.1199	-1.0935	1.1735	0.4760	0.5231	1.1583
0.3211	-2.2038	-0.1411	-0.4442	-0.2869	1.5749	-1.8780	0.3786	-0.1579	1.2129	0.8014
-0.4541	-2.5129	1.4049	-1.0769	2.0136	2.1593	0.7386	0.5943	-0.4884	0.7827	0.6783
-0.5589	-0.2860	0.2963	0.0138	-0.3071	0.1890	-0.4624	-1.0224	1.2983	1.4006	-0.0246
-0.2367	0.4921	-1.0129	0.8514	-1.2627	-0.5605	1.3608	0.6520	0.6445	1.1683	0.0339
0.3841	0.1200	-0.6163	-1.4137	0.6515	-0.2747	0.0241	-0.1763	0.5405	0.9484	1.2751
-0.1081	1.5897	-0.3346	0.6186	-0.1047	-0.5894	1.2300	-0.1828	0.4358	-0.9995	0.6726
-0.4619	-1.4915	-0.7590	2.0721	0.2563	0.5530	1.2741	-0.1231	-0.6948	-0.2463	-0.5178
1.0244	0.6760	-1.9438	-0.4690	0.4469	0.0028	0.4195	-0.4851	-1.0685	-0.6499	-0.7462
0.5581	2.6045	-1.2152	-0.4518	0.9580	0.5387	-1.5166	0.3906	0.1727	0.3573	0.1638
-0.3968	0.9329	0.8845	0.9175	0.4619	-0.9614	1.2673	0.2339	-1.1880	0.6281	0.1470
0.2427	-1.5145	-0.3161	-0.0446	-0.7396	-0.9461	0.3424	0.5834	-0.0922	-0.7194	0.0510
0.2175	0.7573	-0.6680	-0.7693	-0.1702	0.5158	0.9633	0.4862	0.0455	1.3122	-0.9696
3.3363	1.6773	4.6221	-0.6339	-0.7858	-1.0472	-1.3899	-0.3340	-0.3914	-1.3039	0.9755
0.3375	0.2387	1.7679	-0.2758	0.1924	-1.0250	-0.2399	0.9884	1.0213	-0.4782	0.7632
-0.6520	-0.9797	0.1282	-0.2576	-0.1035	0.1891	-1.2007	0.3375	-0.0300	-0.3286	-0.9987
-0.9318	1.2848	0.1202	0.5245	0.7715	-0.8276	0.9607	1.0783	-1.5466	0.6766	-0.9201
-0.2557	-1.8935	3.7494	-0.5411	-2.0503	-0.5762	1.6113	-0.5600	0.1118	0.3254	1.6122
-2.0667	0.8379	-0.8088	-0.2775	-2.1050	-0.5711	-0.4890	0.3684	-0.1481	-0.1884	-0.6114
-0.2383	-0.8160	0.0709	0.6646	0.1010	-1.2272	0.1611	-1.1908	0.3349	0.5328	0.7396
-0.8194	1.5129	-0.0642	0.3261	-0.0923	1.1665	-0.0022	-0.0218	0.8870	1.7740	1.3682

Table D-2 Weights for the First Hidden Layer for BDI Model

-0.324	-0.037	-1.224	0.398	-0.486	0.060	-0.167	0.026	0.080	-0.509	0.796	-1.584	-0.936	0.564	-0.012	-0.230	-0.434	-0.029	-0.177	0.348	0.793	0.305	-0.495	-1.023	1.270	0.536	-0.252	-0.331	0.083	0.595	-0.779	0.440	0.674	0.160	-0.315	0.741
-0.805	0.052	0.336	0.109	0.323	-0.467	-0.973	0.970	-0.222	0.346	-0.358	0.619	-0.321	0.631	-1.345	0.440	-0.523	0.167	-0.638	-0.325	0.015	-0.323	-1.162	1.370	1.136	-0.392	-0.028	0.765	-0.186	0.608	0.883	-0.928	-0.376	-0.073	-0.249	-3.175
0.796	-0.656	0.703	0.156	-0.406	-0.160	0.812	0.114	-0.537	0.682	-0.387	0.771	-0.629	-0.473	0.858	-0.450	0.643	-1.017	0.884	-0.123	-0.064	0.223	-0.259	1.693	-0.409	1.250	1.759	0.566	-0.068	-0.383	0.733	0.353	-1.460	0.086	0.299	-0.546
0.620	0.206	0.830	-0.727	0.194	0.034	0.474	-1.243	2.004	0.085	0.270	-0.394	0.616	0.246	-0.062	0.304	0.587	0.145	-0.978	0.160	0.452	0.148	-0.560	-1.094	0.588	-0.190	0.355	0.958	0.780	-0.391	-0.304	0.261	0.554	0.227	-0.188	-1.417
-0.732	0.429	-0.688	-0.401	0.425	-0.139	-0.471	1.091	-0.309	0.270	0.156	0.381	1.496	0.243	0.938	-0.074	-0.064	-0.128	1.122	-0.624	0.161	0.347	-0.104	0.271	0.662	0.215	0.493	-0.006	-0.260	0.220	-0.017	0.229	0.676	0.368	-0.141	-1.038
0.516	0.073	-0.278	1.602	0.416	0.523	-0.320	-0.088	-0.190	0.073	0.241	-0.180	-0.393	-0.192	1.236	0.050	0.660	-0.773	0.383	0.409	-0.790	-0.096	-0.783	-0.333	0.063	0.722	0.792	0.540	0.122	0.534	0.750	-0.964	-0.025	0.455	0.293	1.616
0.023	0.207	0.400	-0.348	-0.808	-0.310	0.615	-0.218	-0.880	0.243	0.071	-0.445	0.007	-0.807	-0.047	0.239	0.239	0.893	0.072	0.019	0.749	-0.356	0.113	0.794	0.309	0.368	1.309	0.645	0.378	-0.106	-0.532	-0.179	0.499	-0.607	0.290	-0.779
0.451	0.557	0.147	-1.485	0.870	-0.456	0.867	0.481	1.458	0.418	0.647	1.792	0.492	1.148	-0.111	0.065	0.332	0.030	0.875	-0.525	0.195	-0.252	-0.783	-0.180	1.387	0.668	0.224	-0.214	0.569	0.232	-0.296	-0.199	0.323	1.211	-0.328	-1.471
-0.167	1.462	-0.391	-1.438	0.575	0.018	0.928	0.651	1.335	-1.098	0.994	1.960	0.959	-0.172	-0.275	-0.104	-0.651	-1.008	-0.287	0.543	0.930	0.306	-0.231	-0.676	-0.495	-0.973	-0.834	0.035	-0.771	0.016	0.078	1.248	-0.186	0.301	0.387	0.723
-0.781	-0.574	-0.228	-0.286	-1.696	-0.281	-2.284	-0.379	-0.541	0.485	-0.405	0.232	0.223	0.072	-0.195	0.791	0.483	-0.349	-0.903	-0.353	-0.069	-0.156	0.098	-0.313	0.490	0.016	-0.808	0.887	-0.246	0.336	0.240	0.323	-1.240	0.226	-0.208	0.574
0.764	0.022	-0.044	0.857	0.141	0.044	0.420	0.304	-0.153	0.256	-0.587	-0.042	0.026	-0.727	0.328	-0.124	-0.618	0.170	0.130	-0.115	-0.146	0.214	0.273	0.561	0.712	-0.980	0.269	-0.236	-0.116	-0.372	0.009	-0.050	-0.014	0.030	0.011	0.483
-0.208	-0.070	-0.238	-0.801	0.221	0.106	1.589	-1.214	-1.410	-0.208	-0.445	1.121	0.557	0.169	0.719	0.846	-0.666	0.377	-1.014	-1.040	-0.349	-0.070	-0.637	-0.326	-0.184	-0.575	1.571	0.059	1.027	0.527	0.392	0.790	0.502	-0.609	0.019	-0.463
0.448	0.056	0.645	0.873	0.408	0.342	-0.538	1.024	-1.116	0.085	1.216	-2.411	-0.098	-0.872	-0.055	0.086	-0.306	-0.286	-0.127	0.232	-0.210	0.075	0.493	-0.011	-0.176	-1.135	0.094	-0.619	-0.832	0.069	0.784	-1.029	0.558	-0.713	0.182	-0.081
0.102	-0.305	0.570	0.285	0.358	-0.036	0.600	0.363	0.358	-0.073	-0.353	0.697	0.016	-0.027	-0.161	0.561	-0.401	-0.270	0.647	-0.162	0.016	0.637	-0.209	-0.178	0.655	-0.480	-0.332	0.347	-0.190	-0.281	-0.402	-0.593	0.513	-0.007	0.006	-0.247
-0.483	-0.333	0.150	-0.802	-0.979	0.746	-0.890	-0.077	0.171	0.625	-0.552	0.279	0.619	-0.162	-0.137	0.515	0.567	0.051	0.161	0.366	0.088	-0.078	-0.213	-0.342	0.263	-0.153	-1.633	0.255	-0.274	0.564	0.018	0.158	-1.520	0.247	0.052	0.490
-0.923	0.620	-1.373	-0.618	-1.681	-0.529	0.584	-0.367	-0.378	-0.440	-1.165	1.420	-2.262	0.077	-1.605	0.283	0.654	-1.519	0.243	-0.708	0.181	-0.093	0.517	-0.734	-1.095	0.900	-0.254	0.716	0.344	0.761	0.765	-0.338	-0.615	-0.015	-0.374	1.026
-0.070	0.362	-0.785	0.085	0.294	0.034	-0.276	-0.376	-0.243	-0.059	-0.375	2.755	0.790	0.235	-0.390	0.152	0.276	0.506	-0.354	0.039	0.020	-0.169	-0.560	0.634	0.365	-0.105	-1.171	0.112	-0.050	0.309	-0.407	0.298	-1.324	-0.254	0.096	0.010
-0.424	0.286	-1.582	0.552	-2.676	0.051	-0.795	0.244	-0.238	0.065	-0.359	0.060	-0.503	-0.889	-0.236	-0.626	-0.003	0.939	0.269	0.234	-0.385	-0.042	0.733	0.518	-0.107	0.499	-0.563	0.144	-0.118	-0.078	-0.492	-0.331	-0.636	0.485	0.042	-1.394
0.786	-0.125	-0.311	0.421	0.907	-0.219	-0.329	0.996	-0.149	0.701	-0.131	0.229	1.559	-0.387	0.065	-0.972	-0.537	0.341	-0.012	-0.011	0.315	0.131	0.533	0.325	-1.575	0.789	0.402	0.001	-0.230	0.118	0.140	0.985	-0.093	0.122	0.211	-2.494
0.417	-0.158	-0.847	1.344	0.523	0.456	0.651	-0.044	-1.350	0.164	-0.305	-0.404	-0.397	-0.687	0.255	0.154	-0.357	-0.041	0.557	0.226	0.027	0.359	0.585	-0.229	-0.229	0.021	0.390	-0.440	0.050	-0.012	-0.765	0.255	-0.165	-0.139	0.109	0.324
0.674	-0.234	0.150	-0.534	0.117	-0.591	0.209	0.565	-0.023	0.656	0.081	0.040	-0.264	-0.788	-0.429	-0.009	-0.290	0.756	0.415	-0.152	0.644	-0.546	0.065	0.526	-0.403	0.353	0.047	0.564	-0.013	0.373	-0.540	-0.121	-0.177	0.299	-0.339	-0.872
-0.010	0.583	-0.105	-0.618	0.239	0.240	-0.373	0.990	0.319	-1.451	-0.182	-0.716	0.370	0.418	-0.363	0.098	-0.064	0.252	0.807	0.140	-0.388	-0.050	-0.250	-0.665	0.050	-1.286	0.086	-0.969	-0.567	-0.001	-0.282	-0.062	-0.692	-0.752	0.710	0.207
0.315	-0.032	-0.679	0.285	-1.133	-0.152	1.049	0.340	-0.532	-0.173	0.032	-0.300	-0.969	-0.277	0.080	1.026	-0.380	0.121	0.919	0.161	-0.249	0.290	-0.142	0.628	0.643	0.624	-0.088	-0.184	-0.256	0.363	-0.315	-0.121	-0.660	-0.357	0.293	0.115
-0.498	0.297	-0.228	-0.502	0.267	-0.489	0.987	0.368	0.348	0.377	-1.068	0.171	0.410	-0.055	0.471	-0.115	0.373	0.285	-0.161	-0.145	0.011	0.088	-0.030	0.285	-0.139	-0.254	-0.407	-0.540	0.214	0.425	0.210	0.697	-1.164	-0.207	0.022	-0.313
0.118	0.997	-0.570	-0.262	-0.524	-0.512	0.848	0.269	-0.015	-0.283	-0.453	0.906	-0.207	-0.561	0.326	0.289	-0.239	-0.107	0.518	-0.270	-0.056	0.160	1.180	0.092	-0.439	0.485	0.238	-0.625	0.436	0.136	0.527	0.417	0.251	-0.681	0.613	0.526
0.415	0.633	0.649	0.276	-0.387	2.081	-0.943	-0.034	-1.451	-0.232	-0.014	-1.330	-1.380	0.411	-0.861	0.387	-0.238	-0.299	0.077	1.258	0.555	-0.669	0.183	0.151	-1.621	-3.199	0.011	-0.196	-0.724	-0.328	-0.591	-1.409	0.020	0.416	-0.634	1.020
0.246	0.580	-0.255	-0.002	0.149	1.572	0.433	-1.406	-0.218	-0.532	0.143	-1.223	-0.743	-0.245	-0.452	-0.630	-0.814	-0.311	-0.956	0.482	-0.458	-0.171	0.505	1.141	-0.697	-0.743	0.740	-0.539	-0.588	-0.431	0.309	-0.978	-0.045	-0.563	0.596	1.698
-0.328	0.190	0.466	-0.144	1.475	-0.320	0.601	-0.026	0.216	-0.175	-0.074	-0.184	0.357	0.116	-0.061	-0.095	0.005	-0.270	-0.042	-0.042	0.023	0.101	0.141	0.249	-0.379	0.430	-0.291	-0.136	-0.407	0.322	-0.404	-0.273	0.057	-0.030	0.076	0.099
-0.729	-0.120	0.212	-0.215	-0.951	-0.465	0.346	-0.151	0.041	-0.039	-0.337	-0.220	-0.171	0.408	-0.431	0.342	0.256	-0.006	0.435	0.005	0.208	0.151	-0.322	0.166	0.159	-0.929	0.104	-0.421	-0.088	0.423	-0.281	0.248	0.019	-0.105	0.036	0.153
-1.136	0.167	-0.935	0.925	-0.802	0.104	-1.445	0.333	0.595	-1.361	-0.400	-0.533	-0.033	0.012	-1.290	-0.221	-0.048	-0.884	-1.085	-0.281	0.367	0.146	-0.939	1.584	-1.363	-1.356	-0.863	-0.343	-1.234	0.023	0.071	0.055	-0.642	-0.275	-0.360	-1.190
0.242	0.143	0.218	-0.203	0.044	0.514	-0.729	0.126	0.270	0.630	-0.402	-0.516	0.982	-0.527	0.585	-0.407	-0.079	0.121	-0.527	0.100	-0.024	0.176	0.291	0.146	-0.080	0.726	-0.354	-0.418	-0.315	-0.292	0.109	0.730	-0.480	0.206	0.015	0.210
0.186	0.110	-1.122	0.093	-0.352	0.049	1.556	0.410	-0.778	0.358	0.670	-1.434	-0.584	-0.072	0.876	0.607	0.703	0.448	0.418	-0.087	0.330	-0.423	-0.285	0.873	0.795	0.269	1.369	0.809	0.122	-0.150	0.040	0.649	-0.344	-0.449	0.236	0.118
0.570	-0.264	0.023	0.674	1.696	0.460	0.719	0.415	-0.146	-0.310	0.547	-0.473	-0.287	0.448	-0.270	-0.429	0.082	-0.324	-0.359	0.129	0.175	0.098	-0.542	-1.123	-0.310	0.228	1.068	0.483	-0.404	-0.152	-0.431	0.682	1.001	-0.215	0.105	-0.500
-0.115	-0.476	0.260	0.348	-0.473	-0.176	-1.684	-0.848	1.014	-0.587	-0.429	0.553	0.420	0.045	-0.449	-0.621	-0.535	-0.139	-0.205	0.156	-0.032	0.376	0.289	0.338	-0.811	0.094	-0.476	-0.593	-0.163	-0.062	-0.867	-0.019	0.362	0.024	0.170	-0.257
0.028	0.409	-0.270	-0.074	-0.467	0.275	-0.113	-0.461	-0.576	-0.539	0.168	-1.330	-1.041	0.221	0.720	0.100	0.496	0.074	-0.620	0.600	0.389	-0.764	-0.539	-0.233	0.139	0.019	-0.202	-0.247	-0.732	-0.032	-0.270	0.042	0.514	0.252	-0.388	0.154
-0.137	-0.838	-0.957	0.901	0.019	0.529	1.418	-0.654	-0.507	0.032	0.220	-0.354	0.507	0.510	0.336	-0.130	-0.675	-0.088	-0.332	0.614	-0.172	-0.216	0.362	-0.106	-0.195	0.587	0.721	0.131	-0.018	0.713	-1.253	0.018	-0.727	-0.837	0.570	0.400
0.205	0.063	-0.058	-0.796	0.147	0.262	-0.645	-0.003	-0.009	0.212	0.103	-0.693	0.108	-0.361	-1.559	0.640	1.003	-0.009	0.269	0.016	-0.092	0.042	-0.163	0.411	0.519	0.286	-0.822	0.254	-0.078	-0.068	0.710	-1.137	-0.514	-0.223	0.263	0.860
-0.080	0.483	0.483	-0.067	-0.119	0.122	0.673	0.971	-0.305	0.089	0.034	-0.233	0.343	-0.365	-0.163	-0.409	-0.334	0.199	-0.603	-0.328	-0.060	-0.453	0.797	0.284	-0.808	0.284	-0.262	-0.093	0.088	-0.202	0.728	0.475	-0.657	-0.249	0.078	1.094
-0.173	0.292	0.072	-0.020	-1.304	0.468	0.468	-0.518	-0.082	0.446	-0.404	0.591	-0.550	-1.239	0.604	-0.086	0.646	-0.504	0.395	0.424	0.121	-0.074	-0.157	0.996	0.378	-0.330	0.291	-0.447	0.407	-0.216	0.202	-1.461	1.292	-0.021	0.258	0.038
0.379	-0.751	0.895	-1.142	-0.081	-0.599	-0.183	-0.976	0.371	0.994	-0.516	0.567	0.427	0.321	0.316	-0.037	1.070	-0.072	0.039	-0.131	0.223	0.367	-0.470	-0.247	-0.577	1.097	-0.239	-0.054	0.661	0.406	-0.044	-0.122	-0.639	-0.119	0.015	0.370
-0.075	-0.536	-0.377	0.751	-0.079	0.037	0.111	-1.221	-0.519	-0.631	0.470	0.400	-0.240	0.243	1.295	-0.276	-0.536	0.785	-0.479	0.100	-0.453	-0.143	-0.928	1.402	0.310	-1.405	0.300	-2.344	-0.851	0.043	0.063	0.329	0.308	0.771	-0.318	0.201
-0.258	-0.091	0.562	0.715	-0.263	-0.414	-1.375	-0.007	-0.611	0.028	-0.179	-0.430	-2.322	-0.421	0.984	-0.106	-0.209	-0.552	-1.859	-0.790	-0.106	-0.369	0.988	0.707	-0.718	0.562	-0.478	-0.100	0.602	-0.300	-0.068	-0.357	0.294	-0.550	-0.296	1.147
-0.210	0.776	-0.116	-0.820	0.426	0.470	0.718	-0.648	-0.495	-0.921	-1.024	0.233	-0.161	0.131	-1.771	-0.441	-0.429	0.452	-0.340	-0.121	1.016	-0.523	0.493	-0.311	-0.992	-0.443	0.526	-0.404	0.491	-0.752	-0.361	1.360	-0.225	0.398	-0.587	-1.753
-0.802	-0.727	-1.408	-0.241	-0.702	0.214	0.094	-1.630	-0.508	-1.132	0.125	-0.739	-1.225	1.018	0.612	0.808	0.070	-0.775	0.831	0.332	0.251	0.375	-1.824	-0.846	1.594	1.127	1.575	0.323	0.040	-0.141	-0.565	-0.689	1.721	0.219	-0.053	1.284
0.481	0.314	-1.729	-0.849	-0.233	0.282	-0.015	1.704	-0.786	0.584	-0.268	0.311	1.202	0.054	-0.360	-0.052	-0.133	1.283	-0.494	0.057	0.000	0.303	-0.637	1.393	1.256	2.057	0.356	-0.843	-0.536	-0.915	0.931	1.791	-0.086	-0.570	0.502	-2.263
-0.839	0.896	-0.772	-0.101	-1.420	-0.381	0.090	-0.382	-0.580	0.052	-0.356	-0.128	-0.637	-0.517	-0.475	-0.432	0.284	0.045	0.263	-0.105	-0.048	0.051	0.167	1.727	-0.687	0.897	-0.126	0.306	-0.085	0.279	0.333	-0.125	-0.554	-0.236	0.147	0.163
0.048	-0.176	-0.010	-0.024	1.718	-0.436	0.417	0.308	-0.039	-0.064	0.318	1.786	-0.898	0.148	-1.073	0.475	0.866	-0.530	0.202	-0.043	-0.254	0.793	-0.405	-0.889	-0.431	2.003	0.336	-0.272	-0.313	0.287	0.167	-1.289	0.853	0.430	-0.449	-0.493
0.157	0.063	-0.681	-0.049	-0.743	0.594	0.952	-0.243	1.080	-0.609	-0.353	0.151	-0.306	-0.267	0.478	0.039	-0.334	-0.124	0.398	0.733	-0.123	-0.379	-0.612	0.452	-0.063	-1.427	0.206	-0.087	-0.123	0.146	-0.220	-1.217	-0.226	-0.534	0.439	0.446

Table D-3 Weights for Second Hidden Layer for BDI Model

1.845585
-2.04603
0.467209
0.456266
-0.82005
1.343549
-2.64142
-0.30241
0.541163
-1.03749
-1.80845
0.412602
-0.53803
1.059181
0.213116
-0.66512
0.806993
0.862231
-0.50891
-1.63112
1.212438
1.034757
0.607945
-0.39332
0.499743
-0.2115
0.836477
0.858816
-0.82277
0.954818
0.399501
-0.40694
-0.54646
1.692675
2.655687
0.344068

Table D-4 Bias for Hidden Layers in BDI Model

Input layer bias	First hidden layer bias	Second hidden layer bias
-2.409198745	2.085916742	-1.387642107
1.432926658	3.082831015	
-3.073293933	2.542732487	
1.72727215	-1.818339231	
1.237319683	1.804855118	
2.657097372	1.457477522	
-0.546233507	-2.040028674	
-0.365698141	-1.850952775	
1.37235655	0.771755767	
-1.832128722	0.246003628	
-1.186393719	2.092140225	
-1.729124899	1.893177816	
-0.556826715	1.217850912	
1.168106109	1.598691543	
1.752557066	0.501414645	
1.864589615	-0.837745663	
-0.948357744	0.092442715	
0.004676752	-1.045565121	
-1.322460371	0.586245302	
-0.595438292	0.196693665	
0.259216829	0.879354213	
-0.75117297	-0.02678737	
-0.021420139	-1.3521433	
-0.549870846	2.051785055	
0.09060763	-1.049972061	
0.528654229	-1.202301281	
-0.048974538	0.928781951	
-0.785988488	1.678981158	
-0.179416245	-0.206266006	
0.801401574	-0.703904055	
-0.096626387	0.632210209	
0.551197407	2.090965616	
1.31919278	-1.014547449	
-0.420938158	-2.865618197	
-0.759445091	1.296508786	
1.036101173	1.622116834	

0.744983261 -2.172851896 0.796814905 1.133052701 2.37553276 1.609091394 -1.87848552 -2.286972738 2.019142976 -3.366946918 -1.537787338 -1.8414512		

Table D-5 Weights for Input Layer for BCI Model

-1.083	3.208	-1.467	-1.538	0.129	-1.537	-0.033	-0.340	1.353	-0.070	-0.576
-0.988	-0.587	0.340	-1.834	0.083	1.773	1.175	-0.101	-2.337	0.435	1.079
0.117	-1.642	-0.278	-0.934	-0.821	1.539	-1.090	-0.698	-1.891	1.569	0.394
0.028	-0.933	-0.245	0.281	0.906	1.144	-0.558	3.422	0.937	-0.775	1.129
1.350	0.423	0.274	0.021	-1.152	0.975	0.076	-0.233	-0.694	-1.864	0.000
0.087	0.953	-1.345	-0.082	-0.960	0.909	-1.346	0.617	1.438	0.073	-0.959
-0.701	-0.401	0.641	0.273	-0.560	0.185	0.185	-1.370	1.398	0.643	-1.781
0.073	0.025	1.555	0.549	2.900	-1.149	-0.758	-0.469	-1.052	-0.956	1.698
0.162	-0.699	-1.226	1.563	0.534	0.374	-0.249	0.055	-0.373	0.705	-0.469
-0.161	-0.131	-0.193	-0.684	0.399	0.261	-1.077	-2.564	2.221	0.640	1.213
-2.184	0.858	-0.625	1.173	-2.870	-1.419	-0.289	-1.302	0.237	0.870	2.005
3.097	-0.943	-3.491	0.560	2.692	0.628	-2.809	1.221	1.021	2.202	4.544
0.522	-1.162	-0.868	0.295	-1.517	-0.499	-0.273	0.037	-0.077	-1.036	0.050
-0.171	-0.698	-0.698	1.800	0.399	-0.015	-0.829	-0.032	0.783	-0.463	-0.469
3.987	0.435	-1.541	0.513	1.794	-0.530	0.321	-1.097	1.192	1.514	-1.199
0.369	1.892	-1.348	2.220	-0.474	-1.578	1.563	-0.341	1.166	-1.383	-0.559
0.109	-4.658	4.446	1.388	0.733	2.107	-2.412	-0.477	-0.684	0.277	0.148
0.305	-1.806	-0.332	-0.020	-0.272	-0.042	-1.738	-0.078	0.115	0.430	-0.084
0.365	-0.320	1.910	-1.594	0.790	-0.048	1.041	-0.599	-0.867	-0.069	0.040
-0.238	-0.352	-0.695	0.331	-0.115	-0.521	0.117	0.172	0.114	0.991	-0.478
1.385	-0.455	0.591	-0.089	0.083	-0.302	-0.408	1.192	1.558	1.070	0.272
0.063	-1.534	-0.389	-0.505	0.455	-0.513	-0.537	-0.178	1.004	-1.850	-0.310
0.155	1.278	-0.551	0.635	-1.688	-2.480	-0.002	0.162	-1.709	0.923	0.601
1.407	-0.685	0.467	-0.131	0.146	-0.204	-0.428	-0.561	0.641	1.136	-0.929
1.245	-0.001	0.232	0.270	-0.589	-1.372	-0.258	1.322	2.596	-0.471	-0.139
-1.398	-0.383	-2.532	-1.011	1.496	0.026	0.896	0.723	0.085	2.031	-0.868
-0.568	-0.713	-4.420	-0.743	1.626	1.315	1.157	0.186	-1.013	1.380	-0.951
0.314	-0.615	1.562	-0.762	-1.266	-0.375	-0.412	-0.890	-0.381	-0.036	0.955
0.216	0.254	0.503	0.312	-0.270	-0.604	-0.084	1.738	0.631	5.024	2.138
-0.075	-0.775	0.201	-0.968	1.942	1.657	-0.225	0.706	0.078	0.242	-0.447
-2.941	0.011	0.228	-0.270	-1.040	-0.389	0.259	-2.225	-2.215	-1.198	-1.101
-0.651	2.093	1.513	-4.584	-1.194	-0.475	-1.539	0.191	0.775	0.433	0.239
-1.251	-0.327	-0.350	-0.270	-0.761	1.130	0.044	-1.186	0.442	-1.630	-1.223
-0.467	-0.520	0.213	-0.440	0.304	-0.029	0.366	-0.797	0.434	-1.612	0.715
-0.123	-0.185	-0.216	-0.790	1.995	-0.870	-0.290	0.682	0.819	-0.798	0.535
-0.512	1.160	-2.898	0.017	-0.360	-0.076	1.207	1.391	0.530	-0.947	-0.461
0.047	0.520	1.630	-0.244	-0.583	1.601	-0.703	-0.310	-1.420	0.029	0.012
-0.962	-0.612	-0.445	-0.752	0.700	-1.344	0.669	-0.033	-0.292	-1.703	0.230
2.321	-1.062	1.258	-2.434	-2.826	-1.211	1.145	1.081	-1.169	-0.811	-0.738
-1.715	-3.200	0.391	3.765	0.028	-0.291	1.130	0.492	2.905	-1.594	0.715
1.080	-0.408	0.952	-0.079	1.511	-0.186	0.249	0.988	-1.001	-0.608	0.497
0.412	-1.045	0.777	-0.533	-0.693	-1.076	1.875	0.303	-1.519	0.013	0.666
1.396	-1.588	-0.451	-0.768	-1.254	-0.118	0.586	0.022	0.753	1.199	0.400
0.907	0.597	0.433	-0.042	0.852	-1.349	0.621	0.987	0.402	0.148	1.318
-0.984	-0.465	-0.300	0.321	-0.170	0.285	0.258	-0.968	1.176	0.180	-0.416
-0.568	1.034	0.696	0.977	1.222	-0.066	-0.776	0.621	0.150	0.620	-0.484
0.458	-1.452	0.652	0.435	1.201	-0.035	-1.604	-0.688	-1.583	1.573	0.576
0.429	-0.478	2.325	-1.803	-2.098	0.950	-0.414	-1.836	0.937	2.026	2.135

Table D-6 Weights for First Hidden Layer for BCI Model

-0.129	-0.473	-1.838	0.412	0.389	0.935	0.145	2.192	-0.868	0.348	0.518	0.181	0.024	0.983	-0.472	-0.076	2.849	0.243	-0.525	-0.526	-0.441	0.385	-0.597	0.512
0.437	-0.046	0.301	-0.174	0.327	-1.692	-0.466	-0.549	-0.083	0.334	-0.945	0.127	0.660	0.143	0.315	-0.176	-0.777	-0.249	0.332	0.090	0.350	-0.435	-0.541	0.903
-0.030	-0.365	0.520	-0.161	-0.128	0.675	-0.446	0.818	-0.567	-0.285	-0.479	-0.323	-0.733	0.155	0.003	0.478	1.366	0.482	-0.138	0.202	-0.438	-0.310	0.121	0.564
0.022	0.237	-0.923	-0.122	0.364	0.751	-0.200	-0.390	0.368	0.265	0.412	0.374	-0.255	-0.524	0.328	-0.269	-1.242	0.167	0.116	-0.844	0.493	-0.493	-0.088	1.397
-0.662	0.184	-0.283	1.318	0.957	1.630	0.119	0.973	-0.233	-0.272	0.503	-0.543	-0.831	0.030	-0.495	-0.187	-0.377	0.067	-0.633	-0.122	0.091	0.435	0.358	-0.726
-0.152	-0.586	0.839	0.658	-0.304	-0.150	2.215	-0.280	-0.148	-0.431	-0.585	-0.175	1.045	-0.443	-0.035	1.287	2.179	-0.210	0.210	0.588	-1.035	0.041	0.414	-0.333
-0.666	-0.215	-0.099	-0.324	-0.566	1.378	-1.004	0.641	-0.104	-0.742	0.702	-0.080	-0.433	-0.530	-0.517	-0.148	-1.476	-0.098	0.209	-0.285	0.180	-0.035	-0.141	-1.105
0.339	-0.176	-0.771	-0.607	1.760	0.089	1.891	-1.309	0.888	0.094	-0.343	0.054	-0.509	0.647	-0.400	0.507	-0.854	-0.944	-1.154	0.551	0.727	0.012	-0.509	-0.900
0.262	-0.318	-0.027	1.747	0.314	0.490	0.818	0.435	-1.508	0.604	0.282	0.152	-0.663	-1.683	-0.142	0.832	1.842	0.035	1.508	-0.422	-1.441	-1.046	1.368	-2.667
0.277	0.165	0.265	0.165	-0.170	-0.172	0.675	0.294	0.004	-0.412	0.092	0.225	-0.424	0.213	0.043	-0.072	0.046	0.091	-0.135	0.958	0.158	-0.060	0.460	-1.554
0.947	0.021	1.637	-0.427	-0.293	-2.586	0.490	0.851	-0.085	-0.184	0.065	0.085	-0.530	-0.944	-0.023	0.344	-0.589	0.398	-0.343	0.610	0.766	0.502	1.292	-0.003
0.003	0.158	-1.594	0.136	-0.655	1.700	0.274	-0.556	0.002	0.316	0.086	0.142	0.612	-0.479	-0.056	-0.373	0.253	-0.251	0.528	-0.234	0.369	-0.119	0.227	-0.094
-0.608	-0.497	-0.003	-0.071	-1.232	0.939	0.285	0.056	0.217	-1.069	-0.580	0.103	0.148	0.382	-0.423	0.252	-0.380	0.067	0.711	-0.214	0.310	-0.751	0.010	-0.402
0.105	-0.060	0.212	0.422	0.564	0.008	-0.550	-0.555	0.083	0.471	-0.536	0.217	0.414	1.633	-0.133	0.391	0.883	0.578	-0.218	0.184	0.589	-0.096	0.555	4.131
0.051	0.366	-0.393	-0.033	0.674	-0.973	-0.116	-1.297	0.154	-0.140	-0.277	-0.231	-0.252	0.059	-0.222	-0.047	-0.136	0.099	-0.410	0.143	1.282	-0.362	-0.044	0.779
0.017	-0.097	0.760	0.155	0.279	-0.104	0.206	0.189	-0.127	-0.140	-0.668	0.132	-0.399	0.155	-0.331	0.347	-0.357	0.141	-0.391	0.034	-0.496	-0.272	-0.888	1.528
0.112	-0.223	-0.215	0.203	-0.160	0.093	0.240	0.376	-0.036	-0.048	0.508	-0.002	-0.139	0.214	0.229	0.176	-0.319	0.190	0.362	0.071	-0.037	0.050	-0.357	-1.882
0.054	0.276	-0.334	-0.019	0.647	-0.451	-0.899	-0.581	0.063	0.515	-0.072	0.201	0.512	-0.774	-0.454	-0.169	-2.737	-0.483	-0.343	-0.023	-0.042	0.124	-1.790	-0.574
0.546	-0.352	-0.644	-0.011	-0.031	1.199	-0.153	-0.589	-0.094	0.964	-1.403	0.194	0.846	0.679	-0.720	0.108	-0.270	-1.001	-0.171	-0.227	1.208	-0.045	1.486	-1.894
0.176	-0.144	0.523	1.178	0.673	-0.754	1.200	1.390	-0.371	-0.206	0.623	-0.743	-0.529	0.150	0.695	0.450	-2.523	-0.493	-0.072	-0.348	1.045	0.782	0.769	0.335
0.062	0.652	-1.063	0.922	0.726	1.009	-1.659	0.225	0.007	-1.038	-0.808	0.153	0.623	1.230	-0.761	-0.356	-0.594	0.191	-0.053	-0.066	-0.203	-0.449	-1.229	1.514
-0.083	-0.490	-0.268	0.145	0.371	-0.916	1.551	0.487	0.232	-0.005	-0.654	-0.009	0.407	0.546	0.302	0.455	-1.861	0.319	0.176	0.554	-1.172	0.129	1.093	4.191
-0.217	0.134	-0.872	-0.032	-0.563	0.435	-0.281	0.393	-0.670	-0.121	0.279	0.256	-1.277	-0.075	-0.851	-0.075	-0.460	-0.124	-0.342	0.057	1.626	-0.305	-1.299	2.722
-0.706	0.410	-0.706	-1.023	0.170	0.781	-0.281	-1.081	0.404	0.492	-0.707	-0.598	-0.412	-0.598	0.858	-0.225	-0.234	0.468	-0.265	0.191	-0.060	-0.429	0.610	2.830
0.129	0.205	1.296	-0.602	-1.357	-3.037	0.078	0.007	-0.680	-0.096	-0.128	-0.196	-0.151	0.566	1.359	0.128	-1.198	-0.438	0.476	0.205	-0.043	0.245	-0.160	-3.346
-0.101	-0.568	0.780	-0.682	-0.232	-0.477	0.338	-0.682	-0.692	-0.204	0.016	-0.103	0.887	-0.449	-0.203	0.622	-0.125	0.017	0.550	0.032	0.743	-1.159	0.010	-0.121
0.174	-0.225	-1.808	1.126	1.596	-0.269	1.215	-0.572	1.598	-0.579	0.355	0.143	-1.414	0.755	-0.703	0.619	-1.530	-1.268	-1.472	0.207	-0.034	1.268	5.813	-3.783
-0.920	0.099	-0.791	0.375	-0.047	0.194	0.758	-0.749	-0.381	-0.656	0.370	-0.209	-0.746	1.498	-0.184	0.376	0.296	1.266	-0.973	-0.677	0.108	-0.275	0.684	6.053
-1.124	-0.004	0.489	-0.313	0.029	-0.281	0.444	-0.229	0.116	-0.439	-0.254	-0.846	0.170	0.516	-0.033	0.061	-0.430	0.232	-0.013	-0.278	0.710	-0.108	0.191	0.570
0.108	0.828	-1.072	-0.474	0.655	-0.316	-1.053	-0.074	0.066	0.221	-0.353	0.223	-1.941	-0.007	-1.121	-0.586	-0.390	-0.169	-1.771	0.224	0.782	0.644	-0.704	-1.181
0.923	0.362	-2.146	0.363	-0.300	-1.750	-0.079	-0.127	0.007	0.036	-0.223	0.365	0.590	0.489	0.973	-0.022	0.087	0.131	0.609	1.180	0.027	-0.288	-0.953	0.900
0.217	0.265	0.407	-0.055	-0.010	0.106	-0.056	-0.530	-0.257	0.426	-2.018	0.125	0.569	0.025	-0.178	-0.042	-0.465	-1.451	0.439	-0.157	-1.087	-0.102	1.082	-1.808
1.703	0.815	0.345	0.329	0.504	-0.008	-0.605	0.076	-0.206	-1.047	0.856	0.170	-0.133	1.485	0.155	-0.231	-0.662	-0.144	0.281	-0.552	2.177	-0.428	-0.548	0.928
-0.289	0.164	-0.386	0.960	0.817	-0.025	0.124	-0.356	0.051	0.799	0.041	-0.049	-0.793	-0.451	0.639	0.338	0.424	-0.811	-0.320	-0.401	1.198	0.085	-0.695	0.742
-0.993	-0.779	1.099	0.591	-0.418	0.447	-1.672	1.513	-0.203	-1.405	1.528	-0.457	0.793	-0.352	1.139	0.439	0.210	-0.685	0.678	-0.363	1.284	-0.150	-0.423	0.406
-0.504	0.168	0.566	0.485	0.490	-0.438	0.353	-0.404	-0.190	-0.179	-0.539	-0.013	-0.506	-0.072	-0.650	0.011	0.044	0.500	-0.678	0.239	-0.277	-0.163	0.490	3.110
-0.295	-0.350	1.091	0.197	0.384	0.899	1.037	0.070	-0.433	-0.632	-0.273	-0.018	-0.471	0.131	-0.244	0.863	-1.370	-0.780	0.057	-0.589	0.617	-0.533	-0.240	3.021
1.353	0.084	0.765	-0.958	0.237	0.371	0.120	-0.021	0.010	1.266	-0.178	-0.463	0.035	0.392	-0.163	-0.055	0.047	0.185	1.126	-1.204	-0.601	-0.362	0.144	-2.738
0.031	-0.820	0.121	0.254	0.239	-0.099	0.381	0.645	-0.085	0.020	-0.037	0.093	0.330	-0.106	0.058	1.024	2.676	0.070	-0.013	0.646	-0.568	-0.003	0.054	0.788
0.660	-0.570	-0.218	-0.241	1.219	-1.697	-0.049	0.753	0.841	0.568	-1.093	0.338	-1.177	1.221	-0.616	0.887	-1.215	0.364	-0.889	0.585	-0.353	0.000	-0.512	0.892
-0.111	0.559	1.572	-0.395	-1.177	0.029	-0.737	0.381	-0.829	-0.478	-0.776	0.325	0.215	0.022	-1.003	-1.010	1.514	-0.386	-0.100	2.392	-0.875	0.053	-0.072	-0.008
0.116	-0.048	0.318	-0.442	1.071	-2.188	1.165	-0.479	0.690	0.063	-0.378	0.161	0.188	0.124	-0.338	0.737	0.483	0.191	-0.917	0.413	-0.669	0.181	0.410	1.177
-0.183	-0.078	0.559	0.468	-0.283	0.391	-0.309	0.159	0.158	-0.141	0.388	-0.097	0.061	0.212	0.000	-0.352	-0.763	-0.198	0.197	0.140	-0.157	0.468	-0.500	-3.342
0.056	-0.066	-0.170	2.084	0.753	-1.091	0.161	-0.965	-0.014	0.376	0.723	-0.073	1.300	0.420	0.463	0.609	0.346	0.043	0.479	-1.232	1.341	0.021	0.748	0.165
-2.949	0.113	-1.324	-0.172	-2.605	-0.909	-1.147	-0.620	-0.067	-0.611	-2.522	-0.828	-0.289	-1.533	0.553	-1.288	-1.350	-1.213	0.784	-1.594	1.977	-0.750	1.748	-1.703
0.501	0.419	1.295	0.648	0.316	0.059	-0.199	-0.079	-0.180	-0.409	0.634	0.256	0.044	1.060	-0.481	-0.700	-0.078	0.913	-0.042	-0.365	-0.785	0.140	0.148	-1.659
-0.885	-0.445	0.967	2.222	0.610	-2.477	0.974	-0.070	-0.034	-1.093	1.622	-0.657	-0.511	0.601	-0.158	0.219	-0.347	-0.273	1.242	-0.186	-0.688	-0.077	2.144	0.579
-0.097	0.052	1.152	-0.155	0.593	2.572	-2.811	-0.564	-0.349	-0.453	-0.755	-0.096	0.214	1.344	0.628	-0.911	1.243	-1.015	0.042	-0.573	-0.706	-0.476	-1.133	0.145

Table D-7 Weight and Bias for Input and Hidden Layers for BCI Model

Weights for second hidden layer for BCI model	Bias for input layer for BCI model	Bias for first hidden layer for BCI model	Bias for second hidden layer for BCI model
-0.5879	1.5695	0.9470	0.5778
-2.2685	2.2433	2.4129	
0.9219	-1.0847	1.3346	
-0.4783	5.3496	0.9830	
0.6068	-2.1040	-1.2457	
0.1814	-2.1397	3.1198	
1.1383	1.2202	-3.2867	
-0.5278	4.2845	-0.8180	
-0.6015	-1.3881	1.5889	
-0.6778	-1.2412	1.2415	
-0.4969	0.2809	-0.6300	
1.0524	-1.6467	-0.5289	
-0.4512	-1.3464	-1.9308	
-0.3352	-0.1747	-1.9930	
0.6238	-2.0746	-1.0795	
-2.0953	0.3149	-1.1713	
-0.3470	-1.4375	1.5267	
0.5175	-0.5118	2.2570	
0.8376	1.6464	2.8482	
1.0357	0.2760	0.9553	
0.3661	-0.1422	2.1954	
1.0002	-0.0376	-1.9463	
-0.4797	-1.4871	7.0918	
-0.7530	-0.2478	2.7765	
	0.1695		
	-0.6610		
	-0.7470		
	-0.1391		
	0.8241		
	0.8274		
	-1.6184		
	1.2506		
	-1.8785		
	-0.3829		
	-0.2147		
	0.1237		
	-0.7676		
	-1.8734		
	2.2961		
	-2.4575		

	2.4642 1.1604 0.9977 1.9071 -1.7419 -0.9977 2.5845 3.9724		